Representing the present and future release of carbon to rivers in permafrost regions using an earth system model

Simon Bowring

université PARIS-SACLAY

NNT : 2017SACLE035

Thèse de doctorat

université PARIS-SACLAY

UNIVERSITÉ DE VERSAILLES ST-QUENTIN-EN-YVELINES

université PARIS-SACLAY

Representing the Present and Future Release of Carbon to Rivers in Permafrost Regions using an Earth System Model

Thèse de doctorat de l'Université Paris-Saclay
préparée à l'Université de Versailles Saint-Quentin-en-Yvelines

École doctorale N°129: Sciences de l'environnement d'Ile-de-France
Spécialité de doctorat: Météorologie, océanographie, physique de l'environnement

Thèse présentée et soutenue à LSCE, le 23 Mai, 2019

Mr. Simon P. K. Bowring

Composition du Jury :

M. Philippe BOUSQUET Professeur, UVSQ	Président
M. Peter RAYMOND Professeur, Yale University (Etats-Unis)	Rapporteur
Mme. Jorien VONK Associate Professeur, VUA (Amsterdam)	Rapporteur
M. Lars TRANVIK Professeur, Uppsala University (Suède)	Examinateur
M. Samuel ABIVEN Associate Professeur, UZH (Zurich)	Examinateur
M. Philippe CIAIS Professeur, LSCE	Directeur de thèse
M. Bertrand GUENET Chargé de recherche, LSCE	Co-Directeur de thèse
M. Ronny LAUERWALD Chercheur contractuel, ULB (Bruxelles)	Co-Directeur de thèse

Titre : Représenter le rejet présent et futur de carbone dans les rivières dans les régions de pergélisol à l'aide d'un modèle de surface

Mots clés : pergélisol, rivières, carbone organique dissout (COD), alcalinité, changement climatique, couche active

Résumé : Pendant la majeure partie du Pléistocène, les régions de la Terre recouvertes de pergélisol ont été des puits nets de carbone (C) d'origine végétale et transférée au sol. L'accumulation de ce C organique dans les sols de la région de pergélisol circumpolaire nord a conduit à des stocks qui contiennent actuellement une masse C supérieure à celle qui existe dans l'atmosphère par un facteur de plus de deux. Dans le même temps, les rivières du pergélisol arctique rejettent environ 11% du flux d'eau fluvial global dans les océans, et ce dans un océan (l'Arctique) correspondant à 1% du volume d'eau total des océans mais d'une très grande surface ce qui le rend relativement sensible aux afflux de matières dérivées des surfaces terrestres. Ce flux fluvial provient de précipitations sous forme de pluie ou de neige qui, lors du contact initial avec la surface, ont le potentiel immédiat d'interagir avec le C de l'une des deux manières suivantes: d'une part, l'eau qui coule sur des roches carbonatées ou silicatées provoquera une réaction dont le réactif nécessite l'absorption de CO_2 atmosphérique, qui est ensuite transporté dans l'eau des rivières. Ce C inorganique issu de l'interaction de l'eau, de l'atmosphère et de la lithosphère représente donc un vecteur de stockage ou de «puits» du C. D'autre part, l'eau qui interagit avec la matière organique présente dans les arbres, la litière ou le sol peut transporter le C qu'elle contient et le transférer par les eaux de surface et souterraines dans les rivières. Ce carbone peut ensuite être métabolisée vers l'atmosphère ou exportée dans la mer. Des améliorations récentes dans la compréhension de la dynamique du C terrestre indiquent que ce transfert hydrologique de matière organique représente le devenir dominant du carbone organique, après prise en compte de la respiration des plantes et du sol. Dans le contexte du réchauffement climatique d'origine anthropique amplifié de l'Arctique, l'exposition thermique imposée au stock de pergélisol de C, associé à d'une augmentation des précipitations futures, laisse présager des changements importants dans le cycle du carbone organique et inorganique induit par les flux latéraux. Cependant, la totalité des processus impliqués rend difficile la prévision de ce changement. Partant de ce constat, cette thèse s'appuie sur les avancées antérieures en matière de modélisation du système terrestre pour inclure la production et le transport latéral de carbone organique dissous (COD), de CO_2 dérivé de la respiration et d'alcalinité dérivée au sein d'un modèle global de surface terrestre développé précédemment pour résoudre spécifiquement les processus des régions boréales. A l'aide de données issues des plus récent produits sur le sol, l'eau, la végétation et la climatologie pour forcer les conditions aux limites du modèle, nous sommes en mesure de reproduire les processus et les flux de transport latéraux existants ainsi que faire des projections futures. Dans cette thèse, nous montrons que les exportations d'alcalinité panarctique et l'absorption du CO_2 qui l'accompagne augmentent avec le réchauffement, que les flux de COD diminuent en grande partie à cause des circuits d'écoulement d'eau plus profonds dans le sol et des changements qui en résultent dans les interactions carbone-eau. Enfin, nous observons que la libération de COD dans l'Articque n'est pas linéairement liée à la temperaturre. Par conséquent, la future libération de COD dans l'Arctique peut augmenter ou diminuer avec la température en fonction des modifications de l'état thermique et des trajectoires hydrologiques dans les sols profonds. L'effet net de ces flux sur les océans est de réduire l'acidification future de l'eau de mer d'origine terrestre. À l'inverse, nos simulations montrent que l'absorption de CO_2 due à l'altération chimique est supérieure à son évasion de l'eau des rivières, ce qui signifie que, lorsque l'altération est prise en compte, le cycle du carbone dans les eaux intérieures passe d'une source nette de C à un puits net. En outre, ce puit augmente au 21ème siècle, amortissant partiellement la perte de carbone du sol lors du dégel du pergélisol.

Title : Representing the Present and Future Release of Carbon to Rivers in Permafrost Regions using an Earth System Model

Keywords : permafrost, rivers, DOC, alkalinity, climate change, active layer

Abstract: For much of the Pleistocene, regions of the Earth underlain by permafrost have been net accumulators of terrestrially-fixed plant carbon (C), known as organic C, to the extent that in the present day the soils of the northern circumpolar permafrost region alone contain a C mass outweighing that which exists in the modern atmosphere by a factor of over two. At the same time, the rivers of the Arctic permafrost region discharge about 11% of the global volumetric river water flux into oceans, doing so into an ocean (the Arctic) with 1% of global ocean water volume and a very high surface area: volume ratio, making it comparatively sensitive to influxes of terrestrially derived matter. This river flux is sourced from precipitation as either rain or snow, which, upon initial contact with the landscape has the immediate potential to interact with C in one of two ways: Water running over carbonate or silicate –bearing rocks will cause a reaction whose reactant requires the uptake of atmospheric CO_2, which is subsequently transported in river water. This 'inorganic' C derived from interaction of water, atmosphere and lithosphere thus represents a C storage or 'sink' vector. In addition, water interacting with organic matter in tree canopies, litter or soil can dissolve C contained therein, and transfer it via surface and subsurface water flows into rivers, whereupon it may either be metabolised to the atmosphere or exported to the sea. Recent improvements in understanding of terrestrial C dynamics indicate that this hydrologic transfer of organic matter represents the dominant fate of organic carbon, after plant and soil respiration are accounted for. In the context of amplified Arctic anthropogenic warming, the thermal exposure imposed on the permafrost C stock with expectations of enhanced future precipitation point toward substantial shifts in the lateral flux-mediated organic and inorganic C cycle. However, the complex totality of the processes involved make prediction of this shift difficult. Addressing this gap in instrumental power and theoretical understanding, this collection of studies builds upon previous advances in earth system modelling to include the production and lateral transport of dissolved organic C (DOC), respiration-derived CO_2, and rock-weathering derived alkalinity in a global land surface model previously developed to specifically resolve permafrost-region processes. By subjecting the resulting model to state of the art soil, water, vegetation and climatology datasets, we are able to reproduce existing lateral transport processes and fluxes, and project them into the future. In what follows, we show that while Pan-Arctic alkalinity exports and attendant CO_2 uptake increase over the 20th and 21st Centuries under warming, DOC fluxes decline largely as a result of deeper soil water flow-paths and the resulting changes in carbon-water interactions. Rather than displaying a clear continuous (linear or non-linear) temperature sensitivity, future Arctic DOC release can increase or decrease with temperature depending on changes in the thermal state and hydrologic flow paths in the deep soil. The net marine effect of these fluxes is to decrease future terrestrially derived seawater acidification. Conversely, our simulations show that CO_2 uptake from chemical weathering exceeds its evasion from river water, meaning that when weathering is considered, the inland water carbon cycle shifts from being a net C-source to a sink. Further, this sink increases into the 21st C, partially buffering soil C loss from permafrost thaw.

Université Paris-Saclay
Espace Technologique / Immeuble Discovery
Route de l'Orme aux Merisiers RD 128 / 91190 Saint-Aubin, France

Acknowledgements

This was unforeseen. But a PhD thesis on the global numerical modeling of the permafrost, for somebody from a sub-tropical island who started off professionally in writing, was never all that likely. The succession of leaps, many thousands small and some very large over the past three and a half years, have been intellectual, emotional, organisational and –largely less positively –physical, and would have come to little without many people, some of whom I hope have the opportunity, as it were, to be reading these words now. I have gone from somebody who knew next to nothing of the permafrost , of coding, or the importance of the process by which huge masses of the sky are transferred by raindrops over the entire vast stretch of the global land mass into the oceans, to somebody who knows a little bit more. I have met great scientists, colleagues and individuals, and travelled to many places during this time to do so, briefly even acquainting myself with the Lena River in Eastern Siberia. The process itself has been painful, frustrating, stressful, sometimes rewarding, but its outcome has, I hope, somewhat fulfilled its purpose of adding understanding and context to our interpretation of what is happening and what could happen to our planet and the beings that inhabit it, now and onward.

For now, I would like to first raise a glass to my supervisors: Bertrand for his kindness, Philippe for his patience and huge depth of field. A glass more pungent I raise to Ronny for his brilliance, help and humour, and without whom I would likely have abandoned this attempt. Special thanks to Albert, for being there to deal with my code, to Pierre R. and Pierre F. for having and giving belief, and to Jorien, Pete, Samuel and Lars for agreeing to be on the committee tasked with reviewing this document. To my collaborators in life and co-conspirators in laughter and friendship, you know who you are. But here I'll shout out some names. Nefeli, Martin, Isa, Yannis, Ana, Ardalan, Lea, Bob, Rashel, Patrick, Costa, Stefano, Joao, Edo, Imie, Gautham, Taco, Joris, Christos, Giorgos, Niki, Dimi, Omer, Heike, Vale, Tsoef, Fekas, Ola, Timo, Braschi, Ryan, Olivia, Yucca, Crystal, Sim, Matthi, Iain, Alex: Thank you for collectively carrying in you the same flashing, giving, nonchalent and hilarious magic infused of life itself; I'd have been defeated many times in many ways without it. To my parents for their timeless, unconditional support and embodiment of the spirit of questioning, and to my brother for his curiosity and bravery, for always providing a different. And to Monse for being my light, and driving everything which makes everything worth everything.

Chapter 1: Introduction

The Earth's carbon cycle, fundamentally driven at source by volcanic activity, and at sink by the chemical weathering of carbonate-based rocks, is substantially mediated by the existence of life on this planet, in that uptake of carbon dioxide (CO_2) by photosynthetic organisms leads to substantial solid-state storage of CO_2 on the land or sea surface as biomass, causing a buffering or lag-time for the cycling of this element between lithosphere and atmosphere. The terrestrial storage rate of carbon depends on both its uptake rate by photosynthetic organisms, a function of the hospitability of living conditions on the Earth's surface, which is related to temperature and precipitation, and its turnover or release rate by plant and microbial/animal respiration –also a function of climatic conditions. In turn, by altering the concentration of atmospheric CO_2 and its subsequent impact on solar radiative forcing, carbon uptake and storage/release by living organisms themselves modulate climate and hence the conditions of their own existence(Kump, L.R., Kasting, J.F., Crane, 2010).

Soil carbon accumulation occurs when vegetation growth and litter production exceed the capacity of fauna and microfauna to consume them, leading to a net increase in organic matter stocks on the land surface. In the tropics, soil carbon accumulation rates tend to be low, reflecting the efficiency of carbon removal from the land surface due to the relative lack of temperature and moisture limitation on decomposition and mobilisation of photosynthetically-fixed carbon (e.g. ref. (Stuart Chapin et al., 2012)). In the high latitudes, sub-zero mean annual air temperatures can lead to a situation in which organic matter in the subsoil can remain permanently frozen throughout the year, despite seasonal aboveground temperatures far exceeding freezing point. When combined with substantial net primary production and plant litter inputs in boreal forests, sub-zero belowground temperatures result in low rates of soil carbon decomposition and turnover. Additionally, the activity of soil-burrowing organisms and the vertical churning of soil due to repeated freeze-thaw cycles, results in the downward-migration of soil surface matter to depth, where it can remain thermally shielded from decomposition for millennia.

As a result, over multi-millennial timescales this incremental soil accumulation results in the formation of massive organic carbon stocks, collectively known as 'permafrost soil carbon', which can be subdivided into more recent stocks of <10Ky, older >10Ky soils, and 'yedoma' soils, which consist of organic matter 'fixed' during the Pleistocene era (10My-10Ky) that are characterised by both high soil carbon concentrations and volumetric ice content. The soil column produced by this accumulation can reach depths of well over 30m, and are thought to contain 1330–1580 Petagrams (PgC, $=10^{15}$grams or 'billion tonnes') of soil organic carbon (SOC) (Hugelius et al., 2013, 2014; Tarnocai et al., 2009), or the equivalent of ~25 cumulative yrs. of global terrestrial net plant growth or net primary production (NPP) at present day rates (~59PgC yr^{-1})(Regnier et al., 2013).

As planetary warming proceeds with increases in atmospheric CO_2 and other greenhouse gas concentrations in the modern era, temperatures in the Arctic increase disproportionately relative to the global average –a process known as 'Arctic amplification'(Serreze and Barry, 2011). As a result, thermal shielding of permafrost-

region soil has recently diminished, and is expected to do so substantially in the coming centuries. This will both slow the rate of (modern) humic SOC accumulation, and increase the rate at which (older/ancient) stabilised soil carbon is mobilised from its dormant, frozen state(Schädel et al., 2014; Schuur et al., 2009, 2015; Zimov et al., 2006). This extent of this 'awakening' is the subject of a timely focussing of recent scientific research, given the potential perturbations that such a large thermally-vulnerable SOC stock can have on the global carbon cycle.

At the same time, there has been increasing recognition of the role of terrestrial freshwaters in modulating the contemporary carbon cycle. In this regard, the linkage of atmosphere and land with the ocean, with lakes rivers as the spatial conduit between them, has long been understood on geological timescales, and refers to the inorganic atmospheric carbon removal associated with chemical weathering of silicate and carbonate rocks by rainwater. However, the role of inland waters in the contemporary, short-term carbon cycle has only recently been appreciated(Aufdenkampe et al., 2011), and refers to its mediation of the organic carbon component associated with plant matter. Whereas the freshwater transfer of inorganic carbon is relatively 'passive', organic carbon can be rapidly transformed to CO_2 in its transit over the land surface(Raymond et al., 2013; Venkiteswaran et al., 2014), and the freshwater conduit is in this case relatively 'reactive', and has for this reason been dubbed 'the Active Pipe'(Cole et al., 2007).

Thus lateral flows of carbon have 2 major pathways: organic and inorganic, largely reflecting biogenic and lithogenic processes respectively. However, both pathways feed off the same source: atmospheric CO_2. The organic pathway is comprised of dissolved (DOC) and particulate carbon (POC), where the former is derived from the uptake of hydrolysed plant matter to water fluxes in a process known as 'leaching', and the latter either an erosive flux involving the direct removal of plant and soil matter from the land surface, or derived from the in-stream fixation of atmospheric CO_2 by freshwater algae. In addition to weathered material, the inorganic, or dissolved inorganic carbon (DIC) flux includes dissolved carbon dioxide fluxes ($CO_{2(aq.)}$) and ions, both originating from microbial consumption of photosynthetically-fixed carbon. $CO_{2(aq.)}$ can be exported with water fluxes either directly from the soil, or produced in situ, as matter that entered the water column along the organic carbon pathway is respired by river-borne heterotrophs and retained in a dissolved state. Depending (positively) on temperatures, water-atmosphere CO_2 disequilibrium and water turbulence, $CO_{2(aq.)}$ can either be exported to the ocean or outgassed to the atmosphere. Outgassing, in turn, can take either the form of CO_2 or methane (CH_4), depending on prevalence of available oxygen for the decomposition of matter. Thus terrestrial carbon mobilised to inland waters are largely restricted to one of three fates: export to the ocean, outgassing to the atmosphere or settling and sedimentary storage prior to arrival at the coast.

While the first global quantification of the total lateral export of carbon from the land surface was produced in 1981(Schlesinger and Melack, 1981) and estimated at 0.37 PgC yr^{-1}, surging research in this area has produced almost back-to-back increases in this value (Bastviken et al., 2011; Battin et al., 2009; Borges et al., 2015; Cole et al., 2007; Holgerson and Raymond, 2016; Regnier et al., 2013; Sawakuchi et al., 2017; Tranvik et al., 2009). Today, against a backdrop 7.3 PgC yr^{-1} of net ecosystem production

(NEP=Gross primary production -total ecosystem respiration) the total carbon throughput of global inland waters is now estimated at 5.4 PgC yr^{-1} (including weathering (0.3PgC), POC input (0.1 PgC) and in-stream photosynthesis (0.3 PgC)), of which 3.9 PgC is outgassed, 0.6 PgC is stored in sediments, and 0.9 PgC reaches the ocean(Drake et al., 2017) (Fig. 1). Thus, lateral export constitutes the dominant fate of photosynthetically-fixed terrestrial carbon after autotrophic and soil heterotrophic respiration are accounted for.

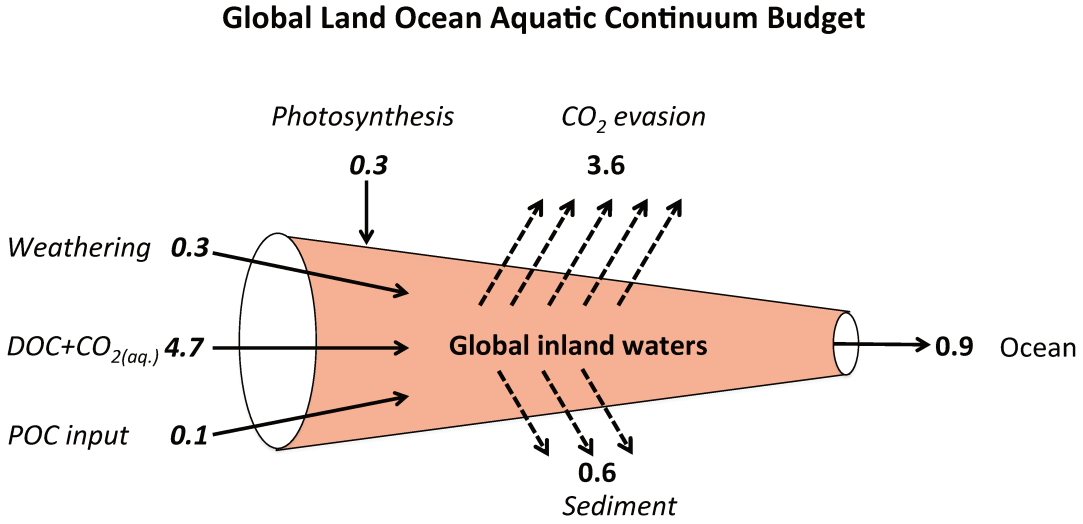

Figure 1: 'Pipe' schematic illustrating the global LOAC budget in a format first employed by Cole et al. (2007) and adapted to include different sources and sinks of carbon as well as updated values for these fluxes (PgC yr^{-1}) per the review paper by Drake et al. (2017). Photosynthesis refers to in-stream ('autochtonous') carbon uptake by river-borne algae.

In the Arctic, a warming environment is expected to increase flows across the LOAC, owing to biotic and physical responses to increases in temperature and atmospheric CO2 concentrations, respectively(Drake et al., 2018; Tank et al., 2012a, 2016). Changes in the flux of organic and inorganic carbon from terrestrial sources to the ocean may likewise have potentially pronounced effects on Arctic marine biogeochemistry, with attendant impacts on regional and global carbon budgets (Feely et al., 2004; Semiletov et al., 2016, 2007; Shakhova et al., 2015; Tesi et al., 2014). These arteries of Arctic riverine carbon are dominated by the six largest river basins north of 45°N: the Ob, Yenisey, Lena, Kolyma, Yukon and Mackenzie, together accounting for ~65% of aggregate water discharge, and drain 67% of the region by area(McClelland et al., 2012). These are followed by eight smaller watersheds, which export a further 15% of aggregate discharge. At present, the total outflow of terrestrially-derived carbon to the Arctic Ocean shelf is thought to total 45-54 teragrams of carbon (TgC, $=10^{12}$g) yr^{-1}. Rivers supply it with an estimated 34 TgC dissolved organic carbon (DOC) per year(Holmes et al., 2012), and deposit 5.8 TgC yr^{-1} particulate organic carbon (POC) on the seabed, these being sourced from those rivers draining low and high elevation headwaters, respectively(McClelland et al., 2016).

The importance of permafrost thaw in the context of lateral carbon fluxes is traced by the following considerations for the high latitude land surface. 1) Do increases in carbon

uptake from primary production due to warming in permafrost areas outweigh increases in carbon loss due to destabilization of permafrost soil stocks, or vice versa? (In other words is net ecosystem production positive or negative?) 2) Will lateral carbon fluxes increase with increases in temperature and precipitation? The combined answer to these questions will drive the rate of change of the carbon system in permafrost regions. For example, if NEP is positive, then lateral transfer of organic carbon represents a potential atmospheric loss, via evasion, of carbon that may be otherwise not metabolized on the land surface itself. In the existing global positive-NEP case, this means that organic carbon that might otherwise have been become part of the soil carbon stock or be respired in the soil is instead exported, a large portion of which is subsequently 'lost' to the atmosphere (Fig. 1). In the hypothetical case that permafrost region NEP is negative in the future, an increase in DOC flux might actually reduce the total stock of carbon available that would otherwise be respired in the soil. In this scenario, an increase of lateral organic carbon fluxes would constitute a 'second chance' for that exported carbon to avoid transformation to gaseous form (if it is not evaded en-route). $CO_{2(aq.)}$ can return to solid-state carbon after export to the river by in-stream algal photosynthetic fixation, while enhanced alkalinity fluxes imply strengthened atmospheric CO_2 uptake by weathering reactions. Thus in this scenario, a strengthened lateral flux system in a weakened or negative NEP system could be a stabilizing force for carbon stocks (Fig. 2).

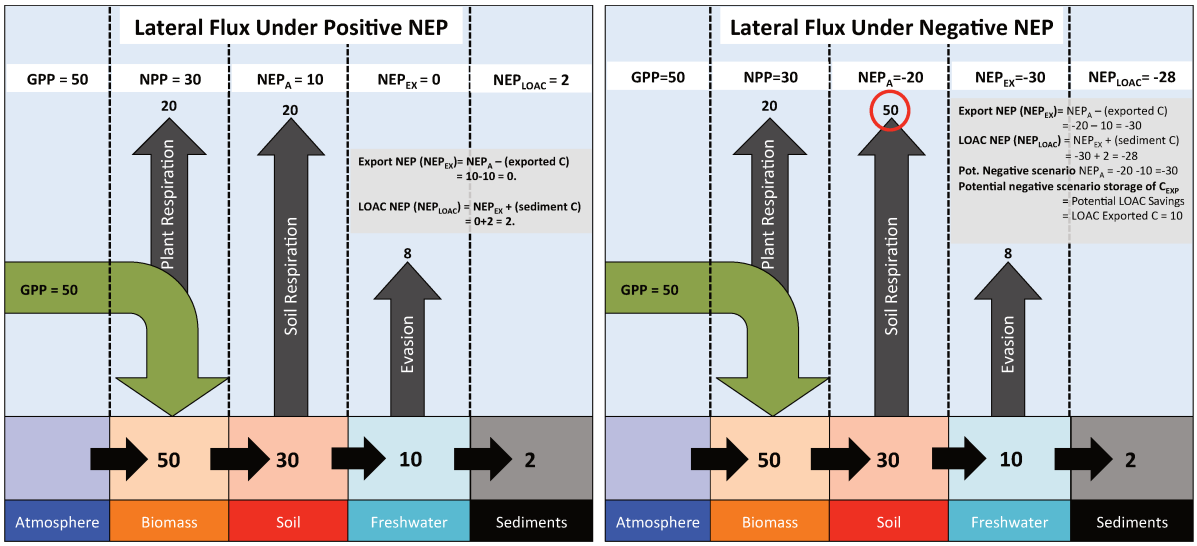

Figure 2: Figure illustrating fluxes between ecosystem scale carbon storage components for **(left)** positive and **(right)** negative NEP cases, to demonstrate how 2 systems with the same fluxes between storage components (lower segment in the images) can be considered to have differing interpretations of the LOAC lateral flux, depending on whether the system is net heterotrophic (negative NEP) or autotrophic (positive NEP). For simplicity, the diagram assumes no in-stream primary production or biomass accumulation in plants themselves (all NPP goes to soil and litter). NEP_A refers to NEP before carbon export to the inland water network, NEP_{EXP} refers to NEP after terrestrial export has occurred, while NEP_{LOAC} refers to NEP after accounting for sedimentary storage (or photosynthetic uptake). See inset box for explanation. On the right hand side, the notion of 'potential LOAC savings' is explored in the case of negative NEP, in which we assume that, because of the optimized conditions for heterotrophic respiration potentially all the river export flux could be respired in the soil if it was not exported, and second, that all the exported C can hypothetically be re-stored on the land through sedimentation. In this situation, we can say that LOAC export potentially stabilizes C that would otherwise be respired.

Permafrost in depth

Characteristic Arctic river processes are largely driven by two latitude-specific controls. First, many key phenomena are determined by phase changes of water, be they in the atmosphere, on the soil surface, in the soil, or in the river network itself. Second, the presence of permafrost –its cap on vertical water flow-paths in the soil, and thermally-determined accommodation/release of the ~1300PgC of SOC underlying it –act as a fulcrum for landscape-scale biogeochemical dynamics. The combination of these permafrost-region characteristics gives rise to the following dynamics. Rapid melting of snow and soil or river ice in Arctic spring (May-June) following ~6 months of continuous accumulation drives massive water runoff rates almost entirely restricted to overland flow by the permafrost barrier. This causes intensely seasonal river discharge, with annual peaks often two orders of magnitude above baseflow rates(Ye et al., 2003). Vigorous water flux rates mean that particulate carbon and nutrients are rapidly eroded from elevated headwater catchments, as observed in the N. American Arctic with high POC:DOC ratios(McClelland et al., 2016). In lower-lying areas, litter and moss material at the soil surface are intensely leached, with mobilization and transformation of this subsequently dissolved matter via inland waters. DOC concentrations tend to be similar to those in the tropics(Holmes et al., 2012; McClelland et al., 2012) particularly in the flatter Eurasian rivers (lower POC:DOC ratio). In some areas, high DOC concentrations are the result of snowmelt-induced soil water saturation, which favours the establishment of moss and sedge-based peat ecosystems characterized by correspondingly high SOC concentrations that are mobilized upon thaw.

In mid-summer, runoff and river discharge rates decline, while the depth to which the soil is unfrozen (referred to as the 'active layer') increases. These are thus periods during which soil respiration rates are highest, and where leached DOC may be of greatest age of origin. Once mobilized to headwaters, it appears that this often-ancient, low molecular weight SOC matter can be preferentially and rapidly metabolized by microbes in headwater streams, to the extent that respiration of ancient plant matter may dominate aggregate summer CO_2 evasion in Arctic rivers(Denfeld et al., 2013; Feng et al., 2013; Vonk et al., 2013; Vonk and Gustafsson, 2013). As Arctic warming proceeds, it has been suggested that volumes of freshwater and total energy flux in runoff and river discharge will increase with rising precipitation and permafrost thaw(Lammers et al., 2007). In addition, guided by rising temperatures, thermal and physical exposure of SOC (see Fig. 3), along with increases in plant growth and litter inputs to the soil, are thought to increase the total pool of carbon available to DOC leaching and transport(Frey and Smith, 2005; Laudon et al., 2012).

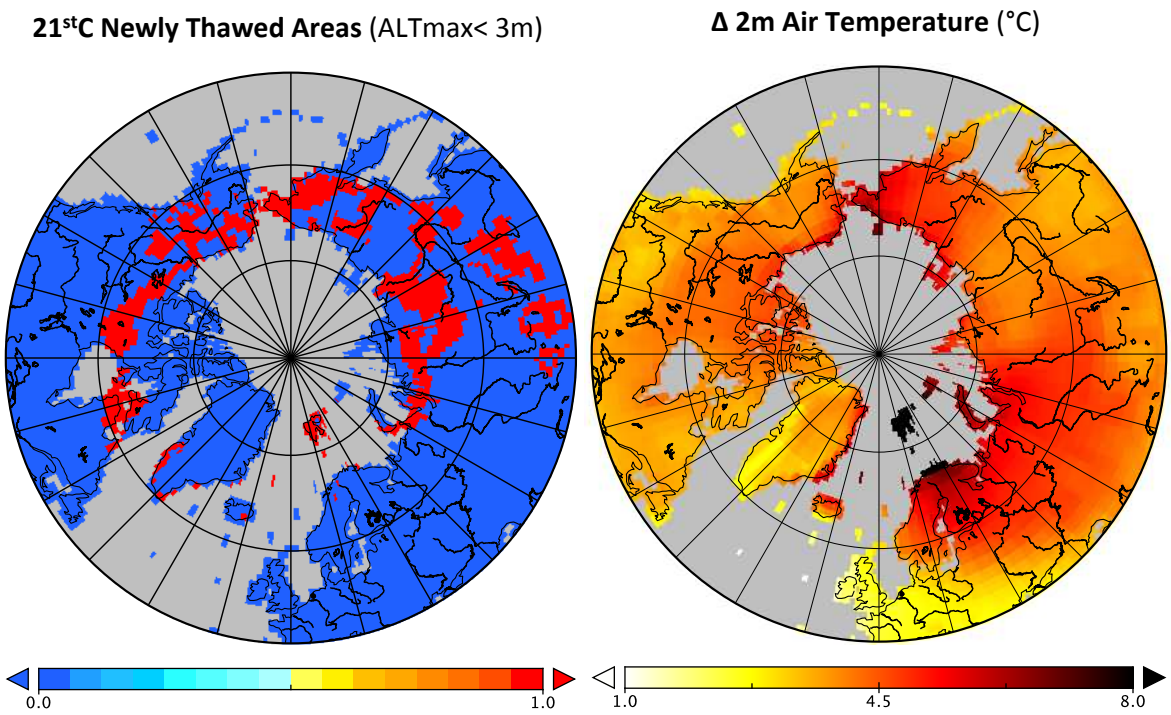

Figure 3: Simulated increases in (left) areas transitioning from continuous to discontinuous permafrost; (right) mean annual 2m air temperatures; over the 21st Century (2090-2099 against a 1996-2005 baseline), under the 'intermediate-high warming' scenario (RCP 6.0), generated by the simulation output from our model. Major rivers are outlined in black.

In addition, high latitude weathering processes are subject to substantial modulation by phenomena such as cryoturbation, glacial action and mineral exposure due to cracking under freeze/thaw cycles. Beyond the focus on the organic carbon cycle, this can further affect the carbon balance of these areas in their impacts on chemical weathering, in which rainwater dissolution of atmospheric CO2 is 'fixed' as to bicarbonate (HCO_3^-) upon weathering of carbonate rocks by its conversion to HCO_3^-, which reduces its chemical susceptibility to atmospheric release. Likewise, the vertical percolation of water through the soil column allows for the fixation of biogenic CO2 residing in soil pore space as HCO_3^-(Beaulieu et al., 2012; Gaillardet et al., 1999; Stets et al., 2017; Tank et al., 2012a, 2016, 2018). The riverine flux of weathering products has been shown to have increased markedly over high latitude regions in the last decades(Drake et al., 2018; Tank et al., 2016), driven by temperature, precipitation, thaw-related increaess in mineral surface area, agricultural liming, mining and acid rain(Kaushal et al., 2018; Maher and Chamberlain, 2014; Raymond and Hamilton, 2018; White and Blum, 1995), and can be expected to increase with time, with the potential to partially offset CO_2 emissions from permafrost thaw(Drake et al., 2018).

Permafrost regions are subject to further processes of potential destabilization:

Under thaw conditions, microbial activity increases and can generate its own heat, which incubation experiments have shown may be sufficient to significantly warm the soil further(Hollesen et al., 2015). 'Thermokarst', or the melting of massive soil ice inclusions can lead to the physical collapse of the soil column and sudden exposure of ancient soil carbon to the surface(Abbott et al., 2015; Kanevskiy et al., 2011; Tanski et

al., 2017). An extreme version collapse/erosion process occurs in coastal areas, exacerbated by water and wind activity there(Fritz et al., 2017; Tanski et al., 2017; Vonk et al., 2012) . Arctic region fire events are on the rise and likely to increase with temperature and severity over time(Ponomarev et al., 2016). The initial burning of biomass is accompanied by active layer deepening, 'priming' of deeper soil horizons(De Baets et al., 2016), and a significant loading of pyrogenic DOC in Arctic watersheds, up to half of which is rapidly metabolized(Myers-Pigg et al., 2015).

The riverine flux of weathering products has been shown to have increased markedly over high latitude regions in the last decades(Drake et al., 2018; Tank et al., 2016), driven by temperature, precipitation, thaw-related increaess in mineral surface area, agricultural liming, mining and acid rain(Kaushal et al., 2018; Maher and Chamberlain, 2014; Raymond and Hamilton, 2018; White and Blum, 1995), and can be expected to increase with time, with the potential to partially offset CO_2 emissions from permafrost thaw(Drake et al., 2018).

Cumulatively, the above processes imply that with warming of Arctic watersheds we might expect a potentially sizeable aquatic mobilization and microbial metabolization (Xue et al., 2016) of dissolved and eroded organic matter, deeper hydrological flow paths, increased thermokarst formation, an increase in total mass, heat and alkalinity transfer to the river network and, ultimately, the Arctic Ocean and atmosphere. As a result of this transfer, both terrestrially-exported and older shelf carbon in the Arctic Ocean face considerable disruption(McGuire et al., 2009; Schuur et al., 2015) from the combined effects of increased freshwater, heat, sediment, nutrient and organic/inorganic carbon flows from rapidly warming Arctic river watersheds, as well as those from melting sea ice, warmer marine water temperatures and geothermal heat sources(Janout et al., 2016; Shakhova et al., 2015).

On the other hand, suggestions of an inevitable increase in Arctic terrestrial DOC throughput may ignore the potential co-variation of increasing water inputs with a deeper active layer, which would promote deeper water flowpaths and a correspondingly different leaching substrate regime (SOC) from that which normally prevails in permafrost systems. This could entail lower leaching rates or concentrations, diminishing the lateral transport of dissolved carbon. Likewise, it assumes that warming won't increase carbon respiration in greater proportion than DOC mobilization (also reducing DOC lateral fluxes), which has yet to be established.

Indeed, theoretical understanding of permafrost region terrestrial systems has been hampered by a dearth of empirical data over permafrost-representative spatio-temporal scales. This is particularly true when attempting to resolve lateral carbon dynamics in these systems, due to the practical difficulties in taking both spot and continuous measurement in some of the coldest, most dynamic and extreme river discharge regimes in the world. It is into this context of great uncertainty over a spectrum of hypothetical outcomes that this thesis assumes its relevance. The spatial, temporal and process scales that projecting the warming-response of the permafrost region and its lateral carbon transfer involves are not at present amenable to resolution by anything other than process based modeling approaches that can incorporate these processes, scales and dimensions to the extent that they are currently perceived to be well-understood.

In what follows, we first trace the development of a spatially-explicit, high temporal resolution model that to our knowledge, is unique in its combination of state-of-the-art theory and representation of both permafrost and lateral flux systems in a global land surface model equipped for coupling with a earth system model. The resulting simulation product, given the name ORCHIDEE MICT-LEAK, simulates the production, transport and transformation of soil and litter carbon to DOC and CO2 in permafrost regions, and is described in detail in **Chapter 1**. This model is subjected to an in-depth evaluation over a wide range of biogeochemical processes and data for its ability to accurately simulate the processes represented over a single, relatively well-studied basin –the Lena –in **Chapter 2**. Chapters 1 and 2 have been written and submitted to the journal Geoscientific Model Development (in review). Having concluded that the model is able to reasonably represent the relevant dynamics for permafrost systems, **Chapter 3** employs state-of-the-art climate projections to 2100 under a given climate warming scenario (RCP 6.0) to examine the lateral-transfer response of the Pan-Arctic to future warming, and finds that contrary to most literature-based expectations, lateral carbon fluxes decline over the 21st Century. The causes of this are explored and explained therein. This manuscript is being prepared for submission to Nature. In **Chapter 4**, we describe and evaluate a simple model developed as an additional module for ORCHIDEE-MICT LEAK, which is able to simulate at a daily timestep chemical weathering/alkalinity production rates and their fluvial transport to the ocean. To our knowledge this is the first such module in a global climate model resolved for both high spatial (integrating both surface and subsurface flows) and temporal (daily/monthly versus yearly) resolution. We then project the response of Pan-Arctic weathering and riverine alkalinity fluxes to climate warming, assessing the implied change in atmospheric carbon uptake that results. This paper is being prepared for submission to the journal Environmental Science and Technology.

Chapter 2
ORCHIDEE MICT LEAK, a global model for the production, transport and transformation of dissolved organic carbon from Arctic permafrost regions : model description and simulation protocol[1]

Summary

High latitude permafrost soils contain very large stores of frozen, often ancient and relatively labile carbon up to depths of over 30m. Surface warming caused by contemporary anthropogenic climate change can be reasonably expected to destabilize these stores via microbial or hydrological mobilization following spring/summer thaw, as the permafrost line migrates pole-ward over time. However, few Earth System models adequately represent the unique permafrost soil biogeochemistry and its respective processes; this significantly contributes to uncertainty in estimating their responses, and that of the planet at large, to warming. The potential feedbacks owing to such a response are of particular acuity and concern. Likewise, the riverine component of what is known as the 'boundless carbon cycle' is seldom recognized in Earth System modeling. Hydrological mobilization of organic material from the Arctic land surface to the river network results either in sedimentary settling or atmospheric 'evasion' within rivers or their geographic end-points, the marine realm. These processes are widely expected to increase in strength and with amplified Arctic climate warming. Thus, representing this spectrum of phenomena, their interaction, and the response of these to changes in environmental drivers (heat, water, their timing, and atmospheric CO_2) are necessary components for the projection of the Arctic's future carbon cycle changes.

Here, the production, transport and atmospheric release of dissolved organic carbon (DOC) from high-latitude permafrost soils into inland waters and the ocean is explicitly represented for the first time in the land surface component (ORCHIDEE) of a CMIP6 global climate model (IPSL). The model, ORCHIDEE MICT-LEAK, mechanistically represents: (1) Vegetation and soil physical processes for high latitude snow, ice and soil phenomena, including snow thermal buffering of the soil surface, mediation of soil temperature by organic carbon concentration, bio- and cryo-turbation of parcticulate and dissolved soil carbon to depth via vertical diffusion over a discretely subdivided soil column and the interaction of these processes with a large-scale soil-carbon stock, representing permafrost soil carbon. (2) The cycling of DOC and CO_2, including atmospheric evasion, along the terrestrial-aquatic continuum from soils through the river network to the coast, at 0.5° to 2° resolution. This dissolved carbon cycling includes the processes of floodplain inundation and flooded mobilisation of dissolved litter and soil organic matter to the river network, soil-type modulation of soil column DOC filtration and decomposition, 'priming' of organic matter decomposition by more reactive carbon, and atmospheric and canopy DOC inputs to the soil. By including these mechanisms in a process-based manner, we hope to capture some of the more

[1] Submitted to *Geoscientific Model Development*, in review.

important landscape-scale emergent phenomena that arise from the interaction of permafrost environments with organic matter and the hydrological realm. This paper, the first in a two-part study, presents the rationale for including these processes in a high latitude specific land surface model, then describes the model with a focus on novel process implementations, followed by a summary of the model configuration and simulation protocol.

The results of the model evaluation simulations, conducted for the Lena River basin, are evaluated against observational data in Chapter 2 of this thesis.

Chapitre 2
ORCHIDEE MICT LEAK, un modèle global pour la production, le transport et la transformation du carbone organique dissous des régions de pergélisol de l'Arctique: description du modèle et protocole de simulation

Résumé

Les pergélisols à haute latitude contiennent de très vastes réserves de carbone gelé, souvent ancien et relativement labile, jusqu'à une profondeur de plus de 30 m. On peut raisonnablement s'attendre à ce que le réchauffement de la surface provoqué par les changements climatiques anthropiques contemporains déstabilise ces réserves via une mobilisation microbienne ou hydrologique après le dégel du printemps / été, à mesure que la ligne de pergélisol migre vers le nord. Cependant, peu de modèles du système Terre représentent de manière adéquate la biogéochimie unique des pergélisol et ses processus respectifs; cela contribue de manière significative à l'incertitude dans l'estimation de leurs réponses, et de celle de la planète dans son ensemble, au réchauffement. Les réactions potentielles résultant d'une telle réponse sont d'une acuité et d'une préoccupation particulières. De même, la composante fluviale de ce que l'on appelle le «cycle du carbone sans bornes» est rarement reconnue dans la modélisation du système Terre. La mobilisation hydrologique de matières organiques de la surface des terres arctiques vers le réseau fluvial entraîne soit un tassement sédimentaire, soit une «évasion» atmosphérique dans les cours d'eau, ou leur limite géographique, le domaine marin. On s'attend généralement à ce que ces processus deviennent plus puissants et entraînent un réchauffement accru du climat arctique. Ainsi, représenter ce spectre de phénomènes, leurs interactions et leur réponse aux changements de facteurs environnementaux (chaleur, eau, leur synchronisation et le CO_2 atmosphérique) sont des éléments nécessaires à la projection des futurs changements du cycle du carbone dans l'Arctique.

Ici, la production, le transport et les rejets atmosphériques de carbone organique dissous (COD) provenant des sols de pergélisol à haute latitude dans les eaux intérieures et l'océan sont explicitement représentés pour la première fois dans la composante de surface terrestre (ORCHIDEE) d'un modèle climatique mondial CMIP6 (IPSL). Le modèle, ORCHIDEE MICT-LEAK, représente mécaniquement: (1) Les processus physiques de la végétation et du sol pour les phénomènes de neige, de glace et de sol sous les hautes latitudes, y compris la compensation thermique de la neige par la surface, la médiation de la température du sol par la concentration de carbone organique, la bio et la cryo-turbation du carbone du sol dissous et dissous jusqu'à sa profondeur par diffusion verticale sur une colonne de sol discrètement divisée et interaction de ces processus avec un stock de carbone sol à grande échelle, représentant le carbone du sol pergélisol. (2) Le cycle du COD et du CO_2, y compris l'évasion atmosphérique, le long du continuum aquatique terrestre des sols à travers le réseau fluvial jusqu'à la côte, à une résolution de 0,5 ° à 2 °. Ce cycle du carbone dissous comprend les processus d'inondation des plaines inondables et de mobilisation COD du sol et de la litère vers le réseau hydrographique, la modulation du type de sol de la filtration et de la décomposition de la colonne de sol DOC, la "préparation" de la décomposition de la matière

organique par du carbone plus réactif, et COD atmosphériques et de la canopée entrant dans le sol. En incluant ces mécanismes d'une manière basée sur les processus, nous espérons capturer certains des phénomènes d'émergence les plus importants à l'échelle du paysage qui résultent de l'interaction des environnements de pergélisol avec la matière organique et le domaine hydrologique. Cet article, le premier d'une étude en deux parties, présente les raisons d'inclure ces processus dans un modèle de surface terrestre spécifique de latitude élevée, puis décrit le modèle en mettant l'accent sur les nouvelles implémentations de processus, suivi d'un résumé de la configuration du modèle et de la simulation. protocole.

Les résultats des simulations, effectuées pour le bassin de la rivière Lena, sont évalués par rapport aux données d'observation présentées au chapitre 2 de cette thèse.

Introduction

High-latitude permafrost soils contain large stores of frozen, often ancient and relatively reactive carbon up to depths of over 30m. Soil warming caused by contemporary anthropogenic climate change can be expected to destabilize these stores (Schuur et al., 2015) via microbial or hydrological mobilization following spring/summer thaw and riverine discharge (Vonk et al., 2015a) as the permafrost line migrates poleward over time. The high latitude soil carbon reservoir may amount to ~1330–1580 PgC (Hugelius et al., 2013, 2014; Tarnocai et al., 2009) –over double that stored in the contemporary atmosphere, while the yearly lateral flux of carbon from soils to running waters may amount to ~40% of net ecosystem carbon exchange (McGuire et al., 2009), the majority as dissolved organic carbon (DOC).

The fact that, to our knowledge, no existing land surface models are able to adequately simultaneously respresent this unique high latitude permafrost soil environment, the transformation of soil organic carbon (SOC) to its eroded particulate and DOC forms and their subsequent lateral transport, as well as the response of all these to warming, entails significant additional uncertainty in projecting global-scale biogeochemical responses to human-induced environmental change.

Fundamental to these efforts is the ability to predict the medium under which carbon transformation will occur: in the soil, streams, rivers or sea, and under what metabolising conditions –since these will determine the process mix that will ultimately enable either terrestrial redeposition and retention, ocean transfer, or atmospheric release of permafrost-derived organic carbon. In the permafrost context, this implies being able to accurately represent (i) the source, reactivity and transformation of released organic matter, and; (ii) the dynamic response of hydrological processes to warming, since water phase determines carbon, heat, and soil moisture availability for metabolisation and lateral transport.

To this end, we take a specific version of the terrestrial component of the IPSL global Earth System model (ESM) ORCHIDEE (Organising Carbon and Hydrology In Dynamic Ecosystems), one that is specifically coded for, calibrated with and evaluated on high latitude phenomena and permafrost processes, called ORCHIDEE-MICT (Guimberteau et al., 2018). This code is then adapted to include DOC production in the soil (ORCHIDEE-SOM, (Camino-Serrano et al., 2018)), 'priming' of SOC (ORCHIDEE-PRIM,(Guenet et al., 2016, 2018)) and the riverine transport of DOC and CO_2, including in-stream transformations, carbon and water exchanges with wetland soils and gaseous exchange between river surfaces and the atmosphere (ORCHILEAK, (Lauerwald et al., 2017)).

The resulting model, dubbed ORCHIDEE MICT-LEAK, herafter referred to as MICT-L for brevity, is therefore able to represent: (a) Permafrost soil and snow physics, thermodynamics to a depth of 38m and dynamic soil hydrology to a depth of 2m; (b) Improved representation of biotic stress response to cold, heat and moisture in high latitudes; (c) Explicit representation of the active layer and frozen-soil hydrologic barriers; buildup of soil carbon stocks via primary production and vertical translocation (turbation) of SOC and DOC; (d) DOC leaching from tree canopies, atmospheric deposition, litter and soil organic matter, its adsorption/desorption to/from soil

particles, its transport and transformation to dissolved CO_2 ($CO^*_{2(aq.)}$) and atmospheric release, as well as the production and hydrological transport of plant root-zone derived dissolved CO_2; (e) Improved representation of C cycling on floodplains; (f) Priming of organic matter in the soil column and subsequent decomposition dynamics. In combination, these model properties allow us to explore the possibility of reproducing important emergent phenomena observed in recent empirical studies (Fig. 1) arising from the interaction of a broad combination of different processes and factors.

To our knowledge very few attempts have been made at the global scale of modelling DOC production and lateral transfer from the permafrost region that explicitly accounts for such a broad range of high latitude–specific processes, which in turn allows us to match and evaluate simulation outputs with specific observed processes, enhancing our ability to interpret the output from theses models and improve our understanding of the processes represented. The only other attempt at doing so is a Pan-Arctic modelling study by Kicklighter et al. (2013)(Kicklighter et al., 2013), which is based on a relatively simplified scheme for soil, water and biology. The following segment briefly overviews the dynamics, emergent properties and their overall significance across scales, of permafrost region river basins.

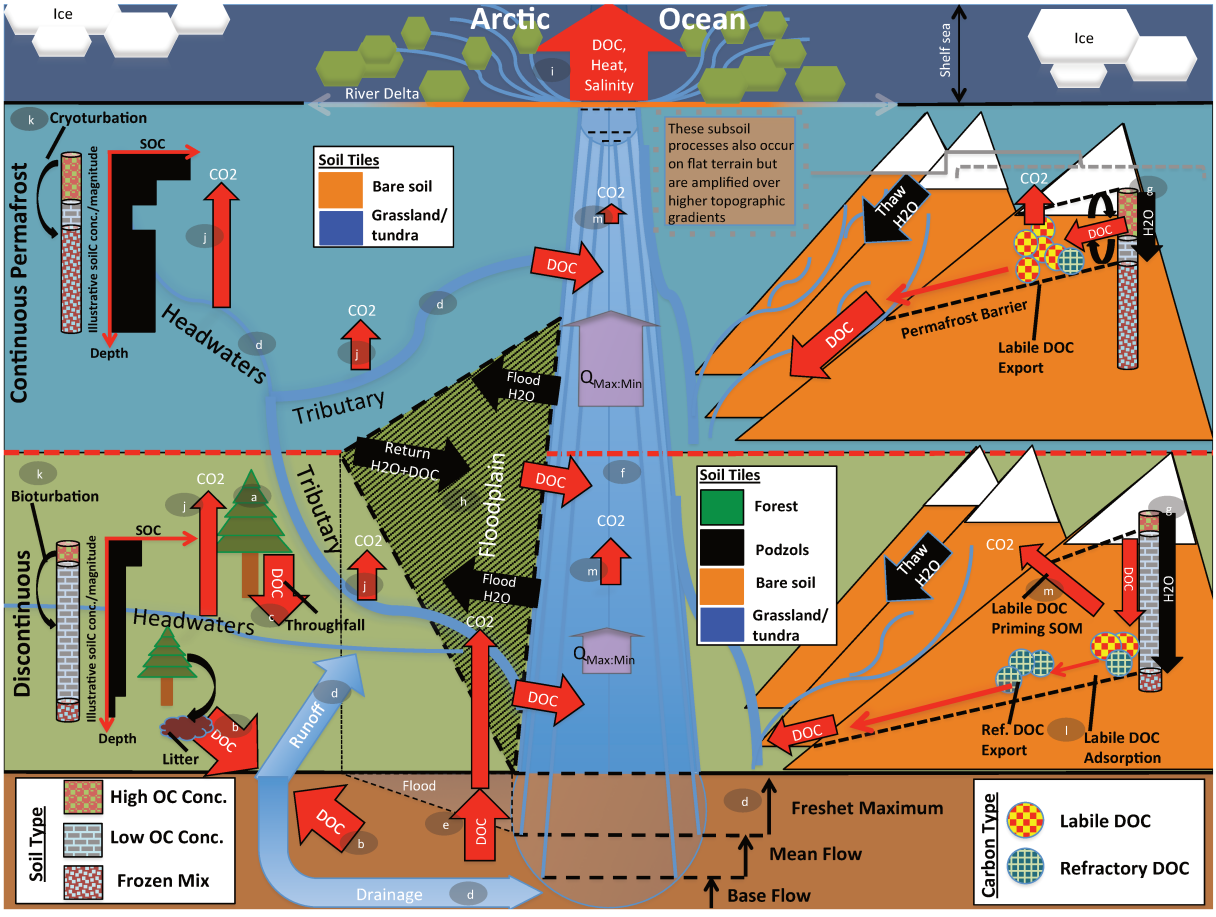

Figure 1: Cartoon diagram illustrating the landscape-scale emergent phenomena observed in high-latitude river systems that are captured by the processes represented in this model. Here, the terrestrial area is shown, in vertically-ascending order, as subsoil, discontinuous permafrost, continuous permafrost and the maritime boundary. Representative soil types, their distributions and carbon concentrations are shown for the two permafrost zones, as well as the different dynamics occuring on 'flat' (left) and 'sloping'

land (right) arising from their permafrost designation. Carbon exports from one subsystem to another are shown in red. The relative strength of the same processes ocurring in each permafrost band are indicated by relative arrow size. Note that the high CO_2 evasion in headwaters versus tributaries versus mainstem is shown here. Proposed and modelled mechanisms of soil carbon priming, adsorption and rapid metabolisation are shown. The arrows $Q_{Max:Min}$ refer to the ratio of maximum to minimum discharge at a given point in the river, the ratio indicating hydrologic volatility, whose magnitude is influenced by permafrost coverage. Soil tiles, a model construct used for modulating soil permeability and implicit/explicit decomposition, are shown to indicate the potential differences in these dynamics for the relevant permafrost zones. Note that the marine shelf sea system, as shown in the uppermost rectangle, is not simulated in this model, although our outputs can be coupled for that purpose. Letter markings mark processes of carbon flux in permafrost regions and implicitly or explicitly included in the model, and can be referred to in subsections of the Methods text. These refer to: (a) Biomass generation; (b) DOC generation and leaching; (c) Throughfall and its DOC; (d) Hydrological mobilisation of soil DOC; (e) Soil flooding; (f) Landscape routing of water and carbon; (g) Infiltration and topography; (h) Floodplain representation; (i) Oceanic outflow; (j) Dissolved carbon export and riverine atmospheric evasion; (k) Turbation; (l) Adsorption; (m) Priming.

1.1 A giant, reactive, fast-draining funnel: A permafrost basin overview

Permafrost has a profound impact on Arctic river hydrology. In permafrost regions, a permanently frozen soil layer acts as a 'cap' on ground water flow (see 'permafrost barrier', right hand side of Fig. 1). This implies that: (i) Near-surface runoff becomes by far the dominant flowpath draining permafrost watersheds (Ye et al., 2009), as shown in Fig. 1d; (ii) The seasonal amplitude of river discharge, expressed by the ratio of maximum to minimum discharge ($Q_{max:min}$ in Fig. 1), over continuous versus discontinuous permafrost catchments is higher as a result of the permafrost barrier; (iii) This concentration of water volume near the surface causes intense leaching of DOC from litter and relevant unfrozen soil layers (Fig. 1g, 1d, and e.g. refs. (Drake et al., 2015; Spencer et al., 2015; Vonk et al., 2013)); (iv) Permafrost SOC stocks beneath the active layer are physically and thermally shielded from aquatic mobilization and metabolization, respectively (Fig. 1g).

Rapid melting of snow and soil or river ice during spring freshet (May-June) drives intensely seasonal discharge, with peaks often two orders of magnitude(Van Vliet et al., 2012, 2013) above baseflow rates (Fig. 1d). These events are the cause of four, largely synchronous processes: (i) Biogenic matter is rapidly transported from elevated headwater catchments (Fig. 1, right hand side) (McClelland et al., 2016); (ii) Plant material at the soil surface is intensely leached, with subsequent mobilization and transformation of this dissolved matter via inland waters (Fig. 1d,b,j); During spring freshet, riverine DOC concentrations increase and bulk annual marine DOC exports are dominated by the terrestrial DOC flux to the rivers that occurs at this time (Holmes et al., 2012). Indeed, DOC concentrations during the thawing season tend to be greater than or equal to those in the Amazon particularly in the flatter Eurasian rivers (Holmes et al., 2012; McClelland et al., 2012), and DOC concentrations are affected at watershed scale by parent material and ground ice content (O'Donnell et al., 2016).

(iii) Sudden inundation of the floodplain regions in spring and early summer (Fig. 1h), (Smith and Pavelsky, 2008), further spurs lateral flux of both particulate and dissolved matter in the process and its re-deposition (Zubrzycki et al., 2013) or atmospheric

evasion (Fig. 1j,m); (iv) Snowmelt-induced soil water saturation, favoring the growth of moss and sedge-based ecosystems (e.g. refs.(Selvam et al., 2017; Tarnocai et al., 2009; Yu, 2011)) and the retention of their organic matter (OM),.i.e., peat formation, not shown in Fig. 1 as this isn't represented in this model version, but is generated in a separate branch of ORCHIDEE (Qiu et al., 2018)).

Mid-summer river low-flow and a deeper active layer allow for the hydrological intrusion and leaching of older soil horizons (e.g. the top part of Pleistocene-era Yedoma soils), and their subsequent dissolved transport(Wickland et al., 2018). These sometimes-ancient low molecular weight carbon compounds appear to be preferentially and rapidly metabolized by microbes in headwater streams (Fig. 1j), which may constitute a significant fraction of aggregate summer CO_2 evasion in Arctic rivers(Denfeld et al., 2013; Vonk et al., 2013) This is likely due to the existence of a significant labile component of frozen carbon(Drake et al., 2015; Vonk et al., 2015 ; Woods et al., 2011) .

CO_2 evasion rates from Arctic inland waters (Fig. 1j,e,m) are estimated to be in the region of 40-84 TgC yr^{-1} (McGuire et al., 2009), to be compared with estimates of Pan Arctic DOC discharge from rivers of 25-36 TgC yr^{-1}. The influx of terrestrial carbon to the shelf zone is thought to total 45-54 TgC yr^{-1} (Holmes et al., 2012; Raymond et al., 2007). Rivers supply the Arctic Ocean (AO) an estimated 34 Tg DOC-C yr^{-1} (Holmes et al., 2012), while depositing 5.8 Tg yr^{-1} of particulate carbon, these being sourced from those rivers draining low and high elevation headwaters, respectively (McClelland et al., 2016). These dynamics are all subject to considerable amplification by changes in temperature and hydrology(Frey and McClelland, 2009; Tank et al., 2018).

Average annual discharge in the Eurasian Arctic rivers has increased by at least 7% between 1936-1999 (Peterson et al., 2002), driven by increasing temperatures and runoff (Berezovskaya et al., 2005), and the subsequent interplay of increasing annual precipitation, decreasing snow depth and snow water equivalent (SWE) mass (Kunkel et al., 2016; Mudryk et al., 2015), and greater evapotranspiration (Zhang et al., 2009). Although net discharge trend rates over N. America were negative over the period 1964-2003, since 2003 they have been positive on average (Dery et al., 2016). These dynamic and largely increasing hydrologic flux trends point towards temperature and precipitation -driven changes in the soil column, in which increased soil water/snow thaw and microbial activity (Graham et al., 2012; MacKelprang et al., 2011; Schuur et al., 2009) converge to raise soil leaching and DOC export rates to the river basin and beyond. Further, microbial activity generates its own heat, which incubation experiments have shown may be sufficient to significantly warm the soil further (Hollesen et al., 2015), in a positive feedback.

Arctic region fire events are also on the rise and likely to increase with temperature and severity over time (Ponomarev et al., 2016). The initial burning of biomass is accompanied by active layer deepening, priming of deeper soil horizons (De Baets et al., 2016), and a significant loading of pyrogenic DOC in Arctic watersheds, up to half of which is rapidly metabolized (Myers-Pigg et al., 2015).

In these contexts, the implications of (polar-amplified) warmer temperatures leading to active layer deepening towards the future (transition from Continuous to Discontinuous Permafrost, as shown in the upper/lower segments of Fig. 1) are clear and unique: potentially sizeable aquatic mobilization and microbial metabolization (Xue, 2017) of dissolved and eroded OM, deeper hydrological flow paths, an increase in total carbon and water mass and heat transfer to the aquatic network and, ultimately, the Arctic Ocean and atmosphere (Fig. 1i).

The advantage of having a terrestrial model that can be coupled to a marine component of an overarching global climate model (GCM) is in this case the representation of a consistent transboundary scheme, such that output from one model is integrated as input to another. This is particularly important given the context in which these terrestrial outflows occur :

Because of its small size, a uniquely large and shallow continental shelf, the global climatological significance of its seasonal sea ice (Rhein et al., 2013) and its rapid decline (Findlay et al., 2015a), the AO has been described as a giant estuary (McClelland et al., 2012), acting as a funnel for the transport, processing and sedimentation of terrestrial OM. Because of its small surface area and shallow seas (Jakobsson, 2002), the AO holds relatively little volume and is consequently sensitive to inputs of freshwater, heat, alkalinity and nutrients that flush out from terrestrial sources, particularly at discharge peak.

High suspended particle loads in river water as they approach the mouth (Heim et al., 2014) cause lower light availability and water albedo and hence higher temperatures (Bauch et al., 2013; Janout et al., 2016), which can affect the near-shore sea ice extent, particularly in spring (Steele and Ermold, 2015). Volumes of riverine freshwater and total energy flux (Lammers et al., 2007) are expected to increase with warmer temperatures, along with an earlier discharge peak (Van Vliet et al., 2012, 2013). In doing so, freshwaters may in the future trigger earlier onset of ice retreat (Stroeve et al., 2014; Whitefield et al., 2015) via a freshwater albedo, ice melt, seawater albedo, ice melt, feedback, amplified by intermediary state variables such as water vapor and cloudiness (Serreze and Barry, 2011).

Both terrestrially-exported and older shelf carbon in the AO face considerable disruption (McGuire et al., 2009; Schuur et al., 2015) from the combined effects of increased freshwater, heat, sediment, nutrient and organic carbon flows from rapidly warming Arctic river watersheds, as well as those from melting sea ice, warmer marine water temperatures and geothermal heat sources (Janout et al., 2016; Shakhova et al., 2015). Because ORCHIDEE is a sub-component of the overarching IPSL ESM, there is scope for coupling riverine outputs of water, DOC, $CO_{2(aq)}$ and heat from the terrestrial model as input for the IPSL marine components (Fig. 1i). Nonetheless, these are not the objectives of the present paper, whose aim is rather to validate the simulated variable output produced by the model described in detail below against observations and empirical knowledge for the Lena basin, but are included here descriptively to scope the plausible future applications of ORCHIDEE MICT-LEAK, given our present empirical understanding of their potential significance.

The Methods section summarises the model structure and associated rationale for each of the model sub-branches or routines relevant to this study, and follows with the setup and rationale for the simulations carried out as validation exercises.

2 Methods

This section overviews the processes represented in the model being described in this manuscript, which is referred to as ORCHIDEE MICT-LEAK, hereafter referred to MICT-L for brevity. MICT-L is at its heart a merge of two distinct models : the high-latitude land surface component of the IPSL Earth System Model ORCHIDEE MICT, and the DOC-production and transport branch of ORCHIDEE's default or 'trunk' version (Krinner et al., 2005), ORCHILEAK. The original merger of these two code sets was between ORCHILEAK and ORCHIDEE-MICT, which are described in ref.(Camino-Serrano et al., 2018; Lauerwald et al., 2017) and ref(Guimberteau et al., 2018) respectively.

However, numerous bug fixes and process additions post-dating these publications have been included in this code. Furthermore, novel processes included in neither of these two core models are added to MICT-L in response to phenomena reported in recent empirical publications, such as the diffusion of DOC (novel in ORCHIDEE-MICT) through the soil column to represent its turbation and preferential stabilisation at depth in the soil, in a process not necessarily the same as its adsorption –also represented here.

In terms of code architecture, the resulting model is substantially different from either of its parents, owing to the fact that the two models were developed on the basis of ORCHIDEE trunk revisions 2728 and 3976 for ORCHILEAK and MICT respectively, which have a temporal model development distance of over 2 years, and subsequently evolved in their own directions. These foundational differences, which mostly affect the formulation of soil, carbon and hydrology schemes, mean that different aspects of each are necessarily forced into the subsequent code. Where these differences were considered scientific or code improvements, they were included in the resulting scheme.

Where these differences were so large as to prove a burden in excess of the scope of this first model version, such as the inclusion of the soil carbon spinup module, they were omitted from this first revision of MICT-L. The direction of the merge –which model was the base which incorporated code from the other –was from ORCHILEAK into MICT, given that the latter contains the bulk of the fundamental (high latitude) processes necessary for this merge. Despite architectural novelties introduced, MICT-L carries with it a marriage of much the same schemes detailed exhaustively in Guimberteau et al. (2018)(Guimberteau et al., 2018) and Lauerwald et al. (2017)(Lauerwald et al., 2017). As such, the following model description details only new elements of the model, those that are critical to the production and transport of DOC from permafrost regions, and parameterisations specific to this study (Fig. 2).

2.1 Model Description

MICT-L is based largely on ORCHIDEE-MICT, into which the DOC production, transport and transformation processes developed by Lauerwald et al. and tested insofar only for the Amazon, have been transplanted, allowing for these same processes to be generated

925 in high latitude regions with permafrost soils and a river flow regime dominated by
926 snow melt. The description that ensues roughly follows the order of the carbon and
927 water flow chain depicted in Fig. 2b. At the heart of the scheme is the vegetative
928 production of carbon, which occurs along a spectrum of 13 plant functional types (PFTs)
929 that differ from one another in terms of plant physiological and phenological uptake and
930 release parameters (Krinner et al., 2005). Together, these determine grid-scale net
931 primary production. In the northern high latitudes, the boreal trees (PFTs 7-9) and C3
932 grasses (PFT 10) dominate landscape biomass and primary production. Thus, in
933 descending order yearly primary production over the Lena basin is roughly broken
934 down between C3 grasses (48%), boreal needleleaf summergreen trees (27%), boreal
935 needleleaf evergreen trees (12%), boreal broadleaf summergreen trees (8%) and
936 temperate broad-leaved evergreen trees (6%). Naturally these basin aggregates are
937 heterogeneously distributed along latitude and temperature contours, with
938 grasses/tundra dominanting at the high latitudes and (e.g.) temperate broadleaf trees
939 existing only at the southern edges of the basin.
940
941 **2.2 Biomass generation** (Fig. 1a)
942
943 Biomass generation, consisting of foliage, roots, above and below –ground sap and heart
944 wood, carbon reserves and fruit pools in the model, results in the transfer of these
945 carbon stores to two downstream litter pools, the structural and metabolic litter (Figure
946 2b). This distinction, defined by lignin concentration of each biomass pool (Krinner et
947 al., 2005), separates the relatively reactive litter fraction such as leafy matter from its
948 less-reactive, recalcitrant counterpart (woody, 'structural' material), with the
949 consequence that the turnover time of the latter is roughly four-fold that of the former.
950 These two litterpools are further subdivided into above and below –ground pools, with
951 the latter explicitly discretised over the first two metres of the soil column, a feature first
952 introduced to the ORCHIDEE model by Camino-Serrano et al. (2014, 2018)(Camino-
953 Serrano et al., 2014, 2018). This marks a significant departure from the original litter
954 formulation in ORCHIDEE-MICT, in which the vertical distribution of litter influx to the
955 soil carbon pool follows a prescribed root profile for each PFT. This change now allows
956 for the production of DOC from litter explicitly at a given soil depth in permafrost soils.
957

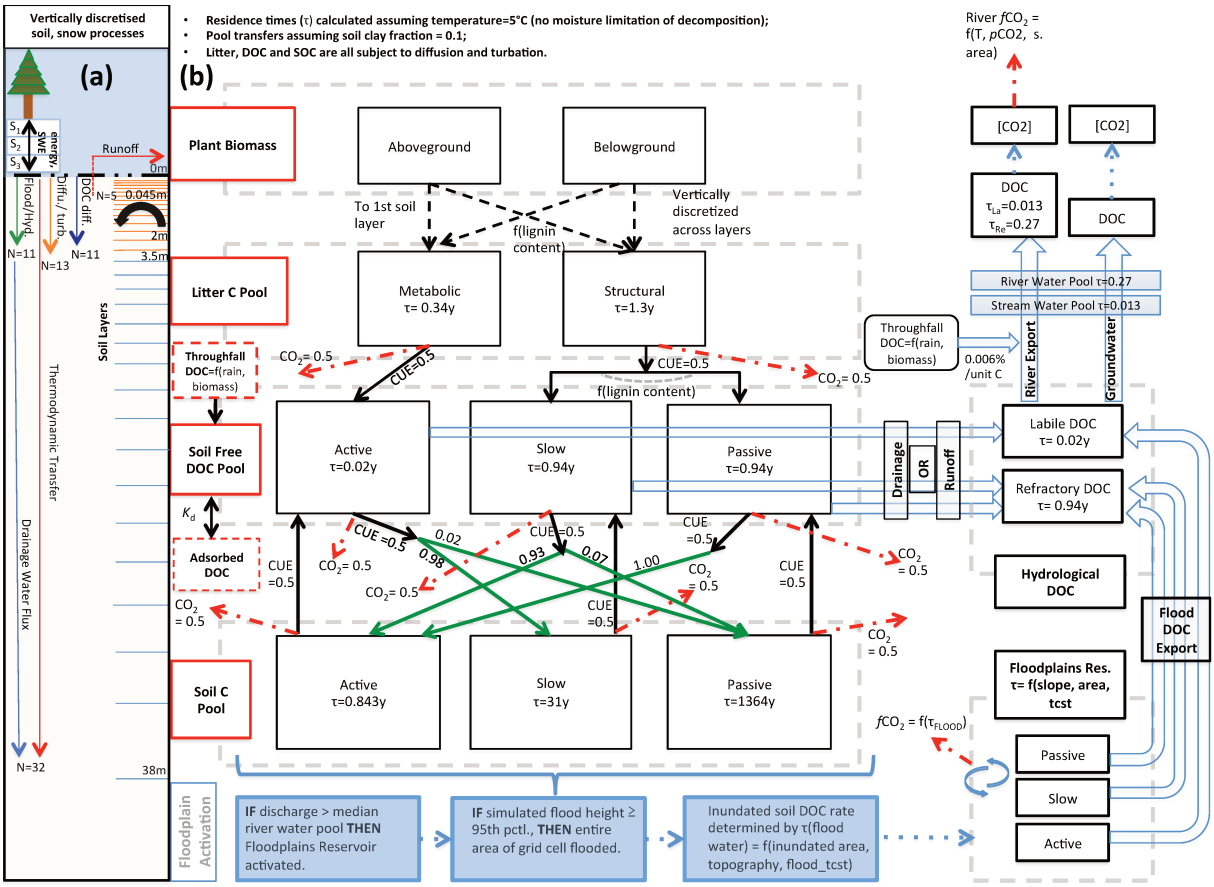

Figure 2 :Carbon and water flux map for core DOC elements in model structure relating to DOC transport and transformation. **(a)** Summary of the differing extent of vertical discretisation of soil and snow for different processes calculated in the model. Discretisation occurs along 32 layers whose thickness increases geometrically from 0-38m. N refers to the number of layers, SWE=snow water equivalent, S_n = Snow layer n. Orange layers indicate the depth to which diffusive carbon (turbation) fluxes occur. **(b)** Conceptual map of the production, transfer and transformation of carbon in its vertical and lateral (i.e., hydrological) flux as calculated in the model. Red boxes indicate meta-reservoirs of carbon, black boxes the actual pools as they exist in the model. Black arrows indicate carbon fluxes between pools, dashed red arrows give carbon loss as CO_2, green arrows highlight the fractional distribution of DOC to SOC (no carbon loss incurred in this transfer), a feature of this model. For a given temperature (5°C) and soil clay fraction, the fractional fluxes between pools are given for each flux, while residence times for each pool (τ) are in each box. The association of carbon dynamics with the hydrological module are shown by the blue arrows. Blue dashed boxes illustrate the statistical sequence which activates the boolean floodplains module. Note that for readability, the generation and lateral flux of dissolved CO_2 is omitted from this diagram, but is described at length in the Methods section.

2.3 DOC generation and leaching (Fig. 1b)

The vast majority of DOC produced by the model is generated initially from the litter pools via decomposition, such that half of all of the decomposed litter is returned to the atmosphere as CO_2, as defined by the microbial carbon use efficiency (CUE) –the fraction of carbon assimilated versus respired by microbes post-consumption –here set at 0.5 following Manzoni et al. (2012)(Manzoni et al., 2012). The non-respired half of the litter feeds into 'Active', 'Slow' and 'Passive' free DOC pools, which correspond to DOC reactivity classes in the soil column. Metabolic litter contributes exclusively to the

Active DOC pool, while Structural litter feeds into the other two, the distribution between them dependent on the lignin content of the Structural litter. The reactive SOC pools then derive directly from this DOC reservoir, in that fractions of each DOC pool, defined again by the CUE, are directly transferred to three different SOC pools, while the remainder adds to the heterotrophic soil respiration. Depending on clay content and bulk density of the soil, a fraction of DOC is adsorbed to the mineral soil and does not take part in these reactions until it is gradually desorbed when concentrations of free DOC decrease in the soil column. This scheme is explained in detail in Camino-Serrano (2018)(Camino-Serrano et al., 2018). The value of the fractional redistributions between free DOC and SOC after adsorption are shown in Fig. 2b.

The approximate ratio of relative residence times for the three SOC (Active :Slow :Passive) is (1 :37:1618) at a soil temperature of 5°C, or 0.843 years, 31 yrs. and 1364 yrs. for the three pools respectively (Fig. 2b). The residence times of the active DOC pool is ~7 days (0.02 yrs.), while the slow and passive DOC pools both have a residence time of ~343 days (0.94 yrs.) at that same temperature. Upon microbial degradation in the model, SOC of each pool reverts either to DOC or to CO_2, the ratio between these determined again by the CUE which is set in this study at 0.5 for all donor pools, in keeping with the parameter configuration in Lauerwald et al., (2017)(Lauerwald et al., 2017) from Manzoni et al. (2012)(Manzoni et al., 2012). This step in the chain of flows effectively represents leaching of SOC to DOC. Note that the reversion of SOC to DOC occurs only along Active-Active, Slow-Slow and Passive-Passive lines in Fig. 2b, while the conversion of DOC to SOC is distributed differently so as to build up a reasonable distribution of soil carbon stock reactivities. Note also that the microbial CUE is invoked twice in the chain of carbon breakdown, meaning that the 'effective' CUE of the SOC-litter system is approximately 0.25.

2.4 Throughfall and its DOC (Fig. 1c)

In MICT-L, DOC generation also occurs in the form of wet and dry atmospheric deposition and canopy exudation, collectively attributed to the throughfall, i.e. the amount of precipitation reaching the ground. Wet atmospheric deposition originates from organic compounds dispersed in atmospheric moisture which become deposited within rainfall, and are assumed here to maintain a constant concentration. This concentration we take from the average of reported rainfall DOC concentrations in the empirical literature measured at sites >55°N (Bergkvist and Folkeson, 1992; Clarke et al., 2007; Fröberg et al., 2006; Lindroos et al., 2011; Rosenqvist et al., 2010; Starr et al., 2003; Wu et al., 2010), whose value is 3 mgC L^{-1} of rainfall. Dry DOC deposition occurs through aerosol-bound organic compounds, here assumed to fall on the canopy ; canopy exudation refers to plant sugars exuded from the leaf surface (e.g. honey dew) or from their extraction by heterotrophs such as aphids. These two are lumped together in our estimates of canopy DOC generation (gDOC per g leaf carbon), which is calibrated as follows.

We take the average total observation-based throughfall DOC flux rate per m^2 of forest from the aforementioned literature bundle (15.7 gC m^{-2} yr^{-1}) and subtract from it the wet deposition component (product of rainfall over our simulation area and the rain DOC content). The remainder is then the canopy DOC, which we scale to the average leaf

biomass simulated in a 107-year calibration run over the Lena river basin, to obtain a constant, non-conservative canopy DOC production rate of $9.2*10^{-4}$ g DOC-C per gram leaf biomass per day (Eq. 1), except for the crop PFTs for which this value equals 0. Note that this production of DOC should be C initially fixed by photpsynthesis, but it is here represented as an additional carbon flux. The dry deposition of DOC through the canopy is given by:

$$(1)\quad \mathbf{TF_{DRY}} = \mathbf{M_{LEAF}} * \mathbf{9.2} * \mathbf{10^{-4}} \frac{\boldsymbol{dt}}{\boldsymbol{day}}$$

Where TF_{DRY} is dry deposition of DOC from the canopy and M_{LEAF} is leaf biomass. This accumulates in the canopy and can be flushed out with the throughfall and percolates into the soil surface or adds to the DOC stock of surface waters. The wet and canopy deposition which hits the soil is then assumed to be split evenly between the labile and refractory DOC pools (following ref.(Aitkenhead-Peterson et al., 2003)).

2.5 Hydrological mobilisation of soil DOC (Fig. 1d)

All DOC pools, leached from the decomposition of either litter and SOC or being throughfall inputs, reside at this point in discrete layers within the soil column, but are now also available for vertical advection and diffusion, as well as lateral export from the soil column as a carbon tracer, via soil drainage and runoff.

Export of DOC from the soil to rivers occurs through surface runoff, soil-bottom drainage, or flooding events (see sections 'soil flooding' and 'floodplain representation'). Runoff is activated when the maximum water infiltration rate of the specific soil has been exceeded, meaning that water arrives at the soil surface faster than it can enter, forcing it to be transported laterally across the surface. DOC is drawn up into this runoff water flux from the first 5 layers of the soil column, which correspond to a cumulative source depth of 4.5cm.

Drainage of DOC occurs first as its advection between the discrete soil layers, and its subsequent export from the 11th layer, which represents the bottom of the first 2m of the soil column, from which export is calculated as a proportion of the DOC concentration at this layer. Below this, soil moisture and DOC concentrations are no longer explicitly calculated, except in the case that they are cryoturbated below this, up to a depth of 3m. DOC drainage is proportional to but not a constant multiplier of the water drainage rate for two reasons. First, in the process of drainage DOC is able to percolate from one layer to another, through the entirety of the soil column, meaning that vertical transport is not solely determined by 11th layer concentrations, given that DOC can be continuously leached and transported over the whole soil column. Secondly, in order to account for preferential flow paths in the soil created by the subsoil actions of flora and fauna, and for the existence of non-homogenous soil textures at depth that act as aquitards, DOC infiltration must account for the fact that area-aggregated soils drain more slowly, increasing the residence time of DOC in the soil. Thus a reduction factor which reduces the vertical advection of DOC in soil solution by 80% compared to

the advection is applied to represent a slow down in DOC percolation through the soil and increase its residence time there.

In MICT-L, as in ORCHILEAK, a 'poor soils' module reads off from a map giving fractional coverage of land underlain by Podzols and Arenosols at the 0.5° grid-scale, as derived from the Harmonized World Soil Database (Nachtergaele, 2010). Due to their low pH and nutrient levels, areas identified by this soil-type criterion experience soil organic matter decomposition rates half that of other soils (Lauerwald et al. (2017)(Lauerwald et al., 2017), derived from Bardy et al. (2011); Vitousek & Sanford (1986); Vitousek & Hobbie (2000)(Bardy et al., 2011; Vitousek and Hobbie, 2000; Vitousek and Sanford, 1986)). To account for the very low DOC-filtering capacity of these coarse-grained, base- and clay-poor soils (DeLuca & Boisvenue (2012)(DeLuca and Boisvenue, 2012), Fig. 2b), no reduction factor in DOC advection rate relative to that of water in the soil column is applied when DOC is generated within these "poor soils"..

By regulating both decomposition and soil moisture flux, the "poor soil" criterion effectively serves a similar if not equal function to a soil 'tile' for DOC infiltration in the soil column (inset box of Fig. 1), because soil tiles (forest, grassland/tundra/cropland and bare soil) are determinants of soil hydrology which affects moisture-limited decomposition. Here however, the 'poor soil' criteria is applied uniformly across the three soil tiles of ecah grid cell. This modulation in MICT-L is of significance for the Arctic region, given that large fractions of the discontinous permafrost region are underlain by Podzols, particularly in Eurasia. For the Arctic as a whole, Podzols cover ~15% of total surface area (DeLuca and Boisvenue, 2012). Further, in modelled frozen soils, a sharp decline in hydraulic conductivity is imposed by the physical barrier of ice, which retards the flow of water to depth in the soil, imposing a cap on drainage and thus potentially increasing runoff of water laterally, across the soil surface (Gouttevin et al., 2012). In doing so, frozen soil layers overlain by liquid soil moisture will experience enhanced residence times of water in the carbon-rich upper soil layers, potentially enriching their DOC load.

Thus, for all the soil layers in the first 2m, DOC stocks are controlled by production from litter and SOC decay, their advection, diffusion, and consumption by DOC mineralization, as well as buffering by adsorption and desorption processes.

2.6 Routing Scheme:

The routing scheme in ORCHIDEE, first described in detail in Ngo-Duc et al. (2007)(Ngo-Duc et al., 2007) and presented after some version iterations in Guimberteau et al. (2012)(Guimberteau et al., 2012), is the module which when activated, represents the transport of water collected by the runoff and drainage simulated by the model along the prescribed river network in a given watershed. In doing so, its purpose is to coarsely represent the hydrologic coupling between precipitation inputs to the model and subsequent terrestrial runoff and drainage (or evaporation) calculated by it on the one hand, and the eventual discharge of freshwater to the marine domain, on the other. In other words, the routing scheme simulates the transport of water by rivers and streams, by connecting rainfall and continental river discharge with the land surface.

To do so, the routing scheme first inputs a map of global watersheds at the 0.5 degree scale (Oki et al., 1999; Vorosmarty et al., 2000) which gives watershed and sub-basin boundaries and the direction of water-flow based on topography to the model. The water flows themselves are comprised of three distinct linear reservoirs within each sub-basin ('slow', 'fast', 'stream'). Each water reservoir is represented at the subgrid scale (here: 4 subgrid units per grid cell), and updated with the lateral in- and outflows at a daily time-step. The 'slow' water reservoir aggregates the soil drainage, i.e. the vertical outflow from the 11^{th} layer (2 m depth) of the soil column, effectively representing the 'shallow groundwater' storage. The 'fast' water reservoir aggregates surface runoff simulated in the model, effectively representing overland hydrologic flow. The 'slow' and 'fast' wast reservoirs feed a delayed outflow to the 'stream' reservoir' of the adjacent subgrid-unit in the downstream direction.

The water residence time in each reservoir depends on the nature of the reservoir (increasing residence time in the order : stream < fast < slow reservoir). More generally, residence time decreases with the steepness of topography, given by the product of a local topographic index and a constant with decreasing values for the 'slow', 'fast' and 'stream' reservoirs. The topographic index is the ratio of the grid-cell length to the square root of the mean slope, to reproduce the effect of geomorphological factors in Manning's equation (Ducharne et al., 2003; Guimberteau et al., 2012; Manning, 1891) and determines the time that water and DOC remain in soils prior to entering the river network. In this way the runoff and drainage are exported from sub-unit to sub-unit and from grid-cell to grid-cell.

2.7 Grid-scale water and carbon routing (Fig. 1f, 1g)

Water-borne, terrestrially-derived DOC and dissolved CO_2 in the soil solution are exported over the land surface using the same routing scheme. When exported from soil or litter, DOC remains differentiated in the numerical simulations according to its initial reactivity within the soil (Active, Slow, Passive). However, because the terrestrial Slow and Passive DOC pools (Camino-Serrano et al., 2018) are given the same residence time, these two pools are merged when exported (Lauerwald et al., 2017): Active DOC flows into a Labile DOC hydrological export pool, while the Slow and Passive DOC pools flow into a Refractory DOC hydrological pool (Fig. 2b). The water residence times in each reservoir of each subgrid-unit determine the decomposition of DOC into CO_2 within water reservoirs, before non-decomposed DOC is passed on to the next reservoir downstream.

The river routing calculations, which occur at a daily timestep, are then aggregated to one-day for the lateral transfer of water, $CO_{2(aq)}$ and DOC from upstream grid to downstream grid according to the river network. Note that carbonate chemistry in rivers and total alkalinity routing are not calculated here.

In this framework, the 'fast' and 'slow' residence times of the water pools in the routing scheme determine the time that water and DOC remains in overland and groundwater flow before entering the river network. Note that while we do not explicitly simulate headwater streams as they exist in a geographically determinant way in the real world, we do simulate what happens to the water before it flows into a river large enough to be

represented in the routing scheme by the water pool called 'stream'. The 'fast' reservoir, which is indicative of the pool of runoff water that is destined for entering the 'stream' water reservoir, is implicitly representative of headwater streams non resolved by the model routing as an explicit stream pool at a given spatial resolution, as it fills the spatial and temporal niche between runoff and the river stem. The dynamics of headwater hydrological and DOC dynamics (Section 2.10) are of potentially great significance with respect to carbon processing, as headwater catchments have been shown to be 'hotspots' of carbon metabolisation and outgassing in Arctic rivers, despite their relatively small areal fraction (Denfeld et al., 2013; Drake et al., 2015; Mann et al., 2015; Venkiteswaran et al., 2014; Vonk et al., 2013, 2015a, 2015c). Thus, in what follows in this study, we refer to what in the code are called the 'fast' and 'stream' pools, which represent the small streams and large stream or river pools, respectively, using 'stream' and 'river' to denote these from hereon in.

Furthermore, the differentiated representation of water pools as well as mean grid cell slope, combined with the dynamic active layer simulated for continuous versus discontinuous permafrost, is important for reproducing the phenomena observed by Kutscher et al. (2017)(Kutscher et al., 2017) and Zhang et al. (2017)(Zhang et al., 2017) for sloping land as shown on the right hand side of Fig. 1. In discontinuous permafrost and permafrost free regions, these phenomena encompass landscape processes (sub-grid in the model), through which water flow is able to re-infiltrate the soil column and so leach more refractory DOC deeper in the soil column, leading to a more refractory signal in the drainage waters. In contrast, in continuous permafrost region, the shallow active layer will inhibit the downward re-infiltration flux of water and encourage leaching at the more organic-rich and labile surface soil layer, resulting in a more labile DOC signal from the drainage in these areas (Fig. 1). These re-infiltration processes are thought to be accentuated in areas with higher topographic relief (Jasechko et al., 2016), which is why they are represented on sloping areas in Fig. 1.

2.8 Representation of floodplain hydrology and their DOC budget (Fig. 1e,1h)

The third terrestrial DOC export pathway in MICT-L is through flooding of floodplains, a transient period that occurs when stream water is forced by high discharge rates over the river 'banks' and flows onto a flat floodplain area of the grid cell that the river crosses, thus inundating the soil. Such a floodplain area is represented as a fraction of a grid-cell with the maximum extent of inundation, termed the 'potential flooded area' being predefined from a forcing file (Tootchi et al., 2019). Here, the DOC pools that are already being produced in these inundated areas from litter and SOC decomposition in the first 5 layers of the soil column are directly absorbed by the overlying flood waters. These flood waters may then either process the DOC directly, via oxidisation to CO_2, (Sections 2.10, 2.11) or return them to the river network, as floodwaters recede to the river main stem, at which point they join the runoff and drainage export flows from upstream.

MICT-L includes the floodplain hydrology part of the routing scheme (D'Orgeval et al., 2008; Guimberteau et al., 2012), as well as additions and improvements described in Lauerwald et al. (2017). The spatial areas that are available for potential flooding are pre-defined by an input map originally based on the map of Prigent et al. (2007)(Prigent

et al., 2007). However, for this study, we used an alternative map of the "regularly flooded areas" derived from the method described in Tootchi et al., (2018), which in this study uses an improved input potential flooding area forcing file specific to the Lena basin, that combines three high-resolution surface water and inundation datasets derived from satellite imagery: GIEMS-D15 (Fluet-Chouinard et al., 2015), which results from the downscaling of the map of Prigent et al. (2007)(Prigent et al., 2007) at 15-arc-sec (ca 500 m at Equator); ESA-CCI land cover (at 300 m ~ 10 arc-sec); and JRC surface water at 1 arc-sec (Pekel et al., 2016). The 'fusion' approach followed by this forcing dataset stems from the assumption that the potential flooding areas identified by the different datasets are all valid despite their uncertainties, although none of them is exhaustive. The resulting map was constructed globally at the 15 arc-sec resolution and care was taken to exclude large permanent lakes from the potential flooding area based on the HydroLAKES database (Messager et al., 2016). In the Lena river basin, the basin against which we evaluate ORCHIDEE MICT-LEAK in Part 2 of this study, this new potential floodplains file gives a maximum floodable area of 12.1% ($2.4*10^5$ km^2) of the $2.5*10^6$ km^2 basin, substantially higher than previous estimates of 4.2%(Prigent et al., 2007).

With this improved forcing, river discharge becomes available to flood a specific pre-defined floodplain grid fraction, creating a temporary floodplains hydrologic reservoir, whose magnitude is defined by the excess of discharge at that point over a threshold value, given by the median simulated water storage of water in each grid cell over a 30 year period. The maximum extent of within-grid flooding is given by another threshold, the calculated height of flood waters beyond which it is assumed that the entire grid is inundated. This height, which used to be fixed at 2 m, is now determined by the 90th percentile of all flood water height levels calculated per grid cell from total water storage of that grid cell over a reference simulation period for the Lena basin, using the same methodology introduced by Lauerwald et al. (2017). The residence time of water on the floodplains (τ_{flood}) is a determinant of its resulting DOC concentration, since during this period it appropriates all DOC produced by the top 5 layers of the soil column.

2.9 Oceanic outflow (Fig. 1i)

Routing of water and DOC through the river network ultimately lead to their export from the terrestrial system at the river mouth (Fig. 1), which for high latitude rivers are almost entirely sub-deltas of the greater 'estuary', described by McClelland et al. (2012), draining into the Arctic Ocean. Otherwise, the only other loss pathway for carbon export once in the river network is through its decomposition to CO_2 and subsequent escape to the atmosphere from the river surface. DOC decomposition is ascribed a constant fraction for the labile and refractory DOC pools of 0.3 d^{-1} and 0.01 d^{-1} at 25°C, respectively, these modulated by a water-temperature dependent Arrhenius rate term. Because the concentration of dissolved CO_2 (referred to as $CO_{2(aq.)}$) in river water is derived not only from in-stream decomposition of DOC, but also from $CO_{2(aq.)}$ inputs from the decomposition of litter, SOC and DOC both in upland soils and in inundated soils, the model also represents the lateral transport of $CO_{2(aq.)}$ from soils through the river network. Note that autochtonous primary production and derivative carbon

transformations are ignored here, as they are considered relatively minor contributors in the Arctic lateral flux system (Cauwet and Sidorov, 1996; Sorokin and Sorokin, 1996).

2.10 Dissolved CO2 export and river evasion (Fig. 1j)

Soil $CO_{2(aq.)}$ exports are simulated by first assuming a constant concentration of $CO_{2(aq.)}$ with surface runoff and drainage water fluxes, of 20 and 2 mgC L^{-1}, corresponding to a *p*CO2 of 50000 μ atm and 5000 μ atm at 25°C in the soil column, respectively. These quantities are then scaled with total (root, microbial, litter) soil respiration by a scaling factor first employed in Lauerwald et al. (2019, *in review*). In the high latitudes soil respiration is dominantly controlled by microbial decomposition, and for the Lena basin initial model tests suggest that its proportional contribution to total respiration is roughly 90%, versus 10% from root respiration. Thus $CO_{2(aq.)}$ enters and circulates the rivers via the same routing scheme as that for DOC and river water. The lateral transfers of carbon are aggregated from the 30 minute time steps at which they are calculated, with a 48 timestep period, so that they occur within the model as a daily flux. The calculation of the river network pCO_2 can then be made from $CO_{2(aq.)}$ and its equilibrium with the atmosphere, which is a function of its solubility (K_{CO2}) with respect to the temperature of the water surface T_{WATER} (Eq.2).

$$(2)\quad \boldsymbol{pCO_{2_{POOL}}} = \frac{[\boldsymbol{CO_{2(aq)}}]}{\boldsymbol{12.011 * K_{CO_2}}}$$

Where the pCO_2 of a given (e.g. 'stream', 'fast', 'slow' and floodplain) water pool (pCO_{2POOL}) is given by $[\boldsymbol{CO_{2(aq)}}]$ the dissolved CO_2 concentration in that pool, and K_{CO2}. Water temperature (T_{WATER}, (°C)) isn't simulated by the model, but is derived here from the average daily surface temperature (T_{GROUND}, (°C)) in the model (Eq. 3), a set up used by Lauerwald et al. (2017) and retained here. Note that while dissolved CO_2 enters from the terrestrial reservoir from organic matter decomposition, it is also generated *in situ* within the river network as DOC is respired microbially.

With our water temperature estimate, both K_{CO2} and the Schmidt number (Sc) from Wanninkhof (1992)(Wanninkhof, 1992) can be calculated, allowing for simulation of actual gas exchange velocites from standard conditions. The CO_2 that evades is then subtracted from the $[CO_2]$ stocks of each of the different hydrologic reservoirs –river, flood and stream.

$$(3)\quad \boldsymbol{T_{WATER} = 6.13^{\circ}C + (0.8 * T_{GROUND})}$$

$$(4)\quad \boldsymbol{Sc = \left((1911 - 118.11) * T_{WATER}\right) + \left(3.453 * T_{WATER}^2\right) - (0.0413 * T_{WATER}^3)}$$

CO_2 evasion is therefore assumed to originate from the interplay of CO_2 solubility, relative gradient in partial pressures of CO_2 between air and water, and gas exchange kinetics. Evasion as a flux from river and floodplain water surfaces is calculated at a daily timestep, however in order to satisfy the sensitivity of the relative gradient of partial pressures of CO_2 in the water column and atmosphere to both CO_2 inputs and evasion, the pCO_2 of water is calculated at a more refined 6 minute timestep. The daily

lateral flux of CO_2 inputs to the water column are thus equally broken up into 240 (6 min.) segments per day and distributed to the pCO_2 calculation. Other relevant carbon processing pathways, such as the photochemical breakdown of riverine OC, are not explicitly included here, despite the suggestion by some studies that the photochemical pathway dominate DOC processing in Arctic streams(Cory et al., 2014). Rather, these processes are bundled into the aggregate decomposition rates used in the model, which thus include both microbial and photochemical oxidation. This is largely because it is unclear how different factors contribute to breaking down DOC in a dynamic environment and also the extent to which our DOC decomposition and CO_2 calculations implicitly include both pathways –e.g. to what extent the equations and concepts used in their calculation confound bacterial with photochemical causation, since both microbial activity and incident UV light are a function of temperature and total incident light.

2.11 Soil layer processes: turbation adsorption

The soil carbon module is discretised into a 32-layer scheme totalling 38m depth, which it shares with the soil thermodynamics to calculate temperature through the entire column. An aboveground snow module (Wang et al., 2013) is discretised into 3 layers of differing thickness, heat conductance and density, which collectively act as a thermodynamically-insulating intermediary between soil and atmosphere (Fig. 2a). Inputs to the three soil carbon pools are resolved only for the top 2m of the soil, where litter and DOC are exchanged with SOC in decomposition and adsorption/desorption processes. Decomposition of SOC pools, calculated in each soil layer, is dependent on soil temperature, moisture and texture (Koven et al., 2009; Zhu et al., 2016), while vertical transfer of SOC is enabled by representation of cryoturbation (downward movement of matter due to repeated freeze-thaw) in permafrost regions, and bioturbation (by soil organisms) in non-permafrost regions in terms of a diffusive flux.

Cryoturbation, given a diffusive mixing rate (Diff) of 0.001 $m^2\ yr^{-1}$ (Koven et al., 2009), is possible to 3 m depth (diffusive rate declines linearly to zero from active layer bottom to 3 m), and extends the soil column carbon concentration depth in permafrost regions from 2 m. Bioturbation is possible to 2 m depth, with a mixing rate of of 0.0001 $m^2\ yr^{-1}$ (Koven et al., 2013b) declining to zero at 2 m (Eq. 5). In MICT-L, these vertical exchanges in the soil column are improved on. Now, we explicitly include the cryoturbation and bioturbation of both belowground litter and DOC. These were not possible in ORCHIDEE-MICT because, for the former, the belowground litter distribution was not explicitly discretised or vertically dynamic, and for the latter because DOC was not produced in prior versions. Diffusion is given by :

$$\left((5)\right) \quad \frac{\delta DOC_i(z)}{\delta t} = IN_{DOC_i}(z) - k_i(z) * \phi * DOC_i(z) + Diff \frac{\delta DOC_i^2(z)}{\delta z^2}$$

Where DOC_i is the DOC in pool i at depth z, ($gC\ m^{-3}$) IN_{DOCi} the inflow of carbon to that pool ($gCm^{-3}d^{-1}$), k_i the decomposition rate of that pool (d^{-1}), Φ the temperature dependent rate modifier for DOC decomposition and *Diff* the diffusion coefficient ($m^2\ yr^{-1}$). The vertical diffusion of DOC in non-permafrost soils represented here (that is, the non-cryoturbated component) appears to be consistent with recent studies reporting an increased retention of DOC in the deepening active layer of organic soils (Zhang et al.,

2017). This vertical translocation of organic carbon, whether in solid/liquid phase appears to be an important component of the high rates of SOC buildup observed at depth in deep permafrost soils.

2.11 Priming (Fig. 1m)

MICT-L also incorporates a scheme for the 'priming' of organic matter decomposition, a process in which the relative stability of SOC is impacted by the intrusion of or contact with SOC of greater reactivity, resulting in enhanced rates of decomposition. This was first introduced by Guenet et al. (2016)(Guenet et al., 2016) and updated in Guenet et al. (2018)(Guimberteau et al., 2018). This process has shown itself to be of potentially large significance for SOC stocks and their respiration in high latitude regions, in empirical in situ and soil incubation studies (De Baets et al., 2016; Walz et al., 2017; Wild et al., 2014, 2016; Zhang et al., 2017), as well as modelling exercises (Guenet et al., 2018). Here, priming of a given soil pool is represented through the decomposition of soil carbon (dSOC/dt) by the following equation :

$$(6) \quad \frac{\boldsymbol{dSOC}}{\boldsymbol{dt}} = \boldsymbol{IN_{SOC}} - \boldsymbol{k} * (\mathbf{1} - \boldsymbol{e}^{-\boldsymbol{c}*\boldsymbol{FOC}}) * \boldsymbol{SOC} * \boldsymbol{\Theta} * \boldsymbol{\phi} * \boldsymbol{\gamma}$$

Where IN_{SOC} is the carbon input to that pool, k is the SOC decomposition rate, FOC is a stock of matter interacting with this SOC pool to produce priming, c is a parameter controlling this interaction, SOC is the SOC reservoir, and θ ,Φ and γ the moisture, temperature and texture functions that modulate decomposition in the code. The variable FOC ('fresh organic carbon') is an umbrella term used for specifying all of the carbon pools which together constitute that carbon which is considered potential priming donor material –ie. more labile – to a given receptor carbon pool. Thus, for the slow soil carbon pool FOC incorporates the active soil carbon pool plus the above and below ground strucutural and metabolic litter pools, because these pools are donors to the slow pool, and considered to accelerate its turnover through priming. Importantly, previous studies with priming in ORCHIDEE employed this scheme on a version which resolves neither the vertical discretisation of the soil column nor the explicit vertical diffusion processes presented here. This is potentially significant, since the vertical diffusion of relatively reactive matter may strongly impact (accelerate) the decomposition of low reactivity matter in the deeper non-frozen horizons of high latitude soils, while the explicit discretisation of the soil column is a significant improvement in terms of the accuracy of process-representation within the column itself.

Other carbon-relevant schemes included in MICT-L are: A prognostic fire routine (SPITFIRE), calibrated for the trunk version of ORCHIDEE (Yue et al., 2016) is available in our code but not activated in the simulations conducted here. As a result, we do not simulate the ~13% of Arctic riverine DOC attributed to biomass burning by Myers-Pigg et al. (2015)(Myers-Pigg et al., 2015), or the ~8% of DOC discharge to the Arctic Ocean from the same source (Stubbins et al., 2017). Likewise, a crop harvest module consistent with that in ORCHIDEE-MICT exists in MICT-L but remains deactivated for our simulations.

A module introduced in the last version of ORCHIDEE-MICT (Guimberteau et al., 2018), in which the soil thermal transfer and porosity and moisture are strongly affected by SOC concentration, is deactived here, because it is inconsistent with the new DOC scheme. Specifically, while carbon is conserved in both MICT and MICT-L soil schemes, MICT-L introduces a new reservoir into which part of the total organic carbon in the soil –the DOC –must now go. This then lowers the SOC concentration being read by this thermix module, causing significant model artefact in soil thermodynamics and hydrology in early exploratory simulations. Ensuring compatibility of this routine with the DOC scheme will be a focal point of future developments in MICT-L. Other processes being developed for ORCHIDEE-MICT, including a high latitude peat formation (Qiu et al., 2018), methane production and microbial heat generating processes that are being optimised and calibrated, are further pending additions to this particular branch of the ORCHIDEE-MICT series.

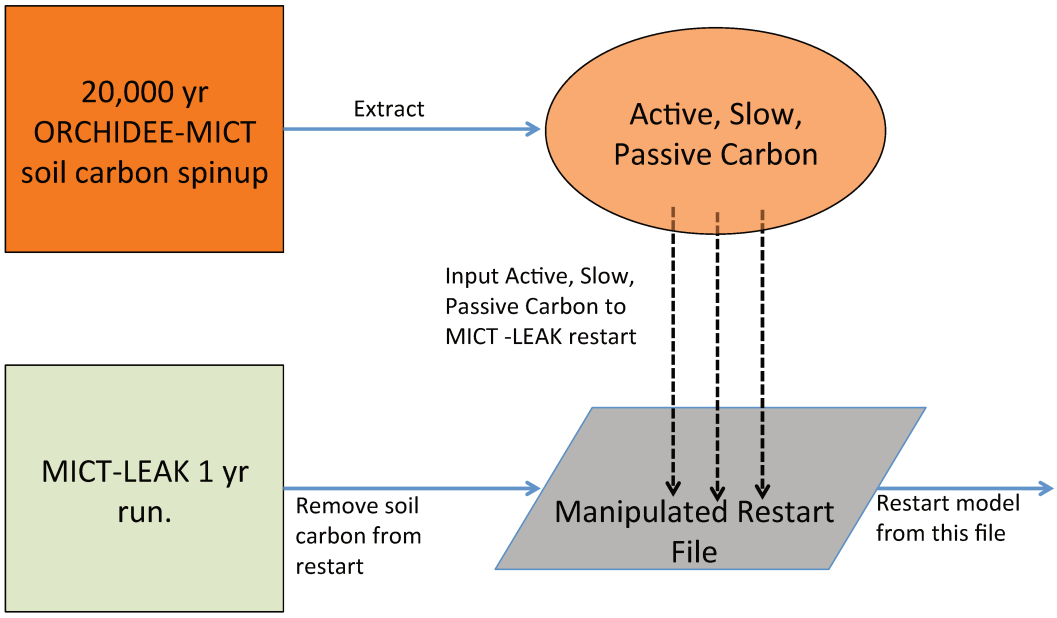

Figure 3: Flow diagram illustrating the step-wise stages required to implement the model's soil carbon stock prior to conducting transient, historical simulations.

Soil Carbon Spinup and Simulation Protocol

The soil carbon spinup component of ORCHIDEE, which is available to both its trunk and MICT branches, was omitted from this first version of MICT-L, owing to the code burden required for ensuring compability with the soil carbon scheme in MICT-L. However, because we are simulating high latitude permafrost regions, having a realistic soil carbon pool at the outset of the simulations is necessary if we are to untangle the dynamics of SOC and DOC with a changing environment. Because the soil carbon spinup in ORCHIDEE-MICT is normally run over more than 10,000 years (Guimberteau et al., 2108), and because running MICT-L for this simulation period in its normal, non-spinup simulation mode would impose an unreasonable burden on computing resources, here we directly force the soil carbon output from a MICT spinup directly into the restart file of a MICT-L simulation.

A 20,000 year spinup loop over 1961-1990 (these years chosen to mimic coarsely warmer mid-Holocene climate) -forced by GSWP-3 climatology, whose configuration derives directly from that used in Guimberteau et al. (2018), was thus used to replace the three soil carbon pool values from a 1-year MICT-L simulation to set their initial values. A conversion of this soil carbon from volumetric to areal units was applied, owing to different read/write standards in ORCHILEAK versus ORCHIDEE-MICT. This artifically imposed, MICT-derived SOC stock would then have to be exposed to MICT-L code, whose large differences in soil carbon module architecture as compared to MICT, would drive a search for new equilibrium soil carbon stocks.

Due to the long residence times of the passive SOC pool, reaching full equilibrium for it requires a simulation length on the order of 20,000y –again an overburden. As we are interested primarily in DOC in this study, which derives mostly from the Active and Slow SOC pools, the model was run until these two pools reached a quasi-steady state equilibria (Part 2 Supplement, Fig. S1). This was done by looping over the same 30 year cycle (1901-1930) of climate forcing data from GSWP-3 during the pre-industrial period (Table 1) and the first year (1901) of a prescribed vegetation map (ESA CCI Land Cover Map(Bontemps et al., 2013)) –to ensure equilibrium of DOC, dissolved CO_2 and Active and Slow SOC pools is driven not just by a single set of environmental factors in one year –for a total of 400 years. The parameter configuration adhered as close as possible to that used in the original ORCHIDEE-MICT spinup simulations, to avoid excessive equilibrium drift from the original SOC state (Fig. 3).

Table 1: Data type, name and sources of data files used to drive the model in the study simulations.

Data Type	Name	Source
Vegetation Map	ESA CCI Land Cover Map	Bontemps et al., 2013
Topographic Index	STN-30p	Vörösmarty et al., 2000
Stream flow direction	STN-30p	Vörösmarty et al., 2000
River surface area		Lauerwald et al., 2015
Soil texture class		Reynolds et al. 1999
Climatology	GSWP3 v0, 1 degree	http://hydro.iis.u-tokyo.ac.jp/GSWP3/
Potential floodplains	Multi-source global wetland maps	Tootchi et al., 2018
Poor soils	Harmonized World Soil Database map	Nachtergaele et al., 2010
Spinup Soil Carbon Stock	20ky ORCHIDEE-MICT soil carbon spinup	Based on config. in Guimberteau et al. (2018)

Conclusion

This first part of a two-part study has described a new branch of the high latitude version of ORCHIDEE-MICT land surface model, in which the production, transport and transformation of DOC and dissolved CO_2 in soils and along the inland water network of explicitly-represented northern permafrost regions has been implemented for the first time. Novel processes with respect to ORCHIDEE-MICT include the discretisation of litter inputs to the soil column, the production of DOC and $CO_{2(aq.)}$ from organic matter and decomposition, respectively, transport of DOC into the river routing network and its

potential mineralisation to $CO_{2(aq.)}$ in the water column, as well as subsequent evasion from the water surface to the atmosphere. In addition, an improved floodplains representation has been implemented which allows for the hydrologic cycling of DOC and CO_2 in these inundated areas. In addition to descriptions of these processes, this paper outlines the protocols and configuration adopted for simulations using this new model that will be used for its evaluation over the Lena river basin in the second part of this study.

Chapter 3

ORCHIDEE MICT-LEAK (r5459), a global model for the production, transport and transformation of dissolved organic carbon from Arctic permafrost regions, Part 2: Model evaluation over the Lena River basin[2].

Summary

In this second part of a two-part study, we perform simulations of the carbon and water budget of the Lena catchment with the land surface model ORCHIDEE MICT-LEAK, enabled to simulate dissolved organic carbon (DOC) production in soils and its transport and fate in high latitudes inland waters. A soil carbon stock representative of permafrost soils carbon concentrations and quantities is equilibrated with the new carbon and DOC modules described in Chapter 1 and the model allowed to run over the 20th Century under state-of-the-art climate forcing data suite. The model results are evaluated in their ability to reproduce the fluxes of DOC and carbon dioxide (CO_2) along the soil-inland water continuum, and the exchange of CO_2 with the atmosphere, including the evasion outgassing of CO_2 from inland waters. We present simulation results over years 1901-2007, and show that the model is able to broadly reproduce observed state variables and their emergent properties across a range of interacting physical and biogeochemical processes, including:

1) Net primary production (NPP), respiration and riverine hydrologic amplitude, seasonality and inter-annual variation; 2) DOC concentrations, bulk annual flow and their volumetric attribution at the sub-catchment level; 3) High headwater versus downstream CO_2 evasion, an emergent phenomenon consistent with observations over a spectrum of high latitude observational studies. (4) These quantities obey emergent relationships with environmental variables like air temperature and topographic slope that have been described in the literature. This gives us confidence in reporting the following additional findings: (5) Of the ~34TgC yr^{-1} left over as input to terrestrial and aquatic systems after NPP is diminished by heterotrophic respiration, 7 TgC yr^{-1} is leached and transported into the aquatic system. Of this, over half (3.6 TgC yr^{-1}) is evaded from the inland water surface back into the atmosphere and the remainder (3.4 TgC yr^{-1}) flushed out into the Arctic Ocean, proportions in keeping with other, empirically derived studies. (6) DOC exported from the floodplains is dominantly sourced from recent, more 'labile' terrestrial production, in contrast to DOC leached from the rest of the watershed with runoff and drainage, which is mostly sourced from recalcitrant soil and litter. (7) All else equal, both historical climate change (a spring/summer warming of 1.8°C over the catchment) and rising atmospheric CO_2 (+85.6ppm) are diagnosed from factorial simulations to contribute similar, significant increases in DOC transport via primary production, although this similarity may not hold in the future.

[2] Submitted to *Geoscientific Model Development*, in review.

The ability of ORCHIDEE MICT-LEAK to reasonably reproduce individual DOC-specific phenomena, and their interaction and response to seasonal and interannual changes in environmental drivers, and the emergent phenomena that arise as a result, demonstrate that this model is a potentially powerful new tool for diagnosing and reproducing past, present and potentially future states of the Arctic carbon cycle. Furthermore, our results appear to suggest that, if the historical response of the Lena basin to environmental drivers is generalisable to its future response, and if the Lena basin can be used to generalise permafrost basins as a whole, DOC cycling in the Arctic may increase under enhanced warming and primary production. Further, if DOC temperature responses follow the pathway witnessed for parts of western Siberia, this likely increase may occur in a highly non-linear fashion. In Chapter 3, these questions are addressed by simulating the past and future of the Pan-Arctic region, driven by climate input data representative of a future intermediate-warming scenario.

Chapitre 3
ORCHIDEE MICT-LEAK (r5459), modèle mondial de production, de transport et de transformation du carbone organique dissous issu des régions de pergélisol de l'Arctique, partie 2: évaluation du modèle sur le bassin de la Lena.

Résumé

Dans cette deuxième partie d'une étude en deux parties, nous effectuons des simulations avec le modèle de surface terrestre ORCHIDEE MICT-LEAK décrit dans le chapitre 1 dans le but de reproduire le bilan carbone et eau du bassin versant de Lena, en particulier la production de carbone organique dissous (COD) dans les sols et son transport dans les eaux intérieures des hautes latitudes au cours du XXe siècle avec une suite de données de forçage climatique ultramoderne. Les capacités du modèle à reproduire les flux de COD et de dioxyde de carbone (CO_2) le long du continuum sol-eaux intérieures et l'échange de CO_2 avec l'atmosphère, y compris l'évacuation dégagée de CO_2 des eaux intérieures sont évaluées. Nous présentons les résultats de la simulation sur les années 1901-2007 et montrons que le modèle est capable de reproduire à grande échelle les variables d'état observées et leurs propriétés émergentes dans une gamme de processus physiques et biogéochimiques en interaction, notamment:

1) Production primaire nette (PPN), la respiration et l'amplitude hydrologique des rivières (saisonnalité et variation interannuelle); 2) les concentrations de COD, le débit annuel global et leur attribution volumétrique au niveau du sous-captage; 3) Évasion du CO_2 en amont et en aval, un phénomène émergent cohérent avec les observations sur un spectre d'études observationnelles à haute latitude. Ces quantités obéissent à des relations émergentes avec des variables environnementales telles que la température de l'air et la pente topographique décrites dans la littérature. Nous estimons grâce au modèle que sur les ~ 34 TgC an^{-1} restants comme intrants dans les systèmes terrestres et aquatiques et après soustraction de la respiration par la respiration hétérotrophe, 7 TgC an^{-1} sont lessivés et transportés dans le milieu aquatique. Sur ce total, plus de la moitié (3,6 TgC an^{-1}) est évacuée de la surface des eaux intérieures vers l'atmosphère et le reste (3,4 TgC an^{-1}) est évacué dans l'océan Arctique. Ces proportions sont conformes à celles estimées par d'autres études empiriques. Le COD exporté des plaines d'inondations provient principalement de la production terrestre récente, plus «labile», contrairement au COD lessivé du reste du bassin versant avec ruissellement et drainage, principalement à partir de sol et de litière récalcitrants. Toutes choses étant égales par ailleurs, les effets directs des changements climatiques historiques (réchauffement printemps / été de 1,8 ° C sur le bassin versant) et de la hausse des émissions de CO_2 dans l'atmosphère (+ 85,6 ppm) ont été diagnostiquées à l'aide de simulations factorielles comme contribuant à des augmentations similaires et significatives du transport de C production, bien que cette similitude puisse ne pas être vraie à l'avenir.

La capacité d'ORCHIDEE MICT-LEAK à reproduire de manière raisonnable des phénomènes individuels spécifiques au COD, leurs interactions et leurs réponses aux changements saisonniers et interannuels des facteurs environnementaux, ainsi que les phénomènes émergents qui en résultent, démontrent que ce modèle constitue un nouvel outil

potentiellement puissant pour diagnostiquer et reproduire les états passés, présents et potentiellement futurs du cycle du carbone arctique. De plus, nos résultats semblent suggérer que, si la réponse historique du bassin de Lena aux facteurs environnementaux est généralisable pour sa réponse future, et si le bassin de Lena peut être utilisé pour généraliser l'ensemble des bassins de pergélisol, le cycle de COD dans l'Arctique pourrait s'accélérer à cause du réchauffement accru et d'un augmentation de la production primaire. En outre, si les réponses de température du COD suivent le chemin observé dans certaines parties de la Sibérie occidentale, cette augmentation risque de se produire de manière très non linéaire. Dans le chapitre 3, ces questions sont traitées en simulant le passé et l'avenir de la région panarctique, à l'aide de données climatologiques représentatives d'un futur scénario de réchauffement intermédiaire.

1 Introduction

A new branch of the high latitude-specific land surface component of the IPSL Earth System model, ORCHIDEE MICT-LEAK (r5459), was enabled to simulate new model processes of soil dissolved organic carbon (DOC) and CO_2 production, and their advective/diffusive vertical transport within a discretized soil column as well as their transport and transformation within the inland water network, in addition to improved representation of hydrological and carbon processes in floodplains. These additions, processes first coded in the model ORCHILEAK (Lauerwald et al., 2017) and implemented within the high latitude base model ORCHIDEE-MICT v8.4.1 (Guimberteau et al., 2018), were described in detail in Part 1 of this study. This second part of our study deals with the validation and application of our model. We validate simulation outputs against observation for present-day and run transient simulations over the historial period (1901-2007) using the Lena River basin as test case. The simulation setup and rationale for choice of simulation basin are outlined below.

2 Simulation Rationale

The Lena river basin, which is bounded by the region 52-72°N; 102-142°E, was chosen as the basin for model evaluation because it is the largest DOC discharge contribution amongst the Arctic rivers, according to some estimates (Raymond et al., 2007; Holmes et al., 2012), with its 2.5 million km^2 area (befitting our coarse-grid resolution) discharging almost 20% of the summed discharge of the largest six Arctic rivers, its large areal coverage by Podzols (DeLuca and Boisvenue, 2012), and the dominance of DOC versus particulate organic carbon (POC) with 3-6Tg DOC-C yr^{-1} vs. 0.03-0.04 Tg POC-C yr^{-1} (Semiletov et al., 2011) in the total OC discharge load –factors all broadly representative of the Eurasian Arctic rivers. Compared to other Eurasian rivers, the Lena is relatively well studied, which provides data across the range of soil, hydrologic, geochemical and ecological domains over space and time, that enable us to perform adequate model evaluation.

Climatological forcing is input from the Global Soil Wetness Project Phase 3 (GSWP3) v.0 data at a 1 degree 3-hourly resolution covering the period 1901 to 2007 (Supplement, Table S1), which is then interpolated to a 30 minute timestep to comply with the timestep of the model's surface water and energy balance calculation period. This dataset was chosen for its suitability as input for reproducing the amplitude and seasonality of Northern Hemisphere high latitude riverine discharge in ORCHIDEE-MICT, as compared to other datasets (Guimberteau et al., 2018). An improved floodplains area input file for the Lena basin(Tootchi et al., 2019) was used to drive the simulation of floodplain dynamics (Supplement, Table S1).

Simulations were run over the Lena river basin (Fig. 3a) at a 1 degree resolution (Fig. 1) for the historical period between 1901 and 2007 to evaluate the simulated output of relevant carbon fluxes and hydrologic variables against their observed values, as well as those of emergent phenomena arising from their interplay (Fig. 1), at both the grid and basin scale. We evaluate at the basin scale because the isolation of a single geographic unit allows for a more refined alaysis of simulated variables than doing the same over

the global Pan-Arctic, much of which remains poorly accounted for in empirical databases and literature.

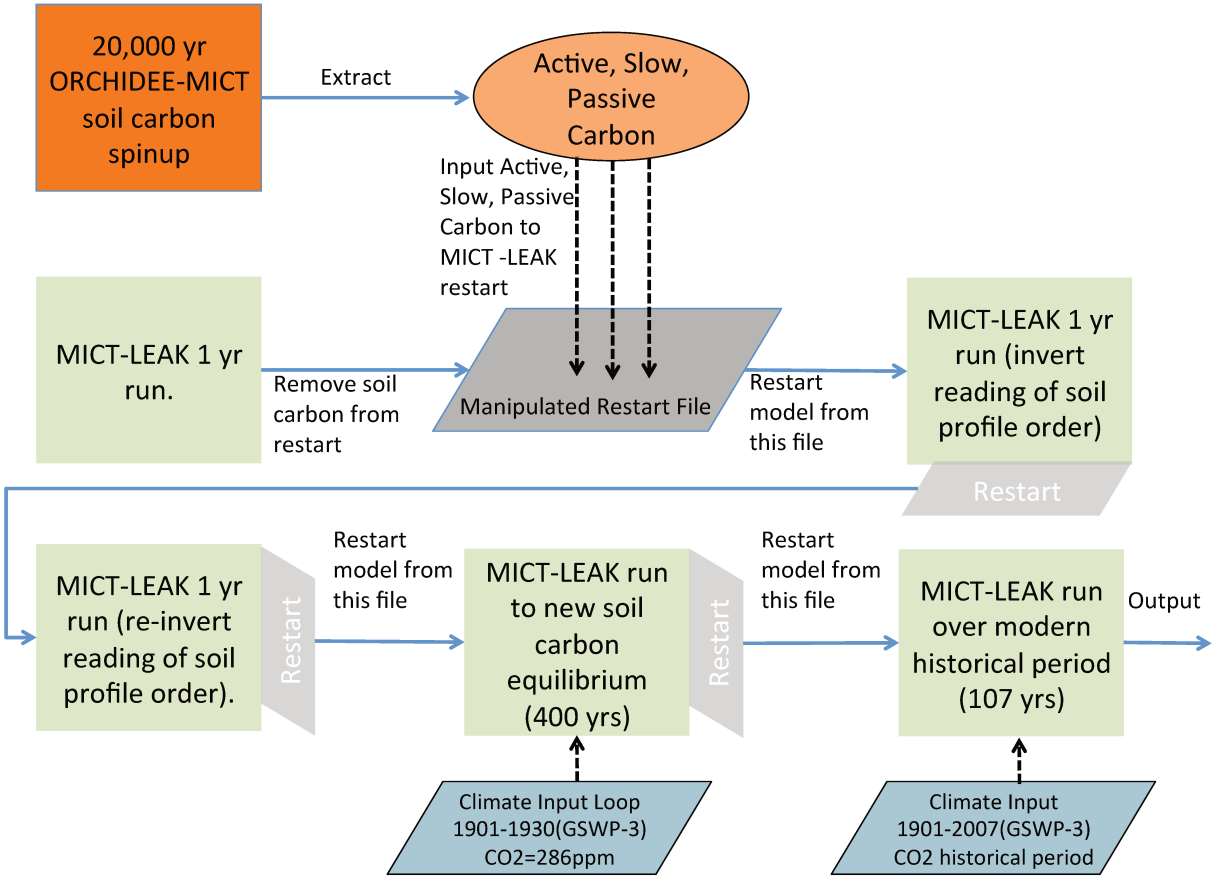

Figure 1: Flow diagram illustrating the step-wise stages required to set up the model, up to and including the historical period. The two stages that refer to the inverted reading of restart soil profile order point to the fact that the restart inputs from ORCHIDEE-MICT are read by our model in inverse order, so that one year must be run in which an activated flag reads it properly, before the reading of soil profile restarts is re-inverted for all subsequent years.

3 Simulation Setup

As detailed in Part 1 (Section 3.1), the soil carbon stock used by our model was reconstituted from the soil carbon spinup of an ORCHIDEE-MICT run from Guimberteau et al. (2018)(Guimberteau et al., 2018) and run to quasi-steady state equilibrium for the Active and Slow carbon pools (Supplement, Fig. S1) under the new soil carbon scheme used in the model configuration of the present study (Fig. 1). After some adjustment runs to account for different data read/write norms between ORCHIDEE-MICT and this model version, the model was then run in transient mode under historical climate, land cover and atmospheric CO_2 concentrations. A summary of the step-wise procedure for simulation setup described above is detailed graphically in Fig. 1. The model was forced with and run over the climate, CO_2 and vegetation input forcing data for the period spanning 1901-2007 (Supplement, Table S1).

Table 1: Summary describing of the factorial simulations undertaken to examine the relative drivers of lateral fluxes in our model.

Simulation Name	Abbreviation	Historical Input Data	Input* Held Constant
Control	CTRL	Climate, CO2, Vegetation	None
Constant Climate	CLIM	CO2, Vegetation	Climate
Constant CO2	CO2	Climate, Vegetation	CO2 (Pre-industrial)

*Historically-variable input

In order to derive an understanding of the environmental drivers of carbon cycling in the Lena watershed and analyze the model sensititivity to the corresponding forcing data, alternative simulations were run with constant climate and CO_2 conditions (Table 1, and Supplement Table S1). Thus a factorial simulation was devised, consisting of 2 factors and 3 simulations whose inputs were otherwise identical but for the investigated factor (Table 1).

4 Results and Discussion

We refer to different simulations performed in this study according to the sensitivity factors to which they are subjected. The 'Control' (CTRL) simulation is that for which transient climate and atmospheric CO_2 forcings are used. CLIM and CO_2 are those simulations for which climate variability and atmospheric CO_2 were held constant at their pre-industriela levels, respectively (Table 1). The following evaluation sections compare observations solely against the CTRL. The subsequent section will evaluate this comparison against the factorial simulations described above.

The overall carbon budgets and their fluxes as generated by each of the simulations are shown in Figs. 2 and 11 and discussed in detail at the end of the evaluation. Below, we examine that budget's component parts, in the following sequential order: In section 4.1 we briefly look through the overall carbon budget of the entire basin, discussing component fluxes of the budget, their values and what they mean. Section 4.2 evaluates DOC discharge, followed by DOC concentrations in export (4.3), dissolved CO_2 transport in rivers and its evasion from the river surface (4.4), emergent phenomena with respect to CO_2 evasion compared to river size (4.5.1) and DOC concentrations and slope (4.5.2), followed by DOC reactivity pools (4.6) and NPP and soil respiration (4.7). Wherever possible, model output are compared with available in situ observations, while emergent relationships between fluxes or concentrations and environmental controls found in observatons are also drawn from the model output, to provide a 'process oriented' evaluation of the model. In Section 4.8 we discuss the overall drivers of the fluxes simulated by our model with respect to the two CLIM and CO_2 factorial simulations and the implications of these for the future.

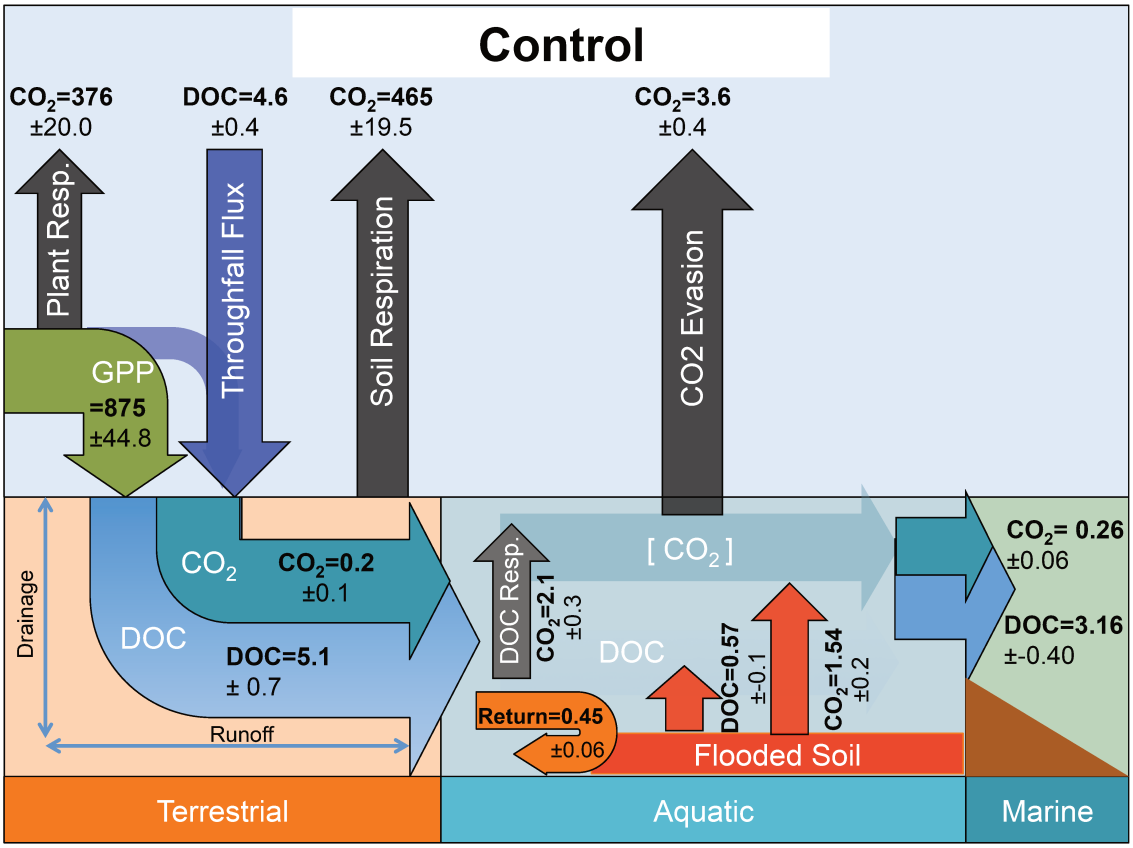

Figure 2: Schematic diagrams detailing the major yearly carbon flux outputs (TgC yr^{-1}) from the Control simulation averaged over the period 1998-2007 as they are transformed and transported across the land-aquatic continuum.

4.1 Carbon Budget: Simulated yearly fluxes

Fig. 2 summarises the components of the carbon cycle across the Lena basin, averaged over the decade 1998-2007. All units are in TgC yr^{-1} and the errors are derived from average yearly standard deviations for each of these fluxes. Modelled carbon inputs to terrestrial ecosystems are dominated by photosynthetic input (GPP). GPP assimilates (875 TgC yr^{-1}) are either used as metabolic substrate by plants and lost as CO_2 by plant respiration processes (376 TgC yr^{-1}) or soil respiration processes (465 TgC yr^{-1}), leaving behind annual terrestrial carbon storage in living biomass and soil, known as net biome productivity (NBP, a sink of atmospheric CO_2 of 34 TgC yr^{-1}). Further carbon inputs are delivered to the terrestrial surface via a combination of atmospheric deposition, rainwater dissolved carbon, and the leaching of canopy carbon compounds, all of which summing up to a flux transported to the soil surface (4.6 TgC yr^{-1}) by throughfall (see Part 1, Section 2.5).

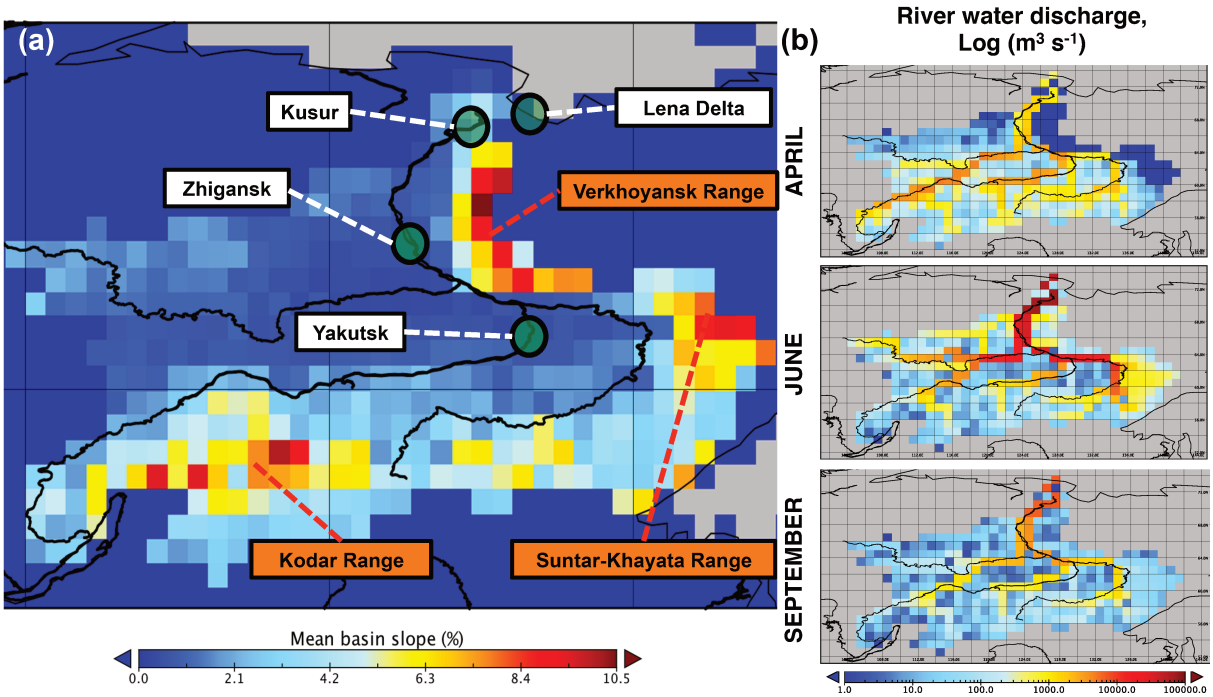
(a)
Kusur
Lena Delta
Zhigansk
Verkhoyansk Range
Yakutsk
Kodar Range
Suntar-Khayata Range
Mean basin slope (%)
0.0
2.1
4.2
6.3
8.4
10.5
(b)
River water discharge,
Log (m³ s⁻¹)
APRIL
JUNE
SEPTEMBER
1.0
10.0
100.0
1000.0
10000.0
100000.0

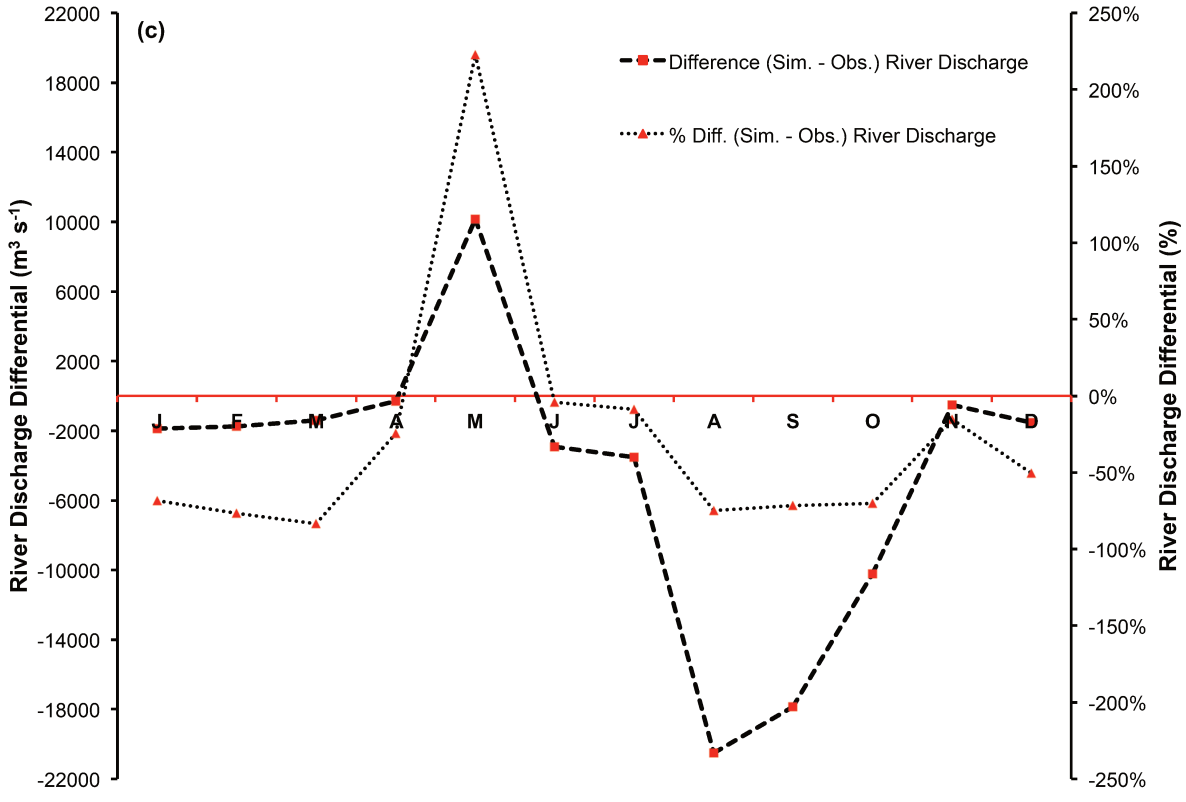
(c)
Difference (Sim. - Obs.) River Discharge
% Diff. (Sim. - Obs.) River Discharge
River Discharge Differential (m³ s⁻¹)
River Discharge Differential (%)
22000
18000
14000
10000
6000
2000
-2000
-6000
-10000
-14000
-18000
-22000
250%
200%
150%
100%
50%
0%
-50%
-100%
-150%
-200%
-250%
J
F
M
A
M
J
J
A
S
O
N
D

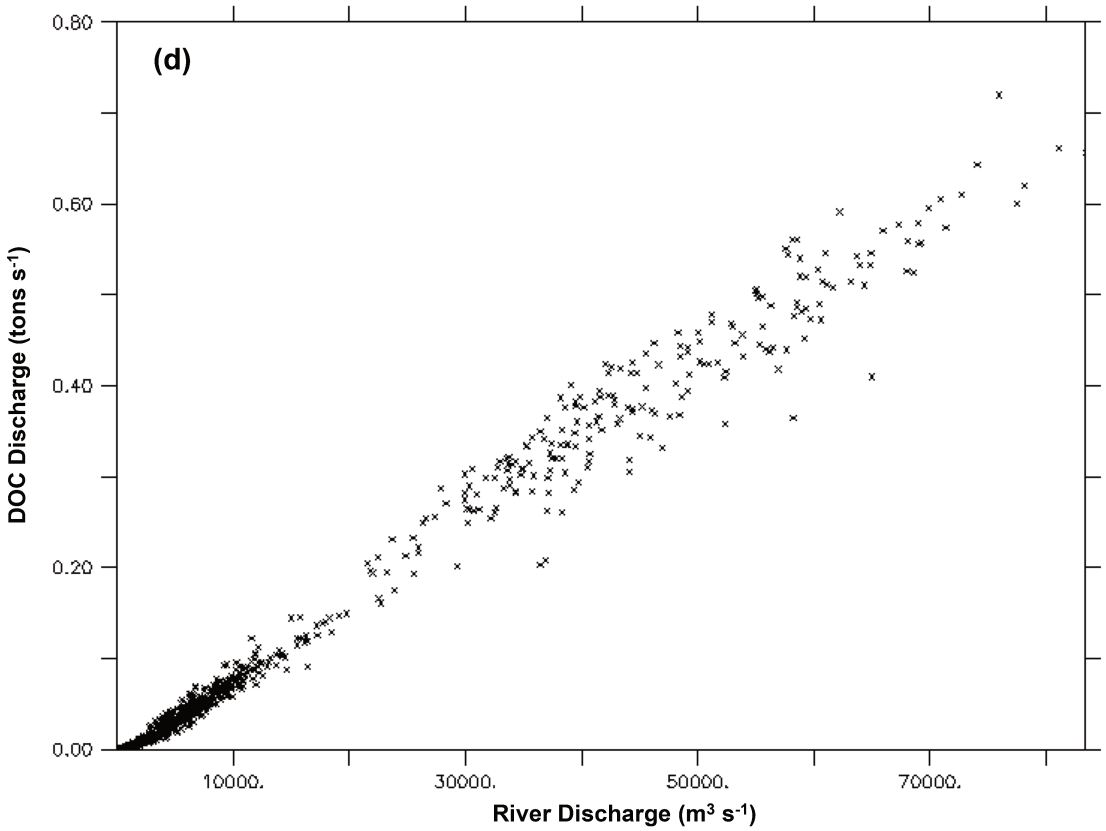

Figure 3: Map of the Lena **(a)** with the scale bar showing the mean grid cell topographic slope from the simulation, and the black line the satellite-derived overlay of the river main stem and sub-basins. Mountain ranges of the Lena basin are shown in orange. Green circles denote the outflow gridcell (Kusur) from which our simulation outflow data are derived, as well as the Zhigansk site, from which out evaluation against data from Raymond et al. (2007) are assessed. The regional capital (Yakutsk) is also included for geographic reference. **(b)** Maps of river water discharge (log(m^3 s^{-1})) in April, June and September, averaged over 1998-2007. **(c)** The mean monthly river discharge differential between observed discharge for the Lena (Ye et al., 2009) and simulated discharge averaged over 1998-2007, in absolute (m^3 s^{-1}) and percentage terms. **(d)** Regression of simulated monthly DOC discharge versus simulated river discharge at the river mouth (Kusur) over the entire simulation period (1901-2007).

In the soil, DOC is produced by the decomposition of litter and soil organic carbon (SOC) pools (see Part 1, Section 2.4 and Fig. 2) and can be ad- or de- sorbed to solid particles (see Part 1, Section 2.11), while there is a continuous exchange of DOC with (solid) soil organic carbon. The interplay between decomposition and sorption leads to DOC concentration changes in the soil solution. DOC in the soil solution as well as a fraction of dissolved CO_2 produced in the root zone from root and microbial respiration is exported to rivers along the model's two hydrological export vectors, surface runoff and deep drainage (Part 1, Section 2.6). For the Lena basin simulations, these fluxes of C exported from soils amount to 5.1 and 0.2 TgC yr^{-1}, for DOC and CO_2 respectively. Three water pools, representing streams, rivers and groundwater and each containing dissolved CO_2 and well as DOC of different reactivity, are routed through the landscape and between grid cells following the river network in the catchment (Part 1, Section 2.7). In addition, seasonally flooded soils located in low, flat grid cells next to the river network (see Part 1, Section 2.8) export DOC (0.57 TgC yr^{-1}) and CO_2 (1.54 TgC yr^{-1}) to the river network when their inundation occurs. Part of this leached inundated material is reinfiltrated

back into the soil from the water column during floodplain recession ('Return' flux, 0.45 TgC yr^{-1}). During its transport through inland waters, DOC can be decomposed into CO_2 (2.1 TgC yr^{-1}) and a fraction of river CO_2 produced from DOC and transferred from soil escapes to the atmosphere (3.6TgC yr^{-1}) through gas exhange kinetics (Part 1, Section 2.10). This flux is termed 'CO_2 evasion' in Fig. 2 of this study. Carbon that 'survives' the inland water reactor is exported to the coastal ocean in the form of DOC (3.16 TgC yr^{-1}) and CO_2 (0.26 TgC yr^{-1}). These fluxes and their interpretation within the context of the Land-Ocean-Aquatic Continuum (LOAC) are returned to in Section 4.8 of this study.

4.2 Discharge and DOC flux to the ocean

Simulated river water discharge captures the key feature of Arctic river discharge – that of a massive increase in flow to ~80,000 m^3s^{-1} in April-June caused by melting snow and ice, otherwise known as ice-out or spring freshet, but underestimates observed river discharge in August to October by around 70% which is in the range of ~15,000-28,000 m^3s^{-1} (Figs. 3c, 4b). Given that DOC fluxes are almost directly proportional to river discharge in the Lena basin (Fig. 3d), this sub-optimal performance with regard to hydrology during August to October seeming to be the main cause of a substantial underestimation in simulated bulk DOC outflow. Another cause may simply be the lack of peat representation in the model, for which DOC flux concentrations in outflowing fluvial water can be very high (e.g. Frey et al., 2005; 2009: see Section 4.5.1).

In addition, the mean spring (June) discharge peak flows are slightly underestimated or out of phase in simulations (Figs. 3c, 4b) compared to observations(Ye et al., 2009): this is caused by a large amount of water throughput being simulated in May (~10,000 $m^3 s^{-1}$) in excess of observed rates. Finally, during the winter low-flow period, it seems that the model consistently under-estimates water flow-through volumes reaching the river main stem (see Fig. 3c, winter months). Although this underestimate is not severe relative to annual bulk flows, the divergence is large as a percentage of observations (see right-hand axis, Fig. 3c), and may point to an issue in how ice is represented in the model, such as the fact that solid ice inclusions in the soil column are not represented, or the possibility that much slower groundwater dynamics than those represented in the model are feeding discharge.

In addition to this, the presence of a dam on the Vilui tributary of the Lena has been shown to reduce main stem winter low-flow rates by up to 90% (Ye et al., 2003), similar to the discrepancy of our low-flow rates: given that our model only simulates 'natural' hydrological flows and thus does not include dams, we expect that this effect is also at play. Evaluating these considerations, if presently possible, remains beyond the scope of this paper. We note that discharge simulations with ORCHIDEE MICT (Fig. 12 of Guimberteau et al. (2018)(Guimberteau et al., 2018)) performed with the same climate forcing over the basin are comparable with those from ORCHIDEE MICT-L, with similar overall seasonality and discharge peaks of ~60,000$m^3 s^{-1}$ in the former over the period 1981-2007. This indicates that the modifications made in Bowring et al. (Part 1) focussing on the DOC cycle did not degrade the hydrological performance of the model in this regard.

Our CTRL simulation shows that the yearly sum of DOC output to the Arctic Ocean has

increased steadily over course of the 20th Century, from ~1.4Tg DOC-C yr^{-1} in 1901 to ~4Tg DOC-C yr^{-1} in 2007 (Fig. 4a). Smoothing the DOC discharge over a 30-year running mean shows that the increasing trend (Fig. 4a) over this averaging scale is almost linear, at ~0.11TgC per decade, or a net increase of 40% using this averaging scale. Empirically based estimates of total contemporary DOC entering the Laptev Sea from Lena river discharge vary around ~2.5-5.8 TgC-DOC (Cauwet and Sidorov, 1996; Dolman et al., 2012; Holmes et al., 2012; Lara et al., 1998; Raymond et al., 2007; Semiletov et al., 2011).

The red bar in Fig. 4a shows the average simulated DOC discharge of the last decade (1998-2007) of 3.2 TgC yr^{-1}, to be compared with estimates of 3.6 TgC yr^{-1} (black bar) from Lara et al. (1998)(Lara et al., 1998) and 5.8 TgC yr^{-1} (orange bar) from Raymond et al. (2007) and 5.7 TgC yr^{-1} from Holmes et al. (2012). These estimates are based on different years, different data and different scaling approaches, whose veracity or accuracy are beyond the scope of this study to address or assess.

Nonetheless, the most recent and elaborate of those estimates is that of Holmes et al. (2012) who used a rating curve approach based on 17 samples collected from 2003 to 2006 and covering the full seasonal cycle, which was then applied to 10 years of daily discharge data (1999-2008) for extrapolation. Given that their estimate is also based on Arctic-GRO-1/PARTNERS data (https://www.arcticgreatrivers.org/data), which stands as the highest temporal resolution dataset to date, we presume that their estimate can be taken to be the most accurate of the actual riverine discharge of DOC from the Lena basin. Compared to their average annual estimate of 5.7 Tg C yr^{-1} then, our simulated DOC export is somewhat low, which can be due to multiple causes:

Firstly, as noted above, the model underestimates observed river discharge. We plot seasonal DOC discharge against river discharge for the Lena outflow grid cell (Kusur station –see Fig. 3a) over 1901-2007 in Fig. 3d, which shows a quasi-linear positive relationship between the two. This dependence is particular to the Arctic rivers, in which the DOC yield of rivers experiences disproportionately large increases in output with increases in discharge yield (Fig. 4, Raymond et al., 2007), relative to the same relationship in e.g. temperate rivers like the Mississippi (Fig. 3, Raymond et al., 2007), owing largely to the 'flushing' out of terrestrially fixed carbon from the previous year's production by the massive runoff generated by ice and snow melt during the spring thaw.

Average river discharge almost doubled between the first and last decades of our simulation (Fig 4b), giving further credence to the relationship between DOC and water discharge. Comparing simulated annual mean discharge rate (m^3 s^{-1}) with long-term observations(Ye et al., 2003) over years 1940-2000 (Fig. 4c) shows that though absolute discharge rates are underestimated by simulations, their interannual variation reasonably tracks the direction and magnitude of observations. Linear regressions through each trend yield very similar yearly increases of 29 vs 38 m^3 s^{-1} yr^{-1} for simulations and observations, respectively, while the mean annual water discharge differential hovers at 30% (Fig. 4c), a fraction similar to that of the simulated and observed(Holmes et al., 2012; Raymond et al., 2007) bulk annual DOC discharge discrepancy (Fig. 4a). Figure 4b plots discharge over the first (1901-1910) and last

(1998-2007) decades of simulated monthly DOC and river discharge with observed river discharge. The bulk of the DOC outflow occurs during the spring freshet or snow/ice-melting period of increased discharge, accounting for ~50-70% of the year's total Lena outflow to the Arctic (Lammers et al., 2001; Ye et al., 2009), with peak river discharge rates in June of ~80,000 $m^3 s^{-1}$. DOC concentrations increase immensely at this time, as meltwater flushes out DOC accumulated from the previous year's litter and SOC generation(Kutscher et al., 2017; Raymond et al., 2007).

(a)

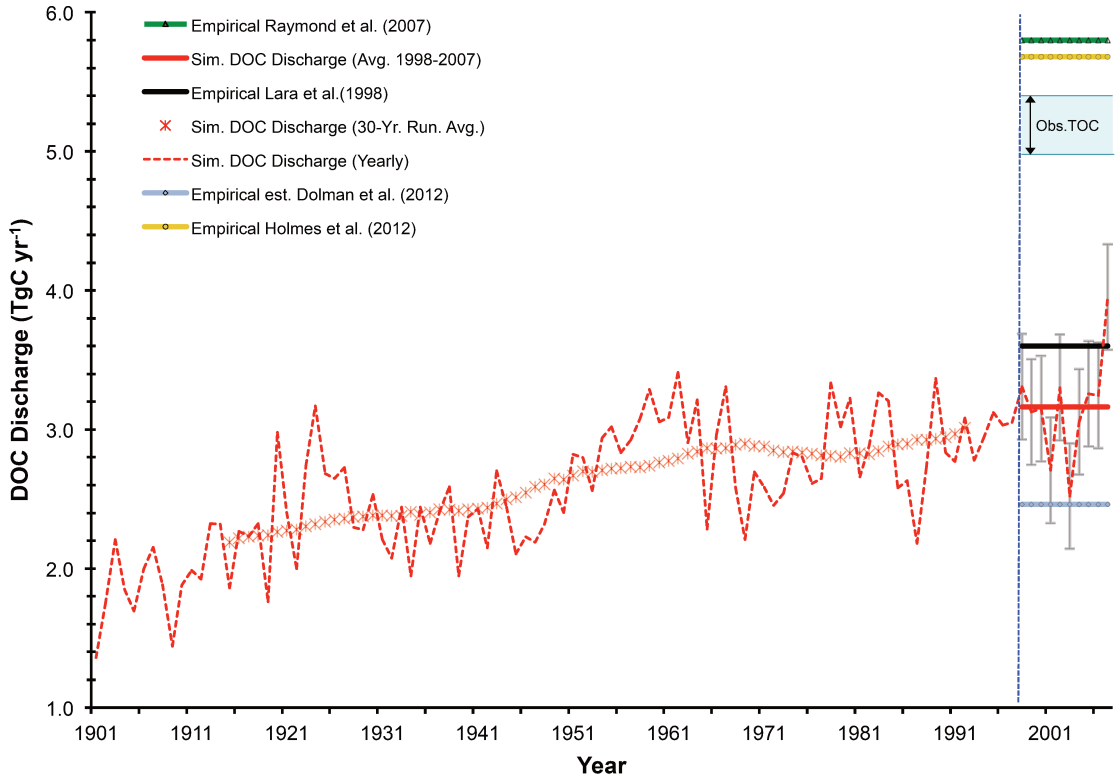

(b)

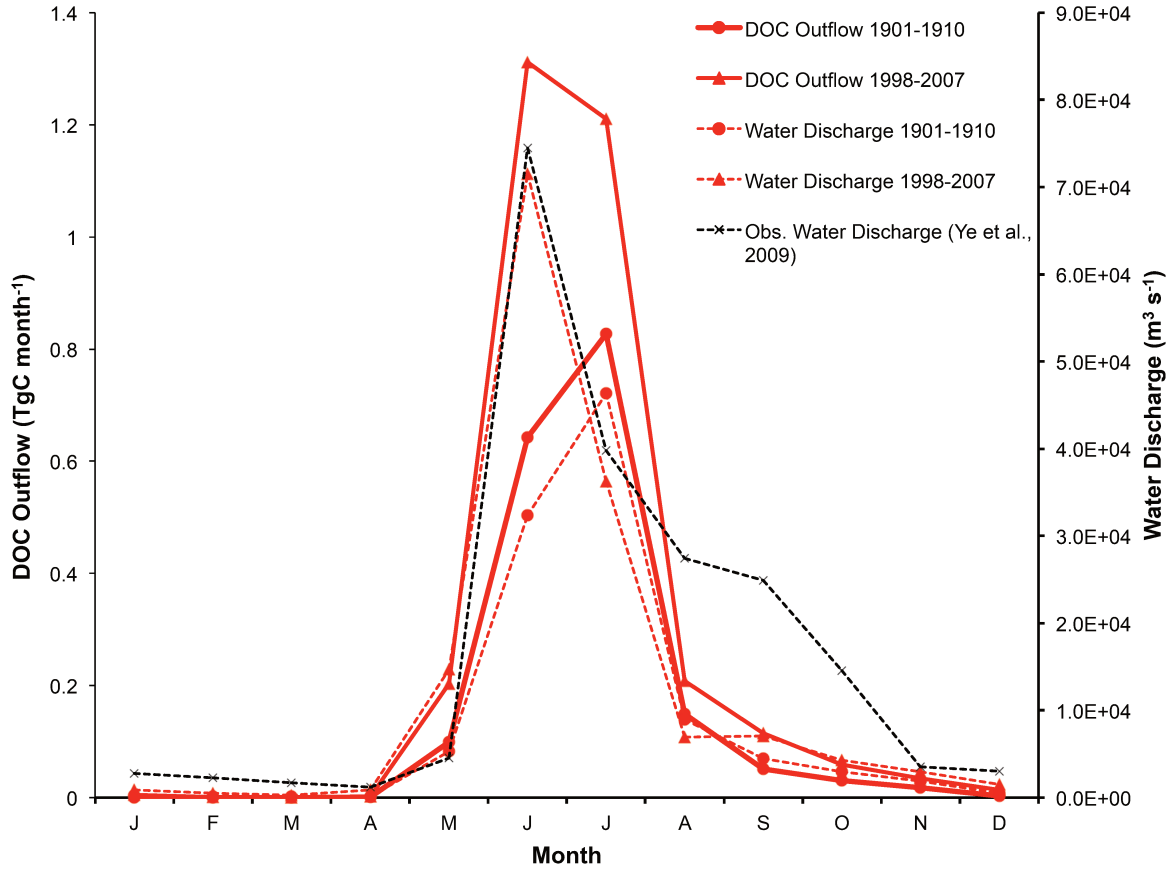

1984

1985 **(c)**

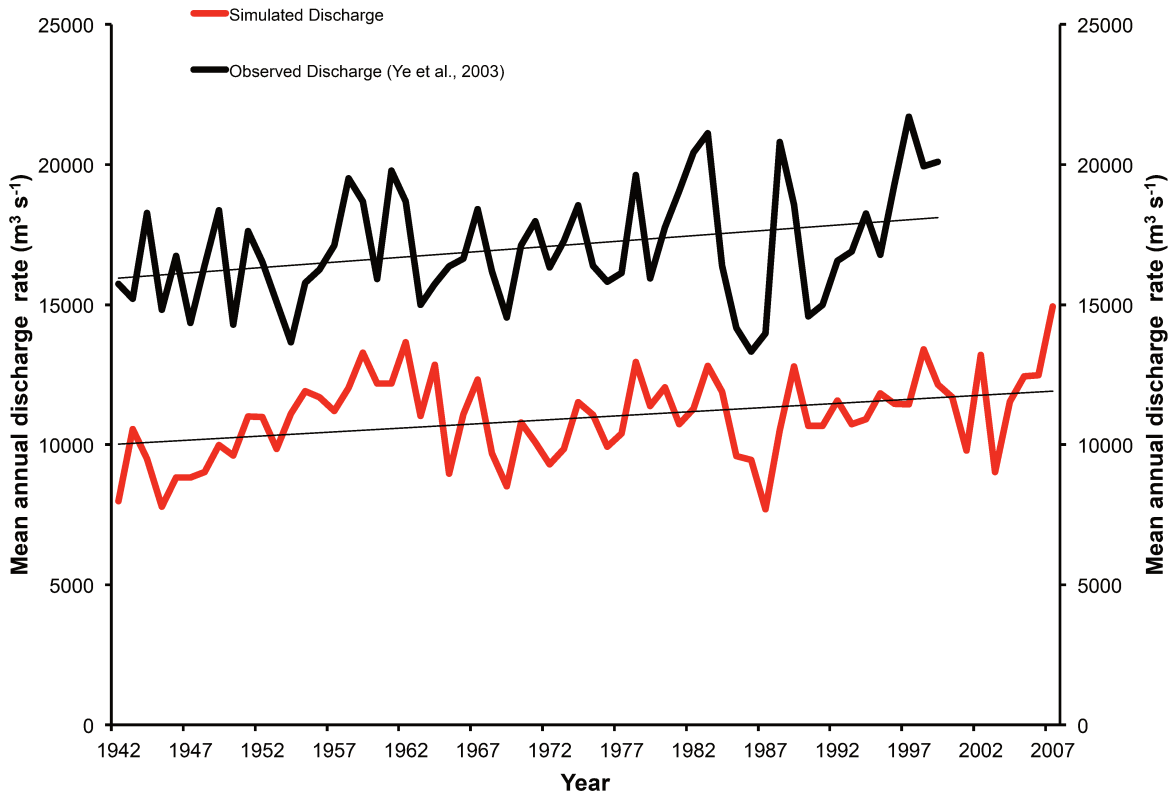

1986

(d)

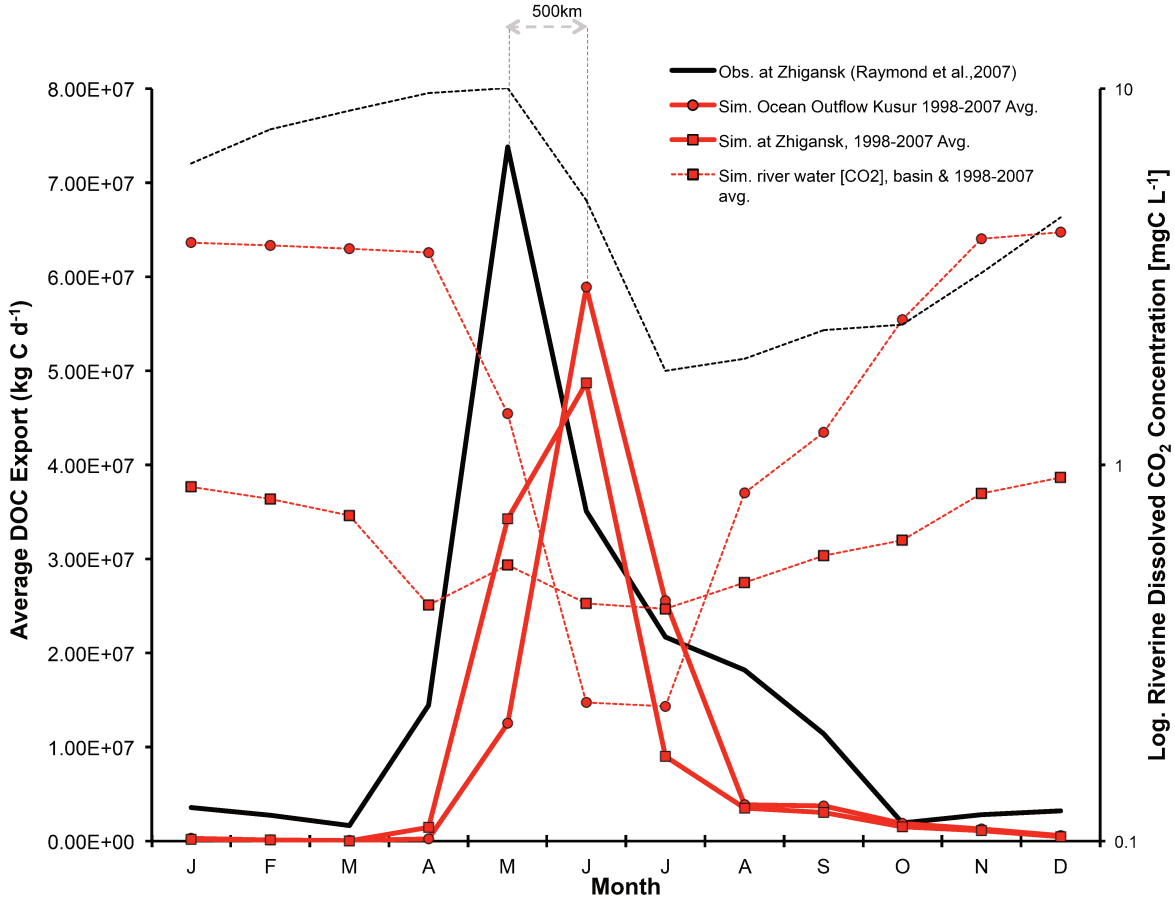

Figure 4: **(a)** Yearly DOC discharged from the Lena river into the Laptev sea is shown here in tC yr^{-1}, over the entire simulation period (dashed red line), with the smoothed, 30-year running mean shown in asterisk. Observation based estimates for DOC discharge from Lara et al. (1998), Raymond et al. (2007), Dolman et al. (2012) and Holmes et al. (2012) are shown by the horizontal black, green triangle, blue diamond and yellow circle line colours and symbols, respectively, and are to be compared against the simulated mean over the last decade of simulation (1998-2007, horizontal red line), with error bars added in grey displaying the standard deviation of simulated values over that period. The range of estimates for total organic carbon discharged as shown in Lara et al. (1998) are shown by the blue bounded region, where TOC here refers to DOC+POC. **(b)** Average monthly DOC discharge (solid red, tC $month^{-1}$) and water discharge (dashed red, m^3 s^{-1}) to the Laptev Sea over the period averaged for 1901-1910 (circles) and 1997-2007 (squares) are compared, with modern maxima closely tracking observed values. Observed water discharge over 1936-2000 from R-ArcticNet v.4 (Lammers et al., 2001) and published in Ye et al. (2009) are shown by the dashed black line. (c) **(d)** Observed (black) and simulated (red) seasonal DOC fluxes (solid lines) and CO_2 discharge concentrations (dashed lines). Observed DOC discharge as published in Raymond et al. (2007) from 2004-2005 observations at Zhigansk, a site ~500km upstream of the Lena delta. This is plotted against simulated discharge for: (i) the Lena delta at Kusur (red circles) and (ii) the approximate grid pixel corresponding to the Zhigansk site (red squares) averaged over 1998-2008. Observed CO_2 discharge from a downstream site (Cauwet & Sidorov, 1996; dashed black), and simulated from the outflow site (dashed circle) and the basin average (dashed square) are shown on the log-scale right-hand axis for 1998-2008.

This is reproduced in our simulations given that DOC discharge peak occurs at the onset of the growing season, meaning that outflow DOC is generated from a temporally prior stock of organic carbon. Simulation of the hydrological dynamic is presented in maps of

river discharge through the basin in Fig. 3b, which show low-flows in April with substantial hydrographic flow from upstream mountainous headwaters and Lake Baikal inflow in the south, peak flow in June with substantial headwater input in the northern portion and a moderate flow through the mainstem with little headwater input in September.

In Fig. 4b we observe that (i) DOC discharge fluxes closely track hydrological fluxes (solid versus dashed lines); (ii) the simulated modern river discharge peak is very close to the historical observed discharge peak, however it slightly overestimates spring fluxes and substantially underestimates fluxes in the Autumn (dashed red versus black lines). Thus the discrepancy between simulated bulk DOC discharge fluxes and empirical estimates may largely be found in the simulated hydrology. (iii) The curve shape of discharge fluxes differs greatly between the first and last decades of simulation.

The difference between the first and last decades of the simulation in Fig. 4b is mostly attributable to a large increase in the DOC flux mobilised by spring freshet waters that culminate in the early summer outflow of DOC to the ocean, which generate the peaks in DOC flux. This suggests both greater peaks in simulated DOC flux and a shift to earlier peak timing, owing to an increase in river discharge indicative of an earlier spring and a progressively warmer environment. (iv) The maximum modeled modern monthly DOC flux rate of ~1.3 TgC $month^{-1}$ (Fig. 4b, solid red line) is comparable to the mean maximum DOC flux rate measured in a recent study, which showed that the aggregate carbon discharge flux of the Lena River over its 2-month peak period in 2013 was 3.5 TgC, giving a mean flux of 1.75 TgC $month^{-1}$ (Kutscher et al., 2017, Fig. 2(Kutscher et al., 2017)).

The monthly pattern of DOC discharge approximates the seasonal pattern found in an empirical Pan-Arctic DOC discharge study by Raymond et al. (2007), which they take to represent total Lena river DOC discharge. The latter study, which looks at Pan-Arctic DOC discharge rates, finding them to be 15-20% higher than in prior estimates, gives discharge maxima in May, whereas our simulated maxima are in June. We compare the Raymond et al. (2007) modern DOC outflow (Fig. 4d, solid black line) from the Lena river at Zhigansk (Raymond et al., 2007) against simulated DOC outflow from the Zhigansk site as well as from the river outflow site (Kusur) 500km downstream (Fig. 4d, solid blue and solid red lines, respectively).

Simulated DOC flux is underestimated for both sites. Peakflow at Zhigansk seems to be attenuated over May and June in simulations, as opposed to May peakflow in observations, while peakflow at Kusur is definitively in June. This suggests that simulated outflow timing at Zhigansk may slightly delayed, causing a split in peak discharge when averaged in the model output. Thus the aggregation of model output to monthly averages from calculated daily and 30 minute timesteps can result in the artificial imposition of a normative temporal boundary (i.e. month) on a continuous series. This may cause the less distinctive 'sharp' peak seen in Fig. 4d (solid blue), which is instead simulated at the downstream Kusur site, whose distance some 500km away from Zhigansk more clearly explains the delay difference in seasonality.

We further evaluate our DOC discharge at the sub-basin scale, to see if the simulated aggregate flux exiting the Lena river mouth is composed of a coarsely realistic breakdown of source matter geography. In other words, whether the fractional contribution of different DOC flows from rivers draining the simulated Lena basin correspond to those in the observed basin. This comparison is depicted in Fig. 5, where, again using data from Kutscher et al., (2017)(Kutscher et al., 2017), the observed and simulated percentage DOC contributions of the Aldan, Vilui, and Upper and Lower Lena sub-basins to total flux rates are 19 (24)%, 20(10%), 33 (38%) and 30 (28)% in simulations (observations) for the four basins, respectively.

While deviations between simulation and observation can be expected given the difference in magnitude and timing of DOC discharge previously discussed, in addition to interannual variability, the nearly twofold value mismatch of the Vilui basin likely has its roots in the fact in its real-word damming, not represented here. On the other hand, we cannot explain the ~5% discrepancies in other sub-basin fluxes, particularly for the Aldan.

Of the shortcomings in our model with respect to observations, year-on-year variations over the decade 1998-2007 may be of significance, given that the Holmes et al. (2012) and Raymond et al. (2007) DOC discharge values are significantly higher than total organic carbon (DOC+POC) outflow estimates (~5.0-5.4 TgC yr^{-1}, Fig. 4a blue boundary) as presented in Lara et al. (1998)(Lara et al., 1998). To this we can add scale-related inaccuracies in the routing protocol that can lead to small geographic inconsistencies in simulated versus observed phenomena, as well as the exclusion of explicit peatland formation and related dynamics in this model, which is the subject of further model developments within the ORCHIDEE-MICT envelope(Qiu et al., 2018) that have yet to be included in this iteration. With peatlands thought to cover ~17% of the Arctic land surface (Tarnocai et al., 2009), and with substantially higher leaching concentrations, this may be a significant omission from our model's representation of high latitude DOC dynamics.

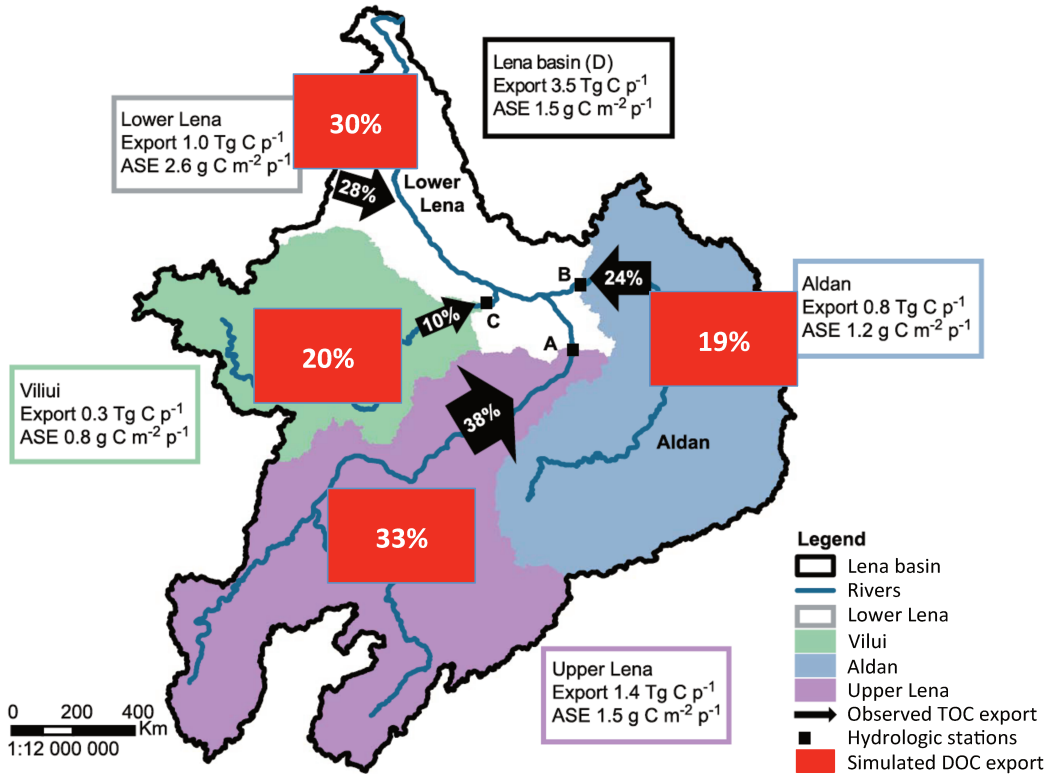

Figure 5: Map adapted from Fig. 2 in Kutscher et al. (2017) showing proportional sub-basin contributions of TOC outflow to total TOC discharge in 2012-2013 as observed in Kutscher et al., 2017 (black arrows), and DOC export contributions as simulated over the period 1998-2007 by ORCHIDEE MICT-L (red boxes). Simulation pixels used in the calculation are correlates of the real-world sampling locations unless the site coordinates deviated from a mainstem hydrographic flowpath pixel –in which case a nearest 'next-best' pixel was used. Here the percentages are out of the summed mean bulk DOC flow of each tributary, not the mean DOC discharge from the river mouth, because doing so would negate the in-stream loss of DOC via degradation to CO_2 while in-stream.

4.3 DOC Concentrations in lateral transport

The range of simulated riverine DOC concentrations approximates those found in the literature for the Lena and other Eurasian high-latitude river basins (e.g. Arctic-GRO 1 (https://www.arcticgreatrivers.org/data); and refs.(Denfeld et al., 2013; Mann et al., 2015; Raymond et al., 2007; Semiletov et al., 2011)). In those for the Lena, observed average DOC concentrations hover at ~10mgC L^{-1}. Likewise, simulated DOC concentrations mostly lie in the range of 0-10 mgC L^{-1}, with monthly grid cell maxima of 1-200 mgC L^{-1}, and on flow-weighted average exhibit the observed seasonal range and amplitude. Figure 6 summarises some of this simulated output, showing maps of mean monthly DOC concentration for stream water, river water and groundwater (Fig. 6a,b,c, respectively) in April, June and September –the beginning, middle and end of the non-frozen period in the basin, respectively, over 1998-2007.

For both the stream and river water reservoirs, DOC concentrations appear to have spatio-temporal gradients correlated with the flux of water over the basin during the thaw period, with high concentrations of 10-15 mgC L^{-1} as the snow and ice melts in April in the upstream portions of the basin, these high concentrations moving

northward to the coldest downstream regions of the basin in June. Lower DOC concentrations of ~5 mgC L^{-1} dominate the basin in September when the bulk of simulated lateral flux of DOC has dissipated into the Laptev Sea, bearing in mind that we underestimate the river discharge flux in the Autumn. In contrast, groundwater DOC concentrations are generally stable with time, although some pixels appear to experience some 'recharge' in their concentrations during the first two of the three displayed thaw months. Significantly, highest groundwater DOC concentrations of up to 20 mgC L^{-1} are focussed on the highest elevation areas of the Lena basin on its Eastern boundary, which are characterized by a dominance of Podzols (SI, Fig. 2b).

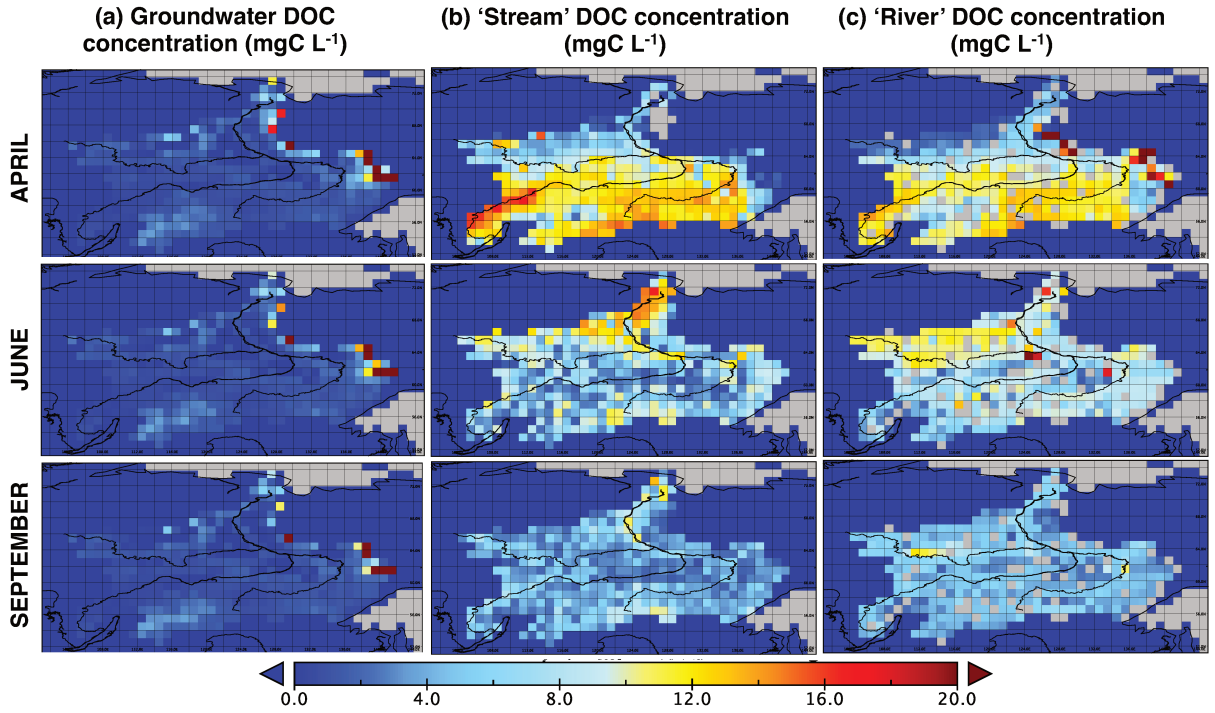

Figure 6: Maps of **(a)** DOC concentrations (mgC L^{-1}) in groundwater ('slow' water pool), **(b)** stream water pool, **(c)** river water pool in April, June and September (first to third rows, respectively), averaged over the period 1998-2007. The coastal boundary and a water body overlay have been applied to the graphic in black, and the same scale applies to all diagrams.

Table 2: Mean observed groundwater CO_2 and DOC concentrations for global permafrost regions subdivided by biogeographic province and compiled by Shvartsev (2008) from over 9000 observations.

	Permafrost Groundwater Provinces				
	Swamp	Tundra	Taiga	Average	Average (-Swamp)
CO_2 (mgC L^{-1})	12.3	14	10.8	12.4	12.4
DOC (mgC L^{-1})	17.6	10.1	9.3	12.3	9.7

This region, the Verkhoyansk range, is clearly visible as the high groundwater DOC concentration(2-20mgC L^{-1}) arc (in red) in Fig. 6a, as well as other high elevation areas

in the south-western portion of the basin (see Fig. 3a for the basin grid cell mean topographic slope), while the central basin of very low mean topographic slope exhibits much smaller groundwater DOC concentrations (0-2mgC L^{-1}). The range of simulated groundwater DOC concentration comes close to those aggregated from the empirical literature by Shvartsev (2008)(Shvartsev, 2008) in his seminal review of global groundwater geochemistry, which finds from >9000 observations that groundwater in permafrost regions exhibit a mean concentration of ~10 mgC L^{-1} after peatlands and swamps (not simulated here) are removed (Table 2).

The high groundwater reservoir DOC concentrations simulated in high altitude regions by ORCHIDEE MICT-L is related to the fact that, in the model, DOC is rapidly produced and infiltrated deep into soil above the permafrost table, to the point that it reaches the simulated groundwater pool relatively quickly, allowing it to enter this reservoir before being metabolised through the soil column –hence allowing for the relatively high groundwater concentrations found in mountain areas. Because of the prevailing low temperatures, this DOC is not quickly decomposed by microbes and instead feed the groundwater DOC pool.

4.4 In-Stream CO2 Production, Transport, Evasion

In our model, the fate of DOC once it enters the fluvial system is either to remain as DOC and be exported to the ocean, or to be degraded to dissolved CO_2 ($CO_{2(aq.)}$), which is itself either also transported to the marine system or outgassed from the fluvial surface to the atmosphere (see Part 1, Section 2.10). The latter two outcomes also apply to $CO_{2(aq.)}$ produced in the soil by organic matter degradation and subsequently transported by runoff and drainage flows to the water column. As shown in Fig. 2, a large proportion of DOC (38%, 2.1 TgC yr^{-1}) that enters the water column is degraded to $CO_{2(aq.)}$ during transport, which adds to the 1.65 TgC yr-1 of direct $CO_{2(aq.)}$ input from the terrestrial land surface. Of this bulk CO_2 exported into and generated within the water column, 3.6 TgC yr^{-1} evades from the water surface to the atmosphere before reaching the river delta. In what follows, we evaluate first inputs of $CO_{2(aq.)}$ to the water column in terms of their seasonality, before evaluating CO_2 evasion rates and the relation of this to smaller and larger water bodies (river versus stream).

The seasonality of riverine dissolved CO_2 concentrations ($CO_{2(aq.)}$, mgC L^{-1}) is evaluated in Fig. 4d to compare $CO_{2(aq.)}$ concentrations with DOC bulk flows, since $CO_{2(aq.)}$ concentrations follow an inverse seasonal pattern to those of DOC, being highest during the winter baseflow period and lowest in summer due to dilution during its high discharge phase (Semiletov et al., 2011). The simulated flow of $CO_{2(aq.)}$ at Kusur (Fig. 4d, dashed red) reproduces the seasonality of observations from Cauwet and Sidorov (1996)(Cauwet and Sidorov, 1996), who sampled the Lower Lena (ship-board, several sites in river delta region (see Fig. 3a)), but somewhat underestimates concentrations, this perhaps due to the absence of peat representation in our model, in combination with underestimated hydrological discharge. Also included in Fig. 4d is the basin average for all non-zero values, whose shape also tracks that of observations. Thus the model represents on the one hand increasing hydrological flow mobilising increasing quantities and concentrations of DOC while on the other hand those same increasing hydrological flows increasing the flux, but decreasing the concentration, of $CO_{2(aq.)}$

throughput.

To our knowledge, no direct measurements for CO_2 evasion from the surface of the Lena river are available in the literature, presumably owing to the notorious difficulty in successfully obtaining such data. We refer to Denfeld et al. (2013)(Denfeld et al., 2013) for evaluating our evasion flux results, since their basin of study, the Kolyma River, is the most geographically proximate existing dataset to the Lena, despite biogeographical differences between the two basins –namely that the Kolyma is almost entirely underlain by continuous permafrost. The Kolyma River CO_2 evasion study measured evasion at 29 different sites along the river basin (~158-163°E; 68-69.5°N), with these sites distinguished from one another as 'main stem', 'inflowing river' or 'stream' on the basis of reach length. The study showed that during the summer low-flow period (August), areal river mainstem CO_2 evasion fluxes were ~0.35 gC m^{-2} d^{-1}, whereas for streams of stream order 1-3 (widths 1-19m), evasion fluxes were up to ~7 gC m^{-2} d^{-1}, and for non-mainstem rivers (widths 20-400m) mean net fluxes were roughly zero (Table 3 of Denfeld et al., 2013). Thus, while small streams have been observed to contribute to roughly 2% of the Kolyma basin surface area, their measured percentage contribution to total basin-wide CO_2 evasion ~40%, whereas for the main stem the surface area and evasion fractions were ~80% and 60%, respectively.

(a)

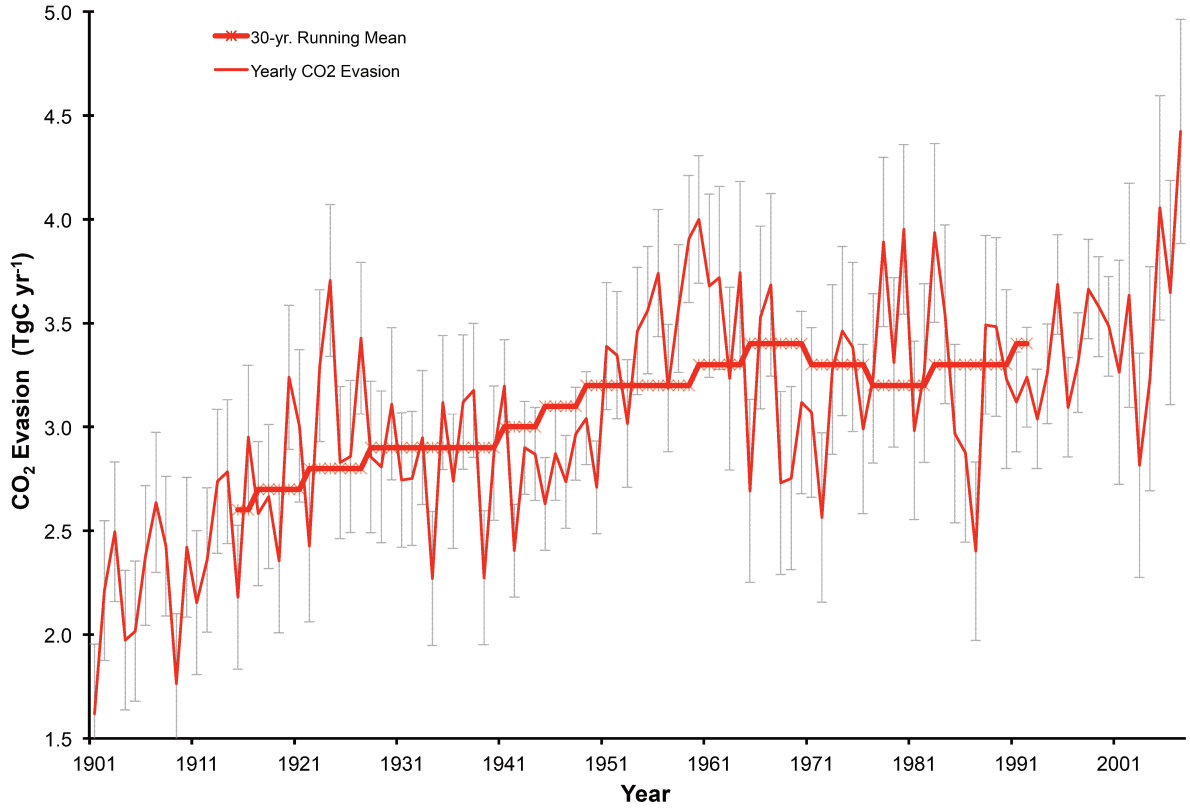

(b)

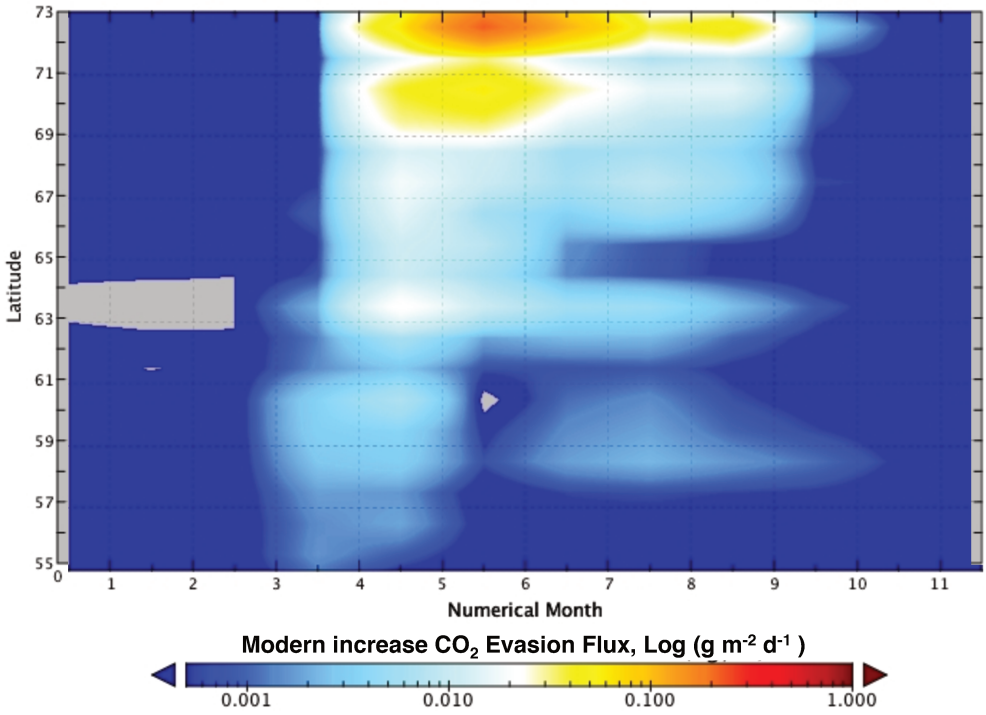
Latitude
73
71
69
67
65
63
61
59
57
55
0
1
2
3
4
5
6
7
8
9
10
11
Numerical Month
Modern increase CO_2 Evasion Flux, Log (g m^{-2} d^{-1})
0.001
0.010
0.100
1.000

(c)

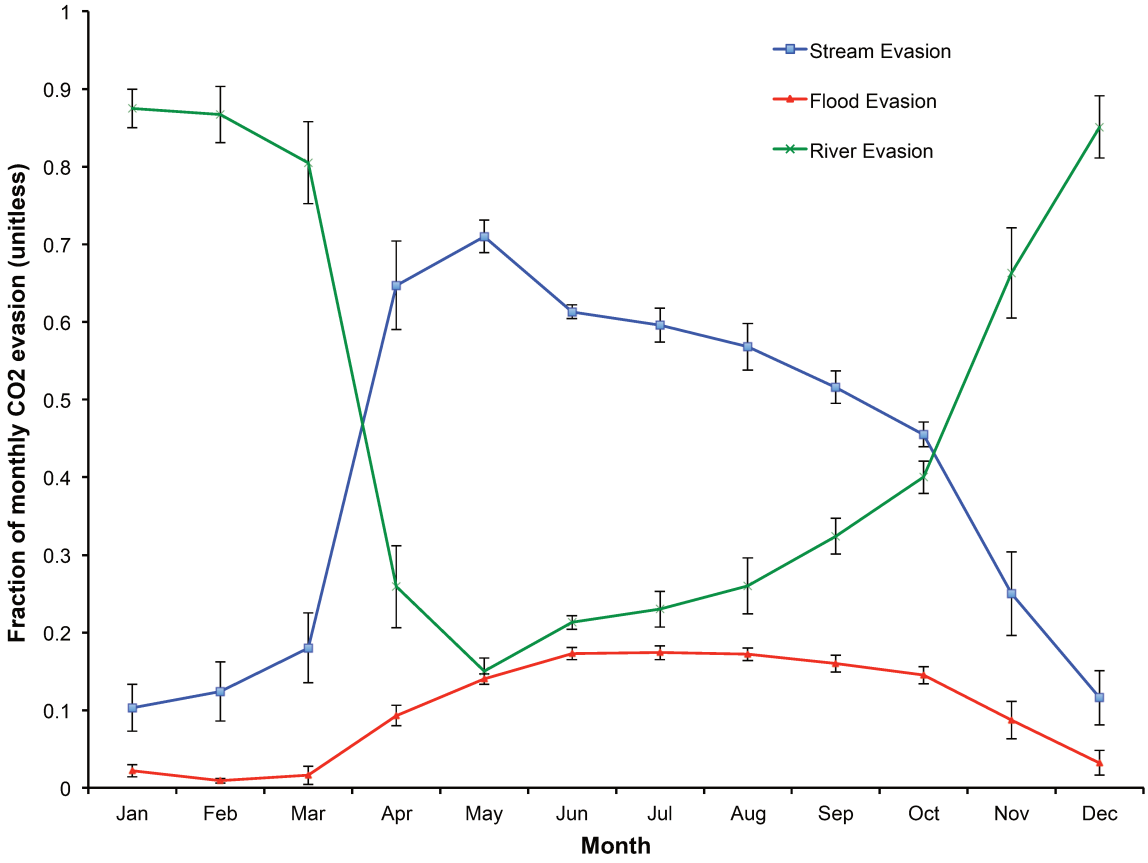
Stream Evasion
Flood Evasion
River Evasion
Fraction of monthly CO2 evasion (unitless)
1
0.9
0.8
0.7
0.6
0.5
0.4
0.3
0.2
0.1
0
Jan
Feb
Mar
Apr
May
Jun
Jul
Aug
Sep
Oct
Nov
Dec
Month

(d)

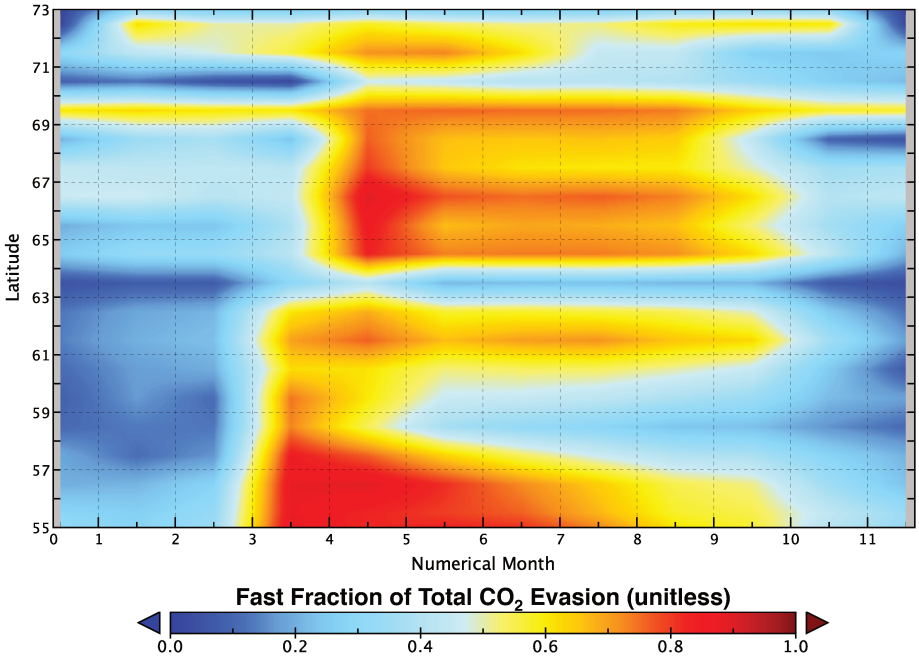

(e)

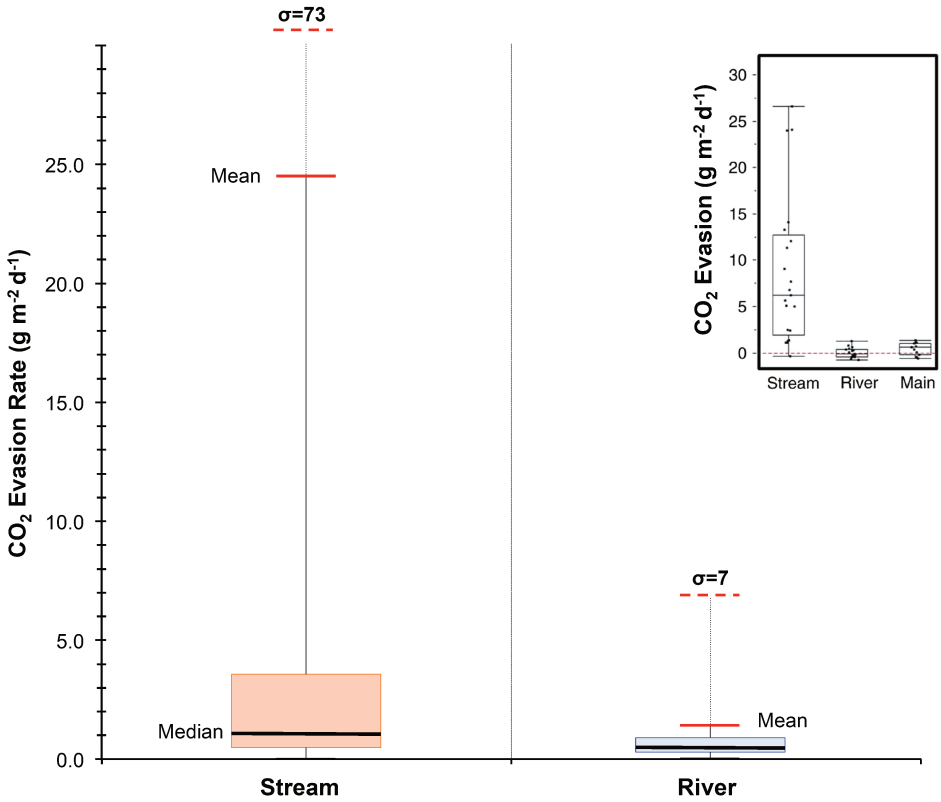

Figure 7: CO_2 evasion from stream, river, flood reservoirs. **(a)** Timeseries of total yearly CO_2 evasion (tC yr^{-1}) summed over the three hydrological pools (red line) with the 30-year running mean of the same variable overlain in thick red (askterisk). Error bars give the standard deviation of each decade (e.g. 1901-1910) for each data point in that decade. **(b)** Log-scale Hovmöller diagram plotting the longitudinally-averaged difference (increase) in total CO_2 evaded from the Lena River basin between the average of the periods 1998-2007 and 1901-1910, over each montly timestep, in (log) gC m^{-2} d^{-1}. Thus as the river drains northward the month-on-month difference in water-body CO_2 flux, between the beginning and end of the 20th Century is shown; **(c)** The fraction of total CO_2 evasion emitted from each of the

hydrological pools for the average of each month over the period 1998-2007 is shown for river, flood and stream pools (blue, green and red lines, respectively), with error bars depicting the standard deviation of data values for each month displayed. **(d)** Hovmöller diagram showing the monthly evolution of the stream pool fraction (range 0-1) per month and per latitudinal band, averaged over the period 1998-2007. **(e)** Boxplot for approximate (see text) simulated CO_2 evasion (gC m^{-2} d^{-1}) from the streamwater reservoir and river water reservoir averaged over 1998-2007. Coloured boxes denote the first and third quartiles of the data range, internal black bars the median. Whiskers give the mean (solid red bar) and standard deviation (dashed red bar) of the respective data. Empirical data on these quantities using the same scale for rivers, streams and mainstem of the Kolyma river from Denfeld et al., 2013 are shown inset.

Results such as these, in addition to permafrost soil incubation experiments (e.g. Drake et al., 2015; Vonk et al., 2013, 2015a) suggest that small streams, which represent the initial (headwater) drainage sites of these basins, rapidly process hydrologically leached carbon to the atmosphere, and that this high-reactivity carbon is a mix of recently thawed ancient permafrost material, as well as decomposing matter from the previous growth year. This is given as evidence that the total carbon processing of high-latitude rivers is significantly underestimated if only mainstem carbon concentrations are used in the accounting framework, since a large amount of carbon is metabolised to the atmosphere before reaching the site of measurement.

Figure 7 summarises some of the results from the simulated water body CO_2 outgassing flux. Year-on-year variation in basin-wide evasion from river, stream and floodplain sources combined exhibits a marked increasing trend over the course of the 20th Century, increasing from a minimum of ~1.6 $TgCO_2$-C yr^{-1} in 1901 to a maximum of ~4.4 $TgCO_2$-C yr^{-1} in 2007, an increase of almost 300% (Fig. 7a). Smoothing the data over a 30 year running average yields a dampened net increase in basin-wide evasion of ~30% over the historical period on this averaging scale (Fig. 7a). Thus yearly evasion flux is some 105% of yearly DOC discharge to the coast from the Lena basin and 51% of C exported from soils to headwaters as CO_2 or DOC. If we compare the mean yearly rate of increase in absolute (TgC yr^{-1}) CO_2 evasion and DOC discharge based on linear regression over the whole simulation period, it appears that the rate of increase of both fluxes has been strikingly similar over the simulated 20th Century, with mean increases of 11.1 GgC yr^{-1} and 11.5 GgC yr^{-1} per year for evasion and export, respectively.

The heterogeneity of CO_2 evasion from different sources in the model is most evident in terms of their geographic distribution and relative intensity, as shown in the evasion flux rate maps (tons grid $cell^{-1}$ d^{-1}) over floodplain, stream and river areas in April, June and September (Fig. 8a-c). Whereas floodplains (Fig. 8a) tend to have some of the highest evasion rates in the basin, their limited geographic extent means that their contribution to basinwide evasion is limited for the whole Lena. Stream evasion meanwhile (Fig.8b), tends to be broadly distributed over the whole basin, representing the fact that small streams and their evasion are the main hydrologic connectors outside of the main river and tributary grid cells, whereas river evasion (Fig. 8c) is clearly linked to the hydrographic representation of the Lena main stem itself, with higher total quantities in some individual grid cells than for the stream reservoir, yet distributed amongst a substantially smaller number of grid cells. Whereas the stream reservoir has greatest absolute evasion flux rates earlier in the year (April-May), maximum evasion rates occur later in the year and further downstream for the river reservoir, reflecting the fact that headwaters are first-order integrators of soil-water carbon connectivity,

whereas the river mainstem and tributaries are of a secondary order. Note that the September values must be interpreted with caution, given the underestimation in our simulations of the river discharge during the Autumn period.

The spatio-temporal pattern of increasing evasion over the simulation period is shown in Fig. 7b as a Hovmöller difference plot, between the last and first decade, of log-scale average monthly evasion rates per latitudinal band. This shows that the vast majority of outgassing increase occurs between March and June, corresponding to the progressive onset of the thaw period moving northwards over this timespan. Although relatively small, outgassing increases are apparent for most of the year, particularly at lower latitudes. This would suggest that the change is driven most acutely by relatively greater temperature increases at higher latitudes ('Arctic amplification' of climate warming, e.g. ref. (Bekryaev et al., 2010)) while less acute but more temporally homogenous evasion is driven by seasonal warming at lower latitudes.

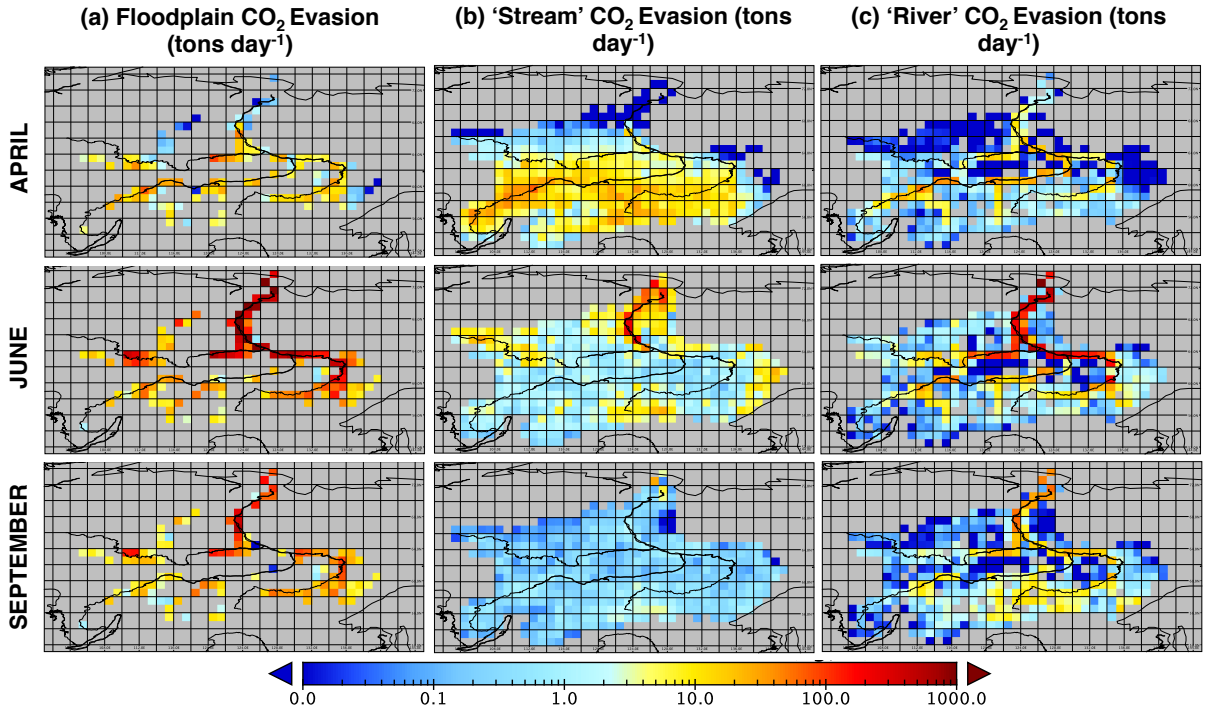

Figure 8: Maps of CO_2 evasion from the surface of the three surface hydrological pools, (a) the floodplains, (b) streams and (c) rivers in April, June and September. All maps use the same (log) scale in units of (tons pixel^{-1} d^{-1}).

As previously discussed, the proportion of total basin-wide CO_2 evasion attributable to headwater streams and rivers is substantially greater than their proportion of total basin surface area. Figure 7c represents the mean monthly fractional contribution of each surface hydrological water pool to the total evasion flux (unitless) over the period 1998-2007. This shows that over the entirety of the thaw period, the stream water pool takes over from the river water pool as the dominant evasion source, particularly at the height of the freshet period, where its fractional contribution rises to >75%.

The stream fraction of August outgassing is roughly 57% of the annual total, which is higher than the ~40% found for streams in the Denfeld et al. (2013) study. However,

the values between the two studies are not directly comparable, different basins notwithstanding. This is because in ORCHIDEE MICT-L, the 'stream' water reservoir is water routed to the river network for all hydrologic flows calculated to not cross a 0.5 degree grid cell boundary (the resolution of the routing module, explained in Part 1, Section 2.6), which may not be commensurate with long, <20m wideth streams in the real-world, that were used in the Denfeld et al. (2013) study. In addition, this 'stream' water reservoir in the model does not include any values for width or area in the model, so we cannot directly compare our stream reservoir to the <20m width criterion employed by Denfeld et al. (2013) in their definition of an observed stream. Thus our 'stream' water reservoir encompasses substantially greater surface area and hydrologic throughput than that in the Denfeld et al. study. We also add the qualification that because of its coarse-scale routing scheme, ORCHIDEE isn't able to simulate stream orders lower than 4 or 5 thus missing a potentially substantial vector for the water-surface evasion of CO_2.

Significantly, also shown in Fig. 7c, is the gradual onset of evasion from the floodplain reservoir in April, as the meltwater driven surge in river outflow leads to soil inundation and the gradual increase of proportional evasion from these flooded areas over the course of the summer, with peaks in June-August as water temperatures over these flooded areas likewise peak. We stress the importance of these simulation results as they concur with large numbers of observational studies (cited above) which show smaller headwater streams' disproportionately large contribution to total outgassing (Fig. 7c), this being due to their comparatively high outgassing rates (Fig. 7e). In addition, the contribution of floodplains to evasion, an otherwise rarely studied feature of high latitude biomes, is shown here to be significant.

A Hovmöller plot (Fig. 7d) of the monthly longitude-averaged stream reservoir fraction of total evasion, gives some indication as to the spatio-temporal pattern under which evasion from this hydrological pool evolves over the course of the year. From this we can infer that: (i) The dominance of stream evasion begins in the most southern upstream headwaters in the lower latitude thaw period (April-May), and trickles northward over the course of the next two months, following the riverflow. (ii) The intensity of stream water evasion is greatest in the lower latitude regions of the basin, which we speculate is the result of higher temperatures causing a greater proliferation of small thaw water-driven flows and evasion. (iii) Areas where the stream fraction is not dominant or only briefly dominant during the summer (58-60°N, 63-64°N, 70-71°N) are all areas where floodplain CO_2 evasion plays a prominent role at that latitudinal band.

Although not directly comparable due to the previously mentioned issues arising from our model-derived representation of 'stream' water versus those in the real world, we evaluate the approximate rate of areal CO_2 efflux from the water surface against obervations from Denfeld et al. (2013) in Fig. 7e. The 'approximate' caveat refers to the fact that model output doesn't define a precise surface area for the stream water reservoir, which is instead bundled into a single value representing the riverine fraction of a grid cell's total surface area. Thus, in order to break down the areal outgassing for the stream versus river water reservoirs, we derive an approximate value for the fractional area taken up by rivers and streams in a simple manner: we weight the total

non-floodplain inundated area of each grid cell by the relative total water mass of each of the two hydrological pools, then divide the total daily CO_2 flux simulated by the model by this value. The per-pool areal estimate is an approximation since it assumes that rivers and streams have the same surface area: volume relationship. This is clearly not the case, since streams are generally shallow, tending to have greater surface area per increment increase in depth than rivers. Thus, our areal approximations are likely underestimated (overestimated) for streams (rivers), respectively.

The comparison of simulated results with those from Denfeld et al. (2013) are displayed in Fig.7e, which shows boxplots for simulated CO_2 evasion (gC m^{-2} d^{-1}) from the stream water reservoir and river water reservoir averaged over 1998-2007. The empirical (Kolyma river) analog of this data, from which this plot is inspired (Fig. 4d in Denfeld et al., 2013), is shown inset in the figure, with whiskers in their case denoting measured maxima and minima. Median efflux was 1.1 (6) versus 0.4 (0.8) for stream and river, respectively, in simulations (observations). Like the observations, simulated stream efflux had a substantially greater interquartile range, mean (24.6) and standard deviation (73) than total river efflux (1.3 and 7.2, respectively). Note that from ~700 non-zero simulation datapoints, 7 were omitted as 'outliers' from the stream reservoir efflux statistics described below, because very low stream:river reservoir values skewed the estimation of total approximate stream surface area values very low, leading to extreme efflux rate values of 1-3000gC m^{-2} d^{-1} and are thus considered numerical artefacts of the areal approximation approach used here.

4.5 Emergent Phenomena

4.5.1 DOC and mean annual air temperature

A key emergent property of DOC concentrations in soils and inland waters should be their positive partial determination by the temperature of the environment under which their rates of production occur, as has been shown in the literature on permafrost regions, most notably in Frey & Smith (2005) (Frey and Smith, 2005)and Frey & McClelland (2009)(Frey and McClelland, 2009).

Increasing temperatures should lead to greater primary production, thaw, decomposition and microbial mobilisation rates, and hence DOC production rates, leading to (dilution effects notwithstanding) higher concentrations of DOC in thaw and so stream waters. Looking at this emergent property allows us to evaluate the soil-level production of both DOC and thaw water at the appropriate biogeographic and temporal scale in our model. This provides a further constraint on model effectiveness at simulating existing phenomena at greater process-resolution.

Figure 9 compares three datasets (simulated and two observational) of riverine DOC concentration (in mgC L^{-1}) plotted against mean annual air temperature (MAAT). The simulated grid-scale DOC versus MAAT averaged over July and August (for comparability of DOC with observational sampling period) of 1998-2007 is shown in red, and observed data compiled by Laudon et al. (2012)(Laudon et al., 2012) and Frey and Smith (2005) (Frey and Smith, 2005)for sites in temperate/cold regions globally and peatland-dominated Western Siberia, respectively. The Laudon et al. (2012) data

are taken from 49 observations including MAAT over the period 1997-2011 from catchments north of 43°N, and aggregated to 10 regional biogeographies, along with datapoints from their own sampling; those in the Frey and Smith study are from 55-68°N and ~65-85°E (for site locations, see Laudon et al. (2012), Table 1 and 2; Frey and Smith (2005), Fig. 1).

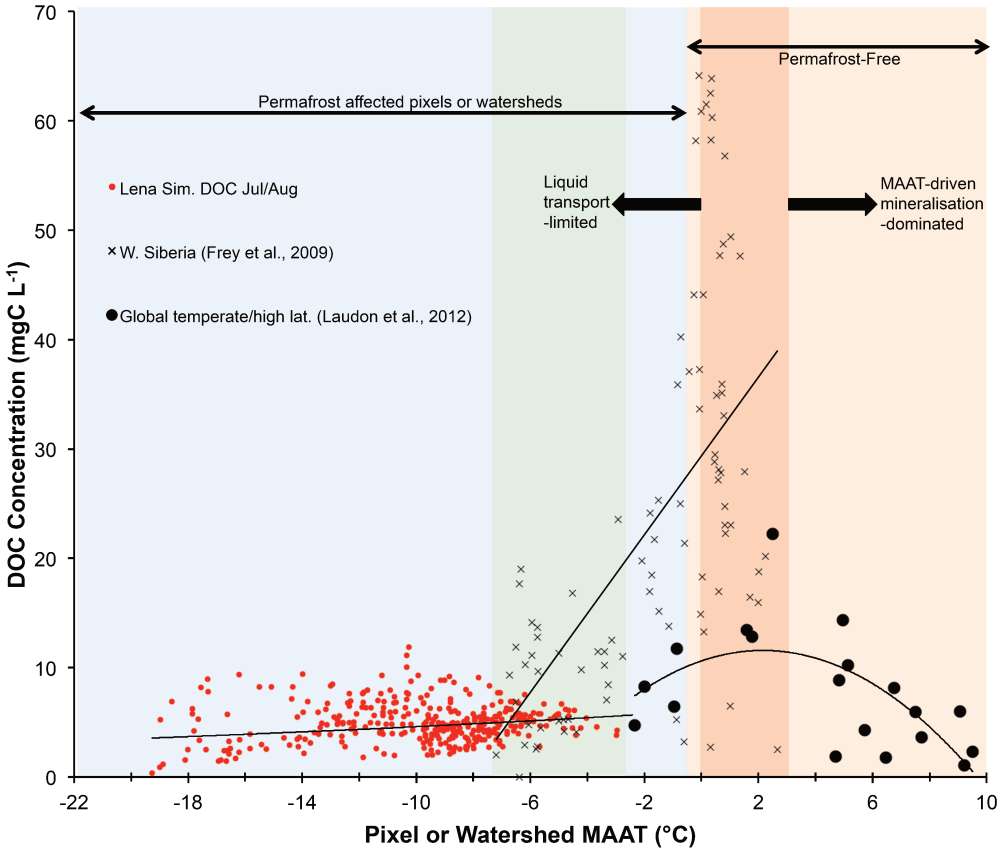

Figure 9: Mean summertime DOC concentrations (mgC L^{-1}) plotted against mean annual air temperature (MAAT, °Celsius) for simulated pixels over the Lena river basin (red circles), and observations for largely peat-influenced areas in western Siberia as reported in Frey et al., 2009 (black crosses), and observations from a global non-peat temperate and high latitude meta-analysis (black circles) reported in Laudon et al. (2012). The blue region represents permafrost-affected areas, while the orange region represents permafrost-free areas. The green region bounds the area of overlap in MAAT between the observed and simulated datasets. The dark red shaded area corresponds to the MAAT 'zone of optimality' for DOC production and transport proposed by Laudon et al. (2012). Regression curves of DOC against MAAT for each of the separate datasets are shown for each individual dataset.

can be interpreted in a number of ways. First, this MAAT continuum spans the range of areas that are both highly and moderately permafrost affected and permafrost free (Fig. 9, blue and green versus orange shading, respectively), potentially allowing us a glimpse of the behaviour of DOC concentration as the environment transitions from the former to the latter. Simulated Lena DOC concentrations, all in pixels with MAAT < -2°C and hence all bearing continuous or discontinuous permafrost ('permafrost-affected' in the figure), only exhibit a weakly positive response to MAAT on the scale used ($y=6.05e^{0.03MAAT}$), although the consistent increase in DOC minima with MAAT is clearly visible.

Second, the Laudon et al. (2012) data exhibit an increasing then decreasing trend over the range of MAAT (-2°C to 10°C) in their dataset, which they propose reflects an 'optimal' MAAT range for the production and transport of DOC, occupying the 0°C to 3°C range (Fig. 9, red shading). Below this optimum range, DOC concentrations may be limited by transport due to freezing, and above this, smaller soil carbon pools and temperature-driven decomposition would suppress the amount of DOC within rivers. Third, the lower end of the Laudon et al. (2012) MAAT values correspond to a DOC concentration roughly in line with DOC concentrations simulated by our model at those temperatures.

Fourth, DOC concentrations in the Frey and Smith (2005) data exhibit a broad scattering in permafrost-affected sites, with concentrations overlapping those of our simulations (Fig. 9, green shading), before rapidly increasing to very high concentrations relative to the Laudon et al. (2012) data, as sites transition to permafrost-free (red shading, $y=3.6_{MAAT}+29.4$). Their data highlight the difference in DOC concentration regime between areas of high (Frey and Smith, 2005) and low (Laudon et al., 2012) peatland coverage and the different response of these to temperature changes. Fifth, because our simulation results largely correspond with the observed data where the MAAT ranges overlap (green shading), and because our model does not include peatland specific processes, we should expect our model to broadly follow the polynomial regression plotted for the Laudon et al. (2012) data as temperature inputs to the model increase. Figure 9 implies that this increase should be on the order of a doubling of DOC concentration as a system evolves from a MAAT of -2°C to 2°C. In addition, as the Arctic environment warms we should expect the response of DOC concentrations as a whole to reflect a mix of both observationally-derived curves, as a function of peatland coverage.

4.5.2 DOC and topographic slope

Subsurface water infiltration fluxes and transformations of dissolved matter represent an important, if poorly understood and observationally under-represented biogeochemical pathway of DOC export to river main stems, involving the complex interplay of slope, parent material, temperature, permafrost material age and soil physical-chemical processes, such as adsorption and priming.

In the Lena basin, as in other permafrost catchments, topographic slope has been shown to be a powerful predictor for water infiltration depth, and concentration and age of dissolved organic carbon (Jasechko et al., 2016; Kutscher et al., 2017; McGuire et al., 2005), with deeper flow paths and older, lower DOC-concentrated waters found as the topographic slope increases. This relationship was shown in Fig. 4 of Kutscher et al. (2017) who surveyed DOC concentrations across a broad range of slope angle values in the Lena basin and found a distinct negative relationship between the two. We compare the Kutscher et al. (2017) values with our model output, by plotting stream and river DOC concentrations averaged per gridpoint over 1998-2007 against the topographic map used in the routing scheme, versus their empirically derived data (Fig. 10). As shown therein, a similar negative relationship between the two variables is clearly apparent.

A similar relationship was found in temperate rivers by Lauerwald et al. (2012)(Lauerwald et al., 2012), and a recent paper by Connolly et al. (2018)(Connolly et al., 2018), based on their observational data and a synthesis of Pan-Arctic empirical literature. They showed that for Arctic catchments in general, the relationship of DOC concentration in fluvial waters scaled in a consistent and strongly negative manner against topographic slope. This was found for all Arctic catchments, globally, prompting Connolly et al. to argue that topographic slope may be a type of 'master variable' for estimating fluvial DOC concentrations in the absence of viable *in* situ measurement programs.

The reasoning for the negative slope-DOC concentration relationship is that as elevation increases, temperature and primary production decreases. This leads to a thinner organic soil layer, meaning that mineral soil plays a stronger role in shallow hydrologic flowpaths, allowing for deeper infiltration and shorter residence time in a given soil layer. In addition, steeper terrain leads to a lower soil water residence time and lower moisture than in flat areas.

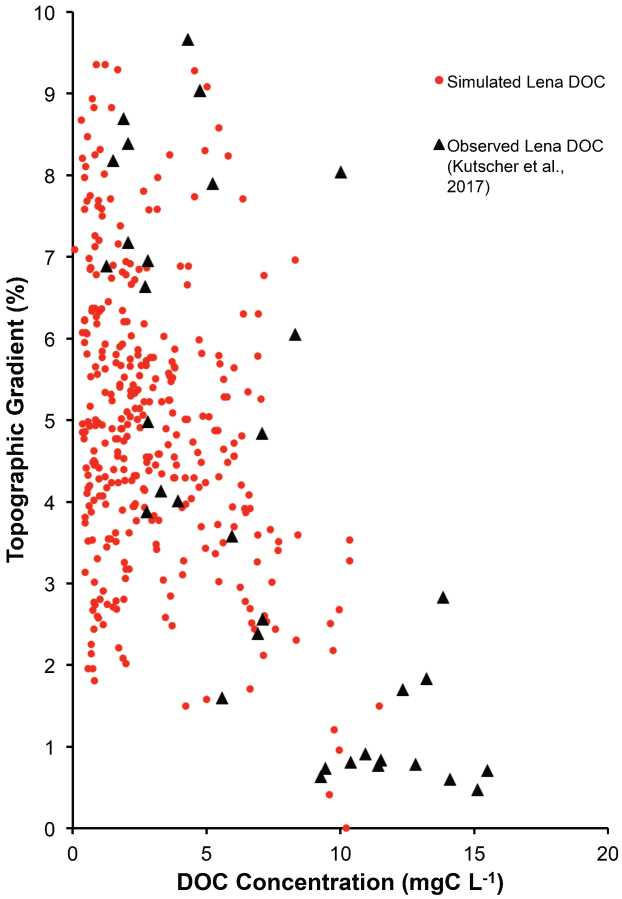

Figure 10: Variation of DOC concentrations versus topographic slope in Kutscher et al., 2017 (black triangles) and (red dots) as simulated and averaged for the summer months (JJA) over 1998-2007; observed values were measured during June and July 2012-2013.

As a result, a given patch of soil matter will be exposed to leaching for less (residence) time, while the organic matter that is leached is thought to be adsorbed more readily to mineral soil particles, leading to either their re-stabilisation in the soil column or

shallow retention and subsequent heterotrophic respiration in situ, cumulatively resulting in lower DOC concentrations in the hydrologic export (Kaiser and Kalbitz, 2012; Klaminder et al., 2011). This line of reasoning was recently shown to apply also to deep organic permafrost soils (Zhang et al., 2017), although the degree to which this is the case in comparison to mineral soils is as yet unknown.

In addition, and as described in Part 1 (Section 2.5) of this study, MICT-L contains a provision for increased soil column infiltration and lower decomposition rates in areas underlain by Podzols and Arenosols. The map from the Harmonized World Soil Database (Nachtergaele, 2010), which is used as the input to this criterion, shows areas underlain by these soils in the Lena basin to also be co-incident with areas of high topographic slope (Fig. 3a, SI, Fig S2b). Their Podzol effect is to increase the rate of decomposition and infiltration of DOC, relative to all other soil types, thus also increasing the rate of DOC flux into groundwater (see Part 1 of this study, Section 2.5).

Our modelling framework explicitly resolves the processes involved in these documented dynamics –soil thermodynamics, solid vertical flow (turbation), infiltration as a function of soil textures and types, adsorption as a function of soil parameters (see Part 1 of this study, Section 2.11), DOC respiration as a function of soil temperature and hence depth (Part 1, Section 2.12), lagging of DOC vertical flow behind hydrological drainage flow (summary Figure in Part 1, Fig. 1). We thus have some confidence in reporting that the simulated negative relationship of DOC concentration with topographic slope may indeed emerge from the model. If generalisable to permafrost basins as a whole, this relationship may be an emergent process-based signal with which to evaluate the biogeographic performance of permafrost-region DOC modelling initiatives in the future, as was recently suggested by Connolly et al. (2018).

4.6 DOC Reactivity Pools

Here we examine the reactivity of DOC leached from the soil and litter to different hydrological export pools. Surface runoff DOC export is dominated by refractory carbon (Fig. 11a), with export rates largely following discharge rates as they drain the basin with an increasing delay when latitude increases. As the thaw period gets underway (April), the fraction of labile carbon in surface runoff DOC increases substantially from south to north, reflecting the hydrologic uptake of the previous year's undecomposed high-reactivity organic matter, as well as the addition of new inputs from the onset of the current year's growing season.

Refractory carbon–dominated drainage DOC export rates (Fig. 11a) are centered on the months June through October, with refractory export rate intensities per latitudinal band during this period largely consistent with the fraction of inundated area (Fig. S1) experienced by these bands during the course of the year, these centering on the areas bounded by 52-65N and 70-72N. The high refractory proportion of drainage flow is expected, as drainage leaches older, relict soil and litter matter. Because of its longer water residence time, labile DOC carried vertically downward through the soil infiltration flux will tend to be metabolised in situ before it can be exported to the hydrological network, thus further increasing the proportion of refractory carbon.

By contrast floodplain DOC export (Fig. 11a) is dominated by the labile carbon pool but is composed of more nuanced mix of both reactivity classes, reflecting its relatively greater dependence on the current year's 'fresh' biomass as source material (62% labile DOC versus 38% refractory DOC, year-averaged) for carbon leaching. This can be expected, since DOC and CO_2 production that would normally occur first in soil free DOC concentrations before being gradually exported into surface runoff and drainage inputs to the hydrological network are instead directly supplied to the water column as they are generated, meaning that there is less of a time lag for the rapid decomposition of the labile portion than through the other two hydrological export pathways.

For both the river and stream pool, mean DOC concentrations are also dominated by refractory carbon sources. Interestingly, very high concentrations in the stream reservoir are maintained year-round in the northernmost reaches of the Lena basin, the causes of which are not directly deducible from our data. Likely, very high stream concentrations are obtained from the confluence of relatively low volumetric water fluxes in these regions that owe themselves to the freezing temperatures, with these low temperatures likewise retarding direct heterotrophic respiration of contemporary plant litter and favouring instead their environmental mobilisation by hydrological leaching, when liquid water is available for matter dissolution.

When averaged over the year, the dominance of the refractory DOC carbon pool over its labile counterpart is also evident for all DOC inputs to the hydrological routing except for floodplain inputs, as well as within the 'flowing' stream and river pools themselves. This is shown in Table 2, where the year-averaged percentage of each carbon component of the total input or reservoir is subdivided between the 'North' and 'South' of the basin, these splits being arbitrarily imposed as the latitudinal mid-point of the basin itself (63N). This reinforces the generalised finding from our simulations that refractory carbon dominates runoff and drainage inflows to rivers (89% refractory, on average), while floodplains export mostly labile DOC to the basin (64%), these values being effectively independent of this latitudinal sub-division (Table 3). This may be expected, given that almost the entire basin is underlain by continuous permafrost, whereas in areas with discontinuous or sporadic permafrost, the combination of higher primary productivity and so litter input, with seasonal thaw of labile permafrost soil matter may be expected to substantially increase the labile portion of the overall sum of these quantities. Nonetheless, there appears to be a small consistent difference between North and South in the stream and river water DOC makeup, in that the labile portion decreases between North and South ; this may be an attenuated reflection of the portion of labile DOC that is decomposed to CO_2 within the water column during its transport northward, affecting the bulk average proportions contained within the water in each 'hemisphere'.

Table 3: Summary of the average carbon reactivity types comprising the hydrological inputs to rivers and streams (runoff, drainage and floodplain inputs), and within the rivers and streams themselves, subdivided between the 'North' and 'South' of the Lena basin (greater or less than 63N, respectively).

Hydrological Source	Model Carbon Reactivity Pool	North	South
Runoff Input	Refractory	81%	83%
	Labile	19%	17%

Drainage Input	Refractory	96%	94%
	Labile	4%	6%
Flood Input	Refractory	36%	37%
	Labile	64%	63%
Streams	Refractory	91%	89%
	Labile	9%	11%
Rivers	Refractory	92%	90%
	Labile	8%	10%

4.7 NPP and Soil Respiration

Rates of yearly net primary production (NPP) for Russian and Siberian forests have been inferred in situ from eddy flux and inventory techniques to range from 123-250 gC m^{-2} yr^{-1} (Beer et al., 2006; Lloyd et al., 2002; Roser et al., 2002; Schulze et al., 1999; Shvidenko and Nilsson, 2003). We likewise simulate a broad range of NPP carbon uptake rates, of 61-469 gC m^{-2} yr^{-1} averaged per grid cell over the Lena basin, with a mean value of 210 gC m^{-2} yr^{-1}. NPP is heterogeneously distributed over space and between PFTs (SI, Fig. S4c), with forests averaging 90 gC m^{-2} yr^{-1} and grasslands averaging 104 gC m^{-2} yr^{-1} over the basin as a whole. Low values tended to originate in basin grid cells with elevated topography or high mean slope, while the maximum value was standalone, exceeding the next greatest by ~100 gC m^{-2} yr^{-1}, and is most likely caused by the edge effects of upscaling a coastal gridcell's small fraction of terrestrial area where high productivity occurs in a small plot, to the grid cell as a whole. By evaluating NPP we are also evaluating at a secondary level litter production, which is at a third level a major component of DOC production.

Taken as a whole, gross primary production (GPP) was performed under simulations by four PFT groups, with the largest basin-wide bulk contributions coming from boreal needleleaf summer-green trees and C3 grasses (SI, Fig. S4a), the highest GPP uptake rates (3 TgC $pixel^{-1}$ yr^{-1}) generated by boreal needleleaf evergreen trees, and the remainder of GPP contributed by Boreal broad-leaved summer-green trees (SI, Fig. S4a).

Soil respiration rates, of combined soil heterotroph and plant root respiration in our Control simulation, averaged 208 gC m^{-2} yr^{-1} (0.57 gC m^{-2} d^{-1}) over the Lena basin over the period 1990-2000, which is somewhat higher than those found by Elberling (2007)(Elberling, 2007) in forest soils over Svalbard, of 103-176 gC m^{-2} yr^{-1} (0.28-0.48 gC m^{-2} d^{-1}). Sawamoto, et al. (2000)(Sawamoto et al., 2000) measured in situ summertime soil respiration over the central Lena basin and found rates of 1.6-34 gC m^{-2} d^{-1}, while Sommerkorn (2008)(Sommerkorn, 2008) observed rates of 0.1-3.9 gC m^{-2} d^{-1} at higher latitudes, these appearing to vary with vegetation and fire history, water table depth and temperature. Mean heterotrophic respiration rates of 1.6 gC m^{-2} d^{-1} are simulated here during July and August, in the range 0.0.5-2.2 gC m^{-2} d^{-1} for each of the above PFT groups. The spatial distribution of, and difference in respiration rates between PFT groups largely mirrors those for NPP (SI Fig. S4c), with maximum rates of 1.4 gC m^2 d^{-1} over forested sites, versus a maximum of 2.2 gC m^2 d^{-1} over grassland/tundra sites (SI, Fig. S4b).

Aggregated over the basin, results show that increases over the course of the 20th Century were simulated for NPP, GPP, River Discharge, DOC, $CO_{2(aq.)}$, autotrophic and heterotrophic respiration and CO_2 evasion, with percentage changes in the last versus first decade of +25%, +27%, 38%, +73%, +60%, +30%, +33% and +63%, respectively. (Fig. 11b). It thus appears that rising temperatures and CO_2 concentrations disproportionately favoured the metabolisation of carbon within the soil and its transport and mineralisation within the water column, fed by higher rates of primary production and litter formation as well as an accelerated hydrological cycle (see Fig. 4b and 13a).

In Figure 11c we run linear regressions through scatter-plots of yearly DOC and CO_2 export and CO_2 evasion fluxes, versus rates of NPP (TgC yr^{-1}). These show that whereas bulk DOC flux appears most sensitive (steeper slope) to increases in NPP, it is also least coupled to it (more scattered, R^2=0.42). CO_2 evasion is least sensitive yet most tightly coupled to NPP (R^2=0.52), while CO_2 export is intermediate between the two for both (R^2=0.43) –this is expected given that CO_2 export is also the intermediate state between DOC export and CO_2 evasion. The greater scattering of DOC:NPP compared to evasion:NPP is understandable, given that the initial of leaching is a covariate of both primary production and runoff, whereas the actual evasion flux is largely dependent on organic inputs (production) and temperature.

(a)

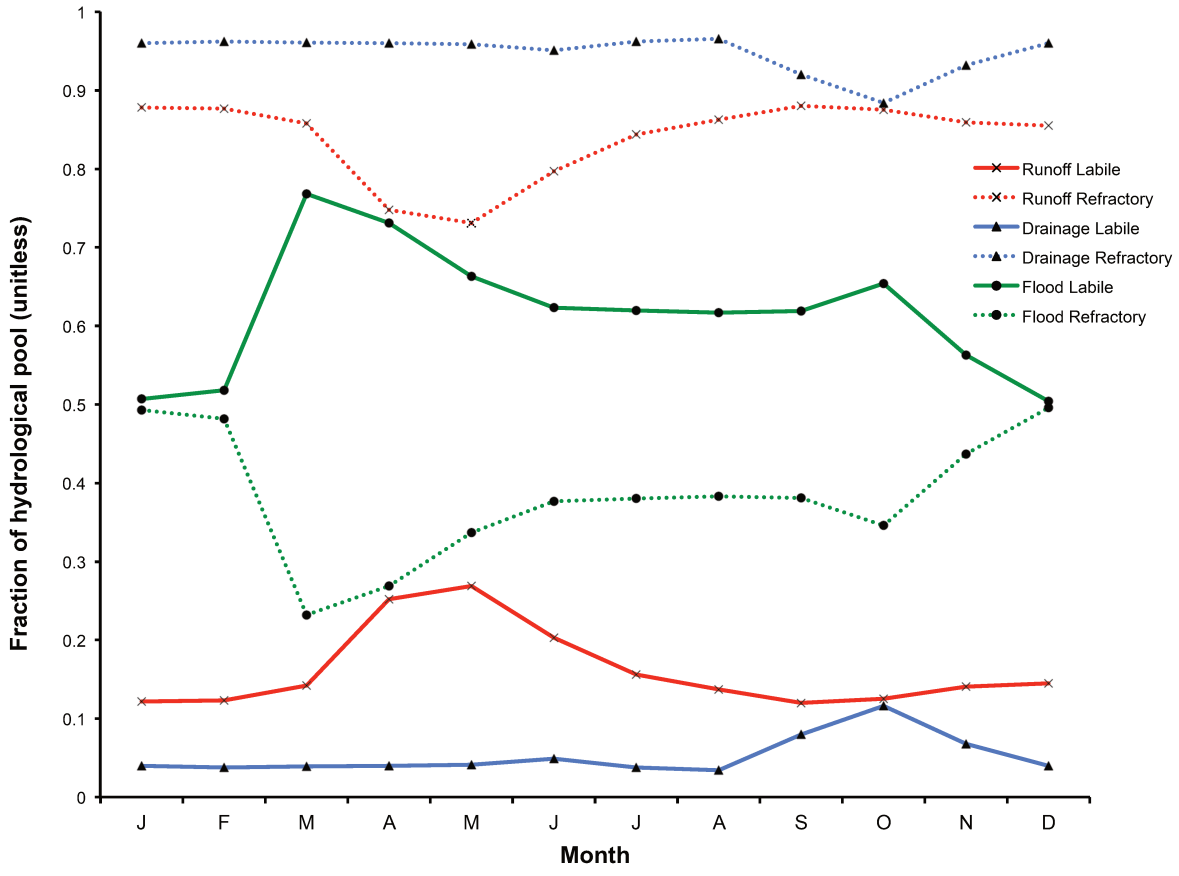

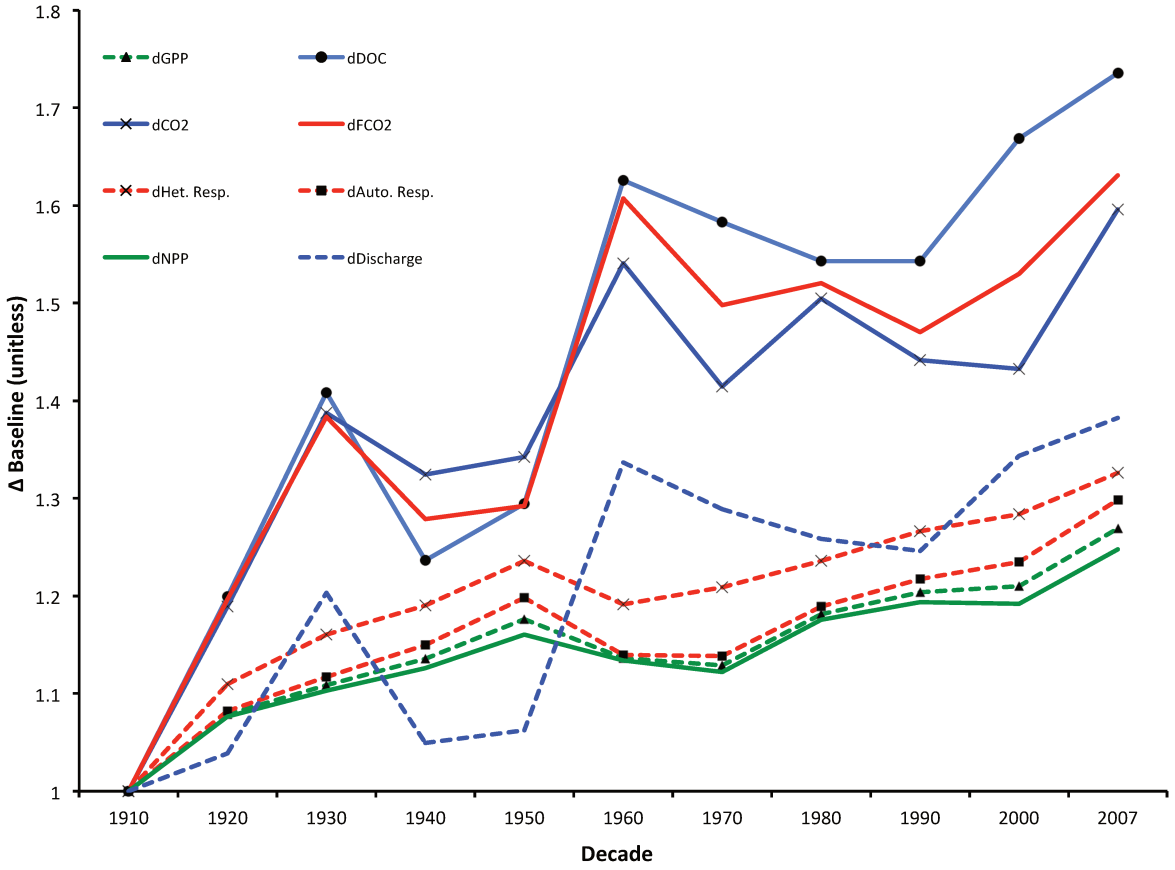
dGPP
dDOC
dCO2
dFCO2
dHet. Resp.
dAuto. Resp.
dNPP
dDischarge
Δ Baseline (unitless)
Decade
1.8
1.7
1.6
1.5
1.4
1.3
1.2
1.1
1
1910
1920
1930
1940
1950
1960
1970
1980
1990
2000
2007

(c)

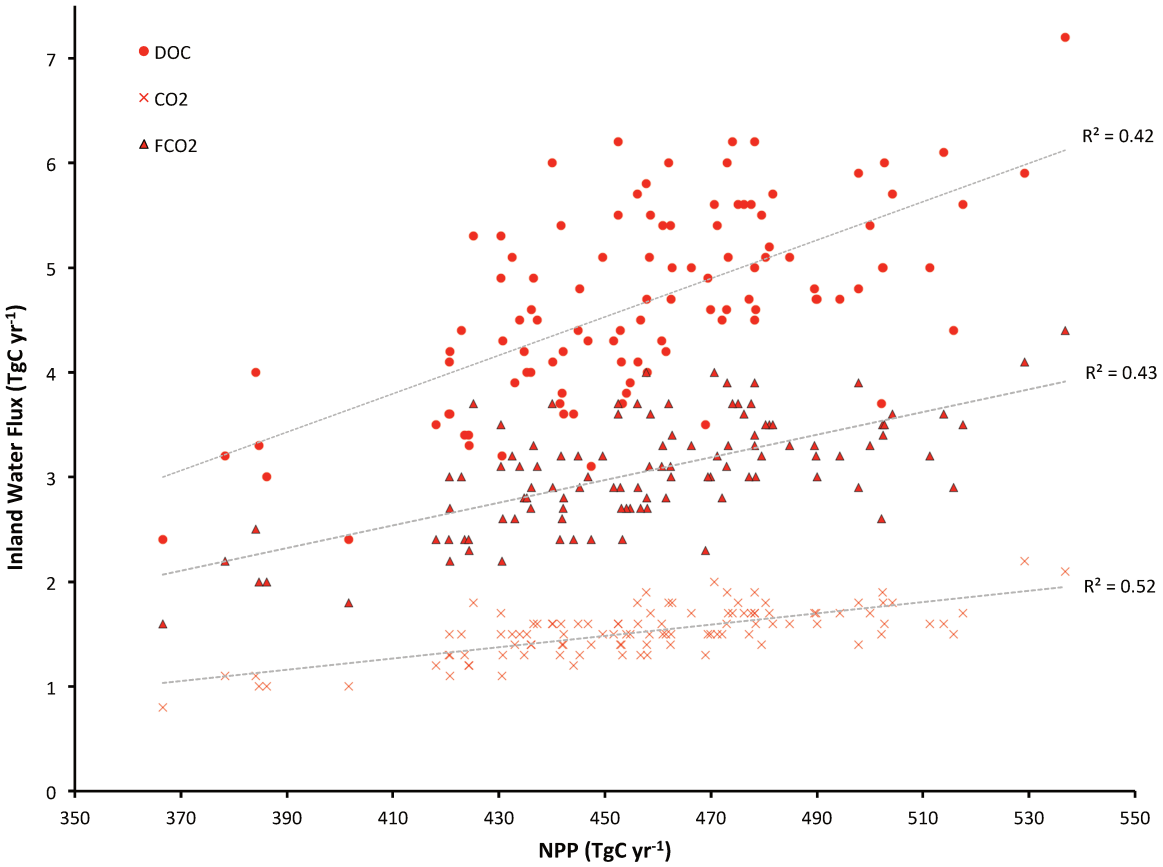
DOC
CO2
FCO2
R² = 0.42
R² = 0.43
R² = 0.52
Inland Water Flux (TgC yr⁻¹)
NPP (TgC yr⁻¹)
7
6
5
4
3
2
1
0
350
370
390
410
430
450
470
490
510
530
550

Figure 11: (a) The mean monthly fraction of each hydrological pool's (runoff, drainage, floodplains) carbon reactivity constituents (labile and refractory) averaged across the simulation area over 1998-2008. **(b)** Time series showing the decadal-mean fractional change in carbon fluxes normalised to a 1901-1910 average baseline (=1 on the y-axis) for NPP, GPP, autotrophic and heterotrophic respiration, DOC inputs to the water column, CO_2 inputs to the water column, CO_2 evasion from the water surface (FCO2), and discharge. **(c)** Summed yearly lateral flux versus NPP values for DOC discharge, CO_2 discharge and CO_2 evasion (FCO2) over the entire simulation period, with linear regression lines shown.

4.8 Land-Ocean Aquatic Continuum (LOAC)

4.8.1 LOAC Fluxes

Overall, our simulation results show that dissolved carbon entering the Lena river system is significantly transformed during its transport to the ocean. Taking the average throughput of carbon into the system over the last ten years of our simulation, our results show that whereas 7 TgC yr^{-1} (after reinfiltration following flooding of 0.45 TgC yr^{-1}; see Fig. 2 'Return' flux) of carbon enters the Lena from terrestrial sources as dissolved carbon and CO_2, only 3.4 TgC yr^{-1} is discharged into the Laptev Sea and beyond from the river mouth. The remainder (3.6TgC yr^{-1}) is metabolised in the water column during transport and evaded to the atmosphere (bottom panel, Fig. 12a). The terrestrial DOC inflow estimate is comparable to that made by Kicklighter et al. (2013)(Kicklighter et al., 2013), who estimated in a modelling study terrestrial dissolved carbon loading of the Lena is ~7.7 TgC yr^{-1}.

The relative quantities of carbon inflow, evasion and outflow in the river system that are presented for the Lena in Fig. 12a can be compared to the same relative quantities –that is, the ratios of evasion:in and out:in, where 'in' refers to dissolved terrestrial input, – from the global study by Cole et al. (2007)(Cole et al., 2007), who estimated these fluxes from empirical or empirically-derived data at the global scale. This is shown in the top panel of Fig. 12a, where we simplify the Cole et al. (2007) data to exclude global groundwater CO_2 flux from the coast to the ocean (because our basin mask has a single coastal pixel whereas coastal groundwater seepage is distributed along the entire continental boundary) and the POC fraction of in-river transport and sedimentation (since ORCHIDEE MICT lacks a POC erosion/sedimentation module) from their budget.

This gives global terrestrial dissolved carbon input of 1.45 PgC yr^{-1}, 0.7 PgC of which is discharged to the ocean, and the other 0.75 PgC evaded to the atmosphere. Taking the previously mentioned [evasion:in] and [out:in] ratios as a percentage, the outflow and evasion fluxes for the Lena versus the global aggregate are remarkably similar, at 48.6 vs. 48.3% and 51.4 vs 51.7%, for the two respective flows. Thus our results agree with the proposition that the riverine portion of the 'land-ocean aquatic continuum' (Regnier et al., 2013) or 'boundless carbon cycle' (Battin et al., 2009) is indeed a substantial reactor for matter transported along it.

4.8.2 LOAC drivers

The constant climate (CLIM) and constant CO_2 (CO2) simulations were undertaken to assess the extent –and the extent of the difference –to which these two factors are drivers of model processes and fluxes. These differences are summarised in Figs. 12(b-

c), in which we show the same 1998-2007 –averaged yearly variable fluxes as in the CTRL simulation, expressed as percentages of the CTRL values given in Fig. 2. A number of conclusions can be drawn from these diagrams.

First, all fluxes are lower in the factorial simulations, which can be expected due to lower carbon input to vegetation from the atmosphere (constant CO_2) and colder temperatures (constant climate) inhibiting more vigorous growth and carbon cycling. Second, broadly speaking, both climate and CO_2 appear to have similar effects on all fluxes, at least within the range of climatic and CO_2 values to which they have subjected the model in these historical runs. With regard to lateral export fluxes in isolation, variable climate (temperature increase) is a more powerful driver than CO_2 increase (see below). Third, the greatest difference between the constant climate and CO_2 simulation carbon fluxes appear to be those associated with terrestrial inflow of dissolved matter to the aquatic network, these being more sensitive to climatic than CO_2 variability. This is evidenced by a 49% and 32% decline in CO_2 and DOC export, respectively, from the land to rivers in the constant climate simulation, versus a 27% and 23% decline in these same variables in the constant CO_2 simulation. Given that the decline in primary production and respiration in both factorial simulations was roughly the same, this difference in terrestrial dissolved input is attributable to the effect of climate (increased temperatures) on the hydrological cycle, driving changes in lateral export fluxes.

This would imply that at these carbon dioxide and climatic ranges, the modelled DOC inputs are slightly more sensitive to changes in the climate rather than to changes in atmospheric carbon dioxide concentration and the first order biospheric response to this. However, while the model biospheric response to carbon dioxide concentration may be linear, thresholds in environmental variables such as MAAT may prove to be tipping points in the system's emergent response to change, as implied by Fig. 9, meaning that the Lena, as with the Arctic in general, may soon become much more temperature-dominated, with regard to the drivers of its own change.

2746 **(a)**

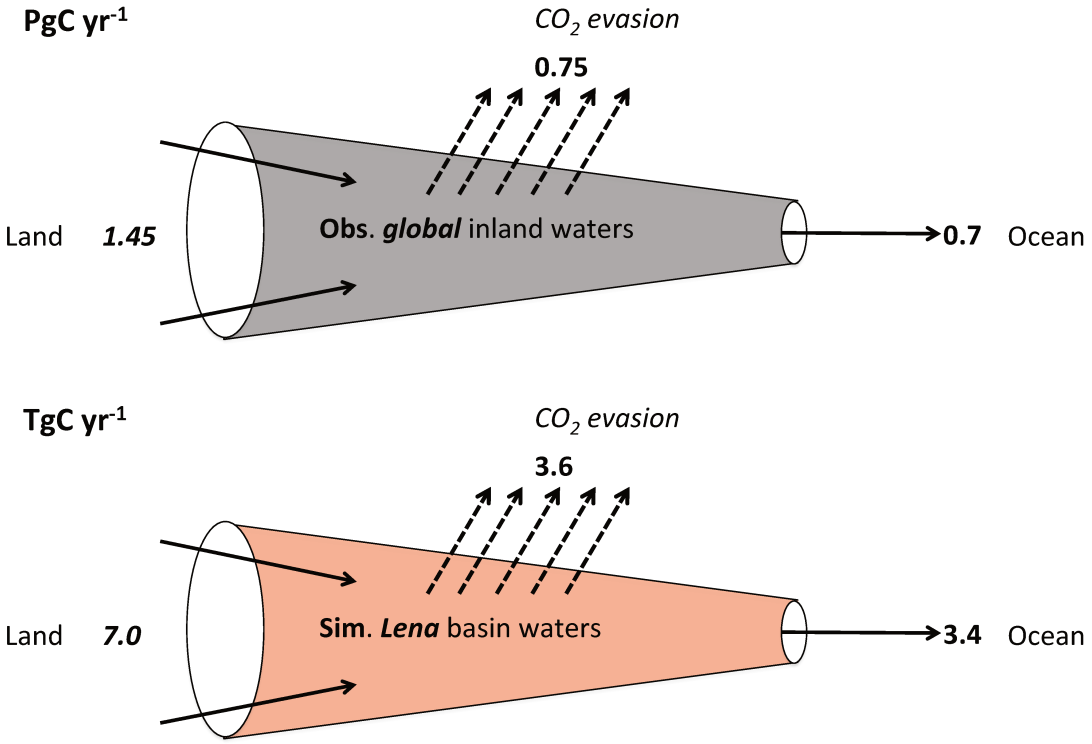

2747
2748 **(b)**

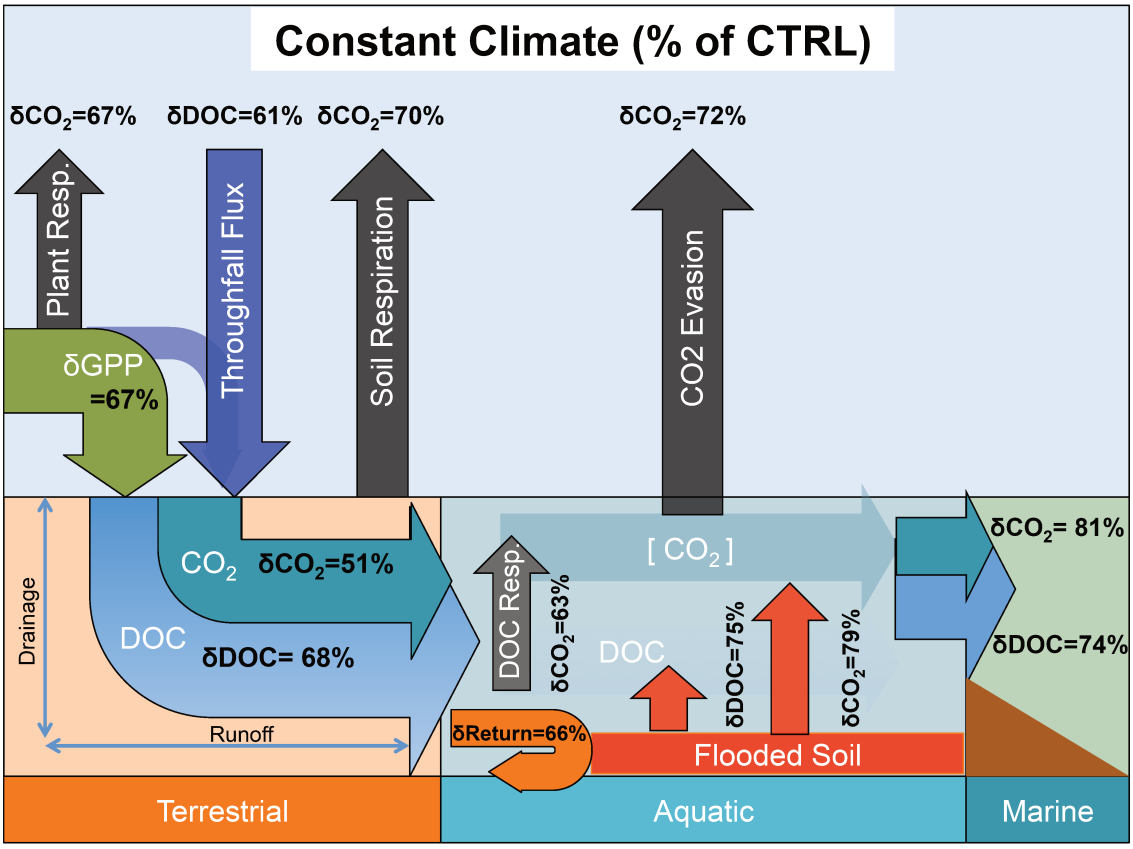

2749
2750 **(c)**

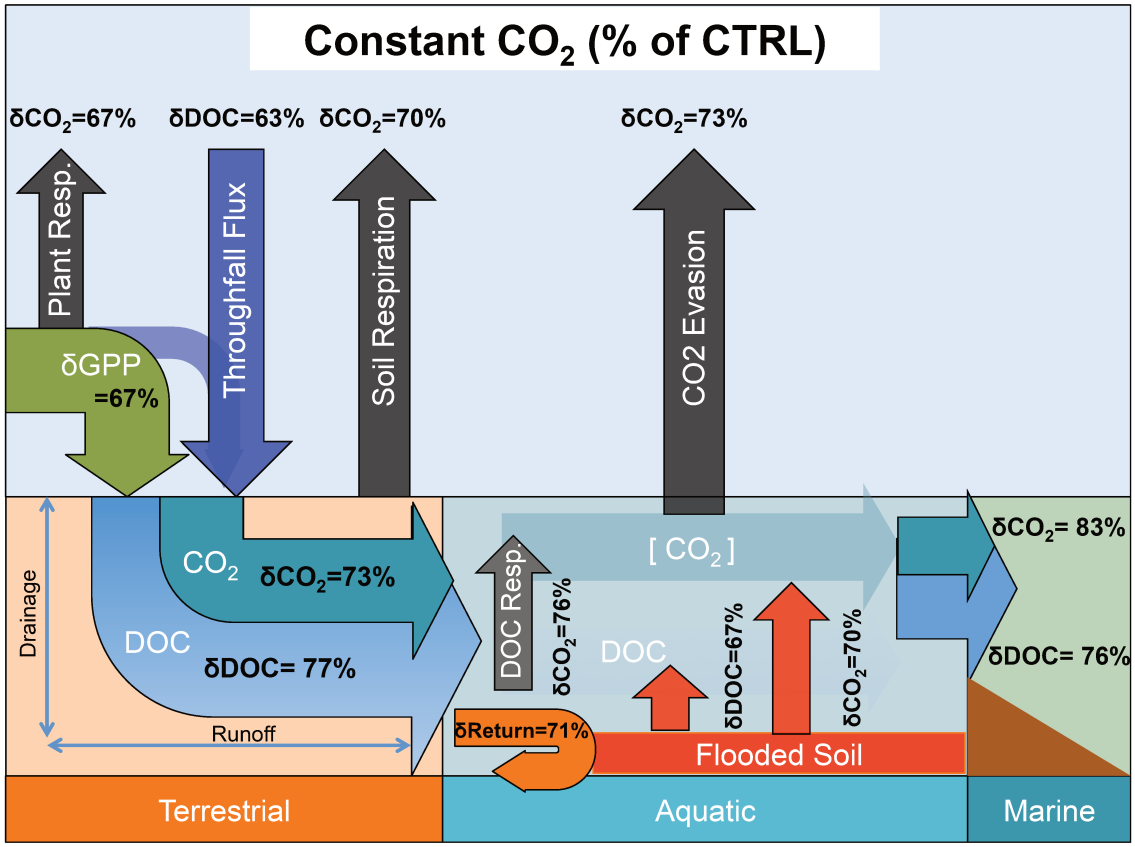

Figure 12: **(a)** Simplified 'leaky pipe' diagram representing the transport and processing of DOC within the land-ocean hydrologic continuum. The scheme template is taken from Cole et al. (2007), where we reproduce their global estimate of DOC and non-groundwater discharge portion of this flow in the top panel (PgC yr^{-1}), and the equivalent flows from our Lena basin simulations in TgC yr^{-1} in the bottom panel. Thus easy comparison would look at the relative fluxes within each system and compare them to the other. **(b-c)**: Schematic diagrams detailing the major yearly carbon flux outputs from simulations averaged over the period 1998-2007 as they are transformed and transported across the land-aquatic continuum. Figures **(b)** and **(c)** give the same fluxes as a percentage difference from the Control (CTRL-Simulation), for the constant climate and CO_2 simulations, respectively.

4.8.3 LOAC export flux considerations

Despite our simulations' agreement with observations regarding the proportional fate of terrestrial DOC inputs as evasion and marine export (Section 4.8.1, Fig. 12a), our results suggest substantial and meaningful differences in the magnitude of those fluxes relative to NPP in the Lena, compared to those estimated by other studies in temperate or tropical biomes. Our simulations' cumulative DOC and CO_2 export from the terrestrial realm into inland waters is equivalent to ~1.5 % of NPP.

This is considerably lower than Cole et al. (2007) and Regnier et al. (2013) who find lateral transfer to approximate ~5% (1.9PgC yr^{-1}) of NPP at the global scale, while Lauerwald et al. (2017)(Lauerwald et al., 2017) found similar rates for the Amazon. The cause of this discrepancy with our results is beyond the scope of this study to definitively address, given the lack of tracers for carbon source and age in our model. Nonetheless, our analysis leads us to hypothesise the following.

Temperature limitation of soil microbial respiration at the end of the growing season (approaching zero by October, SI Fig. S4d) makes this flux neglible from November through May (SI Fig. S4d). In late spring, mobilisation of organic carbon is performed by both microbial respiration and leaching of DOC via runoff and drainage water fluxes. However, because the latter are controlled by the initial spring meltwater flux period, which occurs before the growing season has had time to produce litter or new soil carbon (May-June, Fig. 4b), aggregate yearly DOC transport reactivity is characterised by the available plant matter from the previous year, which is overwhelmingly derived from recalcitrant soil matter (Fig. 11a) and is itself less available for leaching based on soil carbon residence times.

This causes relatively low leaching rates and riverine DOC concentration s(e.g. Fig. 9), as compared to the case of leaching from the same year's biological production. Highlighting this point are floodplains' domination by labile carbon sourced from that year's production with a mean DOC concentration of 12.4 mgC L^{-1} (1998-2007 average), with mean riverine DOC concentrations around half that value (6.9 mgC L^{-1}). Nonetheless the May-June meltwater pulse period dominates aggregate DOC discharge. As this pulse rapidly subsides by late July, so does the leaching and transport of organic matter. Warmer temperatures come in conjunction with increased primary production and the temperature driven soil heterotrophic degradation of contemporary and older matter (via active layer deepening). These all indicate that transported dissolved matter in rivers, at least at peak outflow, is dominated by sources originating in the previous year's primary production, that was literally 'frozen out' of more complete decomposition by soil heterotrophs.

Further, we infer from the fact that all of our simulation grid cells fall within areas of low (<-2°C) MAAT, far below the threshold MAAT (>3°C) proposed by Laudon et al. (2012) for soil respiration-dominated carbon cycling systems (Fig. 9), that the Lena is hydrologically-limited with respect to DOC concentration and its lateral flux. Indeed, the seasonal discharge trend of the Lena –massive snowmelt-driven hydrological and absolute DOC flux, coupled with relatively low DOC concentrations at the river mouth (Fig. 4b, simulation data of Fig. 9), are in line with the Laudon et al. (2012) typology.

We therefore suggest that relatively low lateral transport (as %NPP) in our simulations compared to other biomes is driven by meltwater (vs. precipitation) dominated DOC mobilisation, which occurs during a largely pre-litter deposition period of the growing season. DOC is then less readily mobilised by being sourced from recalcitrant matter, leading to low leaching concentrations relative to those from labile material. As discharge rates decline, the growing season reaches its peak, leaving carbon mobilisation of fresh organic matter to be overwhelmingly driven by in situ heterotrophic respiration.

While we have shown that bulk DOC fluxes scale linearly to bulk discharge flows (Fig. 3d), DOC concentrations (mgC L^{-1}) hold a more complex and weaker positive relationship with discharge rates, with correlation coefficients (R^2) of 0.05 and 0.25 for river and stream DOC concentrations, respectively (Fig. 13). This implies that while increasing discharge reflects increasing runoff and an increasing vector for DOC

leaching, particularly in smaller tributary streams, by the time this higher input of carbon reaches the river main stem there is a confounding effect of dilution by increased water fluxes which reduces DOC concentrations, explaining the difference between stream and river discharge vs. DOC concentration regressions in the Figure. Thus, and as a broad generalisation, with increasing discharge rates we can also expect somewhat higher concentrations of terrestrial DOC input to streams and rivers. Over the floodplains, DOC concentrations hold no linear relationship with discharge rates (R^2=0.003 , SI Fig. S5), largely reflecting the fact that DOC leaching is here limited by terrestrial primary production rates more than by hydrology. To the extent that floodplains fundamentally require flooding and hence do depend on floodwater inputs at a primary level, we hypothesise that DOC leaching rates are not limited by that water input, at least over the simulated Lena basin.

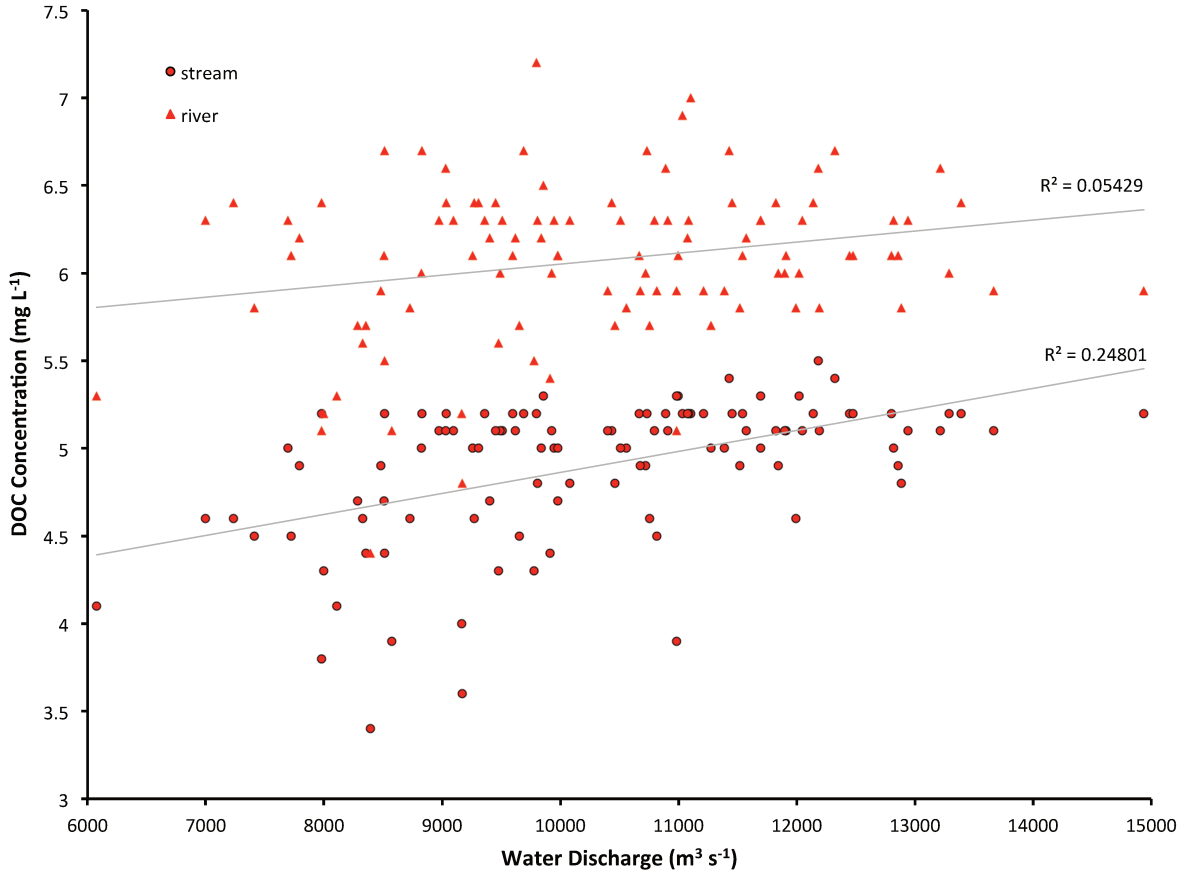

Figure 13: Simulated basin-mean annual DOC concentrations (mg L^{-1}) for the stream and river water pools regressed against mean annual simulated discharge rates (m^3 s^{-1}) at Kusur over 1901-2007. Linear regression plots with corresponding R^2 values are shown.

As discussed above simulated DOC and CO_2 export as %NPP was 1.5% over 1998-2007. However, this proportion appears to be highly dynamic at the decadal timescale. As shown in Fig. 11b, all lateral flux components in our simulations increased their relative throughput at a rate double to triple that of NPP or respiration fluxes over the 20th century, also doing so at a rate substantially higher than the rate increase in discharge. In addition, differentials of these lateral flux rates with the rates of their drivers (discharge, primary production) have on average increased over the century (Fig. 11b).

This suggests that there are potential additive effects of the production and discharge drivers of lateral fluxes that could lead to non-linear reponses to changes in these drivers as the Arctic environment transforms, as suggested by the Laudon et al. (2012)(Laudon et al., 2012) data plotted in Fig. 4. Acceleration of the hydrological cycle compounded by temperature and CO_2 -driven increases in primary production could therefore increase the amount of matter available for leaching, increase the carbon concentration of leachate, and increase the aggregate generation of runoff to be used as a DOC transport vector. Given that these causal dynamics apply generally to permafrost regions, both low lateral flux as %NPP and the hypothesised response of those fluxes to future warming may be a feature particular to most high latitude river basins.

5. Conclusion

This study has shown that the new DOC-representing high latitude model version of ORCHIDEE, ORCHIDEE MICT-LEAK, is able to reproduce with reasonable accuracy modern concentrations, rates and absolute fluxes of carbon in dissolved form, as well as the relative seasonality of these quantities through the year. When combined with a reasonable reproduction of real-world stream, river and floodplain dynamics, we demonstrate that this model is a potentially powerful new tool for diagnosing and reproducing past, present and potentially future states of the Arctic carbon cycle. Our simulations show that of the 34 TgC yr^{-1} remaining after GPP is respired autotrophically and heterotrophically in the Lena basin, over one-fifth of this captured carbon is removed into the aquatic system. Of this, over half is released to the atmosphere from the river surface during its period of transport to the ocean, in agreement with previous empirically-derived global-scale studies. Both this transport and its transformation are therefore non-trivial components of the carbon system at these latitudes that we have shown are sensitive to changes in temperature, precipitation and atmospheric CO_2 concentration. Our results, in combination with empirical data, further suggest that changes to these drivers –in particular climate –may provoke non-linear responses in the transport and transformation of carbon across the terrestrial-aquatic system's interface as change progresses in an Arctic environment increasingly characterised by amplified warming.

Chapter 4
Arctic lateral carbon fluxes decline with future warming[3].

Summary

Release of dissolved organic carbon (DOC) from Arctic soils has been the focus of extensive empirical work over the last decade, with results suggesting that the future thawing of permafrost soils may increase the export of DOC by rivers to Arctic seas. However, to date no studies have reconciled theory and observation with *predictions* of Arctic lateral transport response to anthropogenic forces, owing to the lack of global climate models able to address the complexities of both permafrost soil physics and the mechanics of carbon lateral transport.

Using ORCHIDEE MICT-LEAK, a global-scale land surface model built specifically for addressing this omission (Chapter 1), and successfully evaluated previously for a single permafrost-region river basin (the Lena –Chapter 2), we conduct simulations spanning the 20th and 21st centuries (1898-2099) over the entire Pan-Arctic region (> 45°N), under the Intergovernmental Panel on Climate Change (IPCC) 'RCP 6.0' future (intermediate-range) warming scenario, at a one degree grid-cell resolution. Unlike in Chapter 2, which uses a reanalysis data product to drive the model, future simulations require simulated future climate, land cover and vegetation data to drive them, and are thus necessarily modelling product-driven. This results in some differences in simulated outputs compared with output driven by data used in Chapter 2, driven largely by hydrological and primary production differences. Nonetheless, the model again broadly reproduces modern day bulk riverine DOC fluxes and concentrations that exist in the sparse data record for these regions.

Over the 21st century, our simulations project that mean annual air temperature, CO_2 and precipitation increases relative to the mean of 1996-2005 drive large-scale changes in primary production, biome-scale respiration and soil carbon losses, consistent with the notions that warming will lead to widespread metabolisation of permafrost carbon, and that the latter exceeds increases in carbon uptake by vegetation. Despite this strengthening of the carbon and water cycle, we show that contrary to first-order empirical expectations arising from their trends, lateral carbon flows over the Pan-Arctic decline under RCP6.0 by 2100. This is caused by the complex interaction of temperature with precipitation, soil hydrology and leaching substrate, causing DOC flux temperature response to oscillate in magnitude and sign.

The causes of this result are complex, but are generally driven by deepening hydrological flowpaths resulting from thaw of the permafrost 'cap' on drainage water flows with increases in temperature. Thaw allows drainage of water to depth, which, coupled with increasing soil temperatures, permits increasing water infiltration into the soil, higher rates of soil respiration at depth, and subsequently lower concentrations of carbon in the water-leachate fluxes produced by the deeper hydrological flowpaths. By

[3] Manuscript being prepared for submission to *Nature Climate Change*.

partitioning the aggregate precipitation water flux in favour of infiltraiton flows, these flows are further exposed to leaching substrate with a lower carbon concentration than those that exist at the soil surface, which correspond to recently-produced soil and litter matter. Finally, despite an increase in overall precipitation, we hypothesise that the timing and phase-state of precipitation, drives decreases in DOC flux. Decreasing snowfall in winter and increasing rainfall in late summer demote and promote the massive post-winter leaching flux of contemporary carbon, and that of deeper, lower carbon concentration matter, owing to the deeper active layer and water infiltration regime during this time, respectively, also driving a decline in bulk lateral carbon fluxes. This result appears to be a general result of warming of the permafrost region, and further justifies the necessity of using a model specifically created for representing high-latitude conditions in making these projections. Indeed, whereas the tempearture sensitivity of soil carbon release from the Arctic is unequivocally positive, our simulations show that for lateral carbon fluxes the temperature sensitivity increases and decreases in both magnitude and sign, owing to the response of carbon mobilisation to threshold changes in active layer depth that promote hysteresis as an emergent response.

Chapitre 4
Les flux de carbone latéraux dans l'Arctique diminuent avec le réchauffement futur.

Résumé

La libération de carbone organique dissous (COD) des sols arctiques a fait l'objet de nombreux travaux empiriques depuis une décennie environ avec des résultats suggérant que le dégel futur des sols de pergélisol pourrait accroître les exportations de COD par les rivières vers les mers arctiques. Cependant, à ce jour, aucune étude n'a concilié théorie et observation avec les prévisions de la réponse du transport latéral arctique aux forces anthropiques, en raison de l'absence de modèles climatiques globaux capables de traiter les complexités de la physique des sols du pergélisol et de la mécanique du transport latéral du carbone.

En utilisant ORCHIDEE MICT-LEAK, un modèle de surface terrestre à l'échelle mondiale construit spécifiquement pour remédier à cette omission (chapitre 1) et déjà évalué avec succès pour un seul bassin hydrographique de la région de pergélisol (Lena –Chapitre 2), nous effectuons des simulations couvrant la 20^{ième} et 21^{ième} siècles (1898-2099) sur l'ensemble de la région panarctique (> 45 ° N), dans le cadre du scénario de réchauffement futur du Groupe d'experts intergouvernemental sur l'évolution du climat (GIEC) 'RCP 6.0'. Contrairement au chapitre 2, qui utilise un produit de réanalyse pour piloter le modèle, les simulations futures nécessitent des données simulées sur le climat, la couverture terrestre et la végétation pour les piloter, et sont donc nécessairement modélisées à partir de produits. Cela entraîne certaines différences dans les résultats simulés par rapport aux résultats tirés des données utilisées au chapitre 2, en grande partie dus aux différences hydrologiques et de production primaire. Néanmoins, le modèle reproduit à nouveau de manière générale les flux et les concentrations de COD fluviales modernes de ces régions.

Au 21^{ième} siècle, nos simulations prévoient que la température moyenne annuelle de l'air, les émissions de CO_2 et les précipitations augmentent par rapport à la moyenne de 1996-2005, entraînant des changements à grande échelle dans la production primaire, la respiration à l'échelle du biome et les pertes de carbone du sol, conformément aux notions de réchauffement, entraînera une métabolisation généralisée du carbone du pergélisol, et que ce dernier dépasserait l'augmentation de l'absorption de carbone par la végétation. Malgré ces accélérations des cycles du carbone et de l'eau, nous montrons que, contrairement aux attentes empiriques de premier ordre découlant de leurs tendances, les flux de carbone latéraux serait stable sous un scénario RCP6.0 d'ici 2100. Ceci est dû à l'interaction complexe des températures avec les précipitations, l'hydrologie du sol et le substrat de lessivage, entraînant une variation de la réponse de la température du flux de COD en amplitude et en signe.

Les causes de ce résultat sont complexes, mais sont généralement dues à l'approfondissement des voies hydrologiques résultant du dégel de pergélisol et son impact sur les eaux de drainage lorsque la température augmente. Le dégel permet de drainer l'eau en profondeur, ce qui, associé à l'augmentation de la température du sol, permet une infiltration croissante de l'eau dans le sol, un taux plus élevé de respiration du sol en profondeur et, par la suite, une diminution des concentrations de carbone dans les flux de lixiviat d'eau produits par les

sillons hydrologiques plus profonds. . En diminuant en proportion les flux de ruissèlement de surface par rapport aux flux de drainage, ces flux d'eau sont en outre exposés à un substrat présentant une concentration en carbone inférieure à celle existant à la surface du sol, ce qui correspond au sol et à la litière récemment produits. Enfin, malgré une augmentation des précipitations globales, nous émettons l'hypothèse que le moment et l'état de phase des précipitations entraînent une diminution du flux de COD. La diminution des chutes de neige en hiver et des précipitations croissantes en fin d'été rétablit et favorise le flux de lixiviation massif post-hiver du carbone contemporain, ainsi que celui des matières à plus faible concentration de carbone, en raison de la couche active plus profonde et du régime d'infiltration d'eau pendant cette période, respectivement, entraînant également une diminution des flux de carbone latéraux massifs.

Ce résultat semble être un résultat général du réchauffement de la région de pergélisol et justifie en outre la nécessité d'utiliser un modèle créé spécifiquement pour représenter les conditions de haute latitude lors de la réalisation de ces projections. En effet, alors que la sensibilité à la température du dégagement de carbone du sol de l'Arctique est très positive, nos simulations montrent que, pour les flux de carbone latéraux, la sensibilité à la température augmente et diminue en valeur et en signe, en raison de la réponse de la mobilisation du carbone à des changements de seuil dans la couche active, profondeur qui favorise l'hystérésis en tant que réponse émergente.

Introduction

High-latitude permafrost soils contain large amounts of frozen, often ancient and relatively reactive carbon down to depths of over 30m. Permafrost profoundly affects Arctic river hydrology. A permanently frozen soil layer acts as a barrier to groundwater, so that surface and shallow sub-surface runoff dominates basin-scale waterflow, increasing the inter-seasonal variability of river discharge(Ye et al., 2009). This concentration of water volume near the surface during the thawing season is exacerbated by the accumulation of snow and ice in winter that subsequently melt during the spring freshet(Drake et al., 2015; Spencer et al., 2015) and cause intense leaching of DOC from the topsoil(O'Donnell et al., 2016). The spring pulse of DOC contains mostly modern river carbon(Aiken et al., 2014) and dominates the bulk annual DOC flux(Holmes et al., 2012) to the Arctic Ocean (25-36 TgC yr^{-1})(McClelland et al., 2008). The pronounced seasonality in river flow also drives the summertime inundation of the floodplain regions(Smith and Pavelsky, 2008), whose subsequent recession spurs the lateral transport of terrestrial carbon(Zubrzycki et al., 2013). These dynamics may be subject to amplification by recent and future climate change(Frey and McClelland, 2009; Tank et al., 2018). It is generally expected that rising temperature and enhanced precipitation(Peterson et al., 2002) will increase streamflow and total energy flux(Lammers et al., 2007) and drive an earlier onset of discharge peak(Van Vliet et al., 2012, 2013).

Soil warming can be expected to destabilize soil carbon stocks(Schuur et al., 2015) as active layer deepening exposes old/ancient soil horizons to leaching and transport(Spencer et al., 2015; Vonk et al., 2015c); once mobilised, these carbon compounds appear to be rapidly metabolized in headwater streams(Drake et al., 2015), and may constitute a significant fraction of CO_2 evasion (40-84 TgC yr^{-1}(McGuire et al., 2009)) from Arctic rivers(Vonk et al., 2013). Increasing trends in temperature, soil moisture/snow thaw(McClelland et al., 2004) and microbial activity(Hollesen et al., 2015; Schuur et al., 2009) may converge to raise soil leaching and dissolved organic(Frey and Smith, 2005) and inorganic carbon(Drake et al., 2018; Tank et al., 2012c) export rates into the future. The resulting increase in dissolved and particulate carbon delivery to the Arctic Ocean could lead to local decreases in ocean CO_2 uptake(Manizza et al., 2011) and seawater acidification(Semiletov et al., 2016), conversely contributing to local primary production(Le Fouest et al., 2018): factors all amplified by the Arctic Ocean's high surface area:volume ratio(Jakobsson, 2002).

Despite its importance as both a vehicle for permafrost carbon mobilisation and its effects on the Arctic Ocean, to date, no attempt has been made to mechanistically quantify the Pan-Arctic response of permafrost-region litter/soil carbon leaching and subsequent lateral tranport/evasion to rising temperatures. This omission owes itself to the complexity of representing the interacting processes alluded to above at large scale, which would have to include vegetation and physical processes for high latitude cryo-phenomena, and the leaching and cycling of DOC and CO_2, along the terrestrial-aquatic continuum. This study fills that gap by subjecting a state-of-the-art global land surface model (ORCHIDEE MICT-LEAK) built and evaluated specifically for representing these processes (see Methods and Bowring et al. (2019a, 2019b)), to historical and future

climate change under the IPCC RCP6.0 ("no mitigation") scenario over the Arctic (45-90N) at 1° resolution.

Results

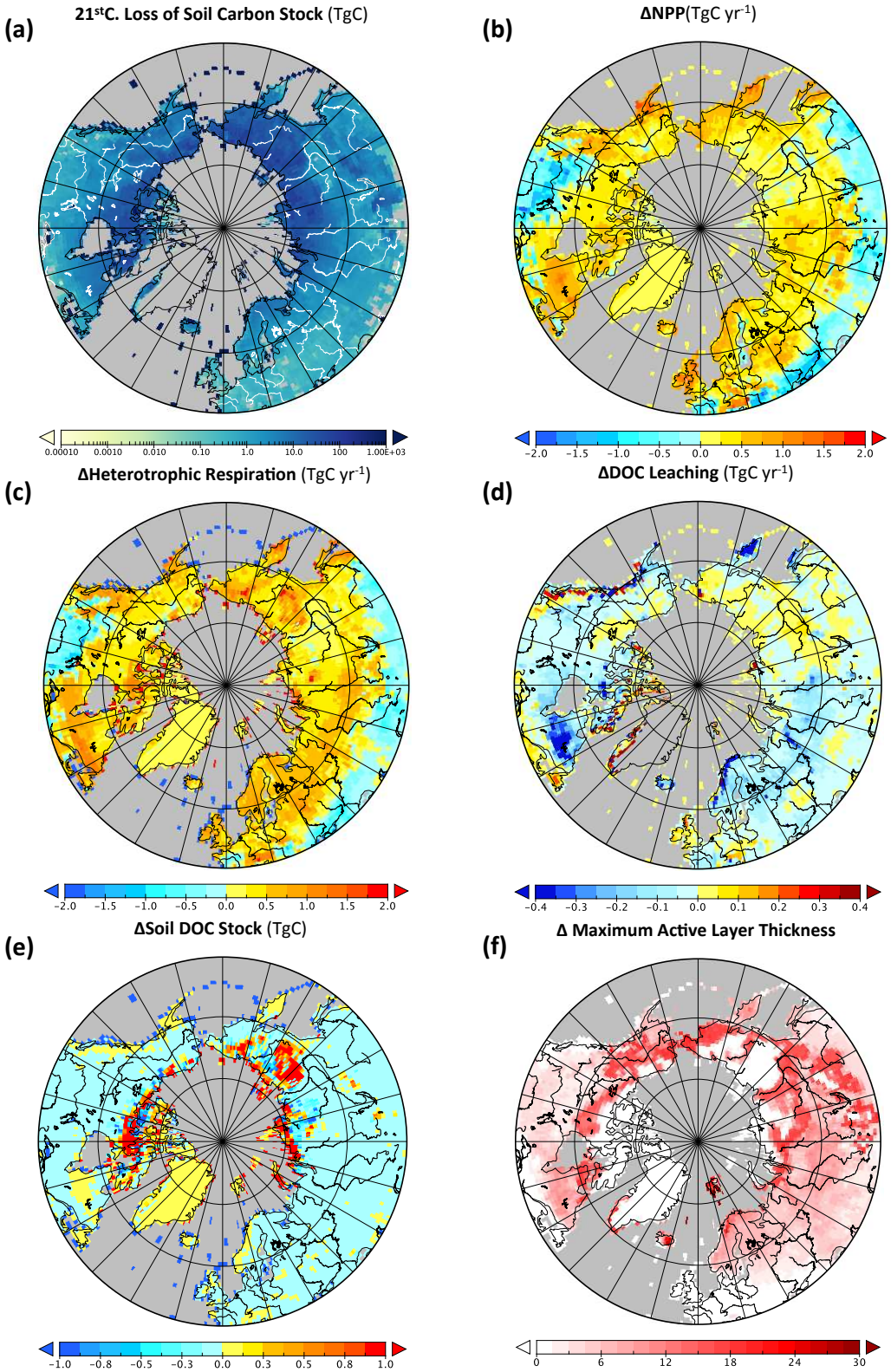

Figure 1: Maps of changes in variables over the 21st century. **(a)** Aggregate loss (TgC) of soil carbon over 2000-2099; (b-f): changes in variables between the mean of (2090-2099) subtracted by that of (1996-

2005) in each pixel for **(b)** NPP (TgC yr^{-1}) **(c)** Heterotrophic soil respiration (TgC yr^{-1}), **(d)** DOC leaching, (TgC yr^{-1}) **(e)** Soil DOC stock (TgC) **(f)** Maximum active layer thickness (m).

21st Century changes and annualised outflow

Over the course of the 21st Century, simulations show that whereas bulk soil carbon loss is concentrated over the coldest regions of the northern hemisphere (Fig. 1a), heterotrophic respiration increases are greatest in warmer (and fastest-warming (SI, Fig.S5e,f) areas like Sweden and western Siberia (Fig. 1c). This spatial difference arises from large increases in net primary production (NPP) in the warmer regions (Fig. 1b) and therefore higher litter production rates. DOC leached from the soil to rivers (Fig. 1d) generally increases in the in northern N. America and Eastern Siberia, where permafrost coverage is highest and temperatures are lower, but decreases substantially in western Siberia, Sweden and Eastern Canada. Indeed, where the change in annual-mean 'active layer' (thawed soil) thickness was near zero (Fig.1f), the soil column experienced large-scale increases in DOC stock over the 21stC, decreasing almost everywhere else (Fig.1e). Furthermore, areas of negligible soil thawing are bounded on the southern edges by regions that experienced huge increases in annualised thaw depth over the century. This suggests that the transition from 'continuous' to discontinuous or sporadic permafrost responds in a highly non-linear manner to climatic change, for which soil thermodynamics appear to hold a threshold in reponse, examined in greater detail below.

Table 1: Simulated and observation-based estimates(Holmes et al., 2012) of DOC discharge by the 'Big Six', and 'Medium 9' river basins. as well as discharge from the remaining Arctic watershed to give the Pan-Arctic river outflow (see Methods). All values are in TgC yr^{-1}. Also shown are the mean annual sum of soil and floodplain DOC and CO_2 input to the Big Six rivers, and CO_2 evasion from their respective water surfaces. Simulated values encompass the mean of the temporal range covering the turn of the millenium (1996-2005) and the last decade of simulation (2090-2099).

		Simulated	Observed	Simulated
		DOC to Ocean (1996-2005)	**DOC to Ocean (Holmes et al., 2012)**	**DOC to Ocean (2090-2099)**
Big Six	Kolyma	1.12 *±0.24*	0.82	1.19*±0.26*
	Lena	4.14 *±0.30*	5.68	4.27 *±0.43*
	Yenisei	5.66 *±0.80*	4.65	4.78 *±0.42*
	Ob	5.07 *±0.70*	4.12	2.38 *±0.61*
	Mackenzie	2.19 *±0.27*	1.38	1.67 *±0.23*
	Yukon	1.19 *±0.14*	1.47	1.11 *±0.22*
	Total	**19.36**	**18.11**	**15.40**
Medium 9				
	Pechora	1.64 *±0.21*	n/a	1.16 *±0.19*
	Pyasina	0.76 *±0.13*	n/a	0.75 *±0.17*
	Verkhnyaya-Taymyra	0.49 *±0.10*	n/a	0.37 *±0.07*
	Khatanga	1.16 *±0.18*	n/a	1.18 *±0.21*
	Olenek	0.46 *±0.07*	n/a	0.44 *±0.10*
	Yana	0.21 *±0.05*	n/a	0.21 *±0.06*
	Indigirka	0.38 *±0.10*	n/a	0.42 *±0.19*
	Anadyr	0.77 *±0.13*	n/a	0.94 *±0.13*
	Kuskokwin	0.40 *±0.07*	n/a	0.34 *±0.08*
	Total	**6.27**	**n/a**	**5.80**
Remaining				
	Total	**6.43**	**n/a**	**6.44**
Pan-Arctic				
	Total	**32.06**	**34.04**	**27.64**

Simulated modern annual DOC flux to the Arctic Ocean, a first order evaluation constraint on model adequacy in representing dissolved carbon dynamics, is in broad agreement with the existing observational literature(Holmes et al., 2012) (Table 1).

Mean DOC discharge over the present day (1996-2005) for each of the Big Six rivers (TgC yr^{-1}) is simulated (observed) to be 1.12 ±0.24 (0.82) for the Kolyma, 4.14 ±0.3 (5.68) for the Lena; 5.66 ±0.8 (4.65) for the Ob; 2.19±0.27 (1.38) for the Mackenzie; and 1.19 ±0.14 (1.47) for the Yukon. With the exception of the Lena and Mackenzie, our model output falls within two standard deviations of observed fluxes. Simulations show that DOC discharge of the 9 next-largest basins ('Medium 9', Table 1), which are largely un-sampled for this metric, is about a third that of the Big 6(~6 vs.~19 TgC yr^{-1}). For the Pan-Arctic as a whole we estimate similar DOC discharge to that found in Holmes et al (2012),(Holmes et al., 2012) of ~32 vs 34 TgC yr^{-1}, for simulations vs. observations. The Supplement contains the full inland water budget breakdown for each basin (SI Fig.S2).

Over the six basins, DOC discharge represents on average 55% (varying from 41-62%) of total dissolved carbon input from the soil to streamflow (runoff+drainage+floodplain), while the combined 'dissolved CO_2' ($CO_{2(aq.)}$)+DOC outflow (Table 1, Supplement Table S2) increases that fraction to 60%. On average, 31% (11-38%) of modelled dissolved C inputs are evaded to the atmosphere as CO_2 in streams and rivers, with the remainder returning to the soil as 'reinfiltration'. This evasion flux as a proportion of carbon inputs from soils is significantly lower than global-scale estimates (~52%)(Cole et al., 2007), a consequence of the temperature-dependence of CO_2 evasion(Lauerwald et al., 2015). Likewise, simulated dissolved carbon influx to streamflow represents only 0.7% (range 0.5-0.9%) of NPP, substantially lower than the global (5% of NPP(Cole et al., 2007; Regnier et al., 2013)) estimate.

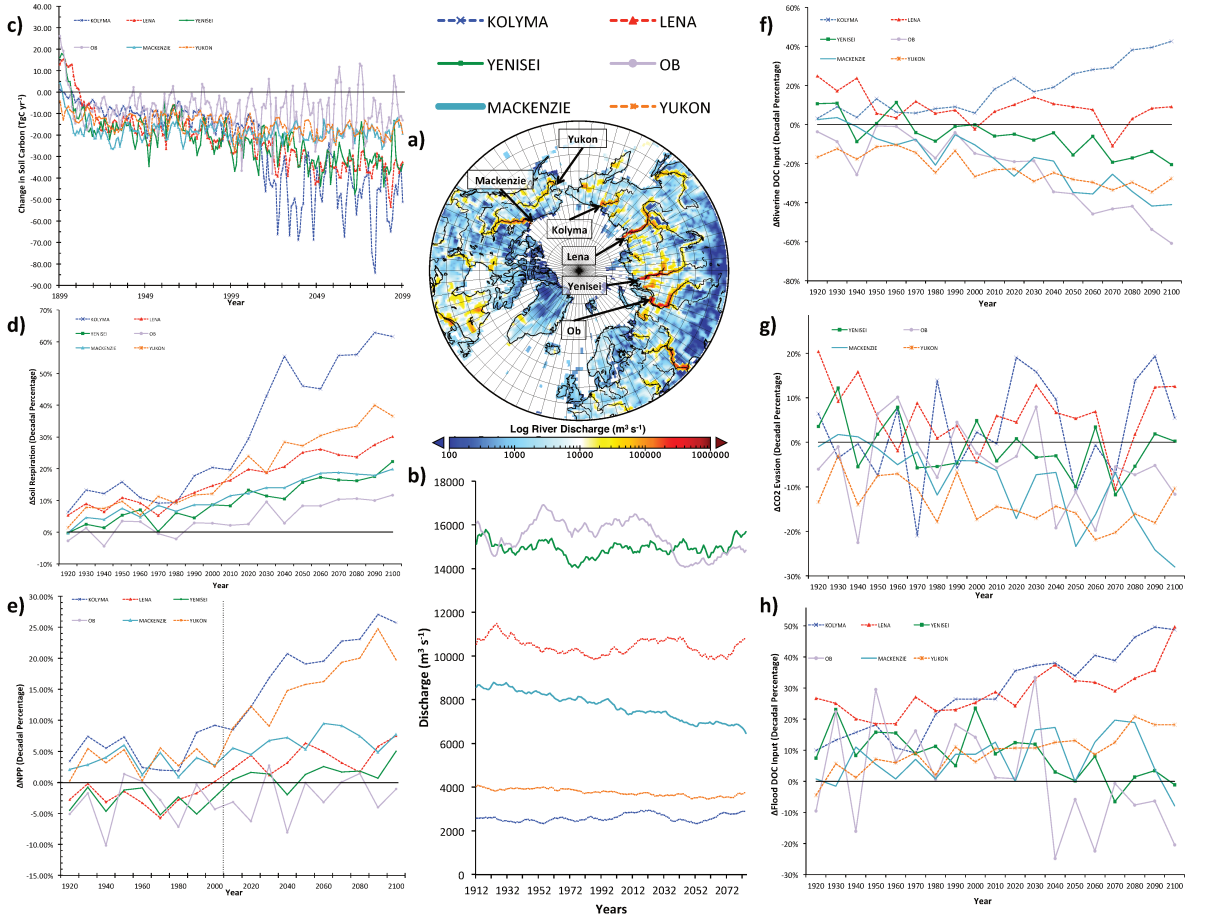

Figure 2: Basin-disaggregated timeseries of variables (periphery) and **(a)** a map of the Pan-Arctic (centre) with major river satellite overlay and mean river discharge plotted, and the Big Six river basins identified by outflow grid cell. **(b)** 30-year moving average of river discharge per basin ($m^3\ yr^{-1}$); **(c)** Yearly change in total soil organic carbon (SOC) for each basin ($TgC\ yr^{-1}$); **(d-h):** These plots show the decadal-mean deviation (%) from a baseline of the first simulation decade (1901-1910), for each decade, for: **(d)** Soil respiration; **(e)** Net primary production (NPP); **(f)** Soil DOC inputs from runoff and drainage fluxes; **(g)** CO_2 evasion from the river surface; **(h)** Floodplain DOC input to the river.

Simulated future (2090-99, Table 1) DOC discharge relative to present day values increases slightly for the Kolyma (+7%) and Lena (+3%) basins, but declines significantly for the Yukon (-7%) and more substantially for the Yenisei (-16%), Ob (-53%) and Mackenzie (-37%). On average, this amounts to a decline of -13% for the Big 6 and -13% for the PanArctic as a whole, over the 21st century. The following examines this general decline.

More carbon–less DOC

From the first (1901-1910) to last (2090-2099) decade of the simulation, net primary production (NPP) increased for all basins except the Ob (Fig. 2e). Soil carbon respiration, changes that are proportionally 2-3 times that of NPP (Fig. 2d, Fig. S4), are partially explained by an increase of soil carbon decomposition inducing a loss in soil carbon stocks across basins (Fig. 2c). These flux trends point towards an accelerated Arctic soil carbon cycle, in line with expectations that increases in primary productivity will be more than outbalanced by increases in biome-scale respiration(Abbott et al., 2016). However, this does not translate into an increasing trend in riverine export of DOC from the soil (Fig. 2f), which generally decreases, except for in the case of the Kolyma basin. The Kolyma may carry the signal of substantial increases in permafrost soil carbon mobilisation, consistent with empirical data(Feng et al., 2017). Marked export decreases can be seen in the Ob, Yukon and Yenisei. Conversely, riverine DOC inputs from flooded regions either carry no trend (Ob, Yenisei) or clearly increase (Kolyma, Lena, Yukon), reflecting this fluxes' dependence on direct litter inputs and primary production. Previous studies have shown that DOC concentration and bulk flow scale positively with discharge(Lauerwald et al., 2017). These are largely volatile, bar a decrease in the Mackenzie (Fig. 2b, Fig. S8). Water discharge trends for the N. American and W. Siberian high latitudes are consistent with those from weighted predictions using global climate model ensembles(Yang et al., 2017). The high signal volatility of the Yenisei and Lena basins has also been suggested by the ensemble model output, however these also mostly suggest a modest discharge increase (<5-10%, RCP4.5-8.5, respectively) in these areas in the future. This discrepancy may arise from either reduced precipitation in the model forcing data, or in the enhanced evaporation and evapotranspiration arising from increased temperatures and primary production, respectively.

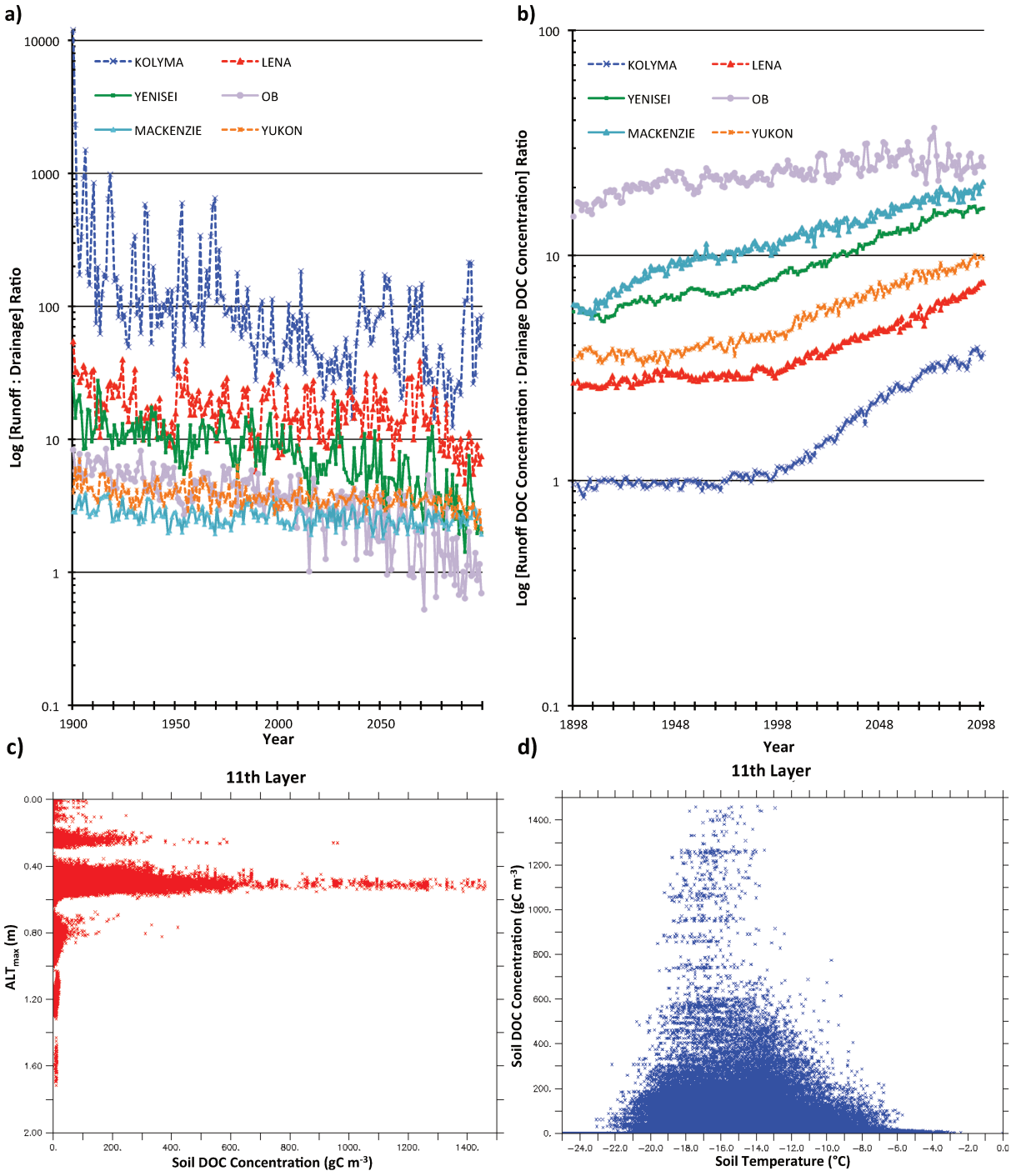

Figure 3: Basin-disaggregated timeseries of **(a)** the yearly mean ratio of (runoff: drainage) water flux over the basin; **(b)** yearly mean ratio of (runoff: drainage) DOC conentrations in those fluxes over the basin. (c-d) The soil DOC concentration (gC m^{-3}) at the model's 11th(2m) layer for each grid cell underlain by continuous permafrost are plotted against **(c)** maximum active layer depth over the pixel and **(d)** mean annual soil temperature.

Where DOC fluxes purely controlled by runoff and river discharge in our simulations, their trends would follow those of the hydrograph. Instead, a more subtle phenomenon is at play. Over 1901-2099, Pan-Arctic soils warmed, permitting an increase in active layer depth and the sudden onset of subsoil water intrusion (drainage) previously inhibited by permafrost shielding. All Arctic basins experienced an order of magnitude

increase in drainage relative to runoff water fluxes over the 200 years (Fig. 3a), where the absolute value of the ratio (runoff:drainage) positively reflects per-basin permafrost coverage. Simultaneously, the relative concentration of DOC in runoff relative to drainage water experienced a similar, ~5-fold increase (Fig. 3b) over that time, spurred by an increase in NPP (+runoff concentration), increased respiration of DOC with depth of its entrainment (drainage concentration decrease of -55 – -74%/200 yrs.), and changes in the seasonal precipitation phase and regime (+runoff). Absolute runoff DOC concentration ratio scales with relative basin permafrost coverage, while its rate of increase accelerates suddenly around the turn of the millenium for the Kolyma and Lena (most permafrost), indicating a basin-wide threshold in active layer thaw and drainage intrusion.

As the mean annual maximum active layer thickness (ALT_{max}) deepens, annual mean soil DOC concentrations at a depth of 2m initially increase (Fig. 3c) up to a thaw depth of ~50cm, before rapidly declining. Correspondingly, the 2m soil DOC concentration responds first positively then negatively to increases in the mean annual soil surface temperature (Fig. 3d), indicating that with increasing temperature, the soil DOC available for lateral transport declines as it is metabolised to CO_2 during the transport into the soil colomn. Furthermore, lower drainage DOC concentrations scale with lower soil particulate carbon concentrations at 2m depth (the depth at which lateral drainage flows occurs) compared to the top 40cm, where runoff DOC fluxes are generated (SI, Fig.S9). This lower substrate concentration leads to a lower leachate concentrations, while carbon concentrations are preferentially depressed at greater soil depths as warming proceeds over the 21st century. Similar dependencies between subsoil carbon fluxes and carbon concentration of their parent material have been found for lateral fluxes of permafrost particulate carbon (Feng et al., 2013).

Increased drainage input to rivers and lower relative concentration of DOC in drainage water combine to lower bulk DOC flow, despite a strengthened carbon cycle, aided by shifting precipitation dynamics. The rain:snowfall ratio increases substantially (SI, Fig. S12a), driven largely by the rain fraction (SI, Fig. S10). This increase largely occurs in mid-late summer (July-October, Fig. S13a-d), with two consequences for DOC: First, it amplifies soil and litter degradation where this is moisture-limited, decreasing the carbon pool build-up normally made available to DOC leaching in the spring snowmelt period, thus decreasing potential DOC input and outflow. Second, late summer corresponds to timing of maximum active layer depth, promoting increased soil water infiltration (feeding massive increases in wintertime groundwater flow (SI, Fig. S14) and lower bulk DOC outflow relative to the case of increased rainfall in e.g. spring (SI, Figs.S12,S13). The relationship of DOC export to rivers with snow and rainfall differs substantially between areas underlain by continuous and discontinuous permafrost (SI, Figs. S12c-f). In permafrost areas, DOC inputs generally increase with rain and snowfall and are more responsive to snowfall (SI, Figs.12c-d). In non-continuous permafrost gridcells, there is no correlation to snowfall and a strong correlation to rainfall (SI, Figs.12e-f). The inference is that the frozen soil layer and cold temperatures in general inhibit DOC flow up until a certain moment in time (late spring/early summer) when the thaw season permits a carbon 'flush'. This is why snow has no relationship with DOC inputs in mon-permafrost areas, since DOC-mobilisation isn't limited by the thawing of a massive snowmelt-derived water flux.

DOC climate sensitivity

Soil-to-river dissolved carbon flux integrates a complex signal, dependent on the interactions between permafrost extent, precipitation, active layer thickness, soil carbon stock, soil type, topography and NPP. These dependencies vary strongly in both strength (R^2) and sign between basins (SI, Fig.S11), highlighting the differing combinations of their interaction. Whereas some basins (e.g., Ob) appear to be clearly driven over the entire simulation period in DOC and CO_2 input by the hydrologic and leaching effects of active layer deepening (SI, Fig.S11b,c,d), others like the Lena appear to lack any response to a full spectrum of drivers (R^2<0.1, SI, Fig.S11a-d) over the whole basin.

This signal between and within catchments is examined with respect to the prime driver of land surface changes, temperature. Sensitivity of combined runoff and drainage DOC exports to temperature for each grid cell grouped under 'permafrost' (ALT_{max}<3m), 'non-permafrost' (ALT_{max}>3m) and 'transitional' (transition from the former to latter over the 21stC, (SI, Fig.S4a) and averaged over the 'modern' (1996-2005) and 'future' (2020-2099)) are plotted against each other (Fig. 4a). DOC input temperature sensitivity between present and future does not follow any distinct pattern between the 3 permafrost groups, although the overall signal appears dominantly controlled by drainage reponse (SI, Fig. S15a,c). The fractal 'star'-shaped response space that results is broken down into an idealised present-future typology (Fig. 4b) to show why such distinct present versus future sensitivity pairings occur. Essentially, the response space indicates high volatility in temperature sensitivity between time periods, in which sensitivity either experiences a change in sign and strong or weak change in value (Fig. 4b, nodes 3,4,7,8), or no change in sign and strong or weak change in value (Fig. 4b, nodes 1,2,5,6).

The DOC input temperature sensitivity is captured by the response of DOC to changes in non-frozen soil or 'active layer' thickness. As temperatures increase, the active layer (ALT_{max}) deepens, causing greater entrainment of water and carbon into the soil. ALT_{max} represents both a temperature and 'DOC-mobilised' soil depth metric. Response of the soil DOC stock and DOC river input (the former the precursor to the latter) to active layer thickness is thus equivalent to a temperature response. This is sinusoidal as the active layer deepens for riverine DOC input and its precursor soil DOC (Figs. 4c,d), reflecting the temperature sensitivity space shown in Fig.4 a-b. The cause for the temperature sensitivity volatility is due to sequential changes in land surface dynamics idealised in Fig. 4e. As temperature, GPP, precipitation and soil carbon loss increase over time in areas underlain by continuous permafrost (no drainage), DOC inputs increase and sensitivity (q) is positive (Fig. , t=0→t=1), but at a temperature threshold (t=2), one soil layer thaws, permitting drainage and causing reduced bulk DOC flux (q=(-)). As the system re-equilibrates, increasing vegetative inputs may cause the sign to switch again (t=3), until a new temperature threshold is reached that thaws another layer of soil (t=4), permitting further diversion of water to drainage another reversal in sensitivity sign, and so on.

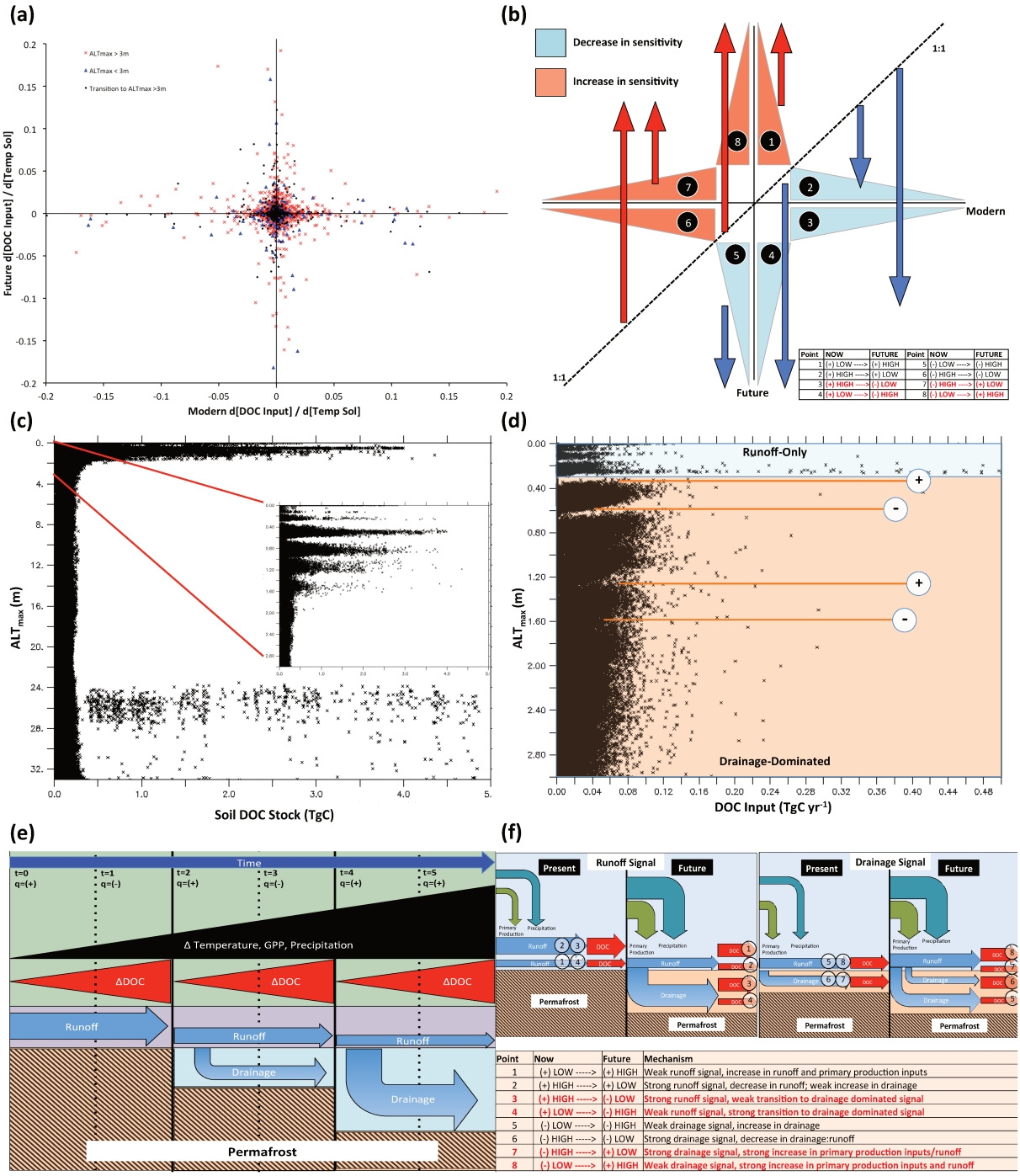

Figure 4: **(a)** Scatter plots showing the year-averaged temperature sensitivity (ground temperature) of DOC inputs to the river (TgC °Celsius^{-1}) in the 'modern' (1996-2005 average) versus 'future' (2020-2099 average) era for 'permafrost' (blue), 'non-permafrost' (red) and 'transitional' (black) grid cells. **(b)** Schematic plot explaining how the 'star'-shaped pattern in (a) results from temperature sensitivity pairs, with each segment of the shape assigned a number and colour. Numbers build a typology of modern versus future temperature sensitivity of DOC (table inset), colours denote an change in sensitivity over time. Arrows indicate the absolute magnitude of change in temperature sensitivity in the future. Red highlights in the inset table indicate changes of sensitivity sign. **(c)** Variation of the summed per-pixel soil DOC stock with the year-mean $ALT_{max)}$ for each pixel and year over the entire simulation period, with inset magnification of the 3m thaw depth. **(d)** Variation of the summed per-pixel DOC input to rivers with the annualised $ALT_{max)}$ for each pixel and year over the entire simulation period, to an ALT_{max} value of 3m. **(e)** Schematic explaining the change in sign and magnitude of total DOC input temperature-sensitivity shown

in (a-b). **(e)** As temperature increases with time GPP inputs with high runoff can cause positive temperature sensitivity (q=(+)); at a temperature threshold, a given permafrost soil layer thaws (middle panel), permitting drainage and causing an abrupt shift in sign of temperature sensitivity to negative (t=2) before regaining positive momentum from runoff and GPP inputs (t=3), etc. **(f):** Specific causal processes explaining the changes in magnitude and sign in (b) with linkages between above and below –ground processes before and after warming (left (LH) and right hand (RH) panels, respectively). **LH panel** corresponds to a situation in which a no-drainage flux soil transitions to one with drainage; **RH panel** corresponds to a situation in which drainage flux increases further with warming. The specific DOC outcomes of warming (red arrows in each right hand panel) map onto the specific modern/future temperature sensitivity pairs in a-b, with an explanation of the potential mechanism for each of these typologies given in the lower panel table.

Expanding on this, we illustrate how each of the temperature sensitivity typology pairs (Fig. 4b) can transition from one side of the pair (present) to the other (future) under second-order environmental drivers, depending on initial conditions (drainage versus no drainage) in Fig.4b,c,d. Thus, nodes (1-4) are cells with no drainage, with DOC input a function of low(1,4)/high(2,3) runoff (Fig. 4f, LHS), and depend on the differing and relative impacts of precipitation, NPP and runoff:drainage to arrive at the specific DOC input outcomes (Fig.4f, RHS) corresponding to the present-future DOC sensitivity pair in Fig. 4b.

These results suggest that despite enhanced water and carbon inputs, bulk DOC outflow to the Arctic Ocean may decline in a warmer future as a result of dynamic water flow paths, their timing, and interaction with a dynamic leaching substrate. This aggregate result is underpinned by substantial divergence between basins in the response of DOC leaching to different variables, which is itself the cause of a necessary volatility, in magnitude and sign, of the temperature sensitivity of DOC leaching between time periods. Given the counter-intuitive nature of these results, we suggest that greater emphasis should be placed on understanding the many non-vegetative interactions from which they emerge.

Chapter 5
CO_2 Uptake By Weathering Increasingly Exceeds CO_2 Evasion From Rivers As Permafrost Thaws [4]

Summary

The potential significance of the rock weathering system to the high latitude inland water and biome-scale carbon cycle has come under increasing recognition in the literature on the topic. In the high latitudes, high carbonate concentrations in bedrock lithologies, their thermal protection from weathering due to the prevalence of permafrost throughout the soil column, and increasing temperatures, soil thaw depths and precipitation caused in part by the amplification of CO_2-driven radiative forcing in high latitude regions, appear on course to combine and drive large-scale increases in CO_2-uptake by chemical weathering. Indeed, recent publications have shown that fluxes of bicarbonate being discharged from major Arctic rivers –a symptomatic measure of rock weathering –have increased on the order of 50-100% in the last few decades alone, with major implications for how the permafrost-region carbon cycle should be viewed and its fate projected into the future. With this in mind, and given the preceding work in this thesis regarding the importance of lateral organic carbon fluxes to the permafrost region, this study integrates a simple simulation module of atmospheric CO2 uptake by chemical rock weathering and carbonate alkalinity generation and export to ocean through rivers in the permafrost region into the land surface component (ORCHIDEE) of an Earth system model (IPSL). To do so, we apply simplified mathematical expressions from the literature relating weathering related CO_2 consumption and alkalinity fluxes to bedrock lithology, surface and subsurface runoff rates and soil temperature. While surface and subsurface runoff rates and soil temperature are simulated by ORCHIDEE at a 30 minute time-step, bedrock lithology is read from a forcing file. After calibrating our model against observed alkalinity fluxes, we are able to reproduce the observed seasonal dynamics in river alkalinity fluxes for present day and to project the long-term evolution of weathering rates and their effect on the CO_2 budget of Arctic watersheds and the exports of carbonate alkalinity to the Arctic Ocean over the 21st century.

To our knowledge, this is the first global-scale model that integrates the specifics of permafrost region soil-thaw dynamics and land-to-river-to-ocean lateral flux tracers to simulate the overland transfer of lithogenically-sourced carbon. Furthermore, by simulating the soil export rate of bicarbonate alkalinity, we are able to estimate the rate of atmospheric carbon dioxide uptake by the chemical weathering process, using some simple literature-derived factors as applied to a lithology map, coupled to the model-generated alkalinity export. All calculated variables are available at daily, monthly or yearly timestep, and at 0.5-2 degree resolution, providing the opportunity to both evaluate and break down the dynamics of these fluxes into their spatial and temporal components and compare them to empirical data. The resulting model version is then subjected to historical and future climatological forcing data to drive simulations of past and future carbonate weathering and alkalinity fluxes for the Pan-Arctic to 2100, under the high/intermediate-warming scenario of RCP-6.0. We show that the model underestimates alkalinity discharge relative to observations by *%. Nevertheless these

[4] Manuscript being prepared for submission to *Global Biogeochemical Cycles.*

flows of DIC (bicarbonates) are similar to DOC fluxes in the present day, and exceed them in projections of the future. Furthermore, and despite the weathering flux underestimate for the current period, CO_2 uptake by chemical weathering is found to exceeds CO_2 evasion from river surfaces across the six largest Arctic rivers, and indeed is nearly double the flux of evasion by the last decade of the 21st C. The upshot of this result is that by including weathering-generated alkalinity fluxes into the calculus of carbon fluxes, the inland water carbon cycle loop including DOC and DIC and their impacts on surface-atmosphere CO_2 fluxes, moves from a net source (via evasion) to a net sink (via chemical weathering uptake) of carbon, and does so increasingly in the future. Furthermore, by including this process, lateral carbon fluxes more than double to ~16% of net biome productivity. Given the shortcomings of both the model and the input data used to drive them, we suggest that this number underestimates the lateral flux contribution by at least a factor of two.

Chapitre 5
L'absorption de CO2 par altération des roches dépasse de plus en plus le relargage de CO2 des rivières à mesure que le pergélisol dégèle

Résumé

L'importance potentielle du système d'altération des roches pour le cycle du carbone des eaux intérieures et des biomes à haute latitude est de plus en plus reconnue dans la littérature sur le sujet. Dans les hautes latitudes, les concentrations élevées en carbonates dans les lithologies du substrat rocheux, leur protection thermique contre les intempéries due à la prévalence du pergélisol dans la colonne de sol, ainsi que l'augmentation des températures, des profondeurs de dégel du sol et des précipitations provoquées en partie par l'amplification du forçage radiatif induit par le CO_2 dans les régions à haute latitude semblent bien vouloir se combiner et entraîner une augmentation à grande échelle de l'absorption de CO_2 par les intempéries. En effet, des publications récentes ont montré que les flux de bicarbonate rejetés par les principaux fleuves arctiques - une mesure symptomatique de l'altération des roches - ont augmenté de l'ordre de 50-100% au cours des dernières décennies seulement, avec des implications majeures sur la façon dont la région du pergélisol le cycle du carbone doit être examiné et son devenir projeté dans le futur. Dans cet esprit, et compte tenu des travaux précédents de cette thèse concernant l'importance des flux de carbone organiques latéraux pour la région du pergélisol, cette étude intègre un module de simulation simple de l'absorption de CO_2 atmosphérique par l'altération chimique des roches et la production d'alcalinité des carbonates et son exportation dans les océans via des rivières de la région du pergélisol dans la composante de surface terrestre (ORCHIDEE) d'un modèle de système terrestre (IPSL). Pour ce faire, nous appliquons des expressions mathématiques simplifiées tirées de la littérature reliant la consommation de CO_2 liée à l'altération et les flux d'alcalinité à la lithologie du substrat rocheux, aux taux de ruissellement superficiel et souterrain et à la température du sol. Alors que les taux de ruissellement en surface et sous la surface et la température du sol sont simulés par ORCHIDEE à un intervalle de temps de 30 minutes, la lithologie du substrat rocheux est lue dans un fichier de forçage. Après avoir calibré notre modèle en fonction des flux d'alcalinité observés, nous sommes en mesure de reproduire la dynamique saisonnière observée dans les flux d'alcalinité des rivières et de projeter l'évolution à long terme des taux d'altération et de leurs effets sur le bilan en CO_2 des bassins versants arctiques et les exportations des produits en question sur l'alcalinité carbonatée dans l'océan Arctique au XXIe siècle.

À notre connaissance, il s'agit du premier modèle à l'échelle mondiale qui intègre les spécificités de la dynamique sol-dégel des régions du pergélisol et des traceurs de flux latéraux de rivières à océan afin de simuler le transfert terrestre de carbone provenant de sources lithogènes. En outre, en simulant le taux d'exportation d'alcalinité en bicarbonate dans le sol, nous pouvons estimer le taux d'absorption de dioxyde de carbone dans l'atmosphère par le processus d'altération chimique, à l'aide de simples facteurs dérivés de la littérature, appliqués à une carte lithologique, couplés aux

modèles générés par le modèle sur exportation d'alcalinité. Toutes les variables calculées sont disponibles à des intervalles de temps quotidiens, mensuels ou annuels et à une résolution de 0,5 à 2 degrés, ce qui permet d'évaluer et de décomposer la dynamique de ces flux en leurs composantes spatiales et temporelles et de les comparer à des données empiriques. La version du modèle résultante est ensuite soumise à des données de forçage climatologiques historiques et futures pour piloter des simulations de flux d'altération et d'alcalinité carbonatés passés et futurs pour le Pan-Arctique jusqu'à 2100, selon le scénario de réchauffement élevé / intermédiaire de RCP-6.0. Nous montrons que le modèle sous-estime le débit d'alcalinité par rapport aux observations de *%. Néanmoins, ces flux de bicarbonates sont similaires aux flux de COD actuels et les dépassent dans les projections sur l'avenir. En outre, et malgré le sous-estimé du flux d'altération climatique pour la période actuelle, l'absorption de CO_2 due à l'altération chimique dépasse l'évasion de CO_2 de la surface des rivières sur les six plus grands fleuves arctiques, et représente en fait presque le double du flux d'évasion de la dernière décennie du 21^{ième} siècle. Ainsi, en intégrant les flux d'alcalinité générés par les intempéries dans le calcul des flux de carbone, le cycle du carbone des eaux intérieures comprenant DOC et DIC et leurs impacts sur les flux de CO_2 passe d'une source nette vers un puits de carbone, avec un effet amplifié à l'avenir. De plus, en intégrant ce processus, les flux de carbone latéraux représentent plus du double, pour atteindre environ 16% de la productivité nette du biome. Étant donné les lacunes du modèle et des données d'entrée utilisées pour les piloter, nous suggérons que ce nombre sous-estime la contribution du flux latéral d'au moins un facteur de deux.

1 Introduction

Chemical weathering of the land surface represents a global CO_2 sink of ~0.26-0.29 $PgCyr^{-1}$ (Amiotte Suchet et al., 2003; Gaillardet et al., 1999). This sink is balanced on oceanic turnover (10^4) or geologic (10^7) -year timescales, depending on whether the weathering product is precipitated in the ocean or outgassed in volcanic activity, respectively (Beaulieu et al., 2012). Fluvial export of weathering products and carbonate precipitation in the coastal ocean have been the primary sink for atmospheric CO_2 over Earth's history and are the reason why today the largest carbon storage term on Earth lies in carbonate rocks, followed by fossil fuel hydrocarbons –themselves partially derived from sedimentation of fluvial organic carbon fluxes (Kump, L.R., Kasting, J.F., Crane, 2010).

In the ocean, the carbonate alkalinity products of weathering (carbonate and bicarbonate) remain important for the contemporary state of the carbon cycle, their input rate and concentration determining the calcium carbonate saturation state of ocean water on which biogenic calcification, including that of many marine primary producers (PP), depend for survival (Feely et al., 2004). Transport by rivers and streams control this oceanic input with weathering reactions occurring in soils over the terrestrial landscape. The chemical products of weathering substantially affect the carbonate alkalinity of terrestrial runoff waters (hereafter referred to as 'alkalinity') through inputs of carbonate and bicarbonate (alkalinity = $\Sigma[HCO_3^-, CO_3^{2-}]$), which are likewise a major component of aggregate dissolved inorganic carbon (DIC, = $\Sigma[CO_2, HCO_3^-, CO_3^{2-}]$) fluxes to the ocean. Weathering is driven by the following idealised reactions:

$$(\mathbf{1})\ \boldsymbol{H_2O + CO_2 \leftrightarrow\ H_2CO_3(carbonic\ acid)}$$
$$(\mathbf{2})\ \boldsymbol{CaCO_3 +\ H_2CO_3 \leftrightarrow\ Ca^{2+} + 2HCO_3^-(bicarbonate)}$$

Rainwater dissolution of CO_2 in the root zone (this CO_2 being of atmospheric origin since it was initially fixed by photosynthesis) is converted into HCO_3^- upon weathering of carbonate rocks, which reduces its chemical susceptibility to atmospheric release (Brantley et al., 2011). Likewise, the vertical percolation of water through the soil column allows for the fixation of CO_2 of atmospheric origin residing in soil pore space as HCO_3^-. Equation 2 acts on short time scales, in that the reaction is reversible, whereby carbonates can also be precipitated in solution in soils, rivers or the ocean, releasing CO_2. The link between freshwater alkalinity and DIC in inland water systems is through carbonate buffering of reaction kinetics, in which high alkalinity waters (pH ~8) cause a small fraction of dissolved CO_2 (H_2CO_3) to dissociate to $H^+ + HCO_3^-$, reducing the air-water CO_2 partial pressure gradient (Stets et al., 2017) and so the river surface flux of CO_2 to the atmosphere, which globally totals ~1.8 PgC yr^{-1} (Raymond et al., 2013). In the high alkalinity case, the HCO_3^- produced by dissociation of carbonic acid is excluded from the summed HCO_3^- in the alkalinity metric defined above, as it is counterbalanced by the proton instead of a base cation. In practice, the weathering substrate responsible for CO_2 uptake is dominated by two globally-prevalent mineral rock sources, silicate and carbonate, similarly weathered as follows for the idealised carbonate and 'silicate' (wollastonite) reactions:

$$(\mathbf{3})\ \boldsymbol{CaSiO_3(silicate) + H_2O\ +\ 2CO_2\ \rightarrow\ Ca^{2+} + 2HCO_3^- + SiO_2}$$

$$(4)\ CaCO_3(carbonate) + H_2O + CO_2 \rightarrow Ca^{2+} + 2HCO_3^-$$

Eqs. (3-4) show that whereas alkalinity ($2HCO_3^-$ above) generated by silicate weathering is fully sourced from atmospheric CO_2 (or in practice free CO_2 in the soil (Calmels et al., 2014)), carbonate alkalinity is equally derived from the atmosphere (50%) and lithogenic source (50%). Soil free CO_2, is mediated by soil microbial activity and root respiration that provide CO_2 and organic acid protons used in the weathering reaction (Kuzyakov, 2006). However, whereas weathering in Eqs. (1-2) uses carbonic acid, the presence of sulphides (pyrite) in parent material (e.g. shales), or in acid rain caused by the burning of sulfur-bearing fuels, can produce weathering via sulphuric acid without consumption of CO_2, and is thus carbon-neutral on short, or a carbon source on ocean turnover, timescales (Tank et al., 2016; Zolkos et al., 2018), e.g. :

$$(5)\ CaCO_3 + H_2SO_4(sulphuric\ acid) \rightarrow +Ca^{2+} + SO_4^{2-} + H_2O + CO_2$$

As suggested, the first-order control on weathering rates are the 'supply' of weatherable minerals -the quantity with which they exist on the land surface and soil (this global distribution driven initially by topographic uplift followed by other 'supply-side' factors like erosion) -and the 'demand' for those weatherable minerals by weathering agents (protons), themselves controlled by atmospheric CO_2 concentrations and the existence of soil flora and fauna for the production of CO_2 and organic acids. The reaction rate between these two is itself sensitive to other environmental drivers. Generally, weathering rates scale positively with temperature (Dessert et al., 2003; Raymond, 2017) due to the knock-on effects on solubility and reaction rates. However, there have been suggestions that the temperature dependence of weathering is limited by hydrological flux -if low, weathering my not be sensitive to temperature (Raymond, 2017; White and Blum, 1995). Likewise, when water throughput is low (residence times long), weathering will equilibrate with the soil solution more quickly, causing it to be 'transport limited' (Maher, 2010; Raymond and Hamilton, 2018) i.e. it will increase with increasing throughput (decreasing residence time) -until a peak is reached at which weathering is reaction-limited. By comparison, dissolved organic carbon (DOC) leaching rates scale positively with runoff but negatively with flowpath length (Maher and Chamberlain, 2014; Millot et al., 2003; Mulholland, 1997).

Globally, the inorganic carbon cycle in cold regions (>50°N) can be characterised by physical and chemical weathering processes, including the grinding action of glaciers and annual freeze-thaw cycles, whose effect is to increase the effective mineral surface area exposed to the weathering reactant. Weathering in these high latitude regions is subject to substantial change due to anthropogenic climate warming. Glacial melting (Gislason et al., 2009) and permafrost thaw and subsequently enhanced soil-water interactions (Tank et al., 2016; Tank, Raymond, et al., 2012a), coupled with increased primary production via higher atmospheric CO_2 and thus biogenic soil CO_2 inputs(Striegl et al., 2007), may all increase weathering and hence riverine alkalinity flux rates (Fig. 1). In addition, temperature increases will spur silicate solubility, enhance chemical reaction rates and, in the high latitudes, probably substantially increase surface and subsurface hydrological runoff, increasing weathering reaction rates. These are presented in idealized form in Figure 1. Such changes may substantially impact the aggregate strength of weathering CO_2 consumption (Drake et al., 2018) and may partly

offset some of the substantial CO_2 release to the atmosphere from microbial metabolisation of thawed permafrost soils projected for the future (Schädel et al., 2014). To date, however, quantification of the high latitude weathering response to a changing climate has been elusive. This is because its process-based representation requires, on the one hand, resolving the nexus of hydro-lithological reaction kinetics with thermal and biotic factors necessary for generating a dynamic above-ground weathering flux rate. Although this has previously been achieved by the WITCH model (Beaulieu et al., 2012), that model requires a very large number of data-based parameters as input, and may thus be difficult to employ outside of extremely well-studied basins, of which very few exist in the high latitudes.

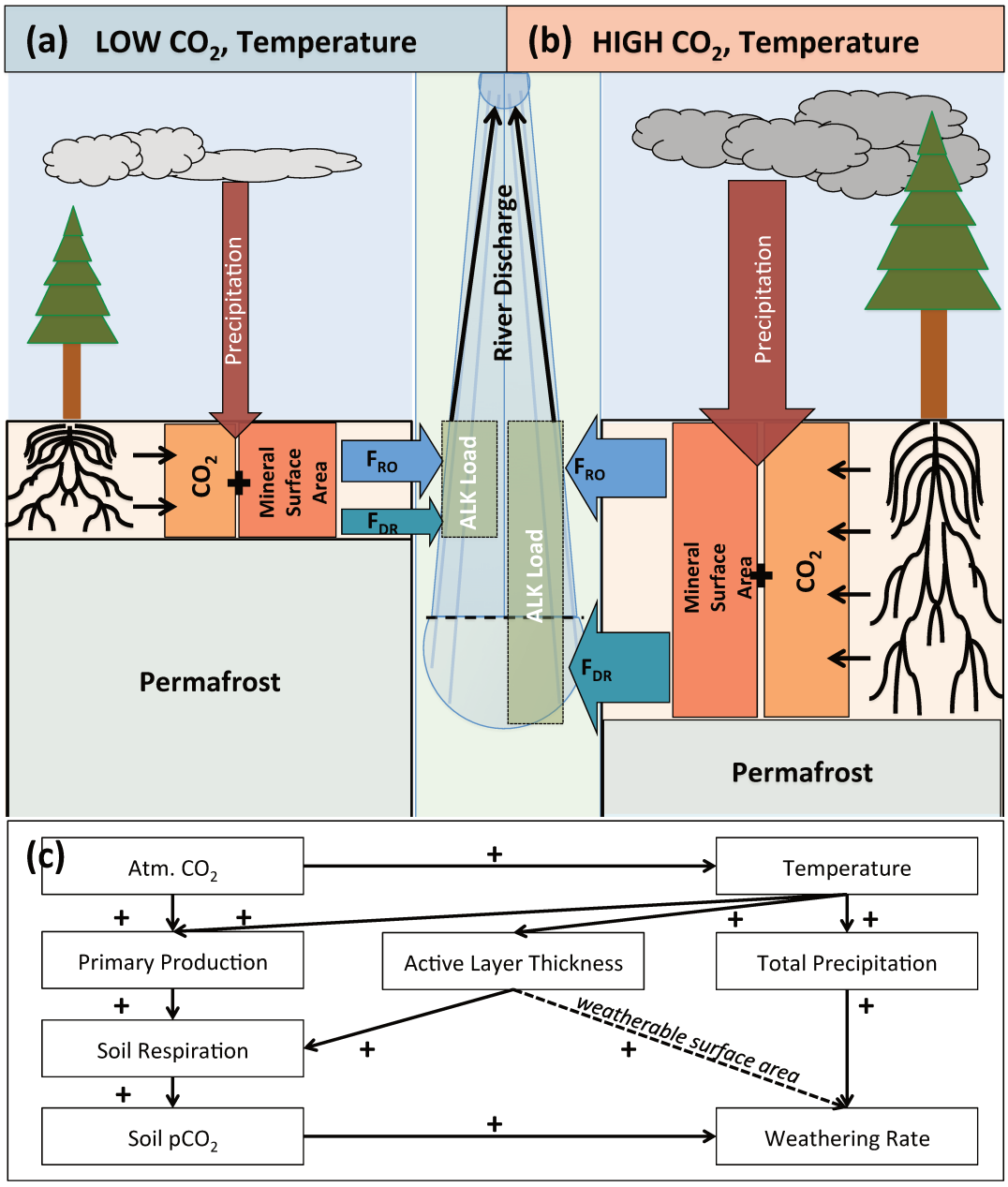

Figure 1: (a-b) Schematic diagram with simplified representation of the main state variables and processes under low (a) and high (b) CO_2 and temperature may affect weathering rate and by extension the alkalinity load ('ALK Load') entering into rivers within the permafrost region. In the diagram, the 'tree' represents primary production, the black lines underneath the rooting depth, 'CO_2' refers to the

partial pressure of CO_2 in the soil, 'Mineral Surface Area' refers to the weatherable soil mineral surface area increasing with active layer), 'F_{RO}' and 'F_{DR}' refer to the surface/near-surface and subsurface/deep soil water flows. The relative size of arrows, boxes and forms is indicative of differences in the volume of these flows between the two states shown.**(c)** System diagram depicting the idealized chain of causality (sign shown) between changes in climatology and changes in weathering rate in a-b.

On the other hand, the complexities of permafrost soil thermodynamics and hydraulics need to be resolved to represent the belowground reaction of these to thaw. The subsequent, dynamic responses of surface and groundwater fluxes likewise determines the flowpath, timing and concentration of weathering products in rivers, these requiring accurate spatio-temporal representation of chemical species lateral transfer across the landscape through the hydrological network. Finally, understanding the response of weathering to environmental change is hampered by the lack of long-term time-series of riverine alkalinity discharge with which to track this response. Globally, only the Mississippi has such data over the 20th Century (Raymond et al., 2008), while in the high latitudes records span a maximum of 50 years, with large data gaps for the Eurasian rivers(Drake et al., 2018; Tank et al., 2012b, 2016; Zolkos et al., 2018). This study aims to address these three problems, by integrating a simple carbonate alkalinity (weathering) generation scheme into a global land surface model developed specifically for resolving permafrost region-specific physical, hydrological and biological dynamics, and the lateral transfer of dissolved species across its landscape, requiring only basic hydrological datasets (alkalinity discharge, river water discharge) for this task. This allows us to simulate seasonal, surface and subsurface fluxes of alkalinity at a 30 minute simulation timestep. High temporal resolution allows us to capture the daily and seasonal cycle of alkalinity fluxes, which are sensitive to short-term variation in the soil environment, rather than bulk annual fluxes. Further, the seasonal variation of terrestrial alkalinity (and CO_2) fluxes into the Arctic ocean of is of particular relevance to the marine realm, where these variations dramatically impact seawater acidification, carbonate saturation state and photosynthetic production (Semiletov et al., 2016). Finally, the ability of our model in reconstructing the interannual trend for those rivers where long-term data exist may give us some confidence in producing datasets of historical fluxes for those where data does not exist. In what follows, we describe the equations and models that were added to the land surface model ORCHIDEE M-L to simulate riverine alkalinity fluxes, as well as the sequence of steps taken for model calibration and optimisation.

2 Materials and Methods

	Basalt	Granite		
Activation Energy (j/mol)	50000	60000	Diff.	Diff. %
Temperature (Kelvin)	Multiplier (F_T)	Multiplier (F_T)		
274.15	0.462	0.396	0.066	14%
276.15	0.542	0.479	0.063	12%
278.15	0.633	0.578	0.055	9%
280.15	0.739	0.696	0.043	6%
282.15	0.861	0.835	0.025	3%
284.15	1.000	1.000	0.000	0%
286.15	1.159	1.194	-0.035	-3%
288.15	1.342	1.423	-0.081	-6%
290.15	1.549	1.691	-0.142	-9%
292.15	1.785	2.005	-0.219	-12%
294.15	2.053	2.371	-0.318	-15%

Table 1: Sensitivity of the temperature-dependent alkalinity flux multiplier (Eq. 6) to the upper and lower bound of the activation energy (E_a) range (for granite and basalt lithologies, respectively) given by Hartmann et al., (2014), calculated for a range of temperatures (1-21°C) against a reference temperature of 10°C. Absolute and percentage difference of the multiplier (F_T) from the mean of the temperature range are shown.

2.1 Global Land Surface Model Description

The land surface model that was adapted to generate alkalinity fluxes in the northern hemisphere is a sub-version of the land surface component of the IPSL Earth System model, ORCHIDEE (Organising Carbon and Hydrology in Dynamic Ecosystems (Krinner et al., 2005)), given the name ORCHIDEE MICT-LEAK (Bowring et al., 2019a), hereafter referred to as ORCHIDEE M-L, which has previously been presented and evaluated for the Lena river basin (Bowring et al., 2019b) as well as the Pan-Arctic (Bowring et al., 2019 in prep.). This model version essentially derives from two other subversions of ORCHIDEE. The first, was specifically coded for representation of high latitude phenomena and permafrost processes, called ORCHIDEE-MICT, has been presented and evaluated for the Pan-Arctic (Guimberteau et al., 2018). Specifically, it includes representation of permafrost soil C stocks and snow physics, and their thermodynamics, to a depth of 38m, soil hydrology to a depth of 2m, explicit simulation of the active layer and subsequent thermal and hydrologic shielding of sub-active layer soil.

The second, ORCHILEAK (Lauerwald et al., 2017) incorporates production of DOC from soil organic matter (Camino-Serrano et al., 2018), soil carbon 'priming' (ORCHIDEE-PRIM (Guenet et al., 2016)) and the riverine transport and transformation of DOC and CO_2, C and water exchanges with floodplains, and CO_2 evasion from rivers and wetlands (Lauerwald et al., 2017). ORCHIDEE M-L thus resolves DOC and CO_2 production, and DOC diffusion, within a vertically-discrete soil column representative of permafrost region soil thermodynamics and snow physics, and their transport/transformation within the inland water network. This combination of process representations is, to our knowledge, unique amongst land surface models and provides the instrumental rationale for using this model sub-version as the basis from which to simulate high latitude alkalinity fluxes at the global scale.

Key to representation of weathering is the explicit, vertically discretised soil column and the hydrological fluxes which flow through them. Hydrological carbon tracers, including alkalinity, are assigned to surface and subsurface water flows, where surface runoff flows are aggregated from the water fluxes that do not permeate below 0.045m while subsurface 'drainage' waters, which flow laterally at depth, are sourced from depths of 0.045-2m. Thus in what follows the "surface runoff" which actually includes a small portion of subsurface flow (to 4.5cm), will be referred to as 'surface runoff', while the deep subsurface flow will be referred to as 'drainage'. This ability to distinguish surface from subsurface flows is important because the seasonality of each is markedly different in the permafrost region. Whereas drainage flows can occur throughout the year in the unfrozen portion of the soil column, surface runoff is highly seasonal. At the same time, we expect alkalinity concentrations in the high latitudes to be substantially higher in drainage versus runoff water flows, given that these flows may currently be accessing parts of the soil column previously inaccessible to them due to soil freezing, as well as higher water residence times and the higher concentration of weatherable surface in the mineral subsoil.

Finally, the soil temperature at the near-surface versus at depth also differ considerably, being cooler at the surface and warmer at depth in the winter, and vice versa in the summer. These temperature differences can drive substantial shifts in the rate of weathering, and can be accounted for in our model. The combination of different timing and concentrations of the surface and subsurface flows and vertically discretised soil temperatures means that we can produce simulated alkalinity at a daily or seasonally and spatially (vertically) disaggregated scale.

2.2 Weathering flux model

Generating a carbonate and silicate weathering flux rate in ORCHIDEE MICT-LEAK required a number of separate steps, described in the following subsections. Our approach was to combine equations linking lithology/hydrological runoff and temperature with weathering, presented first by (Moosdorf et al., 2011) and (Hartmann and Moosdorf, 2012), respectively, who successfully applied these relationships to North America and the globe. We then add in a factor relating weathering to soil respiration (e.g. (Striegl et al., 2007)). Based on an underlying high resolution lithology map (Hartmann and Moosdorf, 2012), and the soil temperature, hydrology and soil respiration, generated by ORCHIDEE M-L, we simulate a weathering and alkalinity flux in the model which is then calibrated against observed data from Tank et al., (2012a) for the six largest Arctic rivers, and used to partition simulated alkalinity fluxes between surface and subsurface flows. The resulting model setup permits us to run long-term model simulations and projections of future weathering.

2.2.1 Step 1: Bulk weathering annual soil solution bicarbonate concentrations

First, to calculate an initial grid cell-specific annualised weathering flux rate, we assume that this flux is determined by hydrological runoff, defined here as the combination of surface and subsurface water flows, and underlying lithology, per the Runoff-Lithology (RoLi) model described in Eq. 2 of Moosdorf et al., (2011) (see Figure 2a). RoLi uses 16 lithological classes to estimate annual alkalinity yield per unit runoff, calibrated over the

entire North American continent, whereby a linear regression parameter for runoff and a exponential parameter for runoff per lithological class are used. Over the lithological classes, carbonate rocks have the highest alkalinity yield per unit increase in runoff, whereas granitic rocks have the lowest (see Fig. 5 in Moosdorf et al., 2011).

To obtain the two weathering drivers (runoff and lithology), we run ORCHIDEE-ML for 30 years at 1° resolution, using the second Inter-Sectoral Impact Model Intercomparison Project (ISIMIP2b (Frieler et al., 2017; Lange, 2016, 2018)) climatology over 1975-2005, to simulate high-latitude (45-90°N) annual river 'total runoff' (surface runoff + drainage in the model) fluxes. The average of this per-grid-cell annual total runoff flux is combined with the high resolution global lithological map GLiM (Hartmann and Moosdorf, 2012) and applied to the equations used in the RoLi Model using ArcGIS 10.6.1 (ESRI, 2018). The result is a high latitude map of mean annual bicarbonate alkalinity concentration (mgC L^{-1}) in runoff and drainage water, i.e. the total runoff (Fig. 2). This methodological sequence is shown for the first three points of Fig. 2a.

2.2.2 Step 2 – Temperature dependence

ORCHIDEE M-L was adapted to read in this annual bicarbonate concentration map, and to allow the model to distribute this annual concentration map into fluxes of alkalinity in surface runoff and drainage fluxes at a 30-minute timestep. To include the sensitivity of weathering rates to temperature we apply a temperature-driven chemical weathering multiplier from Hartmann et al., (2014) to the alkalinity flux generated by the model (concentration*instantaneous hydrological flux) at a 30 minute timestep into its code:

$$F_{T,i} = exp^{(-E_{a,i}/R*(1/T - 1/T_0))} \quad (6)$$

Where F_T is the temperature multiplier, R is the gas constant, T_0 is the reference temperature which is generated from average non-frozen soil temperature generated over the 20th century by the ORCHIDEE-ML at 45-90°N, T is the soil temperature per grid cell and soil layer and timestep (for each of the energy and water calculations module's 30 minutes timesteps) and E_a is the activation energy. Hartmann et al. (2014) give three lithology-dependent activation energies: one each for felsic, mafic, and pyroclastic rocks. For carbonate rocks, they assume that there is no temperature effect as increased weathering rates are counterbalanced by a decreased solubility of carbonates with increasing temperature. We use the mean of their activation energy range for basaltic and granitic rocks (E_a=55000 J mol^{-1}) as input to Eq. 6, justified by the fact that over a 20°C range of realistic non-zero temperatures in high latitudes (1-21°C), the temperature-dependent activation energy varies by a maximum of +/-15% across these two lithological classes (Table 1), while pyroclastic rocks are a relatively scarce underlying lithology, that are thus ignored here. Because ORCHIDEE M-L generates water losses to rivers at both the surface and subsurface, we determine a reference temperature (T_0 in Eq. 6) for each of the runoff and drainage fluxes, determined by the layer thickness-weighted average of the mean annual grid cell soil temperature, in the top five (top 0.045m, 283.2K) and bottom six hydrological soil layers (bottom 1.955m, 280.15) over the 30-year model run period described above, averaged over all grid cells.

(a)

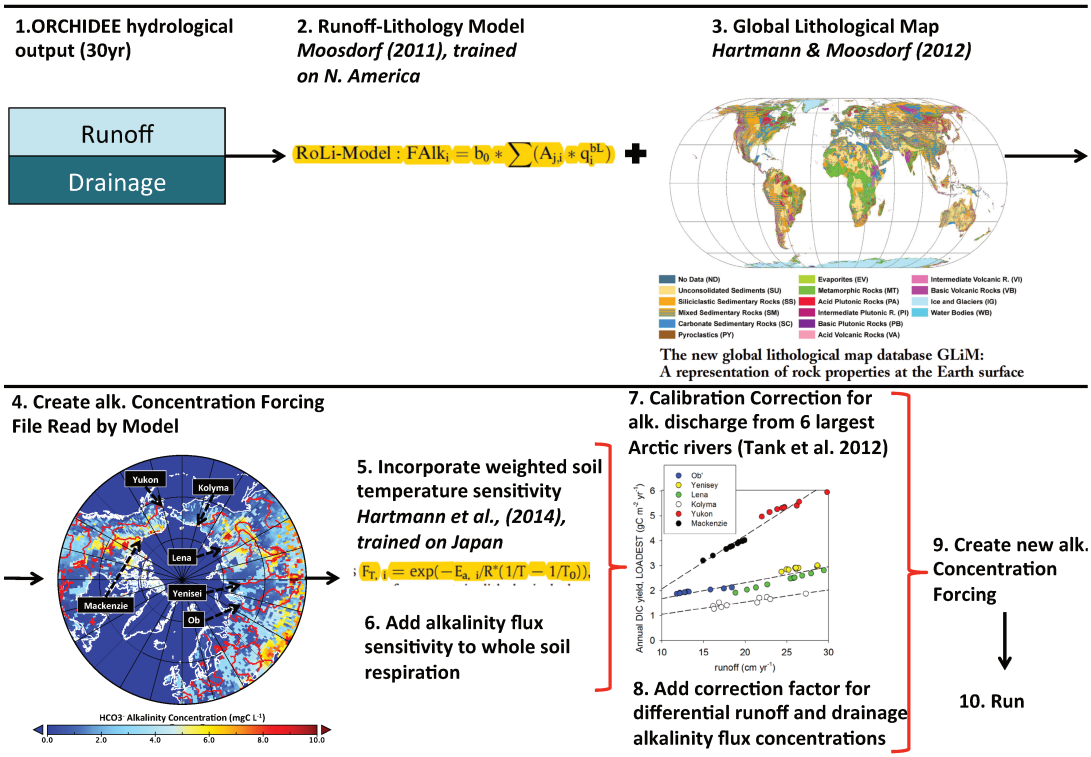

(b)

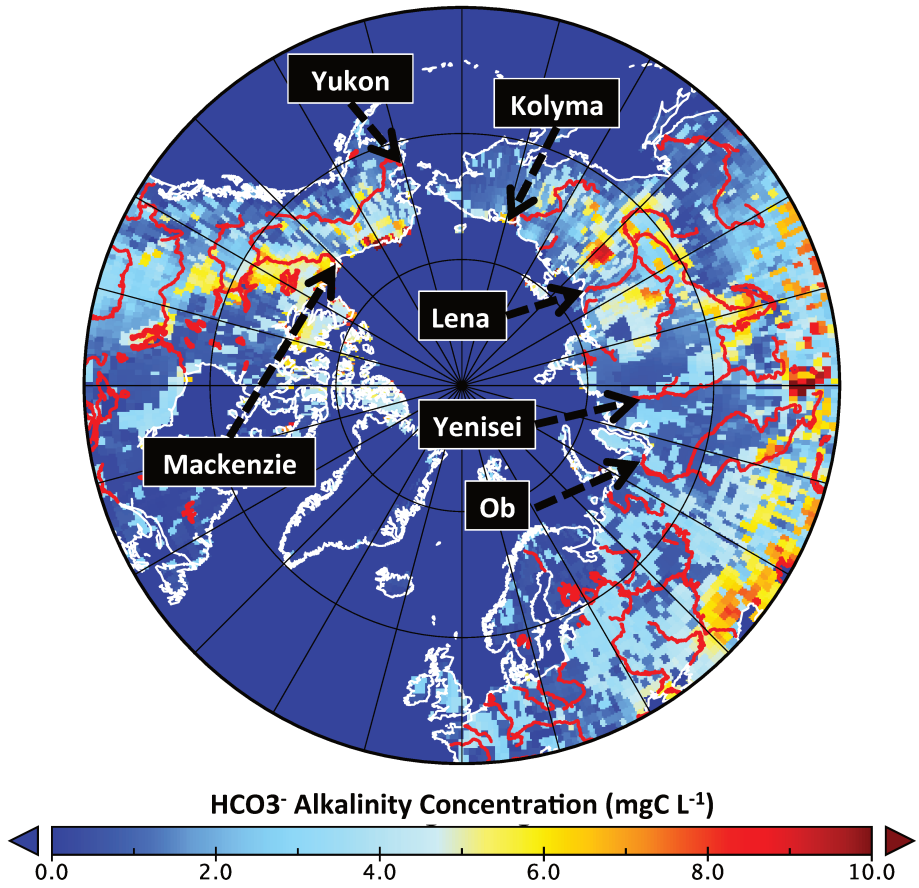

Figure 2: (a) Schematic representation of the sequence of steps by which the simulation of alkalinity fluxes is generated by the model, as described in Section 2.2. (b) Average Pan-Arctic dissolved HCO_3^- alkalinity concentration (mgC L^{-1}) in runoff and drainage water fluxes used as a forcing file to run the

model. Concentrations were calculated using the Moosdorf et al., (2011) Ro-Li model based on the Hartmann and Moosdorf, (2012) Global Lithological Map and the average runoff and drainage fluxes simulated over the years 1975-2005 by ORCHIDEE M-L under ISIMIP2-IPSL climatology. Names of the 'big six' Arctic river basins are given in black boxes, with arrows pointing to the river mouth of each basin.

2.2.3 Step 3 –Respiration dependence of Weathering

As discussed, increases in CO_2 and temperature increase primary production and soil respiration, increasing the availability of the weathering agent (protons) and thus in theory the rate of weathering. To represent this, we scale simulated alkalinity fluxes in runoff and drainage waters to heterotrophic soil (R_{soil}), root (R_{root}), and belowground litter (R_{litt}), respiration, normalised by a reference respiration value (R_{ref}) taken from simulated output of these variables over the Big 6 basins for the approximate period during which most observational data have been gathered for these rivers (1996-2005). Runoff and drainage alkalinity fluxes in a grid cell at a given timestep is scaled to a dimensionless modifier (M) determined by the total soil respiration in that grid cell and timestep, normalised by the R_{ref} calculated, as in Eq. 7:

$$(7)\ \boldsymbol{M} = \frac{\boldsymbol{R_{soil}} + \boldsymbol{R_{root}} + \boldsymbol{R_{litt}}}{\boldsymbol{R_{ref}}}$$

Where R_{ref} depends on the input forcing data being used. Where ISIMIP (IPSL) climatology was fed into the model, R_{ref} = 1.1 gC m^{-2} d^{-1}, whereas for GSWP3 climatology (see Section 3.2) R_{ref} =0.69.

2.2.4 Step 4 –Calibrating Alkalinity Flows to Arctic River Data

In the next step, we calibrated the model to obtain a reasonable ratio between surface runoff and drainage alkalinity concentrations, needed to simulate the seasonality in alkalinity concentrations, with lowest concentrations in late spring when contributions from surface runoff due to spring freshet are the highest, and higher concentrations when the river is mainly sourced by subsurface water flow (due to surface freezing). For this, we fitted the model-generated alkalinity fluxes sourced from both surface runoff and drainage to observation-based estimates of monthly average alkalinity loadings for the Big 6 Arctic Rivers. To obtain those observation-based estimates of monthly average alkalinity loads, we used for each river the rating curve representing the relationship between alkalinity flow and river discharge empirically found by Tank et al., (2012a), and applied them to the average monthly discharges simulated with ORCHIDEE M-L over the period 1976-2005. We preferred the so estimated monthly riverine alkalinity fluxes over the observed fluxes published in Tank et al., (2012a), as seasonality of alkalinity concentrations and discharge are tightly, functionally coupled and the slight but significant mismatch between simulated and observed seasonality and magnitude of discharge, which we had identified for our model results, would lead to erroneous, unrealistic calibrations of surface runoff versus drainage concentrations to compensate for the mismatch in discharge.

In order to calibrate a constant ratio between surface runoff and drainage concentration to be applied to all Arctic Rivers, we first performed a regression of modeled versus observation-driven monthly alkalinity concentrations for the 6 Arctic rivers (eq. 8, n=72). The observation-driven concentrations (C_{obs}) were calculated by dividing observation-driven monthly alkalinity fluxes (see above) by the simulated monthly

discharge . The simulated annual concentrations $C_{sim,RUNOFF}$ and $C_{sim,DRAINAGE}$ were calculated by dividing the simulated surface runoff and drainage alkalinity flux, respectively, by the simulated mean discharge (1976-2005). That means that the sum of $C_{sim,RUNOFF}$ and $C_{sim,DRAINAGE}$ gives the total of simulated alkalinity concentration in the river.

$$(8)\ \boldsymbol{C_{obs} = a1 * C_{sim,RUNOFF} + a2 * C_{sim,DRAINAGE}}$$

The regression yields values for a1 and a2 of 0.58 and 1.22, respectively (R^2=0.77, p-value: < 2.2e-16). From this regression, we obtained a mean ratio of surface runoff to drainage alkalinity concentrations of 0.47. This ratio between surface runoff and alkalinity concentrations explains seasonal variations in alkalinity concentrations, with lowest values during the spring freshet when surface runoff is dominant, but also spatial variations in alkalinity concentrations. For example, areas with high permafrost coverage are dominated by surface runoff and thus exhibit low HCO_3^- concentrations (spatial feature), while during the spring thaw/high river discharge period (temporal feature), alkalinity concentrations plummet as the flux of weathered matter is diluted by the huge water flux at this time (Tank et al., 2012b, 2012c).

2.2.5 Step 5 –Calibration Correction

In the final step, we corrected the alkalinity concentration forcing, developed in Step 1 (2.2.1), to account for the fact that the empirical model from which it is derived was mainly trained on temperate North American watersheds, and thus not necessarily representative of the high latitudes. We found a correction factor for each basin, by applying the [surface runoff:drainage alkalinity] concentration ratio of 0.47 to the surface runoff alkalinity fluxes generated from the alkalinity concentration forcing, while the drainage alkalinity fluxes were kept unchanged (eq. 9). Then, we summed both fluxes up to the simulated monthly fluvial alkalinity transports, which were regressed again against the observation-driven alkalinity fluxes.

$$(9)\boldsymbol{Load_{obs} = b * (0.47 * Load_{sim,RUNOFF} + Load_{sim,DRAINAGE})}$$

Where Load refers to annual alkalinity loading of a river (kgC s^{-1}), with right-hand-side subscripts referring to the source the simulated alkalinity flux and $Load_{obs}$ being the observation-based alkalinity flux. As mentioned above, we fitted that regression for the average monthly alkalinity fluxes for each basin, with regression results listed in Table S1. We applied the b-estimates from the regression as correction factors to the original alkalinity concentration forcing file. For areas outside the Big 6 river basins, we used the correction factor from the closest basin. Through this, we obtained a corrected forcing file representing the alkalinity concentration in the drainage fluxes per grid cell for a reference soil temperature of 280.15 K. The corresponding concentration in the surface runoff flow is calculated by applying the factor of 0.47 obtained above.

2.3 Estimation of CO_2 Uptake by Chemical Weathering

As described in the introduction, chemical weathering of carbonate and silicate rocks drives CO_2 uptake in the weathering reaction between water and carbonate and/or

silicate -bearing rocks. Based on the rate of combined surface and subsurface generation of dissolved product of this reaction (HCO_3^- in solution) –in other words, the export rate of alkalinity from the soil – that is produced by the outputs of our model, we can calculate the atmospheric CO_2 uptake rate associated with weathering, and the spatially explicit changes in that rate over time. To do so, we use the lithology dependent CO_2 uptake/alkalinity flux ratio found in Moosdorf et al. (2011) and apply it to the total export (surface runoff + drainage) of alkalinity per grid cell and year of simulation to arrive at a first-order CO_2 uptake rate per unit land surface area (gC m^{-2} yr^{-1}).

3 Data and Simulation

3.1 Simulation forcing with ISIMIP climatology

The climatological forcing data used to drive ORCHIDEE-ML for historical and future simulations was taken from bias-corrected projected output from the IPSL Earth System Model under the second Inter-Sectoral Impact Model Intercomparison Project (ISIMIP2b (Frieler et al., 2017; Lange, 2016, 2018)) rubric, following the 'intermediate-warming' trajectory of Representative Concentration Pathway 6.0 (RCP 6.0). This scenario projects rising emissions through the 21st Century, which peak in 2080. Climatological input data are at a daily temporal and 1 degree spatial resolution, covering the period 1960 to 2100. The input vegetation and land cover map was taken from the 5th Coupled Model Intercomparison Project 5 (CMIP5-LUHa) output. As previously mentioned, we derived a baseline weathering product concentration map which was read as input to the model (Fig. 2a,b). This input is then mediated by the weighted mean soil temperature experienced by the surface and subsurface water fluxes, as described in the preceding subsections. The water height threshold, used to define the water level at which floodplain inundation is triggered, is obtained statistically over multiple 30 year (1976-2005) model runs using ORCHIDEE MICT-LEAK, in a stepwise procedure first described in Lauerwald et al., (2017) and employed in Bowring et al. (2019).

River Discharge (km^3 yr^{-1})	Yukon	Mackenzie	Ob'	Yenisei	Lena	Kolyma
Observed 2000-2009	**207**	**305**	**415**	**640**	**603**	**78**
ISIMIP sim. 2000-2009	119	245	498	455	327	80
GSWP3 sim. 2000-2009	119	211	593	501	359	98
Observed 1990-1999	**217**	**275**	**405**	**613**	**532**	**68**
ISIMIP sim. 1990-1999	112	253	494	473	295	82
GSWP3 sim. 1990-1999	126	220	558	506	331	89
Observed 1980-1989	**206**	**273**	**376**	**582**	**549**	**68**
ISIMIP sim. 1980-1989	128	260	530	464	327	74
GSWP3 sim. 1980-1989	128	221	524	483	316	96
Observed 1970-1979	**184**	**292**	**441**	**591**	**529**	**65**
ISIMIP sim. 1970-1979	113	232	461	432	317	96
GSWP3 sim. 1970-1979	118	230	574	497	327	90

Table 2: Observed vs. simulated river water discharge using the ISIMIP 2b and GSWP3 climatological forcing datasets. Shown are the decadal-mean simulated (ISIMIP 2b) versus observed total annual river discharge (km^3 yr^{-1}); observations are taken from the NOAA Arctic Report Card by Holmes et al., (2015).

3.2 Rationale for simulation with GSWP3 climatology

Previous studies (Bowring et al., *in prep.*) have shown that the ISIMIP 2b climatology dataset, which we use to drive historical and future projections for alkalinity and

weathering fluxes in our model, tends to underestimate hydrologic runoff when using ORCHIDEE, causing lower-than-observed bulk river fluxes and peak flows. Because bicarbonate weathering and transport rates are dependent on runoff, we are likely to underestimate these alkalinity fluxes in simulations using our model. On the other hand, when using another historical climatology dataset called GSWP3 (http://hydro.iis.u-tokyo.ac.jp/GSWP3/) -ORCHIDEE is able to more successfully reproduce observed Arctic river discharge flows (bulk and seasonal (Guimberteau et al., 2018)). The alkalinity model can be run using this 'optimal' dataset, from which we can compare model performance with respect to observations, and thus provide a yardstick against which to evaluate whether departures from observations are the result of suboptimal input data or suboptimal model representation. To this end, we repeat steps 1 to 3 using the GSWP3 dataset, and run the model over the historical simulation period (1901-2005).

4 Results

4.1 Future Trends

Over the ISIMIP climatology-driven simulation period 1960-2099, bulk alkalinity basin-outflow trends for the 'Big Six' Arctic rivers increased markedly over Eurasia, with ambiguous trends in North America (Fig. 3). If river discharge of alkalinity is disaggregated by source of water flow –that is, if we discriminate between whether a given unit of alkalinity in the river entered the river via the soil surface (runoff) or subsurface (drainage) –as is done in Figure 3, the trend in alkalinity discharge is dominantly driven by large-scale increases in the drainage flux, against smaller increases (Lena, Yenisei, Kolyma) or no noticeable change in runoff fluxes (Ob, Mackenzie, Yukon). This dynamic is particularly apparent for the two largest and least permafrost-affected of the Eurasian rivers considered, the Ob and Yenisei, where the drainage alkalinity flux increases by ~3 (Ob) and ~6 (Yenisei) –fold over the simulation period, or from the order of 1→3 TgC yr^{-1} and 0.2→1.2 TgC yr^{-1} for each river respectively.

The massive increase in drainage water-sourced alkalinity discharge points to a large-scale increase in subsurface flows facilitated by permafrost thaw, a deeper active layer allowing increased vertical entrainment and flow of water from the surface-down. Permafrost thaw in this sense liberates the subsurface soil column from its previous thermal shielding, greatly expanding the surface area subjected to chemical weathering and the subsequent aggregate flux of the weathering product. Indeed, the increase in modeled drainage weathering corresponds with areas of greatest increases in temperature, drainage water flow and active layer depth. Further, the increased vertical distance of water flowpaths and their longer soil residence time (slower flow) converge to increase the concentration of weathered material in drainage flows, as represented in our simple weathering flux module, whose increase thus serves to further enhance the river discharge of alkalinity.

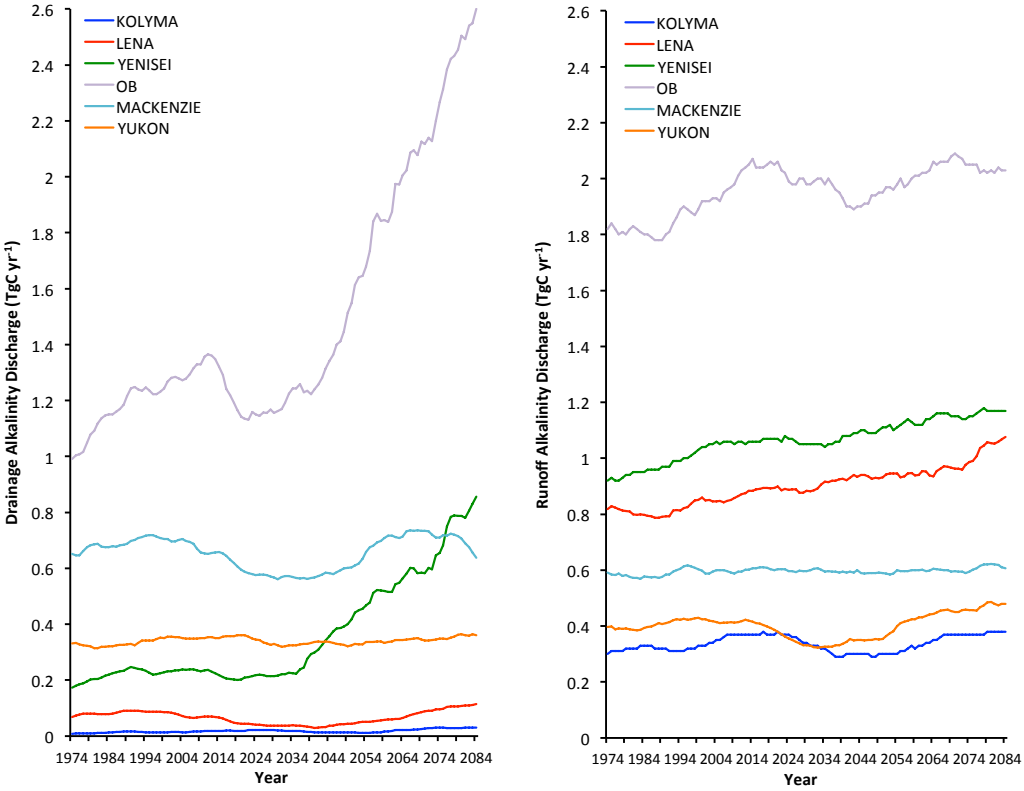

Figure 3: Drainage-sourced (left) and surface runoff-sourced (right) alkalinity discharge trends (TgC-eq. yr^{-1}) at basin outlet for each of the 'Big Six' rivers over the simulation period, with a 30-year moving average applied to each trendline.

As described in the introduction, chemical weathering of carbonate and silicate rocks drives a net atmospheric CO_2 uptake. The change in this land-atmosphere CO_2 flux over the 21st Century is shown in Figure 4a. Carbon uptake rates decline in temperate Western Europe and the inland North American Arctic, but increase strongly in central-Western Siberia, Sweden and along the eastern and western boundaries of North America, and weakly in Eastern Siberia. These same regions correspond to areas of matching sign of changes in alkalinity discharge (Fig. 4b). At the same time, there is a strong spatial correlation (positive) of changes in weathering atmospheric CO_2-sink with changes in subsurface (drainage) soil alkalinity export (compare Fig. 4a and Fig. 4c), and a strong anti-correlation with changes in surface runoff alkalinity export (compare Fig. 4a and Fig. 4d). Thus, deeper vertical flow paths promote CO_2-weathering uptake, whereas an increased flux of water running over the land surface (runoff) is indicative of a shorter water residence time, less weathering per unit volume of water, which implies greater dilution of weathering products and a decrease in CO_2 uptake from weathering.

The trends of CO_2-weathering uptake, when extended to the Big Six rivers, underscore the magnitude of the change of this often-overlooked component of the terrestrial C cycle perturbed by climate change and human activities on short timescales, as well as its potential sensitivity to changes in environmental conditions. Fig. 5 (left) shows that the basin-summed CO_2-weathering uptake rate ranges from ~0.2 TgC yr^{-1} (Kolyma) to up to ~10 TgC yr^{-1} (Yenisei), a range very similar to the maxima and minima of dissolved organic carbon (DOC) export rates for each of the six basins predicted by the model. Like other alkalinity-related variables, the Eurasian basins tend to experience the highest

rates of increase in weathering CO_2 uptake over the simulation period, owing, as previously discussed for Fig. 4, to deeper subsurface flow paths.

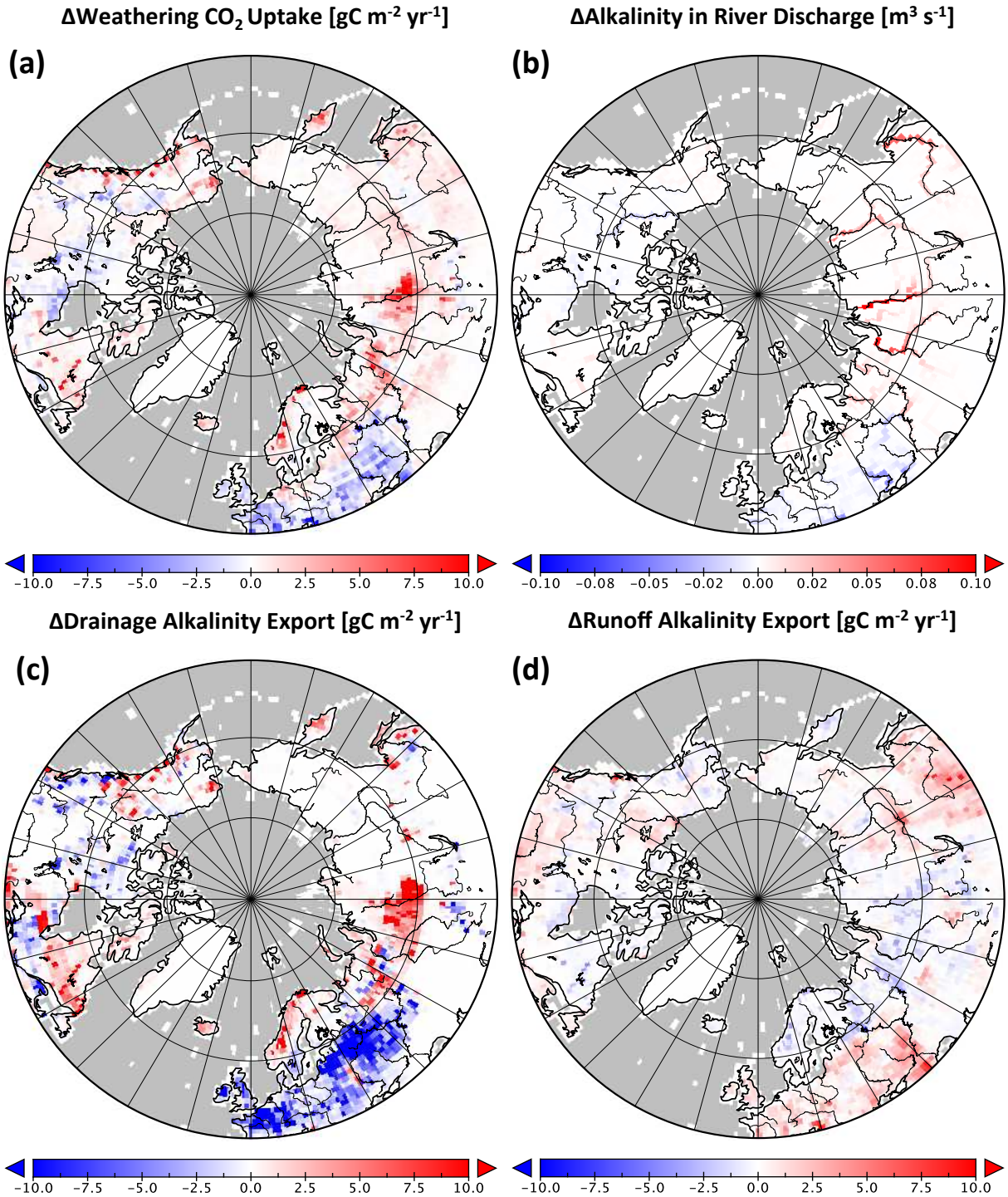

Figure 4: Maps of changes in alkalinity-related variables over the 21st Century, i.e. between the mean of the last decade of simulation (2090-2099) and (1996-2005), for **(a)** weathering-driven CO2 uptake, **(b)** total alkalinity transport in river discharge, **(c)** drainage and **(d)** runoff alkalinity export from the soil column.

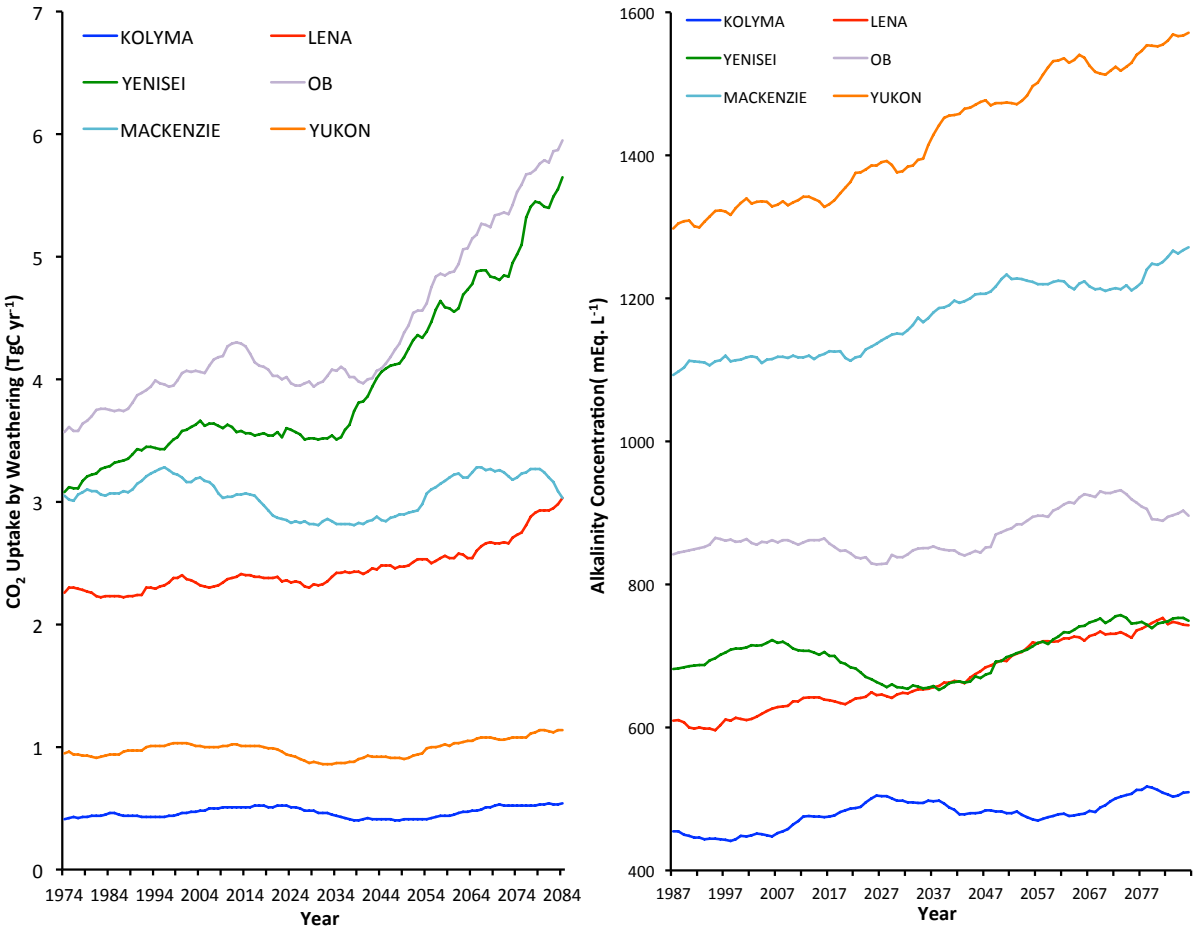

Figure 5: 30-year moving average of (**left**) basin-aggregated CO_2 uptake by weathering (TgC yr^{-1}) and (**right**) annual alkalinity concentrations (mEq. L^{-1}) in outlet discharge, for each of the Big Six river basins.

Whereas the bulk fluxes of terrestrial alkalinity export and discharge previously described are strongly dependent on bulk inputs of precipitation and subsequent surface runoff and drainage water flows, the input of alkalinity made available to each volumetric unit of water flowing from the land surface (mEq L^{-1}) is a measure of the concentration of alkalinity made available by the underlying lithology and soil temperature. The per-basin trends in this alkalinity concentration are shown in Fig. 6 (right) and differ somewhat in magnitude and trend from the other alkalinity variables in this analysis, with highest concentrations in the Mackenzie, Yukon and Ob basins, reflecting the bedrock lithology, and greatest rates of change occurring in the Yukon and Mackenzie, reflecting the whole-soil-column changes in temperature and hence weathering associated with permafrost thaw.

Characteristic features of alkalinity concentration seasonality in permafrost regions are captured by the model output (Figs. 6-8). These include high concentration values in autumn and winter (Fig. 7), as freezing of the top soil hampers runoff flow and facilitates only slow subsurface flow with high concentrations as long as the bottom soil is not yet frozen, followed by an abrupt collapse in concentration values in spring when the freshet or thaw period causes a massive flushing of snow from the land surface whose rapid runoff strongly dilutes concentrations. In the summer, concentrations pick up again as the active layer deepens, causing deeper entrainment of the weathering

reactant and subsequent access to a larger surface area of weatherable material (Fig. 6, right hand side), leading to higher concentrations and fluxes of alkalinity. As expected, alkalinity discharge rates are in proportion with river discharge rates (Fig. 6, left) although it appears that there are clusters of different response rates to river discharge, most likely driven by differing lithology and/or extent of permafrost coverage. These dynamics have been found and explained in greater detail by several studies (Drake et al., 2018; Tank et al., 2012a, 2016).

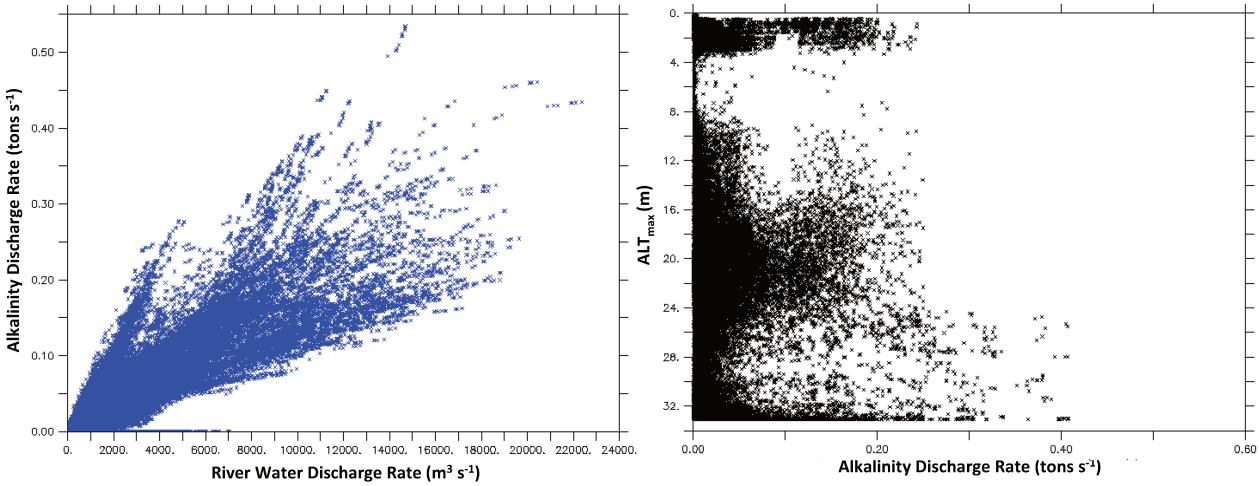

Figure 6: Scatter plots of model output under ISIMIP 2b forcing, where each point represents a given grid cell for a given year over the entire simulation period for the Big 6 rivers combined, to show the variation of bulk alkalinity discharge rate flowing through rivers (tons s^{-1}) with (**left**) annual mean river discharge rate, and (**right**) mean annual maximum active layer depth.

As shown in Fig. 7, the Big 6 basins share common changes in the seasonality of alkalinity concentrations between the end of the 20th and 21st centuries. Generally, the whole seasonal cycle is shifted earlier by one or two months, as warmer temperatures drive ice melt and peak river flow (corresponding to the concentration minimum) earlier in the year. The summertime concentration peak (~Jul-Aug to ~Sept-Oct) increases in magnitude for all rivers as warming deepens the active layer and combines with late summer rain to increase the high-concentration drainage flux of alkalinity. In addition, wintertime concentration peaks (~Dec-Feb) decline in magnitude for all rivers. This suggests that wintertime baseflow rates in river discharge increase in the future, leading to a suppressive dilution effect on alkalinity concentrations.

4.2 Comparing observations with model output per climate input dataset

Previous studies have suggested that weathering rates and attendant riverine alkalinity loading are dominantly driven by runoff and lithology, rather than temperature (Eiriksdottir et al., 2011). At the same time, the climatological datasets from which our models run generally lead to underestimations (with the exception of the Ob) of runoff and river discharge in the Arctic (Table 2), and with a greater negative bias under ISIMIP climatology. Thus by comparing observations of seasonal and inter-annual variations in bulk fluxes and concentrations with simulations performed using two separate datasets, we gain some heuristic grip on the extent to which model-simulation discrepancies reflect issues relating to the forcing data, or issues relating to process-representation in our simple alkalinity-generating module.

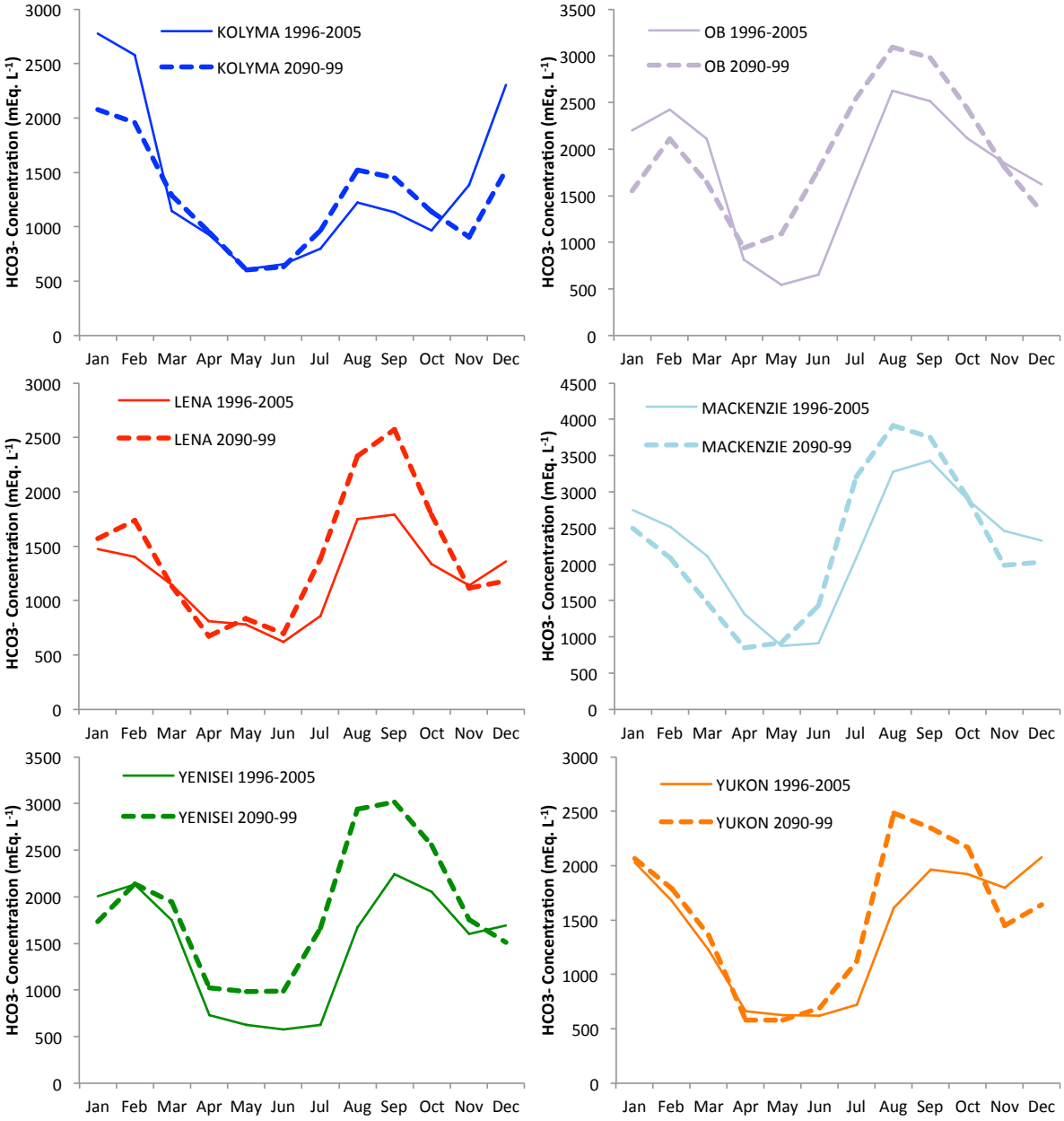

Figure 7: Simulated seasonal variation in alkalinity concentration in the over the decade 1996-2005 (solid) and 2090-2099 (dashed) for the Big Six rivers at outflow grid cell, under ISIMIP 2b forcing.

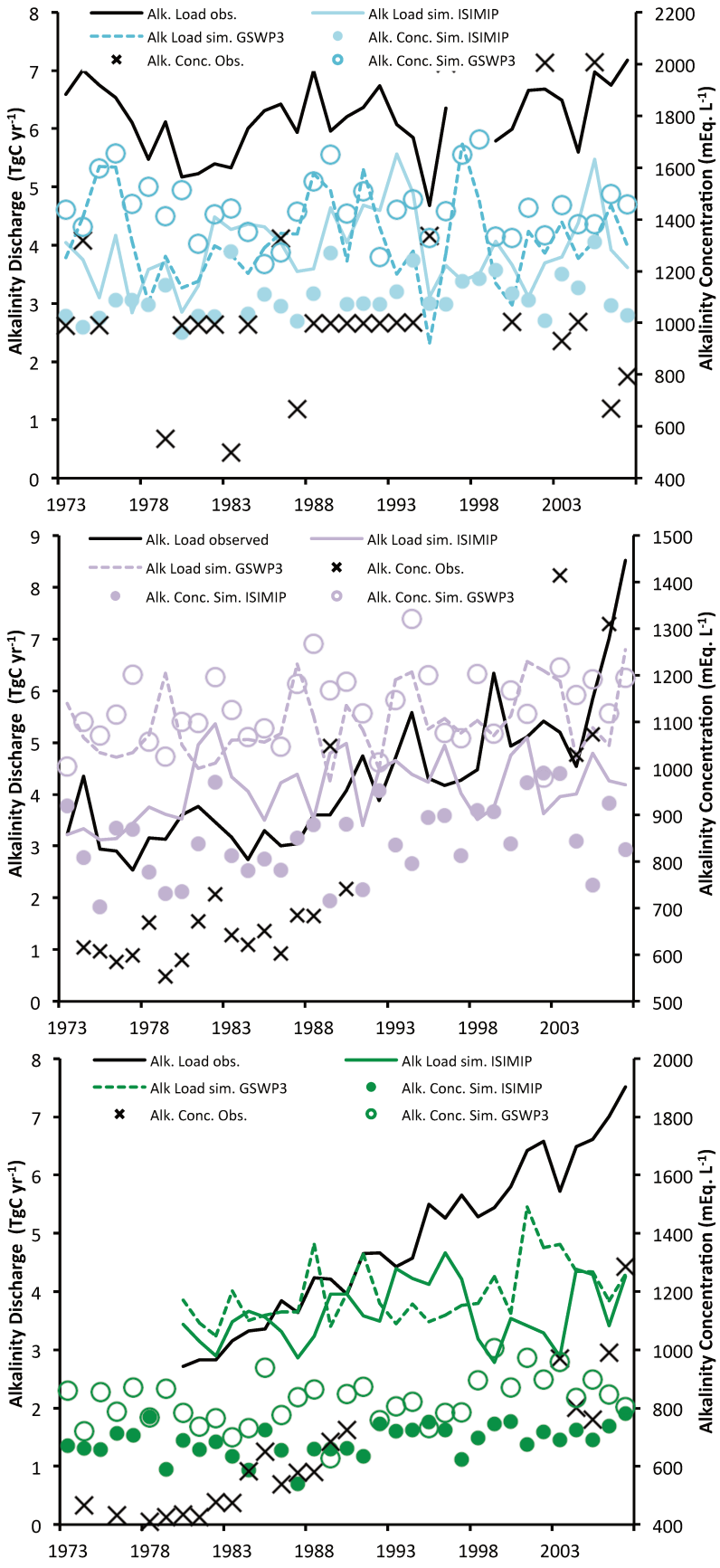
Alk. Load obs.
Alk Load sim. ISIMIP
Alk Load sim. GSWP3
Alk. Conc. Sim. ISIMIP
Alk. Conc. Obs.
Alk. Conc. Sim. GSWP3
Alkalinity Discharge (TgC yr-1)
Alkalinity Concentration (mEq. L-1)
Alk. Load observed
Alk Load sim. ISIMIP
Alk Load sim. GSWP3
Alk. Conc. Obs.
Alk. Conc. Sim. ISIMIP
Alk. Conc. Sim. GSWP3
Alkalinity Discharge (TgC yr-1)
Alkalinity Concentration (mEq. L-1)
Alk. Load obs.
Alk Load sim. ISIMIP
Alk Load sim. GSWP3
Alk. Conc. Sim. ISIMIP
Alk. Conc. Obs.
Alk. Conc. Sim. GSWP3
Alkalinity Discharge (TgC yr-1)
Alkalinity Concentration (mEq. L-1)

4153

Figure 8: Timeseries of bulk annual alkalinity discharge rates at outflow for **(top)** the Ob, **(middle)** Yenisei and **(bottom)** Mackenzie basins, in simulations (solid) and from empirically-determined estimates (dotted) in Drake et al. (2018) and Tank et al. (2016), respectively.

Generally, Figure 8 shows that our model does reasonably well in capturing the magnitude and inter-annual variability of annual alkalinity discharge for the period ~1973-2007 over the Yenisei, Ob (Drake et al. 2018) and Mackenzie (Tank et al. 2016) rivers (those Arctic rivers for which long-term data exist in the published literature). Where the simulated annual river water discharge is low compared to observations (Yenisei, Mackenzie (Table 2)), so too is the simulated alkalinity discharge. Where bulk water outflow is overestimated (Ob under GSWP3 climatology), so the alkalinity discharge is likewise overestimated, suggesting the dominance of runoff as determinant of weathering flux rates. Inter-annual variations in alkalinity discharge appear to be reasonably well captured by our model, particularly for the Ob and Mackenzie, however in Fig. 8 our simulations fail to capture the multi-decadal trends for the two Siberian rivers: a pronounced increase in alkalinity loading (Drake et al., 2018), However, the Drake et al. study did not propose explicit causal mechanisms for the dramatic rise in alkalinity loading, complicating our ability to interpret the apparent shortcomings of our model. It may be that the temperature sensitivity or the weathering correction for soil respiration of the model (see Methods, Step 2) are too low or that it uses too low an activation energy. Similarly, our omission of peat processes or peatland coverage may be significant due to the high areal coverage of peatland in, particularly, West Siberia (for example, Zakharova et al. (2007) show that this can be up to 50% of total watershed area), which may have a significant impact on weathering rates either due to very low-pH soil waters or due to the comparatively low availability of weatherable material in peat soils. Speculatively therefore, changes in this areal peat coverage (expansion/contraction with increasing temperatures) may play a role in long-term weathering rates and alkalinity loading in rivers. On the other hand, the steep alkalinity increases seen in the Siberian region may also reflect changes in human production and consumption systems (e.g. liming or alterations to industrial production and related energy sources). The model is capable of approximating mean annual alkalinity concentrations (Fig. 8). Because simulations driven by the ISIMIP dataset lead to even lower river discharge flows than those driven by GSWP3, alkalinity concentrations tend to be correspondingly higher in the former compared to the latter simulations. For the two Siberian rivers, the model overestimates concentrations for the period preceding 1990, and underestimates them for the period following year 2000. This is unsurprising, given that as previously discussed, our alkalinity model does not reproduce the ~300% increase in alkalinity loading recorded for these two rivers since the 1970s.

Because of this, and because river discharge in West Siberia has not greatly increased over that same time period, the observed increases necessarily ascribe to very large increases in alkalinity concentration. In addition across all rivers, where mean annual alkalinity concentrations are overestimated, this also partly owes itself to the underestimation of summertime river flow in both GSWP3 and ISIMIP climatologies (Fig. 9). This low discharge reduces what would otherwise be a dilution effect, correspondingly raising the mean annual concentration value simulated. Both simulated alkalinity load and concentration suffer from an ability to capture the importance and

extent of other, non temperature/runoff/lithology -related processes which could be important in different basins to different degrees.

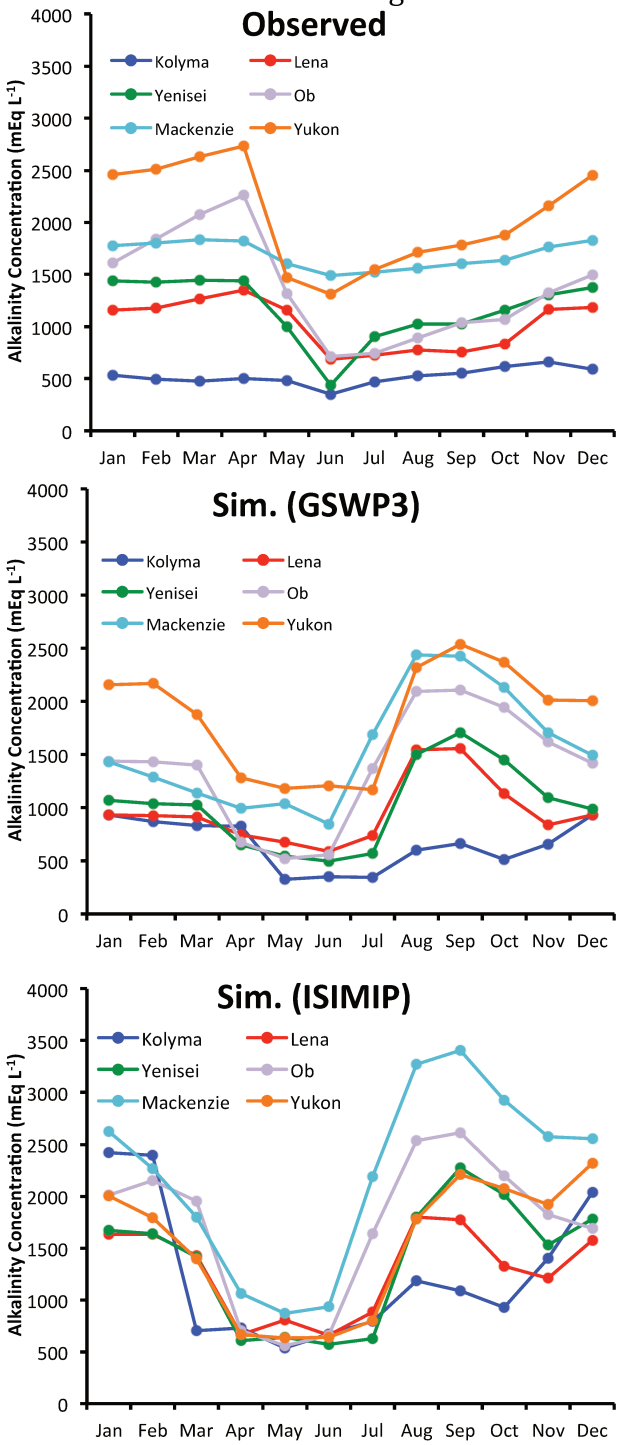

Figure 9: Monthly alkalinity concentrations for the Big Six rivers at coastal outflow as reconstructed from observations in Tank et al. (2012) averaged over the period 2003-2009 and calibrated by river discharge data over 2000-2009 **(top)**, and the average simulated by our model over the period 2000-2007 using **(middle)** ISIMIP 2b and **(bottom)** GSWP3 climatological data.

For example, the impact of glacial processes and glacial thaw, the cracking exposure of weatherable material caused by repeated freeze-thaw cycles and the prevalent exposure of bare rock and soil to precipitation in mountainous Arctic regions are high latitude-

specific factors which by nature would have a high temperature sensitivity that would increase the amount of alkalinity transported in runoff. But the importance of such changes to these fluxes is not known and this is not considered here.

4.3 Alkalinity and weathering in Arctic lateral-flux carbon budgets

To our knowledge, ORCHIDEE M-L is the first and currently only land surface model to include carbonate alkalinity in the geological loop of the carbon cycle perturbed by climate change in the past and future century. This may be a substantial issue for C cycle models. Figure 10 explains why. Our model output suggests that over the Big 6 rivers combined, alkalinity input from soils to rivers in the present day are of the same order as DOC inputs, in C equivalent terms (23.1 vs 27.3, respectively). Likewise, the uptake of CO_2 from weathering in the present day exceeds outgassing from riverine CO_2 evasion (12.1 vs 15.6), which is the major C loss term for the inland-water C cycle, while alkalinity outflow to the Arctic Ocean also exceeds DOC outflow (19.4 vs 23.1). The relative importance of the alkalinity generation/flux and weathering CO_2 uptake only increases in a warmer future, as both processes increase their flux rates by around one-third, while DOC fluxes across the Big Six decline in aggregate. In particular, CO_2 uptake from weathering increases to 180% of evasion, meaning that the inclusion of lateral fluxes that themselves include alkalinity generation shift the inland water C cycle from a status of net C source to net C sink.

Furthermore, while both DOC fluxes and alkalinity fluxes have been shown to be underestimated by our modeling scheme, the former largely due to the poor representation of precipitation in the forcing files and the exclusion of peat in peat-rich basins, the latter also due to the precipitation issue as well as poor representation of some high latitude weathering processes, the factor of this underestimation is substantially higher for alkalinity fluxes, implying that its real importance relative to the organically-generated C fluxes may likewise be significantly higher. At the biome scale, the combined lateral flux process representation enabled by our inclusion of the relevant organic and inorganic dynamics involved in them in the land surface component of an Earth System model suggest that far from being a minor component of the C cycle, the combined lateral flows constitute 16% of net biosphere productivity (51/324 TgC yr^{-1}), or NPP –heterotrophic respiration, in the present day. This is likely an underestimate by a factor of at least two, given the shortcomings of our modeling approach and forcing data inputs used to generate them, when these are compared to empirical data. From this we can conclude that the inland water system offers a C sink to buffer the effect of increased temperatures in permafrost regions, since on the one hand the processes that promote the lateral flux of organic carbon (DOC) tend to decline with warming, decreasing the potential amount of carbon available to be outgassed as evasion to the atmosphere, while on the hand promoting the lateral flux of lithogenically-sourced C, increasing atmospheric C uptake.

5 Conclusions

Despite the shortcomings of this simple alkalinity generation module described above, we have shown that for some Arctic basins it remains capable of reproducing first order bulk alkalinity discharge fluxes as well as their seasonality and concentration. In

addition, we have shown that far from being a minor component of the Arctic C cycle, weathering and alkalinity fluxes are major constituents of it.

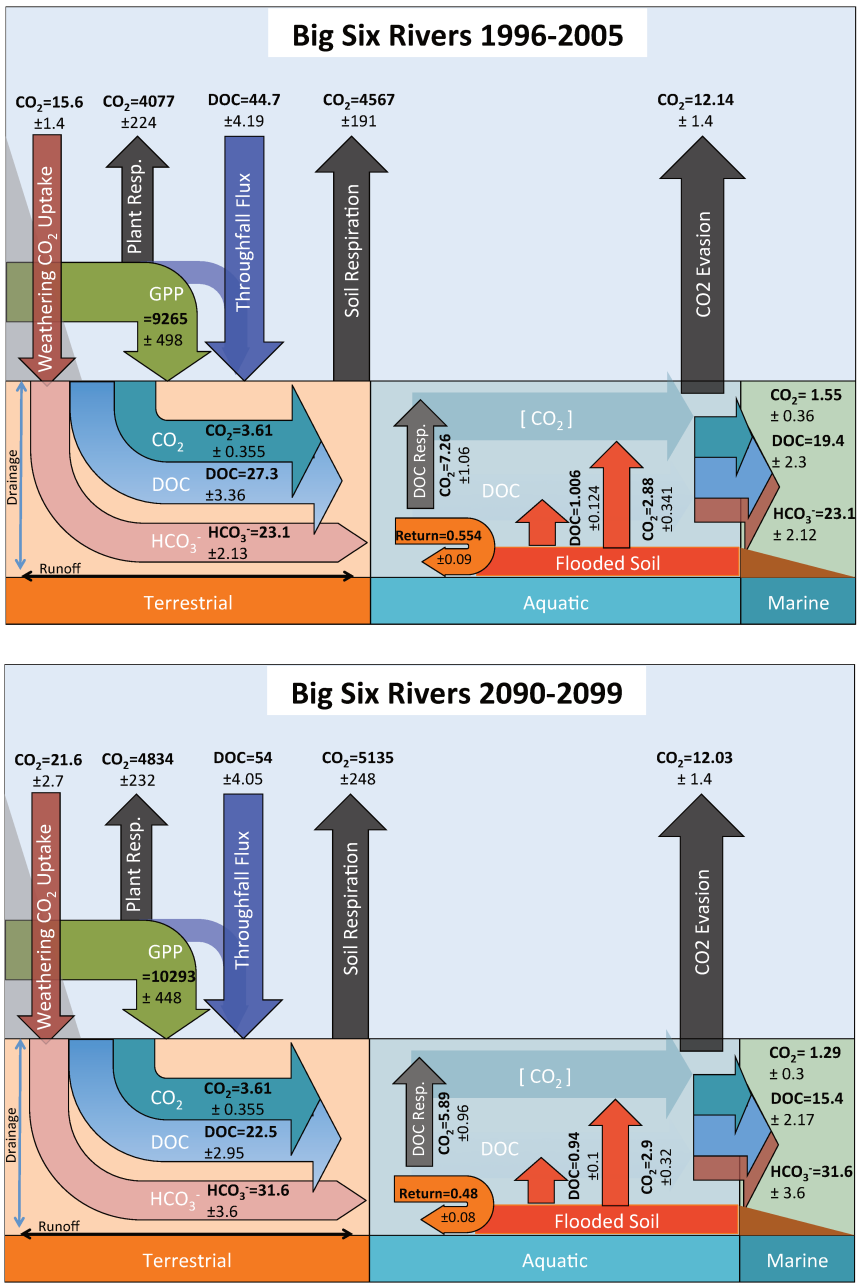

Figure 10: Major carbon fluxes (TgC yr^{-1}) over the terrestrial-aquatic continuum for the Big 6 Arctic rivers combined, averaged over (**top**) 1996-2005 and (**bottom**) 2090-2099.

Chapter 6:
Perspective and Outlook

General Summary

This thesis and the studies of which it is comprised have sought to trace the development of a model that is able to simulate at a broad spatial and temporal scale the dynamics of biogenic and lithogenically -generated lateral carbon (DOC, CO_2 and alkalinity) transfer in permafrost ecosystems. Having described a new DOC-generating model fully coupled to hydrology and terrestrial carbon cycling and evaluated its ability to adequately represent these dynamics at a high spatial, temporal and, for an Earth system model, process resolution in Chapters 2 and 3, respectively, Chapter 4 uses the tool to project the response of the lateral flux system to future changes in the Arctic until the end of the 21st Century. Our simulation results in that study suggest that, contrary to first-order empirical expectations, the response of lateral fluxes to warming in the absence of large scale increases in precipitation-driven runoff, actually decrease the total throughput of carbon to inland waters. Chapter 5 then describes a new, simple module added into ORCHIDEE M-L for the simulation of alkalinity fluxes and shows it is able to broadly simulate present day alkalinity discharge fluxes for the 'Big 6' Arctic rivers, and further, that these fluxes increase substantially in the future when the model is forced by projections of future climatic conditions. Crucially, Chapter 5 also shows that by including the weathering uptake of CO_2, the land inland water lateral carbon transfer system switches from being a net source to a net sink of carbon as weathering carbon uptake exceeds CO_2 evasion from the river surface, even without the representation of authochtonous (in-stream) primary production in our model. Overall, this cumulative work represents a novel and substantial addition to the existing body of research and modelling products available to address such questions. Nonetheless, as with all endeavours in numerical modelling, ours suffers from substantial omission in process representation. In addition the lack of spatio-temporally representative empirical data that would enable greater theoretical understanding, improved input data and stronger baseline for evaluating the model on a Pan-Arctic scale is particularly acute for permafrost-affected areas, owing to the practical and logistical difficulties in acquiring such data. In what follows we summarise some of these data gaps, followed by gaps in the modelling scheme, how these two relate to one another, and discuss the plausible effects of their availability/inclusion.

The Data Gap

The carbon budget of Arctic rivers is poorly constrained with regard to both stocks and fluxes, with land surface flux data at the catchment scale particularly lacking. This limits the ability to understand and predict the amplified surface warming caused by future permafrost thaw and CO_2 release, with current estimates of cumulative terrestrial permafrost-sourced atmospheric loading standing at 65-240 PgC by 2100(Schuur et al., 2015). Given the region's geographical remoteness and the complexity of interacting snow, ice, soil and biology, ground observations are sparse and yet utterly critical for

our understanding. Narrowing gaps will require better understanding of hydrological and biogeochemical dynamics (surface and subsurface) for all watersheds, in particular those outside the 'Big Six' rivers, which feed substantial volumes of Arctic Ocean discharge(Holmes et al., 2012) yet display different dynamics (e.g. base-flow of zero) due to the fact that they are at present entirely underlain by continuous permafrost. Indeed, our simulation output in Chapter 3 shows that the 'Medium 9' –the 9 next-largest rivers after the 'Big 6' –discharge about a third the quantity of DOC as the Big 6, despite proportionally lower water discharge, and that this fraction increases over the 21st Century (Chapter 3, Table 1).

Current estimates for Arctic and boreal region CO_2 evasion are likely to be strong underestimates, given that empirical studies tend to sample from the river main stem over limited time periods, whereas extremely high DOC concentrations and CO_2 evasion rates found in both boreal and Arctic headwater streams are consistently under-sampled (e.g. refs.(Drake et al., 2015; Teodoru et al., 2009)). The current inland water evasion estimate over the high latitudes is around 40-84 TgC yr^{-1} being emitted from Arctic lakes and rivers, of which 15-30 TgC yr^{-1} is thought to be from rivers alone(Mcguire et al., 2009). Our modern-day evasion estimates from the Big 6 rivers alone total 12.14 TgC yr^{-1}, and bring our estimates for that flux close to the mid-range of the first order estimates (20.1 TgC yr^{-1}). Nonetheless, *despite being the dominant pathway for laterally exported carbon*(Drake et al., 2017), the fact that even a river the size of the Lena has, to our knowledge, never been the subject of a CO_2 evasion measurement campaign on either main stem, tributary or headwater scale highlights the extent of what is missing from empirical literature.

In addition, further hydrological data (volumes, timing, temperature) across the spectrum of small and large rivers, upstream, downstream and across the extent of their floodplains and coastlines, on connectivity of lakes (including thermokarst) with each other and to rivers via surface and subsurface flows, as well as higher spatio-temporal resolution maps of subsurface ice content are urgently needed. Without these, reliable estimates of carbon and nutrient transport rates, respective residence times and associated uptake and metabolization pathways and their subsequent flux rates, cannot be generated with much certainty.

Likewise, we recommend further pilot studies exploring the dynamics of POC and DOC parent material, in-stream burial and reaction rates along the length of the river reach. Basin-wide rates of organic carbon mobilization and their relative age, their processing within the aquatic continuum and how all of these factors vary seasonally and with multi-year temperature differentials remains somewhat speculative, despite some progress(O'Donnell et al., 2016). The impact of microbial or photo-degradation 'priming' (De Baets et al., 2016) that might arise from mixing water and or soil masses with constituents of different sources and ages (e.g. ref.(Guenet et al., 2010)) requires comprehensive investigation. In lieu of existing basin-scale data, modeling studies might in the meantime make use of emergent properties such as the scaling relationship found between water retention time and carbon decay rate(Catalán et al., 2016), to derive carbon decomposition in complex Arctic hydro-systems.

Perhaps the most glaring gap in empirical data and process understanding concerns the terrestrial-marine transition zone (the continental shelf), and the effect of lateral fluxes on this region. While the drivers of organic matter outflow from rivers and the coast to the Arctic Ocean are relatively well established, little is known regarding its transport and fate along the Arctic continental shelf, particularly in the East Siberian Arctic Shelf(Semiletov et al., 2012). There, terrestrially-derived DOC behaves non-conservatively(Alling et al., 2010), causing high pCO_2 in, and acidification of, the near-shore zone, a phenomenon previously ascribed to surface water uptake of anthropogenic CO_2(Biastoch et al., 2011; Semiletov et al., 2016). Acidification in addition to changes in riverine OC outflows, may in turn alter the composition of primary producers and heterotrophs along the shelf and beyond (Findlay et al., 2015b) In addition, little is known of marine permafrost stocks and fluxes (~1000±500PgC(Shakhova et al., 2010)) –their extent, distribution, thickness, thermic conductivity, composition – and the response of these to both terrestrial heat and density (freshwater) fluxes over both short and long timescales(Archer, 2015; Janout et al., 2016; Nicolsky et al., 2012; Overduin et al., 2015; Sapart et al., 2017; Shakhova et al., 2014, 2015; Shakhova and Semiletov, 2007).

Finally, the Arctic and boreal land-ocean-aquatic continuum involve a wide range of methane stocks, methane-producing conditions, and transformative processes. These occur across the landscape, from thawing soils, thermokarst formations, lakes and inland waters, to the estuarine and shelf environments. Methane (CH_4) may contribute ~40% of total CO_2-equivalent evasion from boreal rivers(Campeau et al., 2014; Campeau and Del Giorgio, 2014). CH_4 emissions occur dominantly in the winter (post-August) as the active layer is retained despite subzero air temperatures, through snow insulation and the thermal mass of soil water. Significantly, observed emissions are most acute in least inundated areas(Zona et al., 2015), contrary to previous theory(Bohn et al., 2015). Thus methane emissions from tundra wetlands of 16-27 Tg $CH_4 yr^{-1}$(Bruhwiler et al., 2014; McGuire et al., 2012)are comparable to those from non-inundated tundra (23 Tg CH_4 yr^{-1}(Zona et al., 2015))and are likely to increase as Arctic winters warm. CH_4 concentrations (and evasion) have been shown to co-vary significantly with those of CO_2, suggesting common nodes of regulation or origin, despite markedly differing pathways of transformation. Unlike CO_2 concentrations, pCH_4 appears to be tightly coupled to temperature, with a Q_{10} of 4.1, suggesting that emissions therein may increase significantly (~30-100%) in the future(Campeau and Del Giorgio, 2014) In particular, Boreal lakes and ponds have been assessed as 'hot spots' for methane emissions(Bastviken et al., 2011; Tranvik et al., 2009) and thermokarst lakes and subsea methane deposits are thought to play an increasing role under warming conditions(Shakhova et al., 2010). These have been under-represented in the literature, and have a significant role to play in future pilot studies.

The modelling gap

This set of studies has sought to include a wide range of organic and inorganic carbon production, transformation and flux processes from permafrost-specific regions into a global climate model. The resulting product has permitted subsequent analysis and breakdown of the key drivers of this system, as well as their response to change.

However, as it stands the configuration of this broad-scale process representation in our model is far from complete, with multiple areas of potentially substantial impact on the land-ocean-aquatic continuum with respect to permafrost thaw fully omitted from the current scheme.

As discussed in Chapter 3, the exclusion in our model of primary production by bryophytes (mosses, liverworts) as the dominant carbon uptake force in certain high latitude wetland regions (e.g. parts of the Ob river watershed) leads to the exclusion of peatlands, which are formed from these organisms, as well as attendant impacts on soil and soil-water dynamics. Due to their relative inhibition of oxidative decomposition from to soil water saturation, peatland areas tend to be characterised by much higher DOC concentrations, which are readily mobilised to rivers and streams if they are connected to the river network. If not directly connected, as in the aforementioned lakes and ponds, this high concentration can translate into large emissions of CH_4 from the water surface. This gap in process representation is, however, likely to be closed in the near future, given that a recent model version under the high-latitude ORCHIDEE umbrella(Guimberteau et al., 2018; Koven et al., 2013a; Qiu et al., 2018) has been coded to represent precisely these ecosystems, and thus awaits a relatively simple merger with our DOC-producing version to be included.

The anaerobic respiration of organic matter that occurs as a result of water inundation of that matter generally promotes methane as the dominant by-product of respiration. The methane cycle is not represented in our model, and would likely further increase the CO_2-equivalent respiration of the permafrost region, were it included. The process of methane generation is not spatially static, however, in that permafrost thaw over areas of high ice volume can lead to rapid local collapse of the soil column and the formation of depressions overlying carbon-rich soil, known as thermokarst. Thermokarst formation in turn promotes the formation of small, interconnected lakes, which have been shown to be hotspots of both CO_2 and methane emissions, but this phenomenon is as yet omitted from representation in our model, despite it being a characteristic dynamic of permafrost thaw systems. Nonetheless, we are not conceptually far from being able to include them in ORCHIDEE, given the progress and leg-work previously undertaken by (Lee et al., 2014) to include this in the Community Land Model earth system model.

While the high level of CO_2 evasion in headwater streams of permafrost watersheds demonstrated by a large number of empirical studies is likewise evident in our simulation of the high latitudes, as documented in Chapter 3, analysis of this dynamic is hampered by two shortcomings of our model scheme. Firstly, the model lacks explicit representation of 'stream' surface area at the sub-grid scale. This hampers determination of the real CO_2 flux rate, which we have inferred only from the relative size of the cumulative stream versus river water volumes boxes in our model output. Further, given that the surface area:depth or surface area:water volume ratios of small streams versus large rivers are likely to differ substantially, the methodology used in Chapter 3 likely greatly underestimates the true evasion rate being simulated. Furthermore, given that high headwater evasion rates are thought to be related to the mobilisation of once-thermally shielded reactive soil carbon, the lack of a tracer dimension relating a given carbon flux vector to a given soil or litter pool reactivity

source and age remains a significant limitation on evaluating both the model's performance and for understanding what is being mobilised into lateral fluxes in greater proportion in a warmer Arctic: contemporary, CO_2-boosted litter inputs, or newly-exposed, ancient soil matter from the permafrost layer?

Although the fraction of carbon discharged by high latitude rivers in particulate form is relatively small(Raymond et al., 2007), this fraction differs strongly between basins, and is affected by a host of processes including glacial action, bank erosion, and thermokarst. As noted in the Introduction, the exposure of soil matter due to thaw is likely to result in either lateral transport or atmospheric release. If eroded, and passed on to streams, POC may end up being deposited into river or sea bed sediments, removing it once more from the pool of carbon available to metabolisation in the short-term. Thus, the exclusion of this erosive flux, in conjunction with thermokarst processes in the model omit a potentially significant buffering factor with regard to the carbon released in lateral fluxes over the Arctic. This will likely be remedied in the future with the inclusion to this model of a soil erosion emulator that has already been made consistent with the ORCHIDEE soil carbon scheme(Naipal et al., 2018).

Finally, parallel to all the land surface dynamics represented or discussed in the preceding sections and chapters, yet absent from the model code or indeed the context of the discussion thus far, is the role that other nutrients have to play in regulating the carbon cycle, in particular that of nitrogen (N) and phosphorous (P). Additional to the clear benefits of including the cycling of these primary production–limiting elements in any vegetation or land surface model is the expectation that with high latitude warming and permafrost thaw will come the substantial liberation of these nutrients from soil carbon stocks previously under the protection of the permafrost shield. This release may in turn cause previously nutrient-limited production to increase, countering carbon losses implicit in permafrost thaw (Koven et al., 2015). Indeed, this thaw-induced nutrient release has been documented (Keuper et al., 2012) in northern peatland soils, which are N-limited, and may be a major feedback in the Arctic carbon cycle.

While ORCHIDEE incorporates a module that probabilistically simulates fire events and the subsequent combustion of large areas of biomass stock (Yue et al., 2016), this module has not been activated in the simulations documented here. The subsequent lateral transfer of burned material as DOC and POC into rivers, which may constitute a substantial proportion of total bulk DOC discharge(Myers-Pigg et al., 2015), is thus negated from the present modelling framework. Including it will entail some substantive additions to the soil carbon and fire modules, in order to incorporate both the highly stable pyrogenic soil carbon as well as the leaching of DOC from that soil pool.

Despite the above limitations, we remain confident in the broad conclusions drawn from this sequence of studies.

Appendices

Appendix 1
Appendix to Chapter 2:
ORCHIDEE MICT-LEAK (r5459), a global model for the production, transport and transformation of dissolved organic carbon from Arctic permafrost regions, Part 2: Model evaluation over the Lena River basin.

Table S1: Data type, name and sources of data files used to drive the model in the study simulations.

Data Type	Name	Source
Vegetation Map	ESA CCI Land Cover Map	Bontemps et al., 2013
Topographic Index	STN-30p	Vörösmarty et al., 2000
Stream flow direction	STN-30p	Vörösmarty et al., 2000
River surface area		Lauerwald et al., 2015
Soil texture class		Reynolds et al. 1999
Climatology	GSWP3 v0, 1 degree	http://hydro.iis.u-tokyo.ac.jp/GSWP3/
Potential floodplains	Multi-source global wetland maps	Tootchi et al., 2018
Poor soils	Harmonized World Soil Database map	Nachtergaele et al., 2010
Spinup Soil Carbon Stock	20ky ORCHIDEE-MICT soil carbon spinup	Based on config. in Guimberteau et al. (2018)

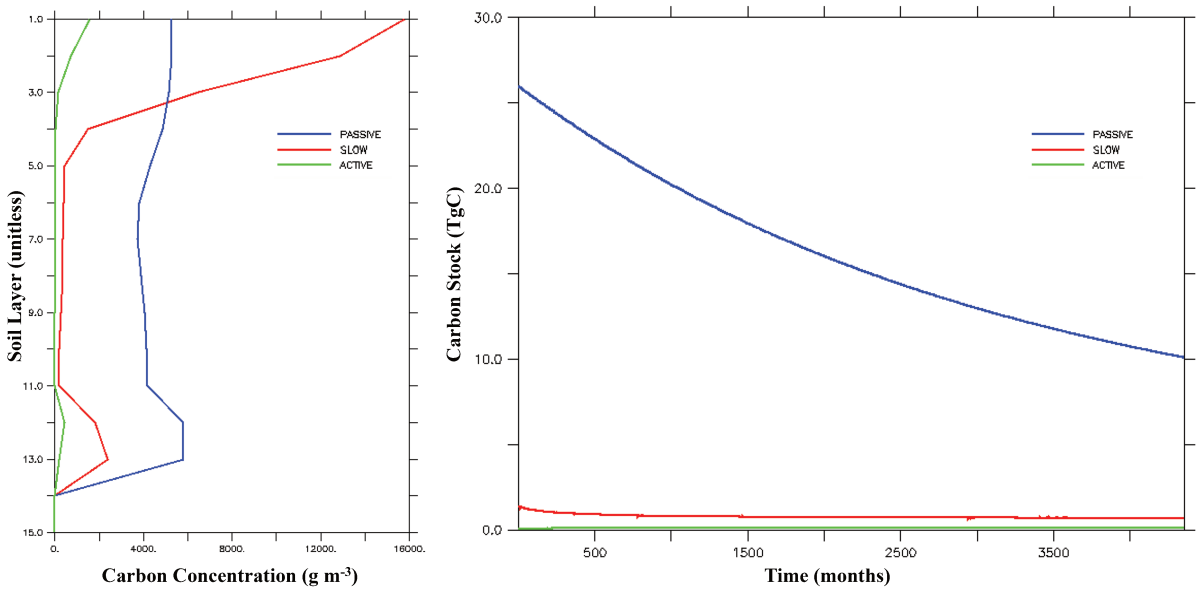

Figure S1: (Left) Soil carbon concentrations per depth level for each soil carbon reactivity pool at the end of the spinup period. (Right) Evolution of each soil carbon pool over the course of the 400-year spinup quasi-eqliuibration period.

(a)

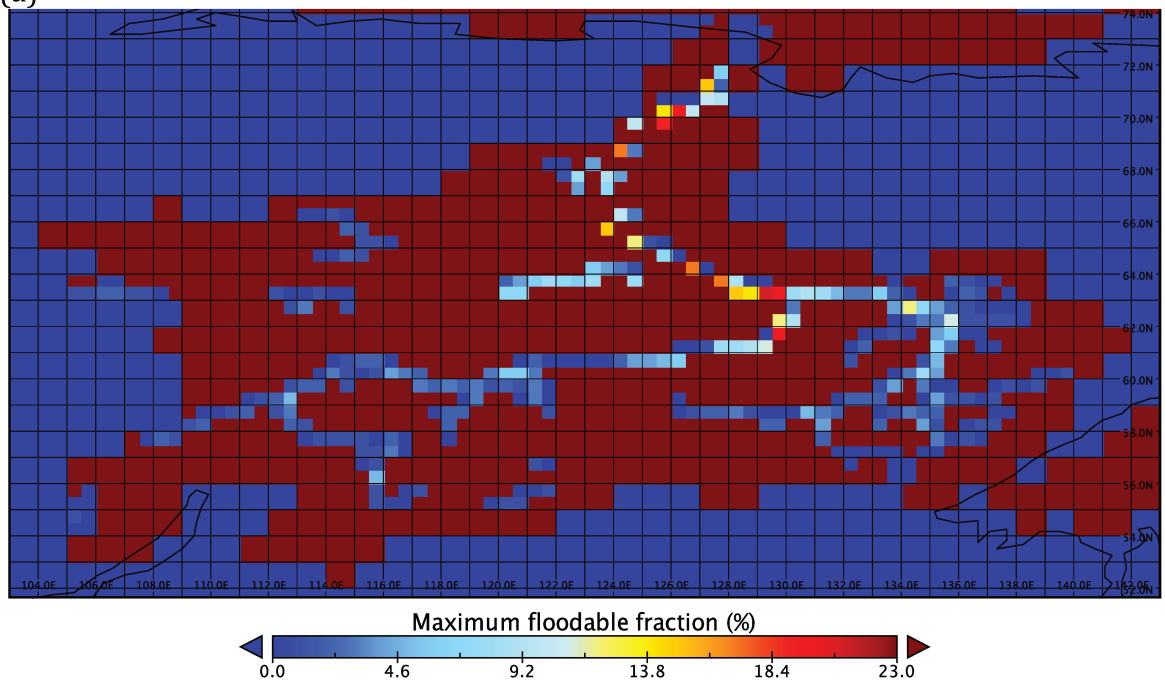

(b)

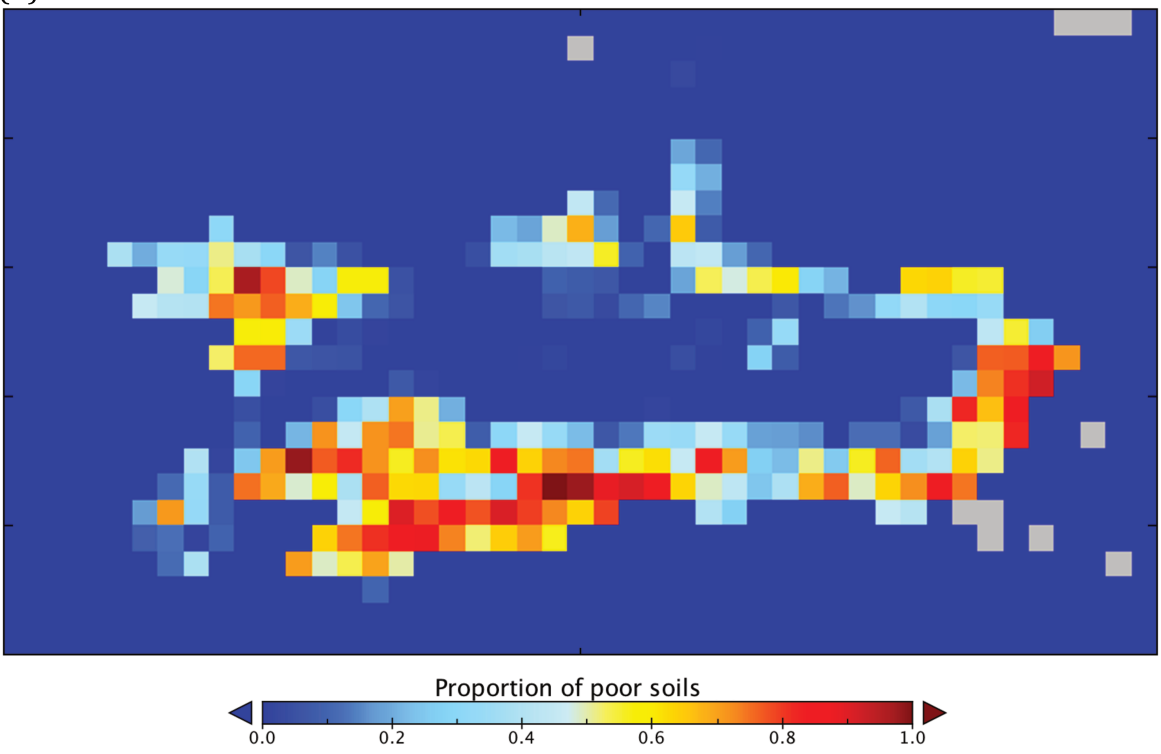

Figure S2: (a) Maximum floodable fraction of grid cells for the Lena basin per the input map from Tootchi et al. (2018). (b) Podzol and Arenosol map (Nachtergaele, 2010) used as input to the 'poor soils' module.

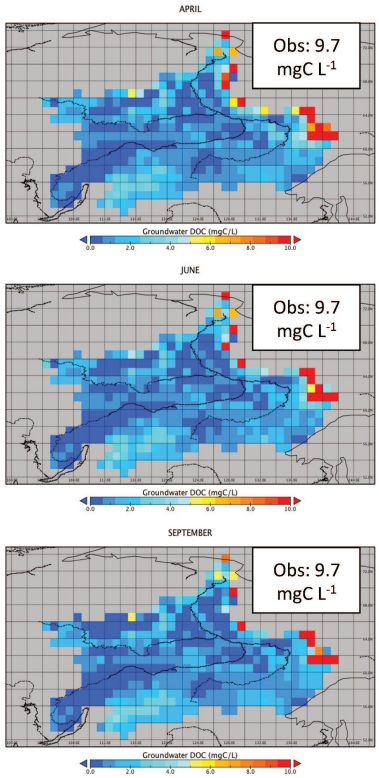

Figure S3: Groundwater DOC concentrations over the Lena basin for April, June and September averaged over 1998-2007, with mean observed concentrations for permafrost groundwater inset.

(a)

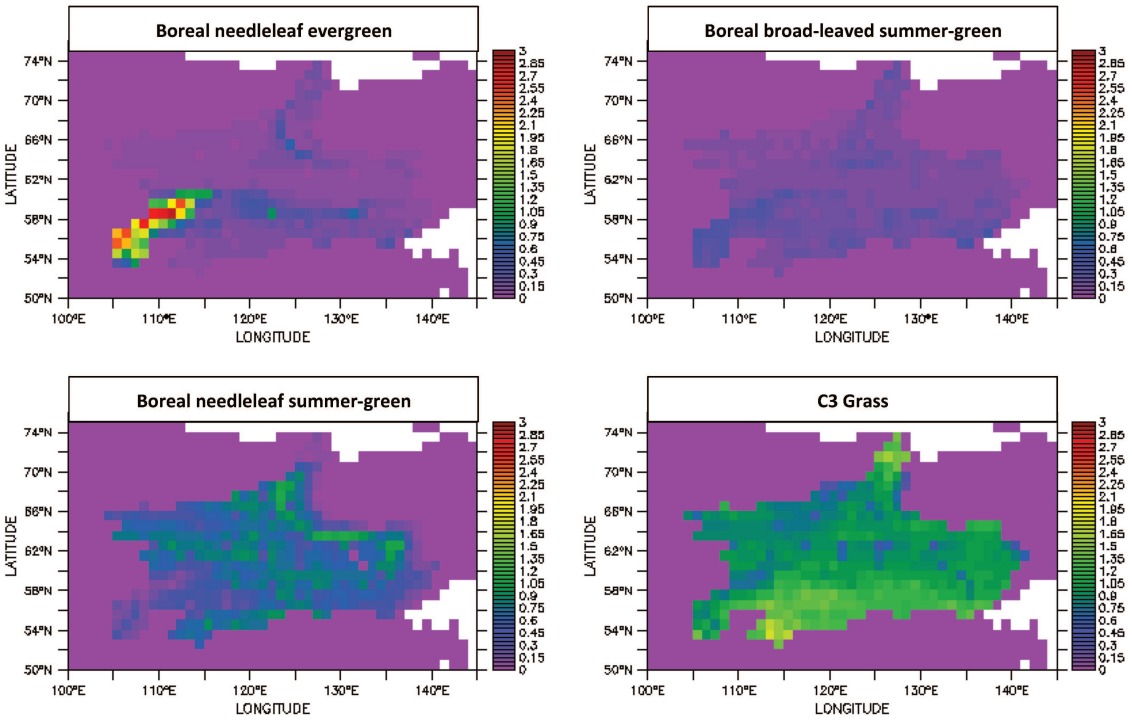

(b)

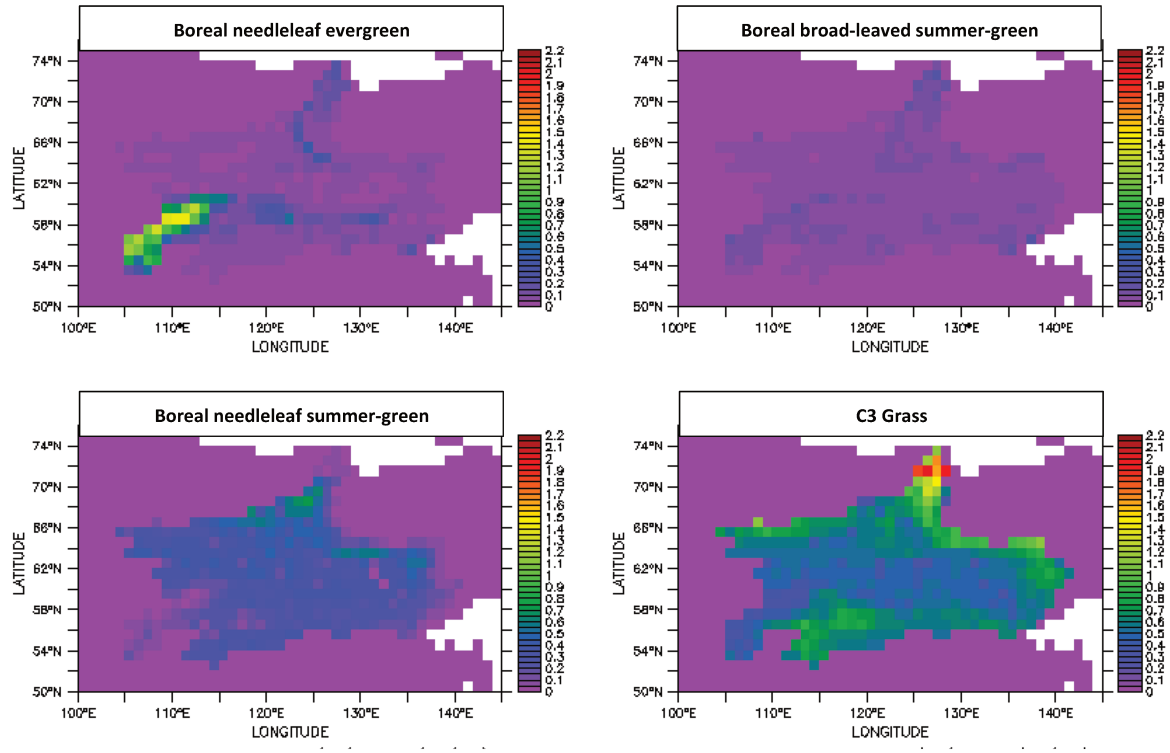
Boreal needleleaf evergreen
Boreal broad-leaved summer-green
Boreal needleleaf summer-green
C3 Grass
LATITUDE
LONGITUDE
74°N
70°N
66°N
62°N
58°N
54°N
50°N
100°E
110°E
120°E
130°E
140°E

(c)

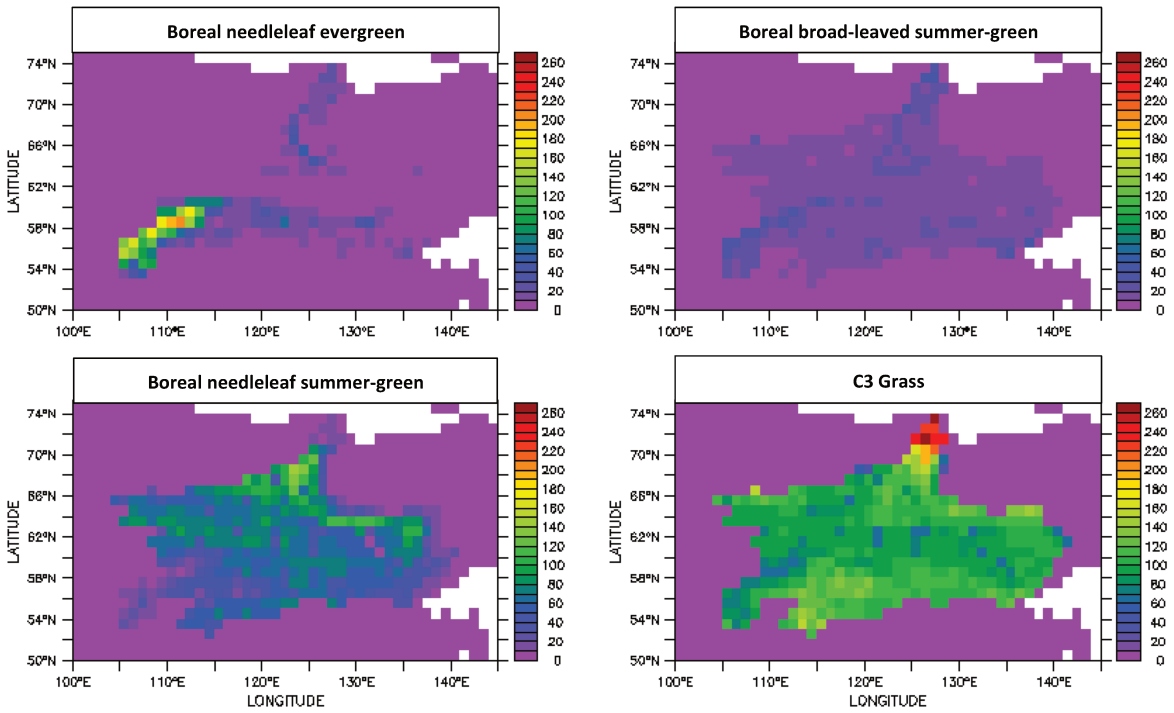
Boreal needleleaf evergreen
Boreal broad-leaved summer-green
Boreal needleleaf summer-green
C3 Grass
LATITUDE
LONGITUDE
74°N
70°N
66°N
62°N
58°N
54°N
50°N
100°E
110°E
120°E
130°E
140°E

(d)

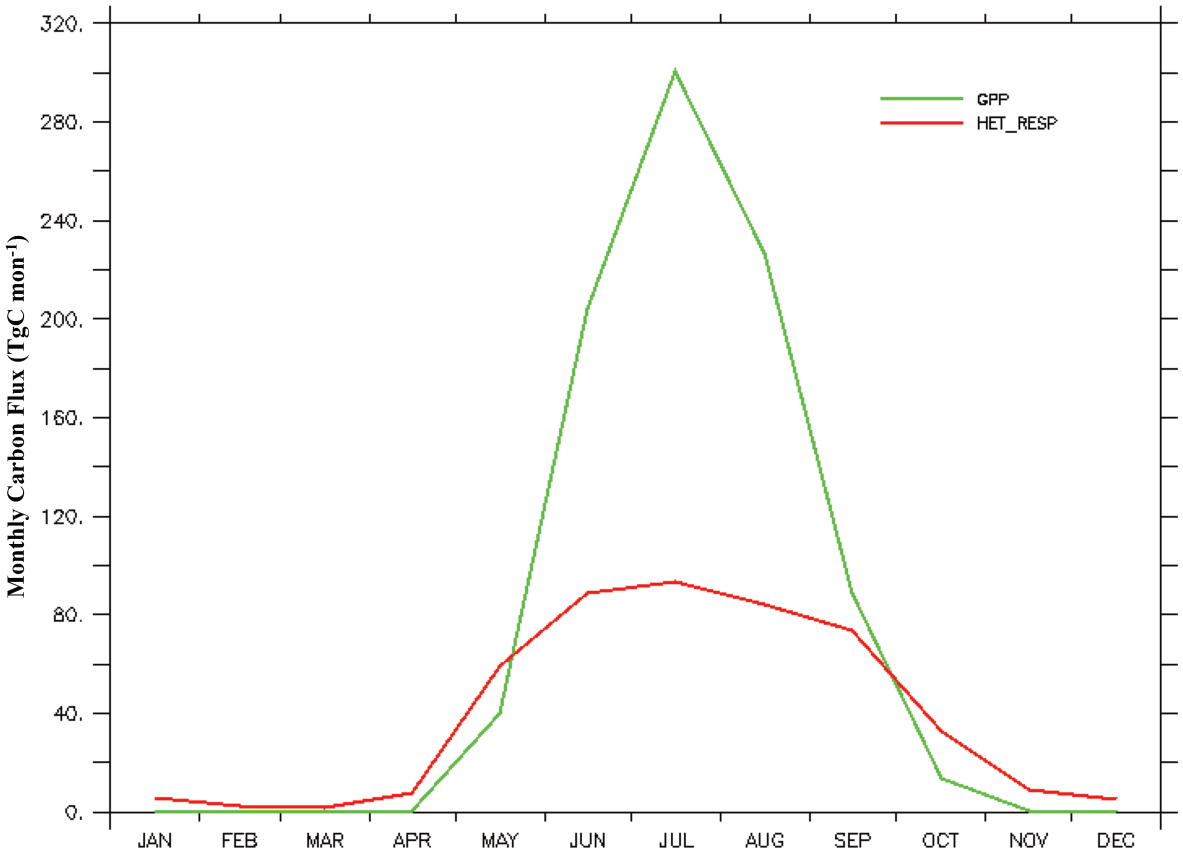

Figure S4: (a) Absolute yearly gross primary productivity (GPP, TgC yr^{-1}) for the four relevant PFT groups over the Lena basin, averaged over 1998-2007. (b) Mean July and August soil heterotrophic respiration rates (g m^2 d^{-1}) for the same PFT groups as in (a), during the period 1998-2007. (c) Average yearly NPP (gC m^2 yr^{-1}) averaged over the period 1998-2007. (d) Mean monthly carbon uptake (GPP) versus its heterotrophic respiration from the soil (Het_Resp) in TgC per month, over the period 1998-2007.

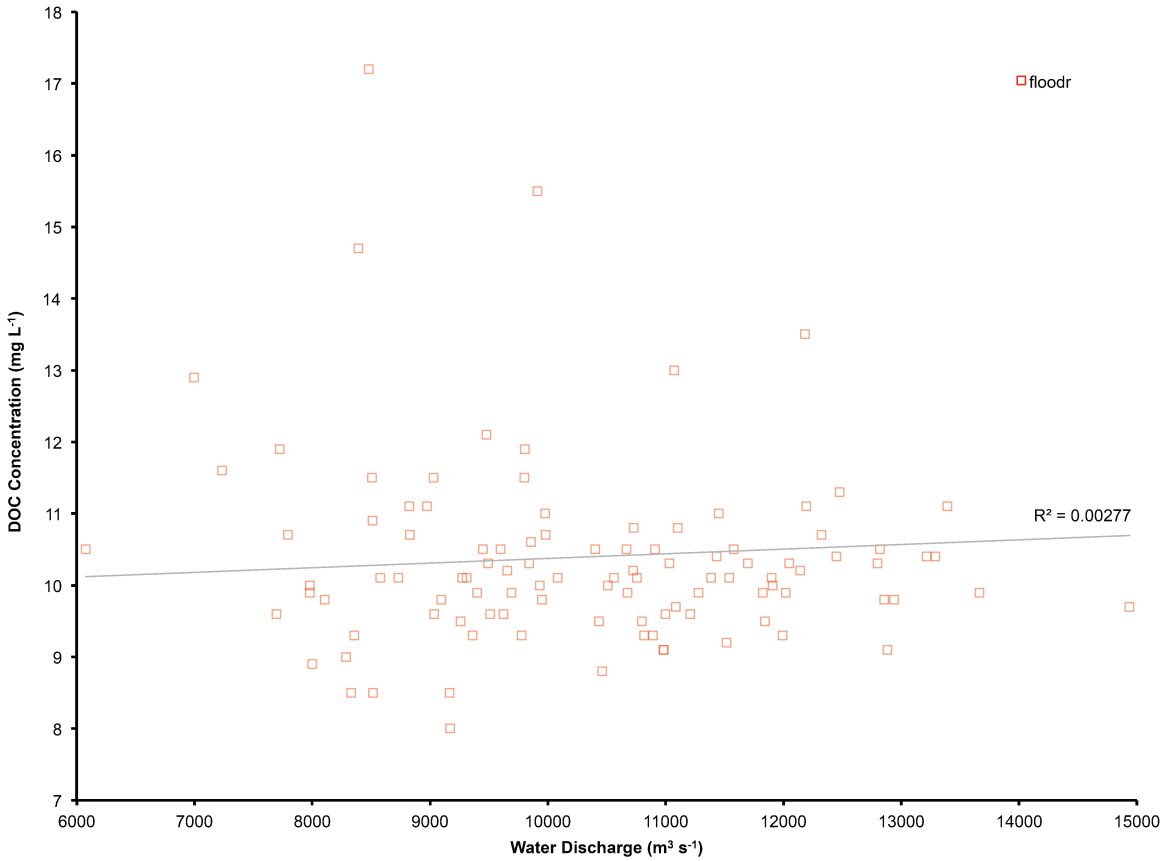

Figure S5: Simulated basin-mean annual DOC concentrations (mg L^{-1}) for the floodplain water pool regressed against mean annual simulated discharge rates at Kusur (m^3 s^{-1}) over 1901-2007. A linear regression with R^2 value is plotted.

Appendix 2
Appendix to Chapter 4:
Arctic lateral carbon fluxes decline with warming.

Methods

Model description

This study uses a new branch version of the land surface model ORCHIDEE (Organising Carbon and Hydrology in Dynamic Ecosystems(Krinner et al., 2005)), the terrestrial component of the IPSL Earth System Model (IPSL-ESM). This model version (ORCHIDEE MICT-LEAK, revision r5459) brings together a recent DOC production module(Camino-Serrano et al., 2018) and DOC and dissolved CO_2 lateral transport module(Lauerwald et al., 2017) with the high latitude-specific ORCHIDEE version(Guimberteau et al., 2018), which includes novel routines and representations of cold region phenomena for snow, ice, soil carbon and permafrost. This new model version has been recently described in detail and evaluated over the Lena River basin ((Bowring et al., 2019a, 2019b)). No changes to the code post-dating those publications were made for the simulations undertaken in this study.

Forcing Data

The climatological forcing data used to drive the model for historical and future simulations was taken from reconstructed and projected output from the IPSL Earth System Model under the second Inter-Sectoral Impact Model Intercomparison Project (ISIMIP2b(Frieler et al., 2017; Lange, 2016, 2018)) rubric, following the trajectory of Representative Concentration Pathway 6.0 (RCP 6.0). Climatological input data are at a daily temporal and 1 degree spatial resolution, covering the period 1898 to 2100. The input vegetation and land cover map was taken from the 5th Coupled Model Intercomparison Project 5 (CMIP5-LUHa) output. The water height threshold, used to define the water level at which floodplain inundation is triggered, is obtained statistically over multiple 30 year (1976-2005) model runs using ORCHIDEE MICT-LEAK, in a stepwise procedure first described in ref. ((Lauerwald et al., 2017)) and employed in (Bowring et al., 2019b). The remaining input forcing data for topographic index, stream flow direction, river surface area, soil texture, potential floodplains, bulk density, pH, 'poor soils' and soil carbon spinup (refs. (Guimberteau et al., 2018; Lauerwald et al., 2015; Nachtergaele, 2010; Reynolds et al., 2000; Tootchi et al., 2019; Vorosmarty et al., 2000), respectively) are summarised in Table 1 of the Supplement.

Simulation Setup

As detailed in (Bowring et al., 2019b, 2019a)the soil carbon stock used to represent the Pan-Arctic permafrost soil carbon stock in our simulation was reconstituted from the 20,000 year carbon stock derived from a soil carbon spinup looped over 1961-1990 (to coarsely approach a warmer mid-Holocene climate) of an ORCHIDEE-MICT simulation used in (Guimberteau et al., 2018). This was run to quasi-steady state equilibrium for the Active and Slow carbon pools over 500 years. (Supplement, Fig. 1), by looping over

the years 1901-1930 and the first year (1901) of the prescribed land cover map. Where possible, the parameter configuration remained faithful to that used in the original ORCHIDEE-MICT spinup simulations, to avoid excessive drift from the original soil organic carbon (SOC) state. This is equilibrium simulation is performed to allow the soil carbon state to adjust to a new equilibrium under the different, DOC and lateral transport-generating soil carbon scheme used by the model branch employed here. After some adjustment simulations to account for differing read/write norms between ORCHIDEE-MICT and this model version, the model was then run in transient mode under historical climate, land cover and atmospheric CO_2 concentrations for the period 1898-2005, and a separate simulation restarted from the latter point over the 'future' period 2006-2099, using the input forcing data under RCP 6.0 described in the preceding section. A summary of the step-wise procedure for simulation setup described is given graphically in Figure 1 of the Supplement. Modules calculating floodplain inundation, water and carbon reinfiltration, poor soils filtration, organic matter priming, canopy and precipitation DOC, all of which have been previously described in detail(Bowring et al., 2019a; Lauerwald et al., 2017)), were all activated for the historical and future simulations.

Simulation Output Analysis and Postprocessing

Output analysis was largely conducted on a basin-by-basin basis for comparison with observational data and to facilitate interpretation of the results with repect to coarse biogeography. In Eurasia, the gradient east-west coarsely corresponds to the gradient pairs colder-warmer, or more-less permafrost. With the exception of the results shown in Table 1, our analysis was restricted to the 'Big Six' Arctic river basins, namely (from East to West) the Kolyma, Lena, Yenisei, Ob, Mackenzie and Yukon. The 'Medium Nine' basins referred to in Table 1 are the nine next-largest basins in the study region. Basins dominantly underlain by continuous or discontinous permafrost (the Kolyma, Lena and Yukon) are denoted in timeseries graphics by a dotted line (versus solid for the remainder). The 'Pan-Arctic' DOC discharge values referred to in Table 1 include all non-Big Six or Medium Nine, non-island coastal grid cells from the western United States to Hudson Bay in North America, and northern Sweden to the northern boundary of the Kamchatka Peninsula, to coarsely match those areas of coastal outflow that correspond to proximate seawater inflow regions of the Arctic Ocean.

Discharge grid cells for each basin were determined from output using the coastal outflow grid cell for each basin. For each basin, these grid cells are as follows (lon,lat): Kolyma (161.5, 69.5); Lena (127.5, 73.5); Yenisei (82.5, 71.5); Ob (69.5, 66.5); Mackenzie (-134.5, 69.5); Yukon (-163.5, 62.5); Pechora (54.5, 68.5); Pyasina (86.5, 73.5); Verkhnyaya-Taymyra (98.5, 76.5); Khatanga (106.5, 73.5); Olenek (119.5, 72.5); Yana (135.5, 72.5); Indigirka (149.5, 71.5); Anadyr (177.5, 64.5); Kuskokwin (-162.5, 60.5).

When referring to standalone values for variables, unless otherwise stated, these are the average for that variable over the period 1996-2005. This same time bracket is used to denote the 'present' or 'modern' period as it marks the last 10 years of the historical (reconstructed) climatological input data used (the 'future' forcing data begin in 2006). Reference to the 'Future', however, implies any time after but including the year 2020. Timeseries displayed in both the main text body and the Supplement use a variety of

aggregation metrics. Most employ a 'decadal-mean percentage change' from a baseline of the 1901-1910 average for a given variable, to enable easy comparison between basins with large differences in variable absolute values. Other metrics, including temperature sensitivities, regressions, 30-year running means, and absolute values for certain variables, are also included in the analysis. The 'present' and 'future' DOC input temperature sensitivities refer to those calculated for the mean of 1996-2005 and 2020-2099, respectively.

Carbon budget closure for the land-ocean-aquatic continuum is determined by the sum of inflows and outflow from a given system (basin), the relevant flows displayed in the Supplement (Fig. S1).

For the inland water carbon cycle of a given basin,

Budget Closure(=0) = [(Soil DOC + CO_2 Input) + (Floodplain DOC + CO_2 Input)] – [(Returnflow + CO_2 Evasion + (DOC+ CO_2 Ocean Outflow)].

Code availability

The source code for ORCHIDEE MICT-LEAK revision 5459 is available online, but its access is restricted. Consequently, one is required to communicate with the corresponding author for a username and password. The source code can be found at the following address: svn://forge.ipsl.jussieu.fr/orchidee/branches/publications/ORCHIDEE_MICT-LEAK_r5459

Primary data and scripts used in the analysis and other supplementary information that may be useful in reproducing the author's work can be obtained by contacting the corresponding author.

This software is governed by the CeCILL license under French law and abiding by the rules of distribution of free software. You can use, modify and/or redistribute the software under the terms of the CeCILL license as circulated by CEA, CNRS and INRIA at the following URL: http://www.cecill.info.

Authors' contribution

SB coded this model version, conducted the simulations and wrote the main body of the paper. RL gave consistent input to the coding process and made several bug fixes. BG advised on the study design and model configuration; DZ gave input on the modelled soil carbon processes and model configuration. PC oversaw all developments leading to the publication of this study. All authors contributed to suggestions regarding the final content of the study.

Competing interests

The authors declare no competing financial interests.

Acknowledgements

Simon Bowring acknowledges funding from the European Union's Horizon 2020 research and innovation program under the Marie Sklodowska-Curie grant agreement No. 643052, 'C-CASCADES' program. Simon Bowring received a PhD grant. RL

acknowledges funding from the European Union's Horizon 2020 research and innovation program under grant agreement no.703813 for the Marie Sklodowska-Curie European Individual Fellowship "C-Leak".

Table S1: Model forcing files used as input for the simulations.

Data Type	Name	Source
Vegetation Map	IPCC AR5 LUHa / IPCC AR5 RCP6.0 AIM	IPCC, 2014
Topographic Index	STN-30p	Vörösmarty et al., 2000
Stream flow direction	STN-30p	Vörösmarty et al., 2000
River surface area	River surface area	Lauerwald et al., 2015
Soil texture class	Soil texture class	Reynolds et al. 1999
Climatology	ISIMIP v2 IPSL-CM5A	Frieler et al., 2017; Lange, 2016,2018.
Potential floodplains	Multi-source global wetland maps	Tootchi et al., 2018
Poor soils	Harmonized World Soil Database map	Nachtergaele et al., 2010
Spinup Soil Carbon Stock	20ky ORCHIDEE-MICT soil carbon spinup	Based on config. in Guimberteau et al. (2018)
Floodwater height	Model vars: floodh_nth, streamr_nth, floodh	Statistically generated from model output
Atmospheric CO2	IPCC AR5 RCP 6.0	IPCC, 2014

Table S2: Simulated present day (1996-2005) and future (2090-2099) CO_2 discharge from the Big Six and Medium Nine river basins into the Arctic.

Big Six		CO2 to Ocean (1996-2005)	s.d.	CO2 to Ocean (2090-2099)	s.d.
	Kolyma	0.180	0.062	0.184	0.057
	Lena	0.203	0.041	0.211	0.043
	Yenisei	0.604	0.198	0.518	0.103
	Ob	0.376	0.111	0.235	0.066
	Mackenzie				
	Yukon	0.049	0.009	0.051	0.014
	SUM	**1.412**	/	**1.199**	/
Medium 9					
	Pechora	0.120	0.027	0.077	0.016
	Pyasina	0.121	0.032	0.108	0.044
	Verkhnyaya-Taymyra	0.050	0.012	0.045	0.019
	Khatanga	0.204	0.049	0.195	0.065
	Olenek	0.060	0.023	0.051	0.018
	Yana	0.028	0.010	0.023	0.009
	Indigirka	0.050	0.019	0.055	0.037
	Anadyr	0.092	0.023	0.114	0.020
	Kuskokwin	0.023	0.008	0.027	0.013
	SUM	**0.748**	/	**0.695**	/

Figures:

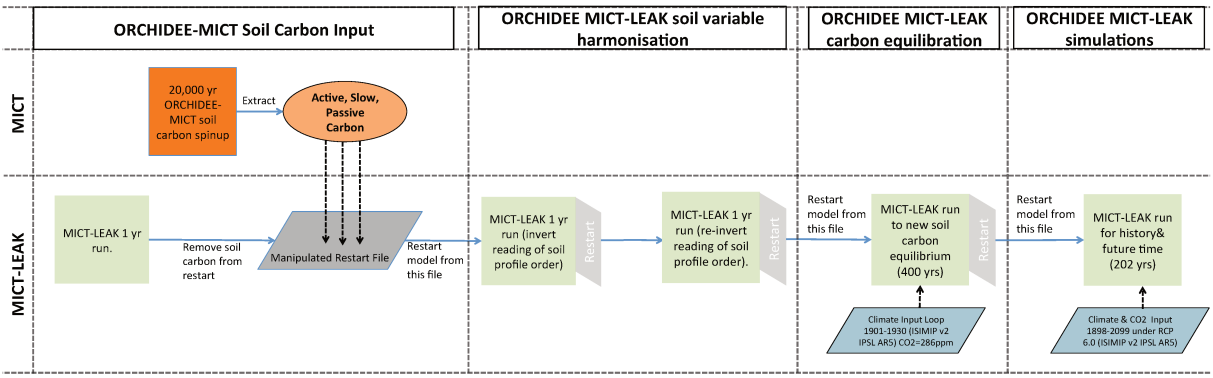

Figure S1: Flow diagram illustrating the step-wise protocol required to set up the model, up to and including the historical and future final simulation runs. The first (left) 'Soil Carbon Input' column refers to the initial steps taken to input permafrost-like soil carbon stocks into our model. The next 'variable harmonisation' column refers to the fact that the restart inputs from ORCHIDEE-MICT are read by our model in inverse order, so that one year must be run in which an activated flag reads it properly, before the reading of soil profile restarts is re-inverted for all subsequent years. 'Carbon equilibration' refers to the quasi-steady state carbon stock subsequently obtained, while 'simulation' refers to the final historical and future simulations whose output is presented in this study.

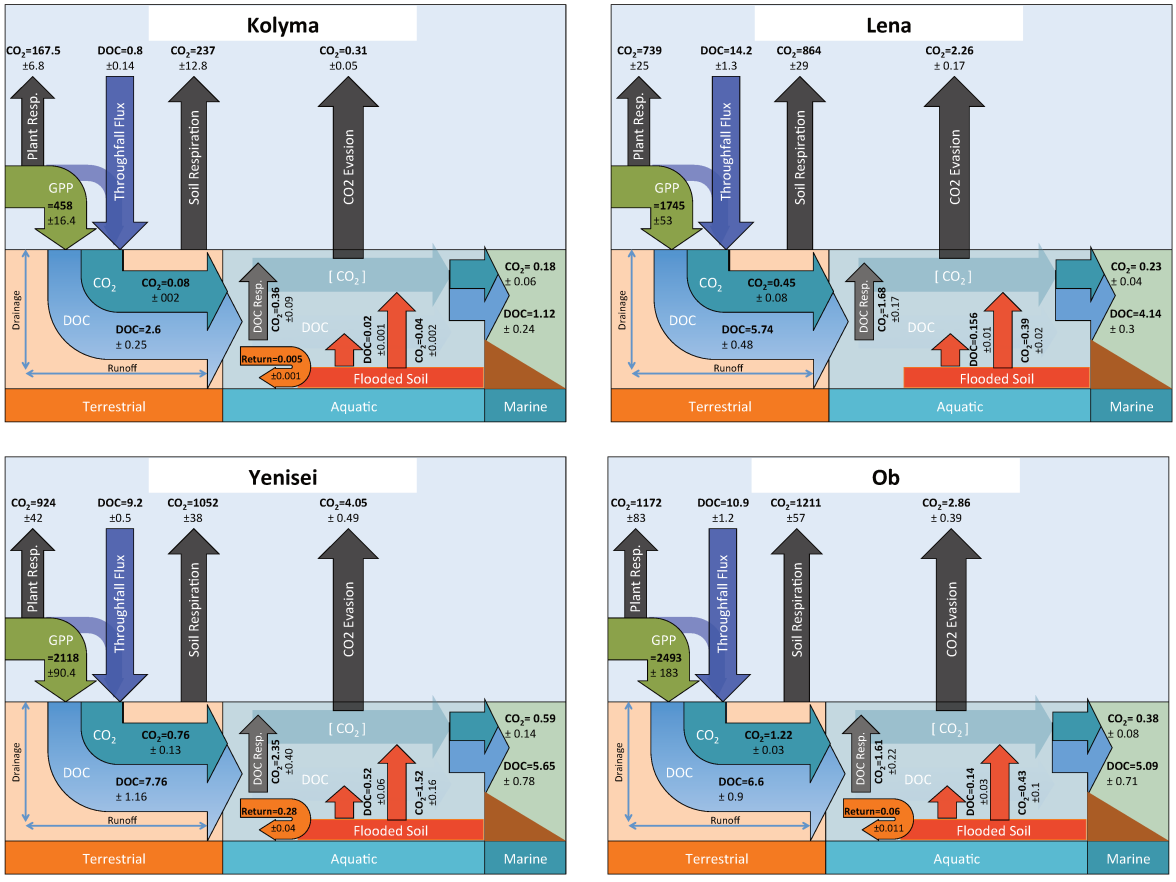

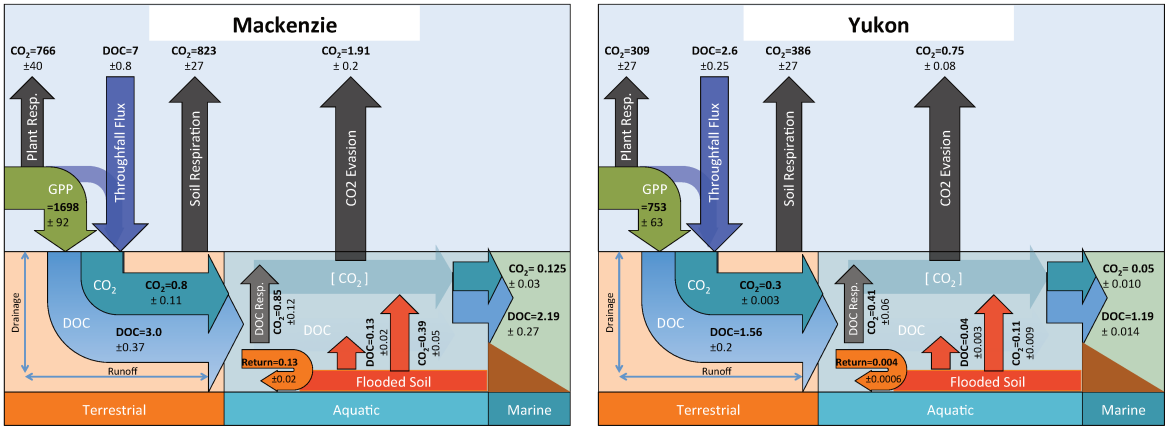

Figure S2: Schematic diagrams detailing the major yearly carbon flux model outputs for each of the Big Six river basins as they are transformed and transported across the land-ocean aquatic continuum (LOAC) for the average of the period 1996-2005. All values represent yearly sums of carbon fluxes in TgC yr^{-1}.

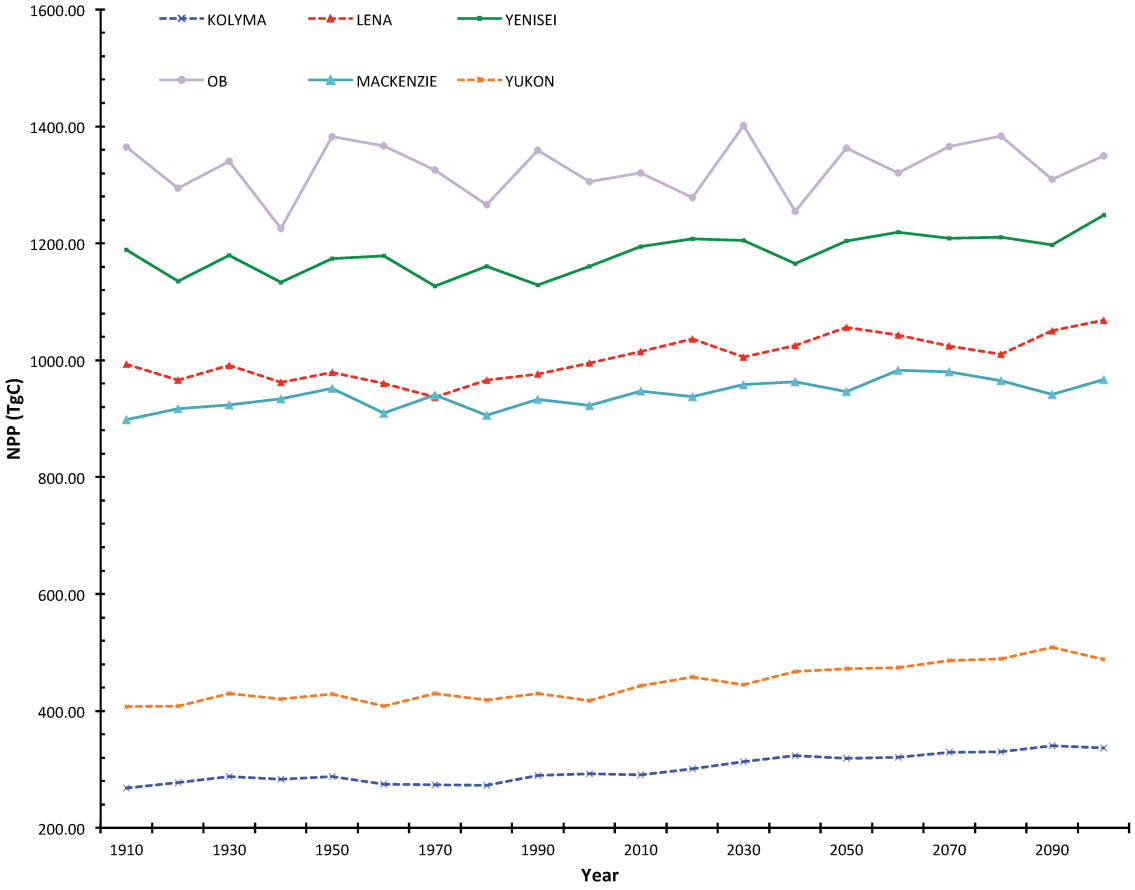

Figure S3: Decadal-averaged annual Net Primary Production (NPP) in TgC yr^{-1} for each of the Bix Six basins over the entire simulation period.

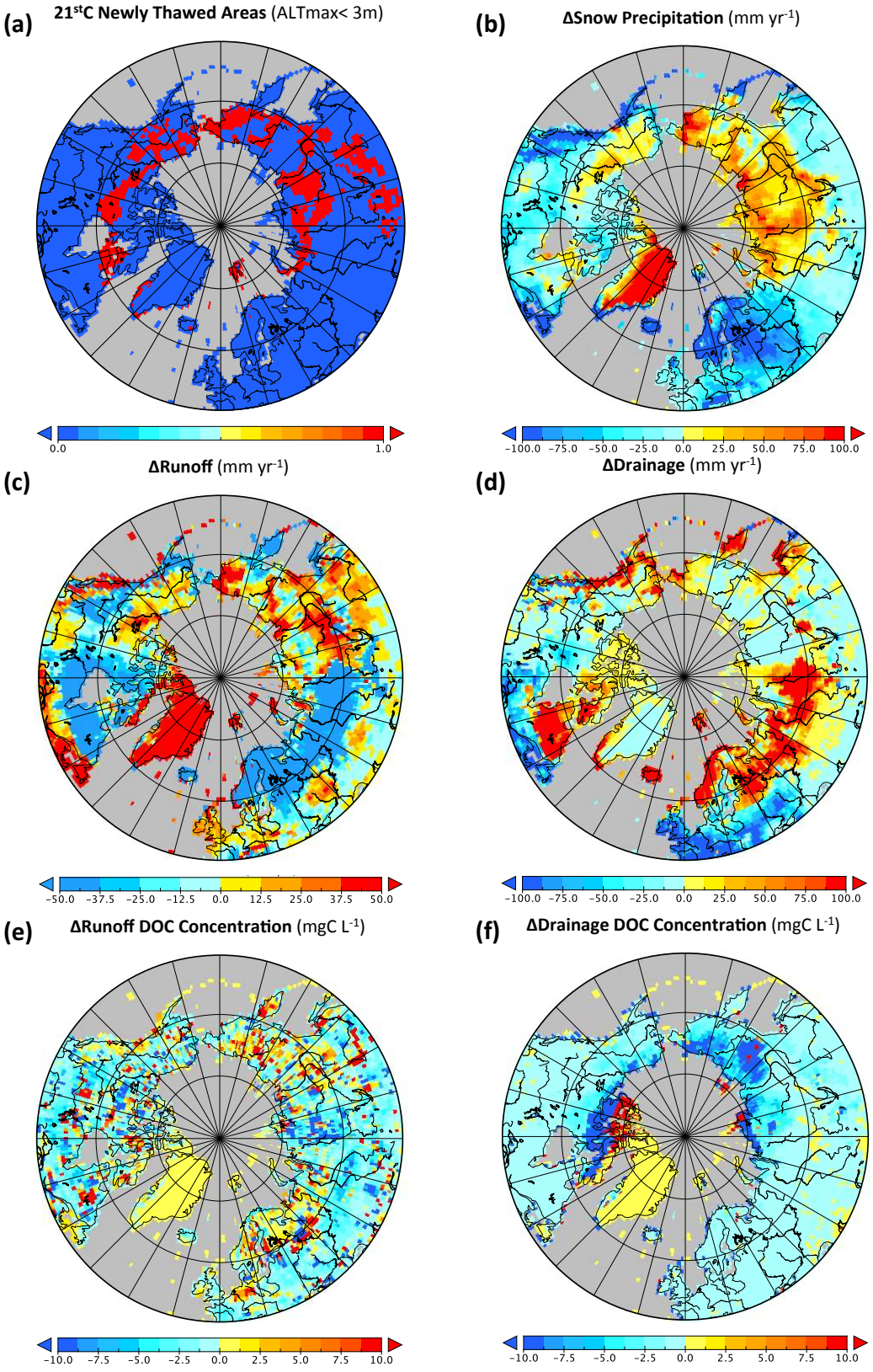

Figure S4: Maps of changes in variables between the mean of (2090-2099) subtracted by that of (1996-2005) in each pixel for. **(a)** Newly thawed permafrost areas; **(b)** Snowfall (mm yr^{-1}) **(c)** Surface runoff (mm yr^{-1}), **(d)** Subsurface drainage(mm yr^{-1}) **(e)** Runoff DOC concentration (mgC L^{-1}) **(f)** Drainage DOC concentration (mgC L^{-1}).

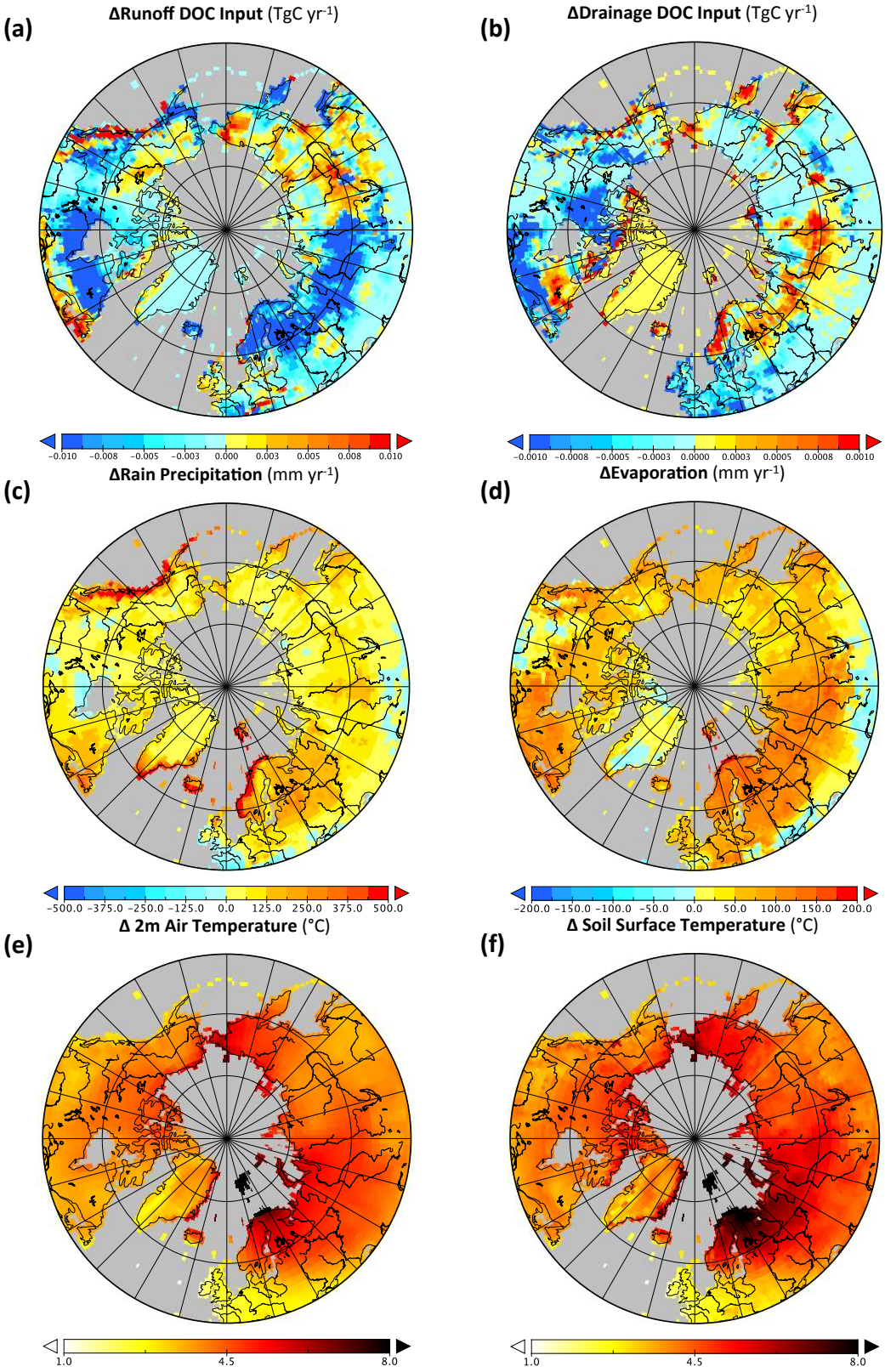

Figure S5: Maps of changes in variables between the mean of (2090-2099) subtracted by that of (1996-2005) in each pixel for. **(a)** Surface runoff DOC input to rivers (TgC yr^{-1}); **(b)** Drainage DOC input to rivers (TgC yr^{-1}) **(c)** Rain precipitation (mm yr^{-1}), **(d)** Evaporation (mm yr^{-1}) **(e)** 2 metre air temperature (Celsius) **(f)** Soil surface temperature (Celsius)..

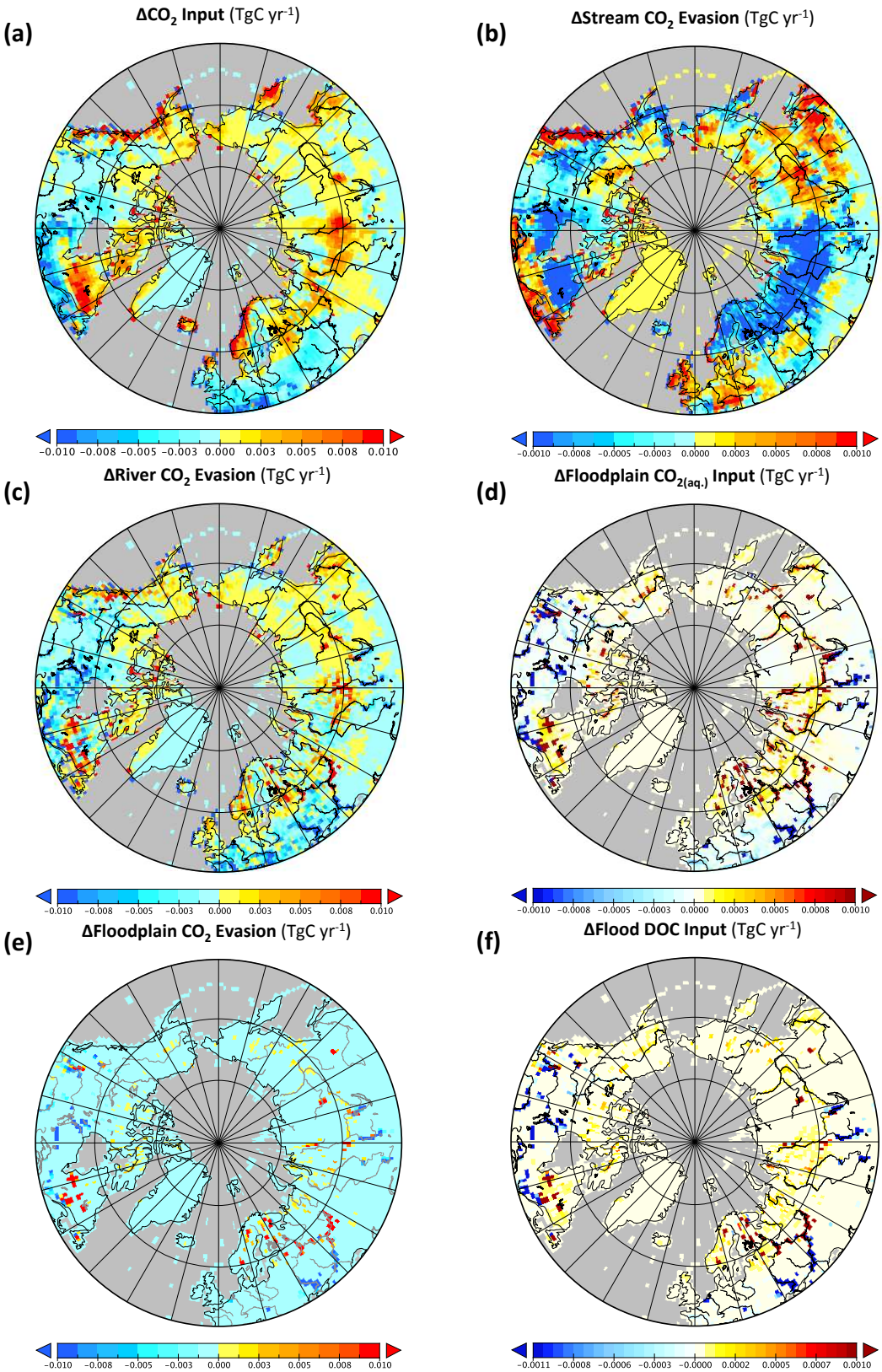

Figure S6: Maps of changes in variables between the mean of (2090-2099) subtracted by that of (1996-2005) in each pixel for. **(a)** CO_2 input to rivers (TgC yr^{-1}); **(b)** Stream water CO2 evasion (TgC yr^{-1}) **(c)** River water surface CO_2 evasion (TgC yr^{-1}); **(d)** Floodplain CO_2 input (TgC yr^{-1}) **(e)** CO_2 evasion from flooded areas (TgC yr^{-1}) **(f)** Floodplain DOC inputs (TgC yr^{-1})..

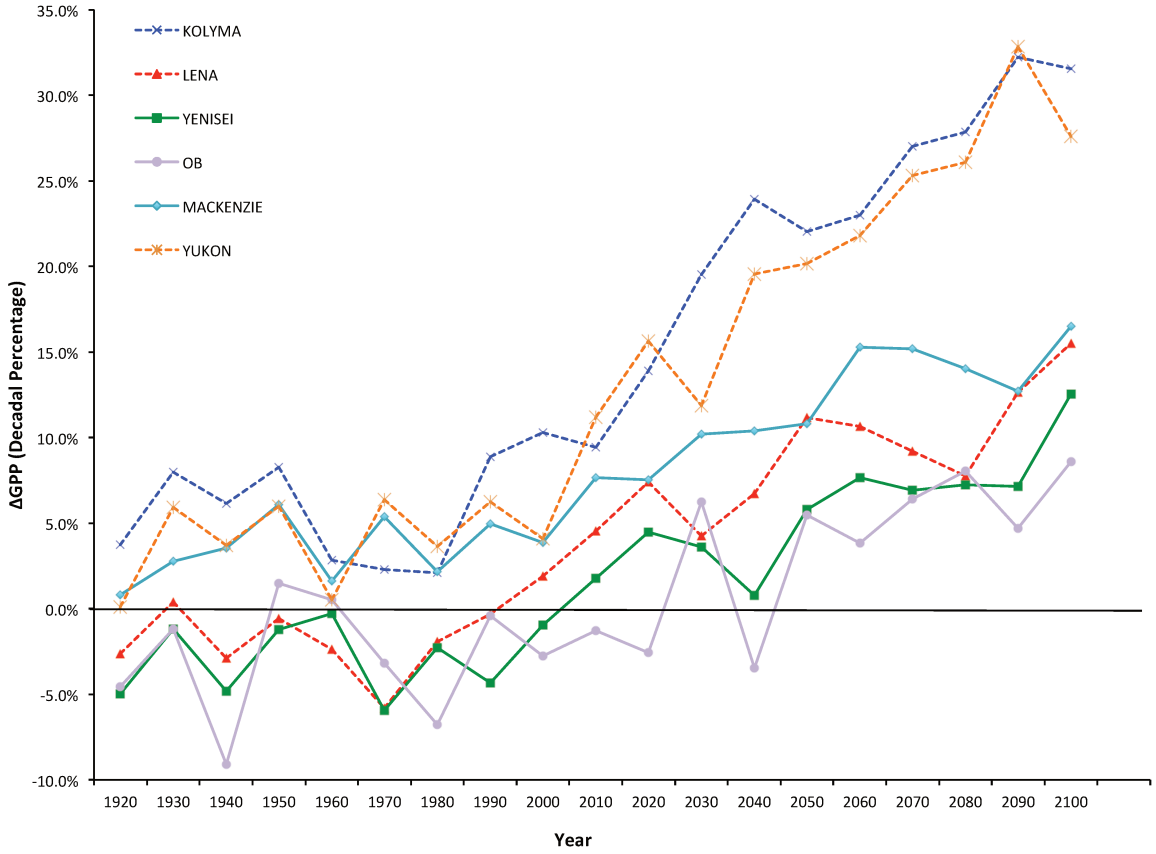

Figure S7: Decadal-average percentage change in Gross Primary Production (GPP) for each of the Big Six basins from a 1901-1910 baseline.

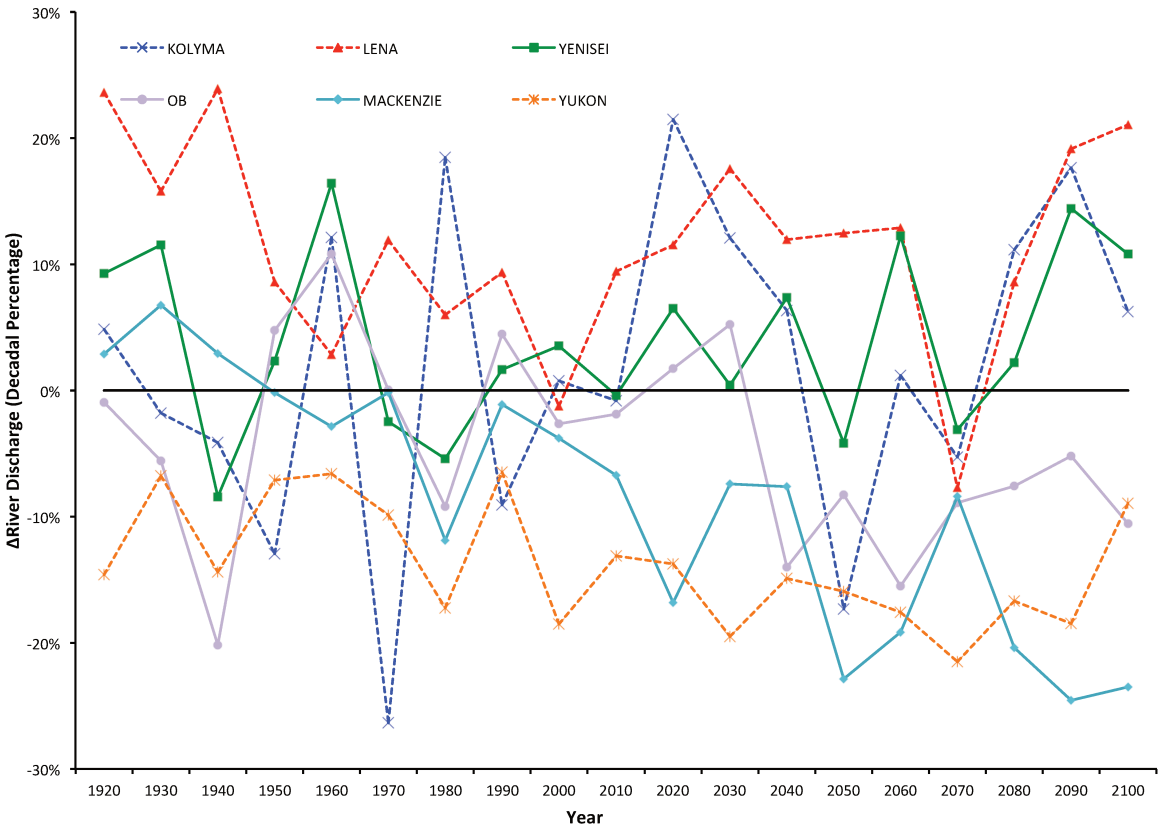

Figure S8: Decadal-averaged percentage change in river discharge for each of the Big Six basins from a 1901-1910 baseline.

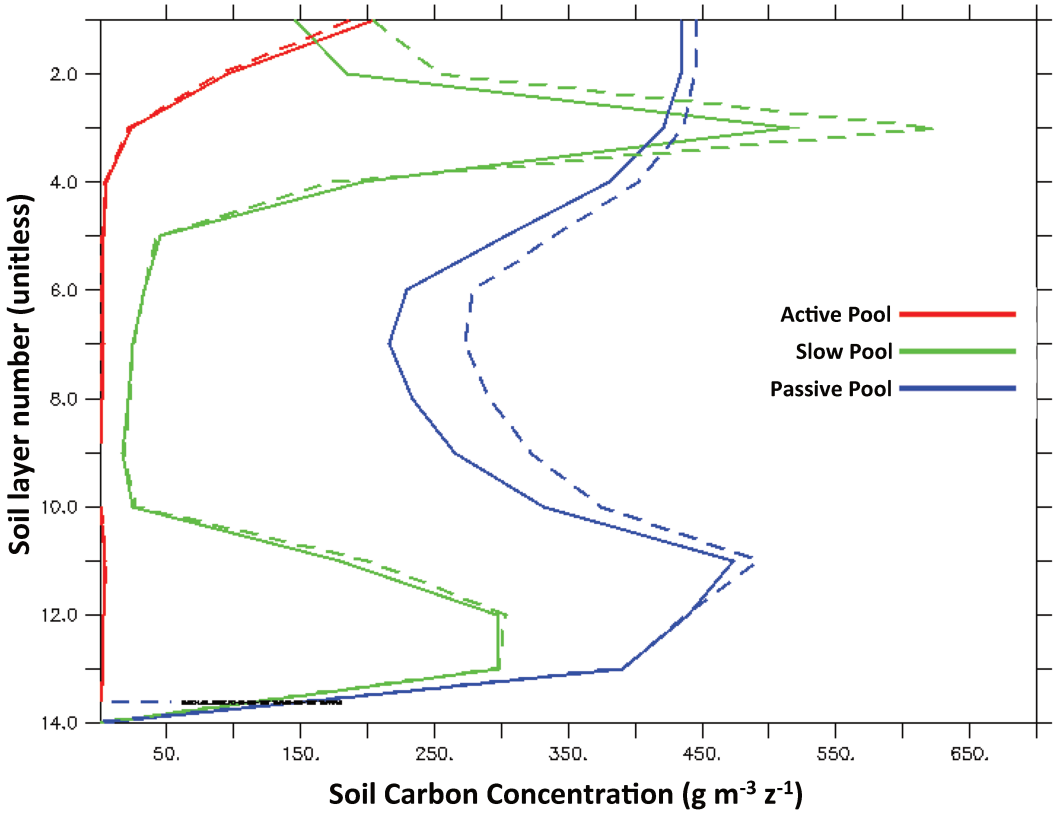

Figure S9: Mean permafrost region soil carbon concentration profiles for each layer in the model soil column (noting that layer thickness increases geometrically from layer 1), for each of the soil carbon pools simulated by the model. Dashed lines are the profiles averaged over 1901-1910, solid lines those averaged over 1996-2005.

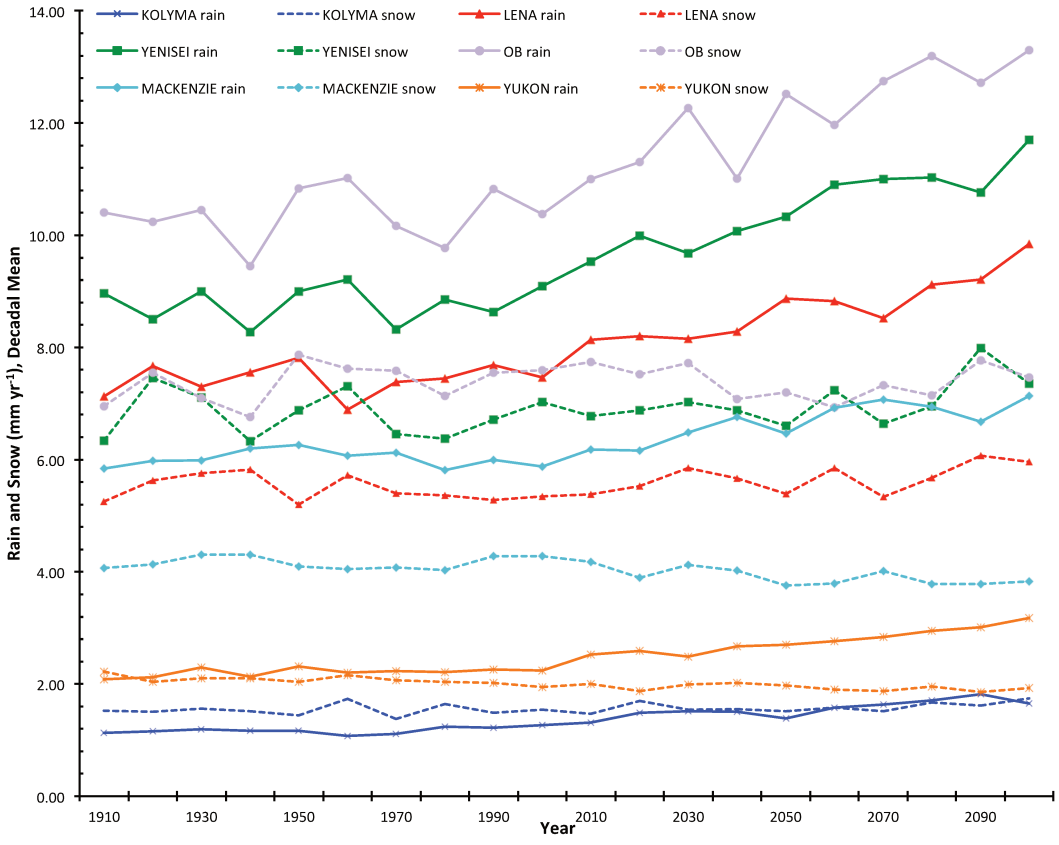

Figure S10: Timeseries for the decade-averaged annual precipitation (mm yr^{-1}) as rain (solid) and snowfall (dashed), given as a grid cell average over each of the basins for the entire simulation period.

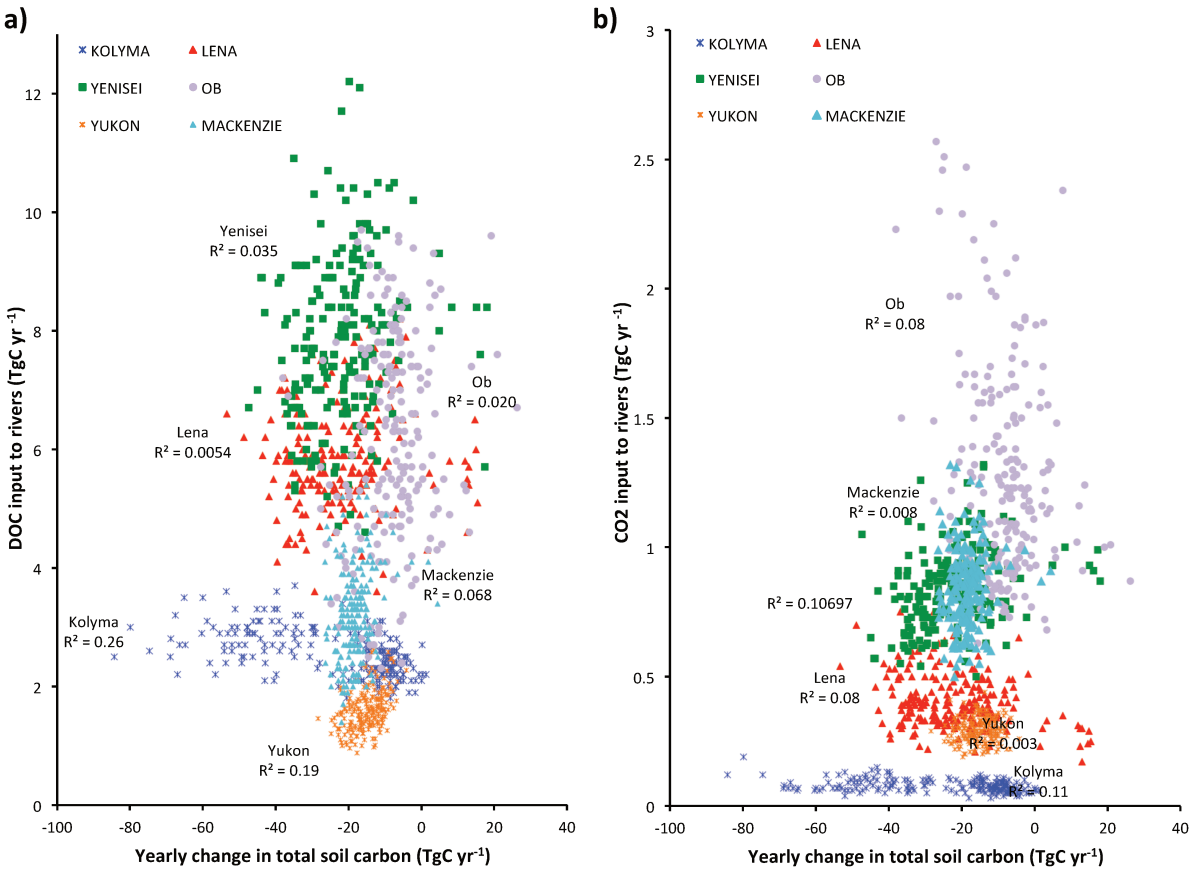
a)
KOLYMA
LENA
YENISEI
OB
YUKON
MACKENZIE
Yenisei
R² = 0.035
Ob
R² = 0.020
Lena
R² = 0.0054
Mackenzie
R² = 0.068
Kolyma
R² = 0.26
Yukon
R² = 0.19
DOC input to rivers (TgC yr⁻¹)
Yearly change in total soil carbon (TgC yr⁻¹)
b)
KOLYMA
LENA
YENISEI
OB
YUKON
MACKENZIE
Ob
R² = 0.08
Mackenzie
R² = 0.008
R² = 0.10697
Lena
R² = 0.08
Yukon
R² = 0.003
Kolyma
R² = 0.11
CO2 input to rivers (TgC yr⁻¹)
Yearly change in total soil carbon (TgC yr⁻¹)

4806

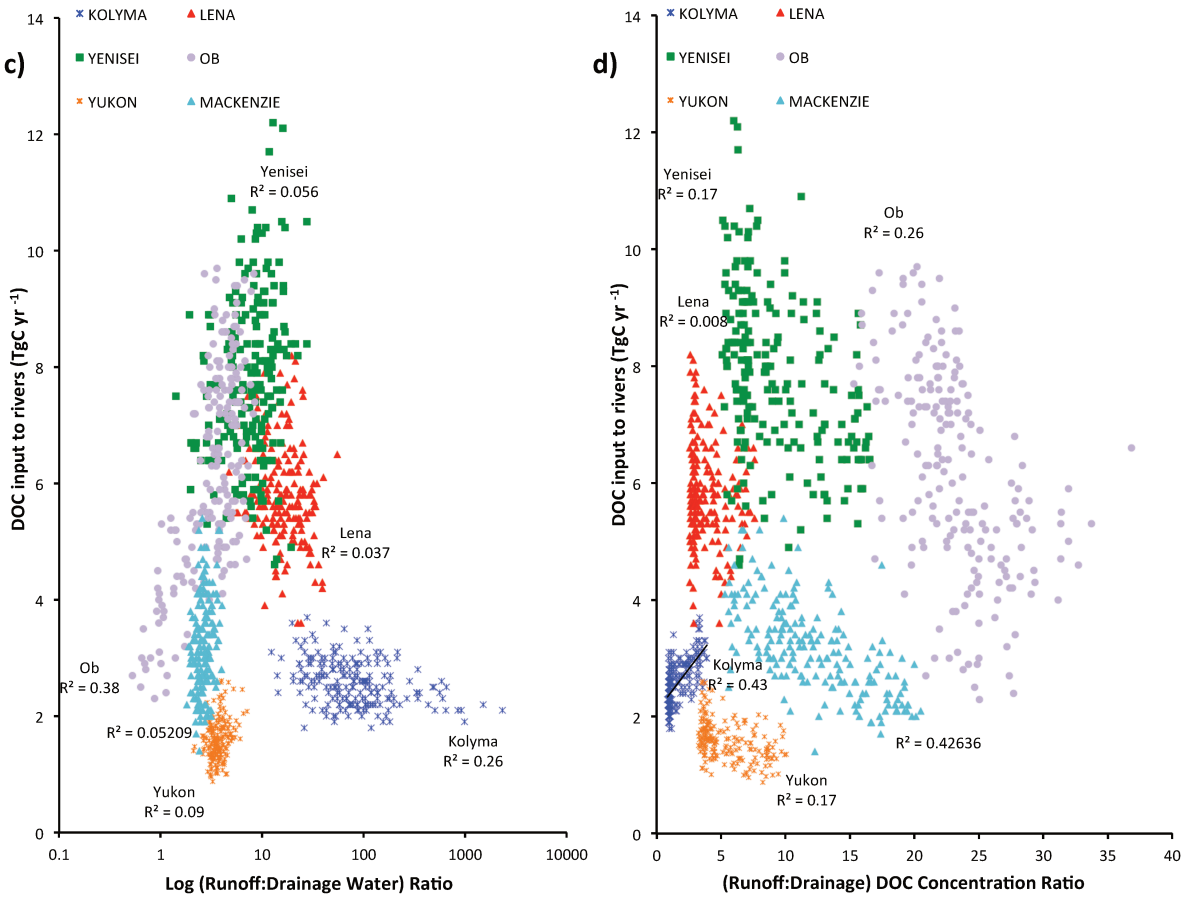
c)
KOLYMA
LENA
YENISEI
OB
YUKON
MACKENZIE
Yenisei
R² = 0.056
Lena
R² = 0.037
Ob
R² = 0.38
R² = 0.05209
Kolyma
R² = 0.26
Yukon
R² = 0.09
DOC input to rivers (TgC yr⁻¹)
Log (Runoff:Drainage Water) Ratio
d)
KOLYMA
LENA
YENISEI
OB
YUKON
MACKENZIE
Yenisei
R² = 0.17
Ob
R² = 0.26
Lena
R² = 0.008
Kolyma
R² = 0.43
R² = 0.42636
Yukon
R² = 0.17
DOC input to rivers (TgC yr⁻¹)
(Runoff:Drainage) DOC Concentration Ratio

4807

Figure S11: Basin-disaggregated regression scatter plots. Each point represents the aggregate over the entire basin for a given year, and thus for each basin the scattering reflects the temporal variability of the plotted variables. **(a)** DOC and **(b)** CO_2 inputs to rivers (TgC yr^{-1}) plotted against yearly basinwide changes in soil organic carbon (TgC yr^{-1}); and DOC input to rivers against the ratio of **(c)** runoff:drainage water flux; and **(d)** DOC concentrations in runoff and drainage (runoff:drainage).

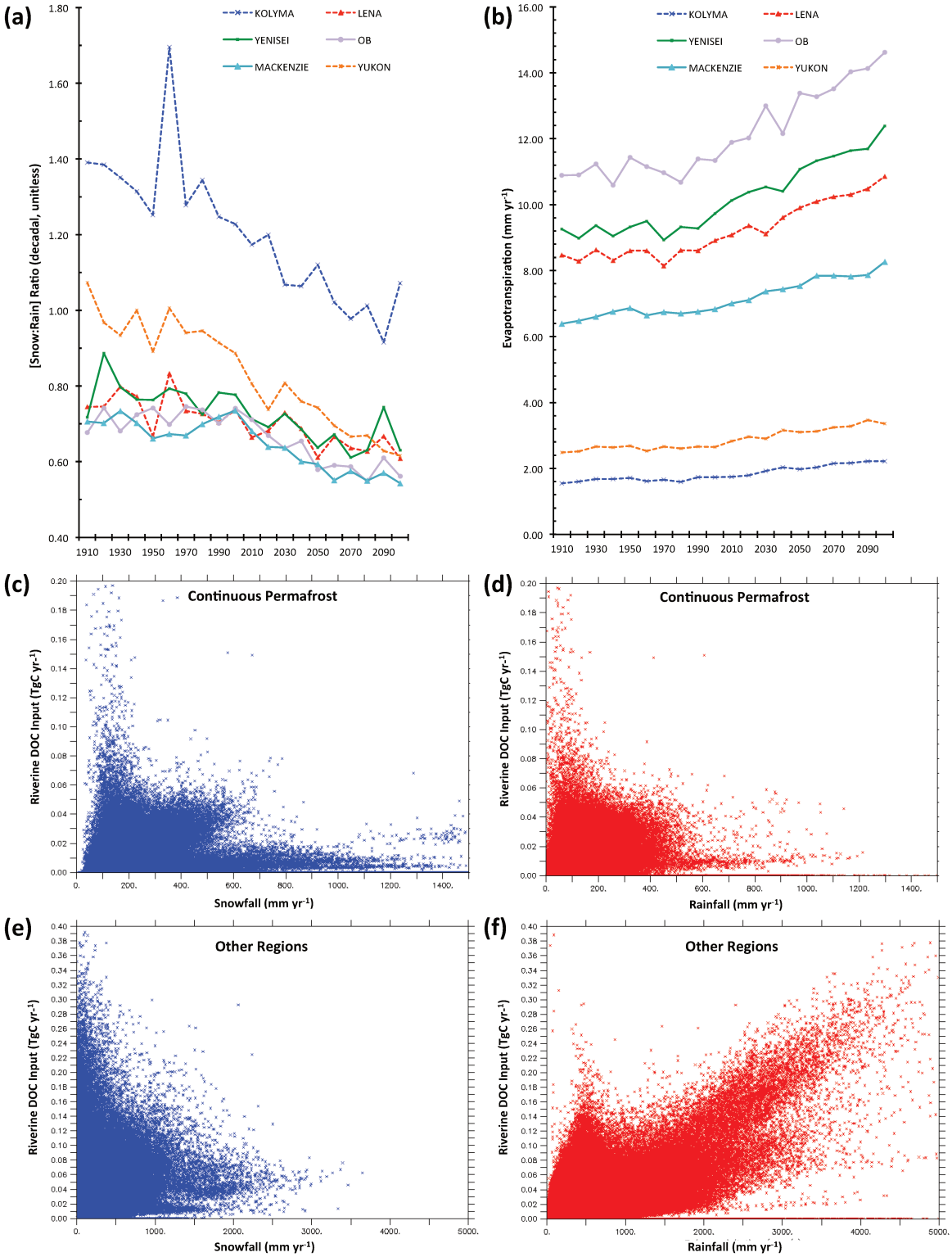

Figure S12: Basin-disaggregated timeseries of **(a)** Decadal-mean (snow:rain) ratio; **(b)** Decadal-mean evapotranspiration rates averaged over each basin. (c-f): Scatter plot of riverine DOC inputs to total

4817 annual snowfall (c,d) and rainfall (d,f) over 'continuous permafrost' and 'non-continuous-permafrost' or
4818 'other', regions, for each grid cell over the entire simulation period.
4819

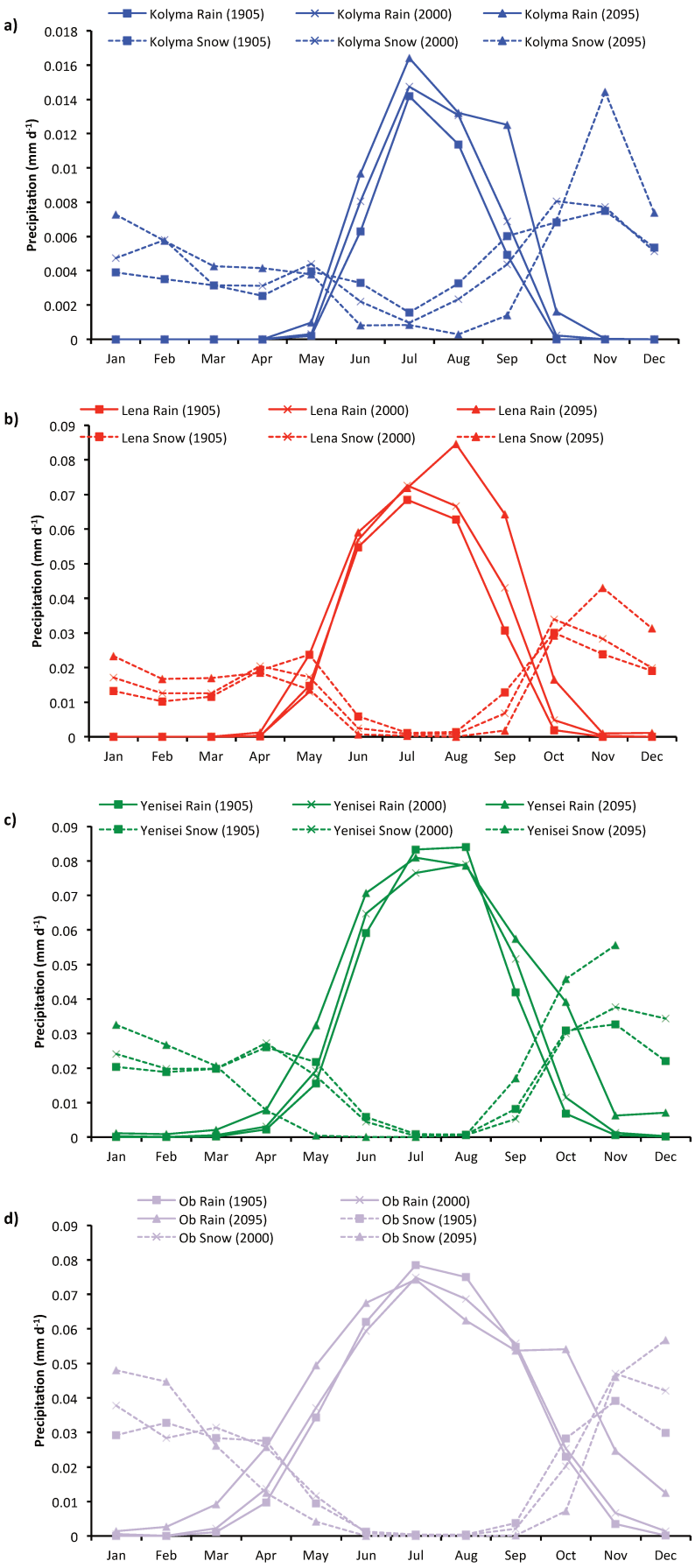
a)
Kolyma Rain (1905)
Kolyma Rain (2000)
Kolyma Rain (2095)
Kolyma Snow (1905)
Kolyma Snow (2000)
Kolyma Snow (2095)
Precipitation (mm d-1)
0.018
0.016
0.014
0.012
0.01
0.008
0.006
0.004
0.002
0
Jan Feb Mar Apr May Jun Jul Aug Sep Oct Nov Dec
b)
Lena Rain (1905)
Lena Rain (2000)
Lena Rain (2095)
Lena Snow (1905)
Lena Snow (2000)
Lena Snow (2095)
Precipitation (mm d-1)
0.09
0.08
0.07
0.06
0.05
0.04
0.03
0.02
0.01
0
Jan Feb Mar Apr May Jun Jul Aug Sep Oct Nov Dec
c)
Yenisei Rain (1905)
Yenisei Rain (2000)
Yensei Rain (2095)
Yenisei Snow (1905)
Yenisei Snow (2000)
Yenisei Snow (2095)
Precipitation (mm d-1)
0.09
0.08
0.07
0.06
0.05
0.04
0.03
0.02
0.01
0
Jan Feb Mar Apr May Jun Jul Aug Sep Oct Nov Dec
d)
Ob Rain (1905)
Ob Rain (2000)
Ob Rain (2095)
Ob Snow (1905)
Ob Snow (2000)
Ob Snow (2095)
Precipitation (mm d-1)
0.09
0.08
0.07
0.06
0.05
0.04
0.03
0.02
0.01
0
Jan Feb Mar Apr May Jun Jul Aug Sep Oct Nov Dec

4820

4821

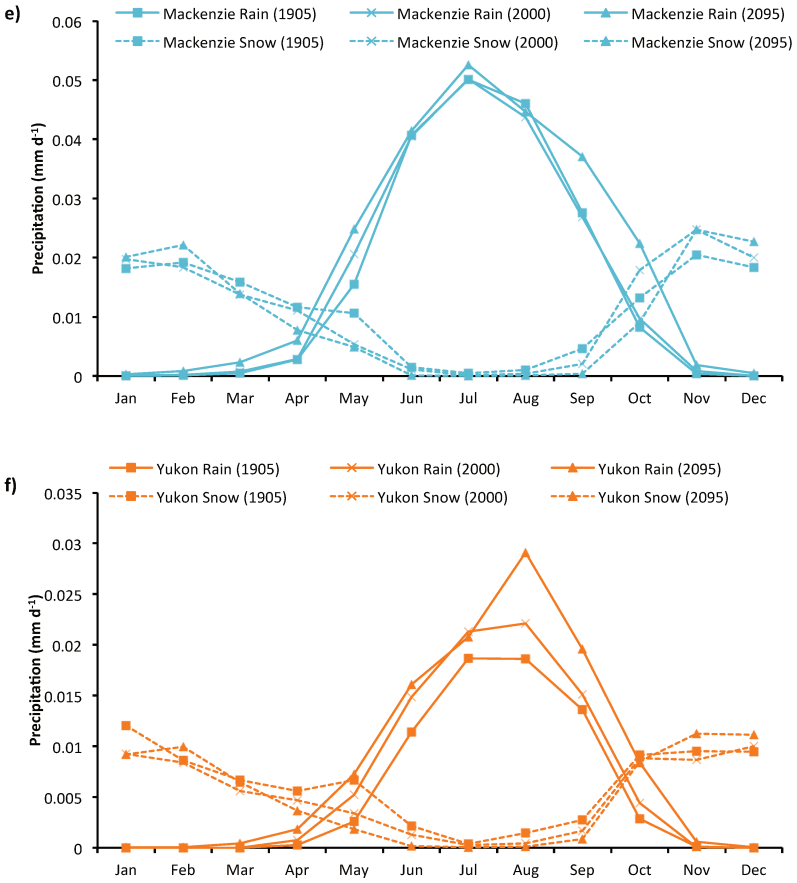

Figure S13: Mean monthly rain (solid) and snow (dashed) in mm d^{-1} averaged over the decades 1901-1910 (squares), 1996-2005 (crosses) and 2090-2099 (triangles) for the average of each of the Big Six basins **(a-f)**. The legend shows the midpoint year of each of the decades concerned.

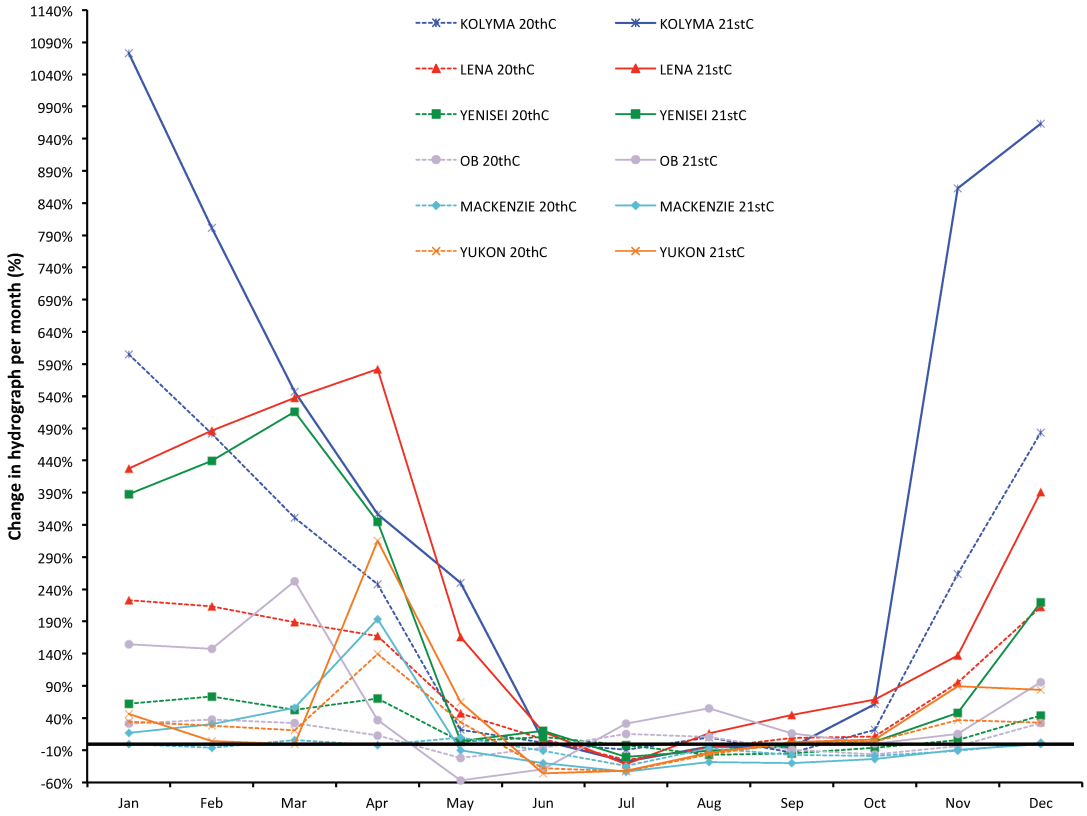

Figure S14: Timeseries of the percentage change in mean monthly river discharge from a baseline of the 1901-1910 average, for the decades 1996-2005 (dashed) and 2090-2099 (solid), for each of the Big 6 rivers. Discharge is taken from the river outflow grid cell (see Methods) of each basin.

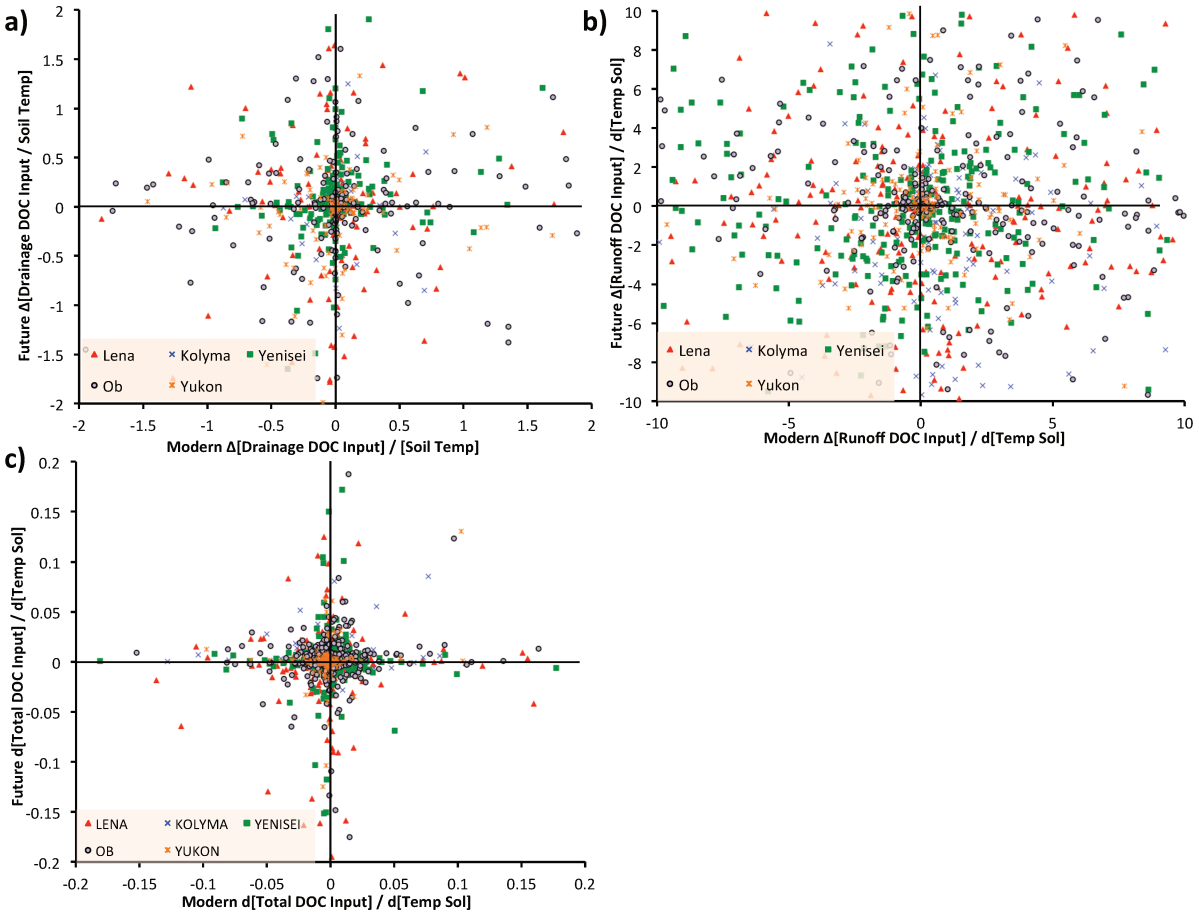

Figure S15: Scatter plots **(a-c)** showing the year-averaged temperature sensitivity (ground temperature) of carbon inputs to the river (TgC °Celsius^{-1}) in the 'modern' (1996-2005 average) versus 'future' (2020-2099 average) era, for **(a)** drainage DOC inputs, **(b)** runoff DOC inputs and **(c)** total DOC input. Basins are disaggregated by colour, with each point representing the mean future/modern temperature sensitivity pair of an individual grid cell.

Appendix 3

Appendix to Chapter 5:

CO_2 Uptake By Weathering Increasingly Exceeds CO_2 Evasion From Rivers As Permafrost Thaws

Introduction

The content of this Supporting Information document covers in greater detail some of the steps taken in the Methods of this paper. Specifically, in Supporting Text S1, we explicitly give the rating curves used for estimating the alkalinity loading of a given river from discharge and, in case of the Ob river, the point in the seasonal cycle. In Table S1, we cover the regression statistics used in estimating a correction factor for per basin alkalinity flux (see 2.2.4 in main text).

Text S1: Per-Basin Calibration Using Tank et al. (2012) Rating Curve

The rating curves set-up by Tank et al. include pre-set 'models' for alkalinity discharge, which differ from basin to basin. The predictor variable in this regression is monthly discharge, and in one case the time in the seasonal cycle (Ob), as predictor, with different models (M) following the following schemes for the Kolyma, Yenisei, Mackenzie and Yukon in Model 1, the Lena in Model 2 and the Ob in Model 4a (here we follow the model numbering convention used in Tank et al.).

$$(\mathbf{1})\ \boldsymbol{ln(Load)} = \boldsymbol{a0} + \boldsymbol{a1} * \boldsymbol{Ln(discharge)^2} \qquad (\boldsymbol{M1})$$

$$(\mathbf{2})\ \boldsymbol{ln(Load)} = \boldsymbol{a0} + \boldsymbol{a1} * \boldsymbol{Ln(discharge)} + \boldsymbol{a2} * \boldsymbol{Ln(discharge)^2} \qquad (\boldsymbol{M2})$$

$$(\mathbf{3})\ \boldsymbol{ln(Load)} = \boldsymbol{a0} + \boldsymbol{a1} * \boldsymbol{Ln(discharge)} + \boldsymbol{a2} * \boldsymbol{sin(2 * \delta time)} + \boldsymbol{a3} * \boldsymbol{cos(2\pi\delta time)} \qquad (\boldsymbol{M4a})$$

where 'Load' is alkalinity load [kgC d^{-1}], discharge is river discharge in m^3s^{-1} and 'dtime' = decimal time - center of decimal time from the empirical data.

Instead of directly using the rating curves established by Tank et al, we simplified those rating curves when information loss was limited. For this, we used the daily discharges and the predicted daily HCO_3^- fluxes from Tank et al., 2012, and performed a regression of these daily HCO_3^- fluxes against daily discharge values.

For the Mackenzie, Yukon, Kolyma, and Yenisei Rivers, we reproduced the original rating curves of the form M1 (see above). Also for the Lena, for which the original rating curve followed the second-order polynomial equation M2 , we chose a linear regression of the form M1 instead, as the difference in R^2 and root mean square error (RMSE) between each form was negligible. Only for the Ob River, for which the original rating curve followed form M4 (see above), we removed the time variant and refitted a second-order polynomial equation of the form M2, using as well only discharge a independent variable. This simplified all basins' regression equation except for the Ob to the form in M1, with a0= 7.424, 9.131, 12.84, 22.924, 8.523, and 9.951, and a1=7.424, 0.762, 0.397, -1.915, 0.881, 0.722, for the Kolyma, Lena, Yenisei, Ob, Yukon and Mackenzie, respectively. For the Ob polynomial, a2=0.1294.

Table S1: Regression statistics for the regression calculations undertaken in Section 2.2.4 of the main text, using the following regression equation $Load_{obs} = b * (0.47 * Load_{sim,RUNOFF} + Load_{sim,DRAINAGE})$. and solved for the factor *b* for each basin.

River	*b*	std	R^2	RMSE	p
Mackenzie	1.542	0.175	0.87	50%	2.54E-06
Yukon	2.472	0.165	0.95	30%	1.16E-08
Kolyma	0.664	0.012	1.00	14%	1.20E-14
Lena	1.032	0.053	0.97	28%	7.20E-10
Yenisei	1.050	0.105	0.89	39%	7.55E-07
Ob	1.077	0.110	0.89	44%	9.18E-07

References

Abbott, B. W., Jones, J. B., Godsey, S. E., Larouche, J. R. and Bowden, W. B.: Patterns and persistence of hydrologic carbon and nutrient export from collapsing upland permafrost, Biogeosciences, doi:10.5194/bg-12-3725-2015, 2015.

Abbott, B. W., Jones, J. B., Schuur, E. A. G., Chapin, F. S., Bowden, W. B., Bret-Harte, M. S., Epstein, H. E., Flannigan, M. D., Harms, T. K., Hollingsworth, T. N., Mack, M. C., McGuire, A. D., Natali, S. M., Rocha, A. V., Tank, S. E., Turetsky, M. R., Vonk, J. E., Wickland, K. P., Aiken, G. R., Alexander, H. D., Amon, R. M. W., Benscoter, B. W., Bergeron, Y., Bishop, K., Blarquez, O., Bond-Lamberty, B., Breen, A. L., Buffam, I., Cai, Y., Carcaillet, C., Carey, S. K., Chen, J. M., Chen, H. Y. H., Christensen, T. R., Cooper, L. W., Cornelissen, J. H. C., De Groot, W. J., Deluca, T. H., Dorrepaal, E., Fetcher, N., Finlay, J. C., Forbes, B. C., French, N. H. F., Gauthier, S., Girardin, M. P., Goetz, S. J., Goldammer, J. G., Gough, L., Grogan, P., Guo, L., Higuera, P. E., Hinzman, L., Hu, F. S., Hugelius, G., Jafarov, E. E., Jandt, R., Johnstone, J. F., Karlsson, J., Kasischke, E. S., Kattner, G., Kelly, R., Keuper, F., Kling, G. W., Kortelainen, P., Kouki, J., Kuhry, P., Laudon, H., Laurion, I., MacDonald, R. W., Mann, P. J., Martikainen, P. J., McClelland, J. W., Molau, U., Oberbauer, S. F., Olefeldt, D., Paré, D., Parisien, M. A., Payette, S., Peng, C., Pokrovsky, O. S., Rastetter, E. B., Raymond, P. A., Raynolds, M. K., Rein, G., Reynolds, J. F., Robards, M., Rogers, B. M., Schdel, C., Schaefer, K., Schmidt, I. K., Shvidenko, A., Sky, J., Spencer, R. G. M., Starr, G., Striegl, R. G., Teisserenc, R., Tranvik, L. J., Virtanen, T., Welker, J. M., et al.: Biomass offsets little or none of permafrost carbon release from soils, streams, and wildfire: An expert assessment, Environ. Res. Lett., doi:10.1088/1748-9326/11/3/034014, 2016.

Aiken, G. R., Spencer, R. G. M., Striegl, R. G., Schuster, P. F. and Raymond, P. A.: Influences of glacier melt and permafrost thaw on the age of dissolved organic carbon in the Yukon River basin, Global Biogeochem. Cycles, doi:10.1002/2013GB004764, 2014.

Aitkenhead-Peterson, J. A., McDowell, W. H. and Neff, J. C.: Sources, Production, and Regulation of Allochthonous Dissolved Organic Matter Inputs to Surface Waters, in Aquatic Ecosystems., 2003.

Alling, V., Sanchez-Garcia, L., Porcelli, D., Pugach, S., Vonk, J. E., Van Dongen, B., Mörth, C. M., Anderson, L. G., Sokolov, A., Andersson, P., Humborg, C., Semiletov, I. and Gustafsson, Ö.: Nonconservative behavior of dissolved organic carbon across the Laptev and East Siberian seas, Global Biogeochem. Cycles, doi:10.1029/2010GB003834, 2010.

Amiotte Suchet, P., Probst, J.-L. and Ludwig, W.: Worldwide distribution of continental rock lithology: Implications for the atmospheric/soil CO 2 uptake by continental weathering and alkalinity river transport to the oceans , Global Biogeochem. Cycles, doi:10.1029/2002gb001891, 2003.

Archer, D.: A model of the methane cycle, permafrost, and hydrology of the Siberian continental margin, Biogeosciences, doi:10.5194/bg-12-2953-2015, 2015.

Aufdenkampe, A. K., Mayorga, E., Raymond, P. A., Melack, J. M., Doney, S. C., Alin, S. R., Aalto, R. E. and Yoo, K.: Riverine coupling of biogeochemical cycles between land, oceans, and atmosphere, in Frontiers in Ecology and the Environment., 2011.

De Baets, S., Van de Weg, M. J., Lewis, R., Steinberg, N., Meersmans, J., Quine, T. A., Shaver, G. R. and Hartley, I. P.: Investigating the controls on soil organic matter decomposition in tussock tundra soil and permafrost after fire, Soil Biol. Biochem., doi:10.1016/j.soilbio.2016.04.020, 2016.

Bardy, M., Derenne, S., Allard, T., Benedetti, M. F. and Fritsch, E.: Podzolisation and exportation of organic matter in black waters of the Rio Negro (upper Amazon basin,

4987 Brazil), Biogeochemistry, doi:10.1007/s10533-010-9564-9, 2011.
4988 Bastviken, D., Tranvik, L. J., Downing, J. A., Crill, P. M. and Enrich-Prast, A.: Freshwater
4989 methane emissions offset the continental carbon sink, Science (80-.).,
4990 doi:10.1126/science.1196808, 2011.
4991 Battin, T. J., Luyssaert, S., Kaplan, L. A., Aufdenkampe, A. K., Richter, A. and Tranvik, L. J.:
4992 The boundless carbon cycle, Nat. Geosci., doi:10.1038/ngeo618, 2009.
4993 Bauch, D., Hölemann, J. A., Nikulina, A., Wegner, C., Janout, M. A., Timokhov, L. A. and
4994 Kassens, H.: Correlation of river water and local sea-ice melting on the Laptev Sea shelf
4995 (Siberian Arctic), J. Geophys. Res. Ocean., doi:10.1002/jgrc.20076, 2013.
4996 Beaulieu, E., Goddëris, Y., Donnadieu, Y., Labat, D. and Roelandt, C.: High sensitivity of the
4997 continental-weathering carbon dioxide sink to future climate change, Nat. Clim. Chang.,
4998 doi:10.1038/nclimate1419, 2012.
4999 Beer, C., Lucht, W., Schmullius, C. and Shvidenko, A.: Small net carbon dioxide uptake by
5000 Russian forests during 1981-1999, Geophys. Res. Lett., doi:10.1029/2006GL026919,
5001 2006.
5002 Bekryaev, R. V., Polyakov, I. V. and Alexeev, V. A.: Role of polar amplification in long-term
5003 surface air temperature variations and modern arctic warming, J. Clim.,
5004 doi:10.1175/2010JCLI3297.1, 2010.
5005 Berezovskaya, S., Yang, D. and Hinzman, L.: Long-term annual water balance analysis of
5006 the Lena River, Glob. Planet. Change, doi:10.1016/j.gloplacha.2004.12.006, 2005.
5007 Bergkvist, B. O. and Folkeson, L.: Soil acidification and element fluxes of a Fagus sylvatica
5008 forest as influenced by simulated nitrogen deposition, Water, Air, Soil Pollut.,
5009 doi:10.1007/BF00482753, 1992.
5010 Biastoch, A., Treude, T., Rpke, L. H., Riebesell, U., Roth, C., Burwicz, E. B., Park, W., Latif,
5011 M., Böning, C. W., Madec, G. and Wallmann, K.: Rising Arctic Ocean temperatures cause
5012 gas hydrate destabilization and ocean acidification, Geophys. Res. Lett.,
5013 doi:10.1029/2011GL047222, 2011.
5014 Bohn, T. J., Melton, J. R., Ito, A., Kleinen, T., Spahni, R., Stocker, B. D., Zhang, B., Zhu, X.,
5015 Schroeder, R., Glagolev, M. V., Maksyutov, S., Brovkin, V., Chen, G., Denisov, S. N., Eliseev,
5016 A. V., Gallego-Sala, A., McDonald, K. C., Rawlins, M. A., Riley, W. J., Subin, Z. M., Tian, H.,
5017 Zhuang, Q. and Kaplan, J. O.: WETCHIMP-WSL: Intercomparison of wetland methane
5018 emissions models over West Siberia, Biogeosciences, doi:10.5194/bg-12-3321-2015,
5019 2015.
5020 Bontemps, S., Defourny, P., Radoux, J., Van Bogaert, E., Lamarche, C., Achard, F., Mayaux,
5021 P., Boettcher, M., Brockmann, C., Kirches, G., Zülkhe, M., Kalogirou, V., Seifert, F. . and
5022 Arino, O.: Consistent global land cover maps for climate modelling communities: current
5023 achievements of the ESA' and cover CCI, in ESA Living Planet Symposium 2013., 2013.
5024 Borges, A. V., Darchambeau, F., Teodoru, C. R., Marwick, T. R., Tamooh, F., Geeraert, N.,
5025 Omengo, F. O., Guérin, F., Lambert, T., Morana, C., Okuku, E. and Bouillon, S.: Globally
5026 significant greenhouse-gas emissions from African inland waters, Nat. Geosci.,
5027 doi:10.1038/ngeo2486, 2015.
5028 Bowring, S. P. K., Lauerwald, R., Guenet, B., Zhu, D., Guimberteau, M., Tootchi, A.,
5029 Ducharne, A. and Ciais, P.: ORCHIDEE MICT-LEAK (r5459), a global model for the
5030 production, transport and transformation of dissolved organic carbon from Arctic
5031 permafrost regions, Part 1: Rationale, model description and simulation protocol,
5032 Geosci. Model Dev. Discuss., 1–29, doi:10.5194/gmd-2018-320, 2019a.
5033 Bowring, S. P. K., Lauerwald, R., Guenet, B., Zhu, D., Guimberteau, M., Regnier, P., Tootchi,
5034 A., Ducharne, A. and Ciais, P.: ORCHIDEE MICT-LEAK (r5459), a global model for the

5035 production, transport and transformation of dissolved organic carbon from Arctic
5036 permafrost regions, Part 2: Model evaluation over the Lena River basin, Geosci. Model
5037 Dev. Discuss., 1–45, doi:10.5194/gmd-2018-322, 2019b.
5038 Brantley, S. L., Megonigal, J. P., Scatena, F. N., Balogh-Brunstad, Z., Barnes, R. T., Bruns, M.
5039 A., Van Cappellen, P., Dontsova, K., Hartnett, H. E., Hartshorn, A. S., Heimsath, A.,
5040 Herndon, E., Jin, L., Keller, C. K., Leake, J. R., Mcdowell, W. H., Meinzer, F. C., Mozdzer, T. J.,
5041 Petsch, S., Pett-Ridge, J., Pregitzer, K. S., Raymond, P. A., Riebe, C. S., Shumaker, K., Sutton-
5042 Grier, A., Walter, R. and Yoo, K.: Twelve testable hypotheses on the geobiology of
5043 weathering, Geobiology, doi:10.1111/j.1472-4669.2010.00264.x, 2011.
5044 Bruhwiler, L., Dlugokencky, E., Masarie, K., Ishizawa, M., Andrews, A., Miller, J., Sweeney,
5045 C., Tans, P. and Worthy, D.: CarbonTracker-CH4: An assimilation system for estimating
5046 emissions of atmospheric methane, Atmos. Chem. Phys., doi:10.5194/acp-14-8269-
5047 2014, 2014.
5048 Calmels, D., Gaillardet, J. and François, L.: Sensitivity of carbonate weathering to soil
5049 CO2production by biological activity along a temperate climate transect, Chem. Geol.,
5050 doi:10.1016/j.chemgeo.2014.10.010, 2014.
5051 Camino-Serrano, M., Gielen, B., Luyssaert, S., Ciais, P., Vicca, S., Guenet, B., Vos, B. De,
5052 Cools, N., Ahrens, B., Altaf Arain, M., Borken, W., Clarke, N., Clarkson, B., Cummins, T.,
5053 Don, A., Pannatier, E. G., Laudon, H., Moore, T., Nieminen, T. M., Nilsson, M. B., Peichl, M.,
5054 Schwendenmann, L., Siemens, J. and Janssens, I.: Linking variability in soil solution
5055 dissolved organic carbon to climate, soil type, and vegetation type, Global Biogeochem.
5056 Cycles, doi:10.1002/2013GB004726, 2014.
5057 Camino-Serrano, M., Guenet, B., Luyssaert, S., Ciais, P., Bastrikov, V., De Vos, B., Gielen, B.,
5058 Gleixner, G., Jornet-Puig, A., Kaiser, K., Kothawala, D., Lauerwald, R., Peñuelas, J.,
5059 Schrumpf, M., Vicca, S., Vuichard, N., Walmsley, D. and Janssens, I. A.: ORCHIDEE-SOM:
5060 Modeling soil organic carbon (SOC) and dissolved organic carbon (DOC) dynamics along
5061 vertical soil profiles in Europe, Geosci. Model Dev., doi:10.5194/gmd-11-937-2018,
5062 2018.
5063 Campeau, A. and Del Giorgio, P. A.: Patterns in CH4 and CO2 concentrations across
5064 boreal rivers: Major drivers and implications for fluvial greenhouse emissions under
5065 climate change scenarios, Glob. Chang. Biol., doi:10.1111/gcb.12479, 2014.
5066 Campeau, A., Lapierre, J. F., Vachon, D. and Del Giorgio, P. A.: Regional contribution of
5067 CO2 and CH4 fluxes from the fluvial network in a lowland boreal landscape of Québec,
5068 Global Biogeochem. Cycles, doi:10.1002/2013GB004685, 2014.
5069 Catalán, N., Marcé, R., Kothawala, D. N. and Tranvik, L. J.: Organic carbon decomposition
5070 rates controlled by water retention time across inland waters, Nat. Geosci.,
5071 doi:10.1038/ngeo2720, 2016.
5072 Cauwet, G. and Sidorov, I.: The biogeochemistry of Lena River: Organic carbon and
5073 nutrients distribution, in Marine Chemistry., 1996.
5074 Clarke, N., Wu, Y. and Strand, L. T.: Dissolved organic carbon concentrations in four
5075 Norway spruce stands of different ages, Plant Soil, doi:10.1007/s11104-007-9384-4,
5076 2007.
5077 Cole, J. J., Prairie, Y. T., Caraco, N. F., McDowell, W. H., Tranvik, L. J., Striegl, R. G., Duarte,
5078 C. M., Kortelainen, P., Downing, J. A., Middelburg, J. J. and Melack, J.: Plumbing the global
5079 carbon cycle: Integrating inland waters into the terrestrial carbon budget, Ecosystems,
5080 doi:10.1007/s10021-006-9013-8, 2007.
5081 Connolly, C. T., Khosh, M. S., Burkart, G. A., Douglas, T. A., Holmes, R. M., Jacobson, A. D.,
5082 Tank, S. E. and McClelland, J. W.: Watershed slope as a predictor of fluvial dissolved

organic matter and nitrate concentrations across geographical space and catchment size in the Arctic, Environ. Res. Lett., 13(10), 104015, doi:10.1088/1748-9326/aae35d, 2018.
Cory, R. M., Ward, C. P., Crump, B. C. and Kling, G. W.: Sunlight controls water column processing of carbon in arctic fresh waters, Science (80-.)., doi:10.1126/science.1253119, 2014.
D'Orgeval, T., Polcher, J. and De Rosnay, P.: Sensitivity of the West African hydrological cycle in ORCHIDEE to infiltration processes, Hydrol. Earth Syst. Sci., doi:10.5194/hess-12-1387-2008, 2008.
DeLuca, T. H. and Boisvenue, C.: Boreal forest soil carbon: Distribution, function and modelling, Forestry, doi:10.1093/forestry/cps003, 2012.
Denfeld, B., Frey, K. and Sobczak, W.: Summer CO 2 evasion from streams and rivers in the Kolyma River basin, north-east Siberia, Polar …, doi:10.3402/polar.v32i0.19704, 2013.
Dery, S. J., Stadnyk, T. A., MacDonald, M. K. and Gauli-Sharma, B.: Recent trends and variability in river discharge across northern Canada, Hydrol. Earth Syst. Sci., doi:10.5194/hess-20-4801-2016, 2016.
Dessert, C., Dupré, B., Gaillardet, J., François, L. M. and Allègre, C. J.: Basalt weathering laws and the impact of basalt weathering on the global carbon cycle, Chem. Geol., doi:10.1016/j.chemgeo.2002.10.001, 2003.
Dolman, A. J., Shvidenko, A., Schepaschenko, D., Ciais, P., Tchebakova, N., Chen, T., Van Der Molen, M. K., Belelli Marchesini, L., Maximov, T. C., Maksyutov, S. and Schulze, E. D.: An estimate of the terrestrial carbon budget of Russia using inventory-based, eddy covariance and inversion methods, Biogeosciences, doi:10.5194/bg-9-5323-2012, 2012.
Drake, T. W., Wickland, K. P., Spencer, R. G. M., McKnight, D. M. and Striegl, R. G.: Ancient low–molecular-weight organic acids in permafrost fuel rapid carbon dioxide production upon thaw, Proc. Natl. Acad. Sci., doi:10.1073/pnas.1511705112, 2015.
Drake, T. W., Raymond, P. A. and Spencer, R. G. M.: Terrestrial carbon inputs to inland waters: A current synthesis of estimates and uncertainty, Limnol. Oceanogr. Lett., doi:10.1002/lol2.10055, 2017.
Drake, T. W., Tank, S. E., Zhulidov, A. V., Holmes, R. M., Gurtovaya, T. and Spencer, R. G. M.: Increasing Alkalinity Export from Large Russian Arctic Rivers, Environ. Sci. Technol., doi:10.1021/acs.est.8b01051, 2018.
Ducharne, A., Golaz, C., Leblois, E., Laval, K., Polcher, J., Ledoux, E. and De Marsily, G.: Development of a high resolution runoff routing model, calibration and application to assess runoff from the LMD GCM, J. Hydrol., doi:10.1016/S0022-1694(03)00230-0, 2003.
Eiriksdottir, E. S., Gislason, S. R. and Oelkers, E. H.: Does runoff or temperature control chemical weathering rates?, Appl. Geochemistry, doi:10.1016/j.apgeochem.2011.03.056, 2011.
Elberling, B.: Annual soil CO2effluxes in the High Arctic: The role of snow thickness and vegetation type, Soil Biol. Biochem., doi:10.1016/j.soilbio.2006.09.017, 2007.
Feely, R. A., Sabine, C. L., Lee, K., Berelson, W., Kleypas, J. A., Fabry, V. J. and Millero, F. J.: Impact of Anthropogenic CO_2 on the $CaCO_3$ System in the Oceans, Science (80-.)., doi:10.1126/science.1097329, 2004.
Feng, X., Vonk, J. E., van Dongen, B. E., Gustafsson, O., Semiletov, I. P., Dudarev, O. V., Wang, Z., Montlucon, D. B., Wacker, L. and Eglinton, T. I.: Differential mobilization of terrestrial carbon pools in Eurasian Arctic river basins, Proc. Natl. Acad. Sci., doi:10.1073/pnas.1307031110, 2013.

Feng, X., Vonk, J. E., Griffin, C., Zimov, N., Montluçon, D. B., Wacker, L. and Eglinton, T. I.: ^{14}C Variation of Dissolved Lignin in Arctic River Systems, ACS Earth Sp. Chem., doi:10.1021/acsearthspacechem.7b00055, 2017.
Findlay, H. S., Gibson, G., Kędra, M., Morata, N., Orchowska, M., Pavlov, A. K., Reigstad, M., Silyakova, A., Tremblay, J.-É., Walczowski, W., Weydmann, A. and Logvinova, C.: Responses in Arctic marine carbon cycle processes: conceptual scenarios and implications for ecosystem function, Polar Res., doi:10.3402/polar.v34.24252, 2015a.
Findlay, H. S., Gibson, G., Kedra, M., Morata, N., Orchowska, M., Pavlov, A. K., Reigstad, M., Silyakova, A., Tremblay, J. É., Walczowski, W., Weydmann, A. and Logvinova, C.: Responses in Arctic marine carbon cycle processes: Conceptual scenarios and implications for ecosystem function, Polar Res., doi:10.3402/polar.v34.24252, 2015b.
Fluet-Chouinard, E., Lehner, B., Rebelo, L. M., Papa, F. and Hamilton, S. K.: Development of a global inundation map at high spatial resolution from topographic downscaling of coarse-scale remote sensing data, Remote Sens. Environ., doi:10.1016/j.rse.2014.10.015, 2015.
Le Fouest, V., Matsuoka, A., Manizza, M., Shernetsky, M., Tremblay, B. and Babin, M.: Towards an assessment of riverine dissolved organic carbon in surface waters of the western Arctic Ocean based on remote sensing and biogeochemical modeling, Biogeosciences, doi:10.5194/bg-15-1335-2018, 2018.
Frey, K. E. and McClelland, J. W.: Impacts of permafrost degradation on arctic river biogeochemistry, Hydrol. Process., doi:10.1002/hyp.7196, 2009.
Frey, K. E. and Smith, L. C.: Amplified carbon release from vast West Siberian peatlands by 2100, Geophys. Res. Lett., doi:10.1029/2004GL022025, 2005.
Frieler, K., Lange, S., Piontek, F., Reyer, C. P. O., Schewe, J., Warszawski, L., Zhao, F., Chini, L., Denvil, S., Emanuel, K., Geiger, T., Halladay, K., Hurtt, G., Mengel, M., Murakami, D., Ostberg, S., Popp, A., Riva, R., Stevanovic, M., SuzGBRi, T., Volkholz, J., Burke, E., Ciais, P., Ebi, K., Eddy, T. D., Elliott, J., Galbraith, E., Gosling, S. N., Hattermann, F., Hickler, T., Hinkel, J., Hof, C., Huber, V., Jägermeyr, J., Krysanova, V., Marcé, R., Müller Schmied, H., Mouratiadou, I., Pierson, D., Tittensor, D. P., Vautard, R., Van Vliet, M., Biber, M. F., Betts, R. A., Leon Bodirsky, B., Deryng, D., Frolking, S., Jones, C. D., Lotze, H. K., Lotze-Campen, H., Sahajpal, R., Thonicke, K., Tian, H. and Yamagata, Y.: Assessing the impacts of 1.5ĝ€°C global warming - Simulation protocol of the Inter-Sectoral Impact Model Intercomparison Project (ISIMIP2b), Geosci. Model Dev., doi:10.5194/gmd-10-4321-2017, 2017.
Fritz, M., Vonk, J. E. and Lantuit, H.: Collapsing Arctic coastlines, Nat. Clim. Chang., doi:10.1038/nclimate3188, 2017.
Fröberg, M., Berggren, D., Bergkvist, B., Bryant, C. and Mulder, J.: Concentration and fluxes of dissolved organic carbon (DOC) in three Norway spruce stands along a climatic gradient in Sweden, Biogeochemistry, doi:10.1007/s10533-004-0564-5, 2006.
Gaillardet, J., Dupré, B., Louvat, P. and Allègre, C. J.: Global silicate weathering and CO2consumption rates deduced from the chemistry of large rivers, Chem. Geol., doi:10.1016/S0009-2541(99)00031-5, 1999.
Gislason, S. R., Oelkers, E. H., Eiriksdottir, E. S., Kardjilov, M. I., Gisladottir, G., Sigfusson, B., Snorrason, A., Elefsen, S., Hardardottir, J., Torssander, P. and Oskarsson, N.: Direct evidence of the feedback between climate and weathering, Earth Planet. Sci. Lett., doi:10.1016/j.epsl.2008.10.018, 2009.
Gouttevin, I., Menegoz, M., Dominé, F., Krinner, G., Koven, C., Ciais, P., Tarnocai, C. and Boike, J.: How the insulating properties of snow affect soil carbon distribution in the

continental pan-Arctic area, J. Geophys. Res. Biogeosciences, doi:10.1029/2011JG001916, 2012.
Graham, D. E., Wallenstein, M. D., Vishnivetskaya, T. A., Waldrop, M. P., Phelps, T. J., Pfiffner, S. M., Onstott, T. C., Whyte, L. G., Rivkina, E. M., Gilichinsky, D. A., Elias, D. A., MacKelprang, R., Verberkmoes, N. C., Hettich, R. L., Wagner, D., Wullschleger, S. D. and Jansson, J. K.: Microbes in thawing permafrost: The unknown variable in the climate change equation, ISME J., doi:10.1038/ismej.2011.163, 2012.
Guenet, B., Danger, M., Abbadie, L. and Lacroix, G.: Priming effect: Bridging the gap between terrestrial and aquatic ecology, Ecology, doi:10.1890/09-1968.1, 2010.
Guenet, B., Moyano, F. E., Peylin, P., Ciais, P. and Janssens, I. A.: Towards a representation of priming on soil carbon decomposition in the global land biosphere model ORCHIDEE (version 1.9.5.2), Geosci. Model Dev., doi:10.5194/gmd-9-841-2016, 2016.
Guenet, B., Camino-Serrano, M., Ciais, P., Tifafi, M., Maignan, F., Soong, J. L. and Janssens, I. A.: Impact of priming on global soil carbon stocks, Glob. Chang. Biol., doi:10.1111/gcb.14069, 2018.
Guimberteau, M., Drapeau, G., Ronchail, J., Sultan, B., Polcher, J., Martinez, J. M., Prigent, C., Guyot, J. L., Cochonneau, G., Espinoza, J. C., Filizola, N., Fraizy, P., Lavado, W., De Oliveira, E., Pombosa, R., Noriega, L. and Vauchel, P.: Discharge simulation in the sub-basins of the Amazon using ORCHIDEE forced by new datasets, Hydrol. Earth Syst. Sci., doi:10.5194/hess-16-911-2012, 2012.
Guimberteau, M., Zhu, D., Maignan, F., Huang, Y., Yue, C., Dantec-N d lec, S., Ottl, C., Jornet-Puig, A., Bastos, A., Laurent, P., Goll, D., Bowring, S., Chang, J., Guenet, B., Tifafi, M., Peng, S., Krinner, G., Ducharne, A. s., Wang, F., Wang, T., Wang, X., Wang, Y., Yin, Z., Lauerwald, R., Joetzjer, E., Qiu, C., Kim, H. and Ciais, P.: ORCHIDEE-MICT (v8.4.1), a land surface model for the high latitudes: model description and validation, Geosci. Model Dev., doi:10.5194/gmd-11-121-2018, 2018.
Hartmann, J. and Moosdorf, N.: The new global lithological map database GLiM: A representation of rock properties at the Earth surface, Geochemistry, Geophys. Geosystems, doi:10.1029/2012GC004370, 2012.
Hartmann, J., Moosdorf, N., Lauerwald, R., Hinderer, M. and West, A. J.: Global chemical weathering and associated p-release - the role of lithology, temperature and soil properties, Chem. Geol., doi:10.1016/j.chemgeo.2013.10.025, 2014.
Heim, B., Abramova, E., Doerffer, R., Günther, F., Hölemann, J., Kraberg, A., Lantuit, H., Loginova, A., Martynov, F., Overduin, P. P. and Wegner, C.: Ocean colour remote sensing in the southern laptev sea: Evaluation and applications, Biogeosciences, doi:10.5194/bg-11-4191-2014, 2014.
Holgerson, M. A. and Raymond, P. A.: Large contribution to inland water CO2and CH4emissions from very small ponds, Nat. Geosci., doi:10.1038/ngeo2654, 2016.
Hollesen, J., Matthiesen, H., Møller, A. B. and Elberling, B.: Permafrost thawing in organic Arctic soils accelerated by ground heat production, Nat. Clim. Chang., doi:10.1038/nclimate2590, 2015.
Holmes, R.M., Shiklomanov, A. I., Tank, S. E., McClelland, J. W., Tretiakov, M.: Arctic Report Card 2016 Arctic Report Card 2016. https://arctic.noaa.gov/Report-Card/Report-Card-2015/ArtMID/5037/ArticleID/227/River-Discharge, Arct. Rep. Card -River Disch., 2015.
Holmes, R. M., McClelland, J. W., Peterson, B. J., Tank, S. E., Bulygina, E., Eglinton, T. I., Gordeev, V. V., Gurtovaya, T. Y., Raymond, P. A., Repeta, D. J., Staples, R., Striegl, R. G., Zhulidov, A. V. and Zimov, S. A.: Seasonal and Annual Fluxes of Nutrients and Organic

Matter from Large Rivers to the Arctic Ocean and Surrounding Seas, Estuaries and Coasts, doi:10.1007/s12237-011-9386-6, 2012.
Hugelius, G., Bockheim, J. G., Camill, P., Elberling, B., Grosse, G., Harden, J. W., Johnson, K., Jorgenson, T., Koven, C. D., Kuhry, P., Michaelson, G., Mishra, U., Palmtag, J., Ping, C.-L., O'Donnell, J., Schirrmeister, L., Schuur, E. A. G., Sheng, Y., Smith, L. C., Strauss, J. and Yu, Z.: A new data set for estimating organic carbon storage to 3m depth in soils of the northern circumpolar permafrost region, EARTH Syst. Sci. DATA, doi:10.5194/essd-5-393-2013, 2013.
Hugelius, G., Strauss, J., Zubrzycki, S., Harden, J. W., Schuur, E. A. G., Ping, C. L., Schirrmeister, L., Grosse, G., Michaelson, G. J., Koven, C. D., O'Donnell, J. A., Elberling, B., Mishra, U., Camill, P., Yu, Z., Palmtag, J. and Kuhry, P.: Estimated stocks of circumpolar permafrost carbon with quantified uncertainty ranges and identified data gaps, Biogeosciences, doi:10.5194/bg-11-6573-2014, 2014.
Jakobsson, M.: Hypsometry and volume of the Arctic Ocean and its constituent seas, Geochemistry, Geophys. Geosystems, doi:10.1029/2001GC000302, 2002.
Janout, M., HÃ¶lemann, J., Juhls, B., Krumpen, T., Rabe, B., Bauch, D., Wegner, C., Kassens, H. and Timokhov, L.: Episodic warming of near-bottom waters under the Arctic sea ice on the central Laptev Sea shelf, Geophys. Res. Lett., doi:10.1002/2015GL066565, 2016.
Jasechko, S., Kirchner, J. W., Welker, J. M. and McDonnell, J. J.: Substantial proportion of global streamflow less than three months old, Nat. Geosci., doi:10.1038/ngeo2636, 2016.
Kaiser, K. and Kalbitz, K.: Cycling downwards - dissolved organic matter in soils, Soil Biol. Biochem., doi:10.1016/j.soilbio.2012.04.002, 2012.
Kanevskiy, M., Shur, Y., Fortier, D., Jorgenson, M. T. and Stephani, E.: Cryostratigraphy of late Pleistocene syngenetic permafrost (yedoma) in northern Alaska, Itkillik River exposure, Quat. Res., doi:10.1016/j.yqres.2010.12.003, 2011.
Kaushal, S. S., Likens, G. E., Pace, M. L., Utz, R. M., Haq, S., Gorman, J. and Grese, M.: Freshwater salinization syndrome on a continental scale, Proc. Natl. Acad. Sci., doi:10.1073/pnas.1711234115, 2018.
Keuper, F., van Bodegom, P. M., Dorrepaal, E., Weedon, J. T., van Hal, J., van Logtestijn, R. S. P. and Aerts, R.: A frozen feast: Thawing permafrost increases plant-available nitrogen in subarctic peatlands, Glob. Chang. Biol., doi:10.1111/j.1365-2486.2012.02663.x, 2012.
Kicklighter, D. W., Hayes, D. J., Mcclelland, J. W., Peterson, B. J., Mcguire, A. D. and Melillo, J. M.: Insights and issues with simulating terrestrial DOC loading of Arctic river networks, Ecol. Appl., doi:10.1890/11-1050.1, 2013.
Klaminder, J., Grip, H., Mörth, C. M. and Laudon, H.: Carbon mineralization and pyrite oxidation in groundwater: Importance for silicate weathering in boreal forest soils and stream base-flow chemistry, Appl. Geochemistry, doi:10.1016/j.apgeochem.2010.12.005, 2011.
Koven, C., Friedlingstein, P., Ciais, P., Khvorostyanov, D., Krinner, G. and Tarnocai, C.: On the formation of high-latitude soil carbon stocks: Effects of cryoturbation and insulation by organic matter in a land surface model, Geophys. Res. Lett., doi:10.1029/2009GL040150, 2009.
Koven, C. D., Riley, W. J. and Stern, A.: Analysis of permafrost thermal dynamics and response to climate change in the CMIP5 earth system models, J. Clim., doi:10.1175/JCLI-D-12-00228.1, 2013a.
Koven, C. D., Riley, W. J., Subin, Z. M., Tang, J. Y., Torn, M. S., Collins, W. D., Bonan, G. B., Lawrence, D. M. and Swenson, S. C.: The effect of vertically resolved soil biogeochemistry and alternate soil C and N models on C dynamics of CLM4, Biogeosciences,

doi:10.5194/bg-10-7109-2013, 2013b.
Koven, C. D., Lawrence, D. M. and Riley, W. J.: Permafrost carbon–climate feedback is sensitive to deep soil carbon decomposability but not deep soil nitrogen dynamics, Proc. Natl. Acad. Sci., doi:10.1073/pnas.1415123112, 2015.
Krinner, G., Viovy, N., de Noblet-Ducoudré, N., Ogée, J., Polcher, J., Friedlingstein, P., Ciais, P., Sitch, S. and Prentice, I. C.: A dynamic global vegetation model for studies of the coupled atmosphere-biosphere system, Global Biogeochem. Cycles, doi:10.1029/2003GB002199, 2005.
Kump, L.R., Kasting, J.F., Crane, R. G.: Kump, L.R., Kasting, J.F. and Crane, R.G., 2004. The Earth System 3rd edition (Vol. 432). Upper Saddle River, NJ: Pearson Prentice Hall., , doi:10.1017/s0016756800243823, 2010.
Kunkel, K. E., Robinson, D. A., Champion, S., Yin, X., Estilow, T. and Frankson, R. M.: Trends and Extremes in Northern Hemisphere Snow Characteristics, Curr. Clim. Chang. Reports, doi:10.1007/s40641-016-0036-8, 2016.
Kutscher, L., Mörth, C. M., Porcelli, D., Hirst, C., Maximov, T. C., Petrov, R. E. and Andersson, P. S.: Spatial variation in concentration and sources of organic carbon in the Lena River, Siberia, J. Geophys. Res. Biogeosciences, doi:10.1002/2017JG003858, 2017.
Kuzyakov, Y.: Sources of CO2 efflux from soil and review of partitioning methods, Soil Biol. Biochem., doi:10.1016/j.soilbio.2005.08.020, 2006.
Lammers, R. B., Shiklomanov, A. I., Vörösmarty, C. J., Fekete, B. M. and Peterson, B. J.: Assessment of contemporary Arctic river runoff based on observational discharge records, J. Geophys. Res. Atmos., doi:10.1029/2000JD900444, 2001.
Lammers, R. B., Pundsack, J. W. and Shiklomanov, A. I.: Variability in river temperature, discharge, and energy flux from the Russian pan-Arctic landmass, J. Geophys. Res. Biogeosciences, doi:10.1029/2006JG000370, 2007.
Lange, S.: EartH2Observe, WFDEI and ERA-Interim data Merged and Bias-corrected for ISIMIP (EWEMBI), GFZ Data Serv., doi:10.5880/pik.2016.004, 2016.
Lange, S.: Bias correction of surface downwelling longwave and shortwave radiation for the EWEMBI dataset, Earth Syst. Dyn., doi:10.5194/esd-9-627-2018, 2018.
Lara, R. J., Rachold, V., Kattner, G., Hubberten, H. W., Guggenberger, G., Skoog, A. and Thomas, D. N.: Dissolved organic matter and nutrients in the Lena River, Siberian Arctic: Characteristics and distribution, Mar. Chem., doi:10.1016/S0304-4203(97)00076-5, 1998.
Laudon, H., Buttle, J., Carey, S. K., McDonnell, J., McGuire, K., Seibert, J., Shanley, J., Soulsby, C. and Tetzlaff, D.: Cross-regional prediction of long-term trajectory of stream water DOC response to climate change, Geophys. Res. Lett., doi:10.1029/2012GL053033, 2012.
Lauerwald, R., Hartmann, J., Ludwig, W. and Moosdorf, N.: Assessing the nonconservative fluvial fluxes of dissolved organic carbon in North America, J. Geophys. Res. Biogeosciences, doi:10.1029/2011JG001820, 2012.
Lauerwald, R., Laruelle, G. G., Hartmann, J., Ciais, P. and Regnier, P. A. G.: Spatial patterns in CO2evasion from the global river network, Global Biogeochem. Cycles, doi:10.1002/2014GB004941, 2015.
Lauerwald, R., Regnier, P., Camino-Serrano, M., Guenet, B., Guimberteau, M., Ducharne, A., Polcher, J. and Ciais, P.: ORCHILEAK (revision 3875): A new model branch to simulate carbon transfers along the terrestrial-aquatic continuum of the Amazon basin, Geosci. Model Dev., doi:10.5194/gmd-10-3821-2017, 2017.
Lee, H., Swenson, S. C., Slater, A. G. and Lawrence, D. M.: Effects of excess ground ice on

projections of permafrost in a warming climate, Environ. Res. Lett., doi:10.1088/1748-9326/9/12/124006, 2014.
Lindroos, A. J., Derome, J., Derome, K. and Smolander, A.: The effect of scots pine, norway spruce and silver birch on the chemical composition of stand throughfall and upper soil percolation water in northern Finland, Boreal Environ. Res., 2011.
Lloyd, J., Shibistova, O., Zolotoukhine, D., Kolle, O., Arneth, A., Wirth, C., Styles, J. M., Tchebakova, N. M. and Schulze, E. D.: Seasonal and annual variations in the photosynthetic productivity and carbon balance of a central Siberian pine forest, Tellus, Ser. B Chem. Phys. Meteorol., doi:10.1034/j.1600-0889.2002.01487.x, 2002.
MacKelprang, R., Waldrop, M. P., Deangelis, K. M., David, M. M., Chavarria, K. L., Blazewicz, S. J., Rubin, E. M. and Jansson, J. K.: Metagenomic analysis of a permafrost microbial community reveals a rapid response to thaw, Nature, doi:10.1038/nature10576, 2011.
Maher, K.: The dependence of chemical weathering rates on fluid residence time, Earth Planet. Sci. Lett., doi:10.1016/j.epsl.2010.03.010, 2010.
Maher, K. and Chamberlain, C. P.: Hydrologic regulation of chemical weathering and the geologic, Science (80-.)., doi:10.1126/science.1250770, 2014.
Manizza, M., Follows, M. J., Dutkiewicz, S., Menemenlis, D., McClelland, J. W., Hill, C. N., Peterson, B. J. and Key, R. M.: A model of the Arctic Ocean carbon cycle, J. Geophys. Res. Ocean., doi:10.1029/2011JC006998, 2011.
Mann, P. J., Eglinton, T. I., McIntyre, C. P., Zimov, N., Davydova, A., Vonk, J. E., Holmes, R. M. and Spencer, R. G. M.: Utilization of ancient permafrost carbon in headwaters of Arctic fluvial networks, Nat. Commun., doi:10.1038/ncomms8856, 2015.
Manning, R.: On the Flow of Water in Open Channels and Pipes, Trans. Inst. Civ. Eng. Irel., doi:10.1021/bi2010619, 1891.
Manzoni, S., Taylor, P., Richter, A., Porporato, A. and Ågren, G. I.: Environmental and stoichiometric controls on microbial carbon-use efficiency in soils, New Phytol., doi:10.1111/j.1469-8137.2012.04225.x, 2012.
McClelland, J. W., Holmes, R. M., Peterson, B. J. and Stieglitz, M.: Increasing river discharge in the Eurasian Arctic: Consideration of dams, permafrost thaw, and fires as potential agents of change, J. Geophys. Res. Atmos., doi:10.1029/2004JD004583, 2004.
McClelland, J. W., Holmes, R. M., Peterson, B. J., Amon, R., Brabets, T., Cooper, L., Gibson, J., Gordeev, V. V., Guay, C., Milburn, D., Staples, R., Raymond, P. A., Shiklomanov, I., Striegl, R., Zhulidov, A., Gurtovaya, T. and Zimov, S.: Development of Pan-Arctic database for river chemistry, Eos (Washington. DC)., doi:10.1029/2008EO240001, 2008.
McClelland, J. W., Holmes, R. M., Dunton, K. H. and Macdonald, R. W.: The Arctic Ocean Estuary, Estuaries and Coasts, doi:10.1007/s12237-010-9357-3, 2012.
McClelland, J. W., Holmes, R. M., Peterson, B. J., Raymond, P. A., Striegl, R. G., Zhulidov, A. V., Zimov, S. A., Zimov, N., Tank, S. E., Spencer, R. G. M., Staples, R., Gurtovaya, T. Y. and Griffin, C. G.: Particulate organic carbon and nitrogen export from major Arctic rivers, Global Biogeochem. Cycles, doi:10.1002/2015GB005351, 2016.
Mcguire, A. D., Anderson, L. G., Christensen, T. R., Scott, D., Laodong, G., Hayes, D. J., Martin, H., Lorenson, T. D., Macdonald, R. W. and Nigel, R.: Sensitivity of the carbon cycle in the Arctic to climate change, Ecol. Monogr., doi:10.1890/08-2025.1, 2009.
McGuire, A. D., Anderson, L. G., Christensen, T. R., Dallimore, S., Guo, L., Hayes, D. J., Heimann, M., Lorenson, T. D., Macdonald, R. W. and Roulet, N.: Sensitivity of the carbon cycle in the Arctic to climate change, Ecol. Monogr., doi:10.1890/08-2025.1, 2009.
McGuire, A. D., Christensen, T. R., Hayes, D., Heroult, A., Euskirchen, E., Kimball, J. S.,

5371 Koven, C., Lafleur, P., Miller, P. A., Oechel, W., Peylin, P., Williams, M. and Yi, Y.: An
5372 assessment of the carbon balance of Arctic tundra: Comparisons among observations,
5373 process models, and atmospheric inversions, Biogeosciences, doi:10.5194/bg-9-3185-
5374 2012, 2012.
5375 McGuire, K. J., McDonnell, J. J., Weiler, M., Kendall, C., McGlynn, B. L., Welker, J. M. and
5376 Seibert, J.: The role of topography on catchment-scale water residence time, Water
5377 Resour. Res., doi:10.1029/2004WR003657, 2005.
5378 Messager, M. L., Lehner, B., Grill, G., Nedeva, I. and Schmitt, O.: Estimating the volume and
5379 age of water stored in global lakes using a geo-statistical approach, Nat. Commun.,
5380 doi:10.1038/ncomms13603, 2016.
5381 Millot, R., Gaillardet, J., Dupré, B. and Allégre, C. J.: Northern latitude chemical weathering
5382 rates: Clues from the Mackenzie River Basin, Canada, Geochim. Cosmochim. Acta,
5383 doi:10.1016/S0016-7037(02)01207-3, 2003.
5384 Moosdorf, N., Hartmann, J., Lauerwald, R., Hagedorn, B. and Kempe, S.: Atmospheric CO2
5385 consumption by chemical weathering in North America, Geochim. Cosmochim. Acta,
5386 doi:10.1016/j.gca.2011.10.007, 2011.
5387 Mudryk, L. R., Derksen, C., Kushner, P. J. and Brown, R.: Characterization of Northern
5388 Hemisphere snow water equivalent datasets, 1981-2010, J. Clim., doi:10.1175/JCLI-D-
5389 15-0229.1, 2015.
5390 Mulholland, P. J.: Dissolved Organic Matter Concentration and Flux in Streams, JJournal
5391 North Am. Benthol. Soc. 16, no. 1 (Mar., 1997) 131-141.ournal North Am. Benthol. Soc.,
5392 16(1), 131–141., doi:10.2307/1468246, 1997.
5393 Myers-Pigg, A. N., Louchouarn, P., Amon, R. M. W., Prokushkin, A., Pierce, K. and Rubtsov,
5394 A.: Labile pyrogenic dissolved organic carbon in major Siberian Arctic rivers:
5395 Implications for wildfire-stream metabolic linkages, Geophys. Res. Lett.,
5396 doi:10.1002/2014GL062762, 2015.
5397 Nachtergaele, F. et al.: The harmonized world soil database, FAO, ISRIC,ISSCAS, JRC,
5398 doi:3123, 2010.
5399 Naipal, V., Ciais, P., Wang, Y., Lauerwald, R., Guenet, B. and Van Oost, K.: Global soil
5400 organic carbon removal by water erosion under climate change and land use change
5401 during AD-1850-2005, Biogeosciences, doi:10.5194/bg-15-4459-2018, 2018.
5402 Ngo-Duc, T., Laval, K., Ramillien, G., Polcher, J. and Cazenave, A.: Validation of the land
5403 water storage simulated by Organising Carbon and Hydrology in Dynamic Ecosystems
5404 (ORCHIDEE) with Gravity Recovery and Climate Experiment (GRACE) data, Water
5405 Resour. Res., doi:10.1029/2006WR004941, 2007.
5406 Nicolsky, D. J., Romanovsky, V. E., Romanovskii, N. N., Kholodov, A. L., Shakhova, N. E. and
5407 Semiletov, I. P.: Modeling sub-sea permafrost in the East Siberian Arctic Shelf: The
5408 Laptev Sea region, J. Geophys. Res. Earth Surf., doi:10.1029/2012JF002358, 2012.
5409 O'Donnell, J. A., Aiken, G. R., Swanson, D. K., Panda, S., Butler, K. D. and Baltensperger, A.
5410 P.: Dissolved organic matter composition of Arctic rivers: Linking permafrost and parent
5411 material to riverine carbon, Global Biogeochem. Cycles, doi:10.1002/2016GB005482,
5412 2016.
5413 Oki, T., Nishimura, T. and Dirmeyer, P. A.: Assessment of annual runoff from land surface
5414 models using Total Runoff Integrating Pathways (TRIP), J. Meteorol. Soc. Japan, 1999.
5415 Overduin, P. P., Liebner, S., Knoblauch, C., Günther, F., Wetterich, S., Schirrmeister, L.,
5416 Hubberten, H. W. and Grigoriev, M. N.: Methane oxidation following submarine
5417 permafrost degradation: Measurements from a central Laptev Sea shelf borehole, J.
5418 Geophys. Res. Biogeosciences, doi:10.1002/2014JG002862, 2015.

Pekel, J.-F., Cottam, A., Gorelick, N. and Belward, A. S.: Global Surface Water - Data Users Guide (JRC) High-resolution mapping of global surface water and its long-term changes, Nature, doi:10.1038/nature20584, 2016.
Peterson, B. J., Holmes, R. M., McClelland, J. W., Vörösmarty, C. J., Lammers, R. B., Shiklomanov, A. I., Shiklomanov, I. A. and Rahmstorf, S.: Increasing river discharge to the Arctic Ocean, Science (80-.)., doi:10.1126/science.1077445, 2002.
Ponomarev, E. I., Kharuk, V. I. and Ranson, K. J.: Wildfires dynamics in Siberian larch forests, Forests, doi:10.3390/f7060125, 2016.
Prigent, C., Papa, F., Aires, F., Rossow, W. B. and Matthews, E.: Global inundation dynamics inferred from multiple satellite observations, 1993-2000, J. Geophys. Res. Atmos., doi:10.1029/2006JD007847, 2007.
Qiu, C., Zhu, D., Ciais, P., Guenet, B., Krinner, G., Peng, S., Aurela, M., Bernhofer, C., Brümmer, C., Bret-Harte, S., Chu, H., Chen, J., Desai, A. R., Dušek, J., Euskirchen, E. S., Fortuniak, K., Flanagan, L. B., Friborg, T., Grygoruk, M., Gogo, S., Grünwald, T., Hansen, B. U., Holl, D., Humphreys, E., Hurkuck, M., Kiely, G., Klatt, J., Kutzbach, L., Largeron, C., Laggoun-Défarge, F., Lund, M., Lafleur, P. M., Li, X., Mammarella, I., Merbold, L., Nilsson, M. B., Olejnik, J., Ottosson-Löfvenius, M., Oechel, W., Parmentier, F. J. W., Peichl, M., Pirk, N., Peltola, O., Pawlak, W., Rasse, D., Rinne, J., Shaver, G., Peter Schmid, H., Sottocornola, M., Steinbrecher, R., Sachs, T., Urbaniak, M., Zona, D. and Ziemblinska, K.: ORCHIDEE-PEAT (revision 4596), a model for northern peatland CO2, water, and energy fluxes on daily to annual scales, Geosci. Model Dev., doi:10.5194/gmd-11-497-2018, 2018.
Raymond, P. A.: Temperature versus hydrologic controls of chemical weathering fluxes from United States forests, Chem. Geol., doi:10.1016/j.chemgeo.2017.02.025, 2017.
Raymond, P. A. and Hamilton, S. K.: Anthropogenic influences on riverine fluxes of dissolved inorganic carbon to the oceans, Limnol. Oceanogr. Lett., doi:10.1002/lol2.10069, 2018.
Raymond, P. A., McClelland, J. W., Holmes, R. M., Zhulidov, A. V., Mull, K., Peterson, B. J., Striegl, R. G., Aiken, G. R. and Gurtovaya, T. Y.: Flux and age of dissolved organic carbon exported to the Arctic Ocean: A carbon isotopic study of the five largest arctic rivers, Global Biogeochem. Cycles, doi:10.1029/2007GB002934, 2007.
Raymond, P. A., Oh, N. H., Turner, R. E. and Broussard, W.: Anthropogenically enhanced fluxes of water and carbon from the Mississippi River, Nature, doi:10.1038/nature06505, 2008.
Raymond, P. A., Hartmann, J., Lauerwald, R., Sobek, S., McDonald, C., Hoover, M., Butman, D., Striegl, R., Mayorga, E., Humborg, C., Kortelainen, P., Dürr, H., Meybeck, M., Ciais, P. and Guth, P.: Global carbon dioxide emissions from inland waters, Nature, doi:10.1038/nature12760, 2013.
Regnier, P., Friedlingstein, P., Ciais, P., Mackenzie, F. T., Gruber, N., Janssens, I. A., Laruelle, G. G., Lauerwald, R., Luyssaert, S., Andersson, A. J., Arndt, S., Arnosti, C., Borges, A. V., Dale, A. W., Gallego-Sala, A., Goddéris, Y., Goossens, N., Hartmann, J., Heinze, C., Ilyina, T., Joos, F., Larowe, D. E., Leifeld, J., Meysman, F. J. R., Munhoven, G., Raymond, P. A., Spahni, R., Suntharalingam, P. and Thullner, M.: Anthropogenic perturbation of the carbon fluxes from land to ocean, Nat. Geosci., doi:10.1038/ngeo1830, 2013.
Reynolds, C. A., Jackson, T. J. and Rawls, W. J.: Estimating soil water-holding capacities by linking the Food and Agriculture Organization soil map of the world with global pedon databases and continuous pedotransfer functions, Water Resour. Res., doi:10.1029/2000WR900130, 2000.
Rhein, M., Rintoul, S., Aoki, S., Campos, E., Chambers, D., Feely, R. A., Gulev, S., Johnson, G.,

5467 Josey, S., Kostianoy, A., Mauritzen, C., Roemmich, D., Talley, L., Wang, F. and IPCC:
5468 Observations: Ocean. In: Climate Change 2013: The Physical Science Basis. Contribution
5469 of Working Group I to the Fifth Assessment Report of the Intergovernmental Panel on
5470 Climate Change., 2013.
5471 Rosenqvist, L., Hansen, K., Vesterdal, L. and van der Salm, C.: Water balance in
5472 afforestation chronosequences of common oak and Norway spruce on former arable
5473 land in Denmark and southern Sweden, Agric. For. Meteorol.,
5474 doi:10.1016/j.agrformet.2009.10.004, 2010.
5475 Roser, C., Montagnani, L., Schulze, E.-D., Mollicone, D., Kolle, O., Meroni, M., Papale, D.,
5476 Marchesini, L. B., Federici, S. and Valentini, R.: Net CO2 exchange rates in three different
5477 successional stages of the "Dark Taiga" of central Siberia, Tellus B, doi:10.1034/j.1600-
5478 0889.2002.01351.x, 2002.
5479 Sapart, C. J., Shakhova, N., Semiletov, I., Jansen, J., Szidat, S., Kosmach, D., Dudarev, O., Van
5480 Der Veen, C., Egger, M., Sergienko, V., Salyuk, A., Tumskoy, V., Tison, J. L. and Röckmann,
5481 T.: The origin of methane in the East Siberian Arctic Shelf unraveled with triple isotope
5482 analysis, Biogeosciences, doi:10.5194/bg-14-2283-2017, 2017.
5483 Sawakuchi, H. O., Neu, V., Ward, N. D., Barros, M. de L. C., Valerio, A. M., Gagne-Maynard,
5484 W., Cunha, A. C., Less, D. F. S., Diniz, J. E. M., Brito, D. C., Krusche, A. V and Richey, J. E.:
5485 Carbon Dioxide Emissions along the Lower Amazon River, Front. Mar. Sci.,
5486 doi:10.3389/fmars.2017.00076, 2017.
5487 Sawamoto, T., Hatano, R., Yajima, T., Takahashi, K. and Isaev, A. P.: Soil respiration in
5488 siberian taiga ecosystems with different histories of forest fire, Soil Sci. Plant Nutr.,
5489 doi:10.1080/00380768.2000.10408759, 2000.
5490 Schädel, C., Schuur, E. A. G., Bracho, R., Elberling, B., Knoblauch, C., Lee, H., Luo, Y., Shaver,
5491 G. R. and Turetsky, M. R.: Circumpolar assessment of permafrost C quality and its
5492 vulnerability over time using long-term incubation data, Glob. Chang. Biol.,
5493 doi:10.1111/gcb.12417, 2014.
5494 Schlesinger, W. H. and Melack, J. M.: Transport of organic carbon in the world's rivers,
5495 Tellus, doi:10.3402/tellusa.v33i2.10706, 1981.
5496 Schulze, E. D., Lloyd, J., Kelliher, F. M., Wirth, C., Rebmann, C., Luhker, B., Mund, M., Knohl,
5497 A., Milyukova, I. M., Schulze, W., Ziegler, W., Varlagin, A. B., Sogachev, A. F., Valentini, R.,
5498 Dore, S., Grigoriev, S., Kolle, O., Panfyorov, M. I., Tchebakova, N. and Vygodskaya, N. N.:
5499 Productivity of forests in the eurosiberian boreal region and their potential to act as a
5500 carbon sink - a synthesis, Glob. Chang. Biol., doi:10.1046/j.1365-2486.1999.00266.x,
5501 1999.
5502 Schuur, E. A. G., Vogel, J. G., Crummer, K. G., Lee, H., Sickman, J. O. and Osterkamp, T. E.:
5503 The effect of permafrost thaw on old carbon release and net carbon exchange from
5504 tundra, Nature, doi:10.1038/nature08031, 2009.
5505 Schuur, E. A. G., McGuire, A. D., Schädel, C., Grosse, G., Harden, J. W., Hayes, D. J., Hugelius,
5506 G., Koven, C. D., Kuhry, P., Lawrence, D. M., Natali, S. M., Olefeldt, D., Romanovsky, V. E.,
5507 Schaefer, K., Turetsky, M. R., Treat, C. C. and Vonk, J. E.: Climate change and the
5508 permafrost carbon feedback, Nature, doi:10.1038/nature14338, 2015.
5509 Selvam, B. P., Lapierre, J. F., Guillemette, F., Voigt, C., Lamprecht, R. E., Biasi, C.,
5510 Christensen, T. R., Martikainen, P. J. and Berggren, M.: Degradation potentials of
5511 dissolved organic carbon (DOC) from thawed permafrost peat, Sci. Rep.,
5512 doi:10.1038/srep45811, 2017.
5513 Semiletov, I., Pipko, I., Gustafsson, Ö., Anderson, L. G., Sergienko, V., Pugach, S., Dudarev,
5514 O., Charkin, A., Gukov, A., Bröder, L., Andersson, A., Spivak, E. and Shakhova, N.:

5515 Acidification of East Siberian Arctic Shelf waters through addition of freshwater and
5516 terrestrial carbon, Nat. Geosci., doi:10.3233/978-1-61499-868-6-158, 2016.
5517 Semiletov, I. P., Pipko, I. I., Repina, I. and Shakhova, N. E.: Carbonate chemistry dynamics
5518 and carbon dioxide fluxes across the atmosphere-ice-water interfaces in the Arctic
5519 Ocean: Pacific sector of the Arctic, J. Mar. Syst., doi:10.1016/j.jmarsys.2006.05.012,
5520 2007.
5521 Semiletov, I. P., Pipko, I. I., Shakhova, N. E., Dudarev, O. V., Pugach, S. P., Charkin, A. N.,
5522 Mcroy, C. P., Kosmach, D. and Gustafsson, Ö.: Carbon transport by the Lena River from its
5523 headwaters to the Arctic Ocean, with emphasis on fluvial input of terrestrial particulate
5524 organic carbon vs. carbon transport by coastal erosion, Biogeosciences, doi:10.5194/bg-
5525 8-2407-2011, 2011.
5526 Semiletov, I. P., Shakhova, N. E., Sergienko, V. I., Pipko, I. I. and Dudarev, O. V.: On carbon
5527 transport and fate in the East Siberian Arctic land-shelf-atmosphere system, Environ.
5528 Res. Lett., doi:10.1088/1748-9326/7/1/015201, 2012.
5529 Serreze, M. C. and Barry, R. G.: Processes and impacts of Arctic amplification: A research
5530 synthesis, Glob. Planet. Change, doi:10.1016/j.gloplacha.2011.03.004, 2011.
5531 Shakhova, N. and Semiletov, I.: Methane release and coastal environment in the East
5532 Siberian Arctic shelf, J. Mar. Syst., doi:10.1016/j.jmarsys.2006.06.006, 2007.
5533 Shakhova, N., Semiletov, I., Salyuk, A., Yusupov, V., Kosmach, D. and Gustafsson, Ö.:
5534 Extensive methane venting to the atmosphere from sediments of the East Siberian Arctic
5535 Shelf, Science (80-.)., doi:10.1126/science.1182221, 2010.
5536 Shakhova, N., Semiletov, I., Leifer, I., Sergienko, V., Salyuk, A., Kosmach, D., Chernykh, D.,
5537 Stubbs, C., Nicolsky, D., Tumskoy, V. and Gustafsson, Ö.: Ebullition and storm-induced
5538 methane release from the East Siberian Arctic Shelf, Nat. Geosci., doi:10.1038/ngeo2007,
5539 2014.
5540 Shakhova, N., Semiletov, I., Sergienko, V., Lobkovsky, L., Yusupov, V., Salyuk, A.,
5541 Salomatin, A., Chernykh, D., Kosmach, D., Panteleev, G., Nicolsky, D., Samarkin, V., Joye, S.,
5542 Charkin, A., Dudarev, O., Meluzov, A. and Gustafsson, O.: The East Siberian Arctic Shelf:
5543 Towards further assessment of permafrost-related methane fluxes and role of sea ice,
5544 Philos. Trans. R. Soc. A Math. Phys. Eng. Sci., doi:10.1098/rsta.2014.0451, 2015.
5545 Shvartsev, S. L.: Geochemistry of fresh groundwater in the main landscape zones of the
5546 Earth, Geochemistry Int., doi:10.1134/S0016702908130016, 2008.
5547 Shvidenko, A. and Nilsson, S.: A synthesis of the impact of Russian forests on the global
5548 carbon budget for 1961-1998, Tellus, Ser. B Chem. Phys. Meteorol., doi:10.1034/j.1600-
5549 0889.2003.00046.x, 2003.
5550 Smith, L. C. and Pavelsky, T. M.: Estimation of river discharge, propagation speed, and
5551 hydraulic geometry from space: Lena River, Siberia, Water Resour. Res.,
5552 doi:10.1029/2007WR006133, 2008.
5553 Sommerkorn, M.: Micro-topographic patterns unravel controls of soil water and
5554 temperature on soil respiration in three Siberian tundra systems, Soil Biol. Biochem.,
5555 doi:10.1016/j.soilbio.2008.03.002, 2008.
5556 Sorokin, Y. I. and Sorokin, P. Y.: Plankton and primary production in the Lena River
5557 Estuary and in the south-eastern Laptev sea, Estuar. Coast. Shelf Sci.,
5558 doi:10.1006/ecss.1996.0078, 1996.
5559 Spencer, R. G. M., Mann, P. J., Dittmar, T., Eglinton, T. I., McIntyre, C., Holmes, R. M., Zimov,
5560 N. and Stubbins, A.: Detecting the signature of permafrost thaw in Arctic rivers, Geophys.
5561 Res. Lett., doi:10.1002/2015GL063498, 2015.
5562 Starr, M., Lindroos, A. J., Ukonmaanaho, L., Tarvainen, T. and Tanskanen, H.: Weathering

release of heavy metals from soil in comparison to deposition, litterfall and leaching fluxes in a remote, boreal coniferous forest, Appl. Geochemistry, doi:10.1016/S0883-2927(02)00157-9, 2003.
Steele, M. and Ermold, W.: Loitering of the retreating sea ice edge in the Arctic Seas, J. Geophys. Res. Ocean., doi:10.1002/2015JC011182, 2015.
Stets, E. G., Butman, D., McDonald, C. P., Stackpoole, S. M., DeGrandpre, M. D. and Striegl, R. G.: Carbonate buffering and metabolic controls on carbon dioxide in rivers, Global Biogeochem. Cycles, doi:10.1002/2016GB005578, 2017.
Striegl, R. G., Dornblaser, M. M., Aiken, G. R., Wickland, K. P. and Raymond, P. A.: Carbon export and cycling by the Yukon, Tanana, and Porcupine rivers, Alaska, 2001-2005, Water Resour. Res., doi:10.1029/2006WR005201, 2007.
Stroeve, J. C., Markus, T., Boisvert, L., Miller, J. and Barrett, A.: Changes in Arctic melt season and implications for sea ice loss, Geophys. Res. Lett., doi:10.1002/2013GL058951, 2014.
Stuart Chapin, F., Matson, P. A. and Vitousek, P. M.: Principles of terrestrial ecosystem ecology., 2012.
Stubbins, A., Mann, P. J., Powers, L., Bittar, T. B., Dittmar, T., McIntyre, C. P., Eglinton, T. I., Zimov, N. and Spencer, R. G. M.: Low photolability of yedoma permafrost dissolved organic carbon, J. Geophys. Res. Biogeosciences, doi:10.1002/2016JG003688, 2017.
Tank, S. E., Raymond, P. A., Striegl, R. G., McClelland, J. W., Holmes, R. M., Fiske, G. J. and Peterson, B. J.: A land-to-ocean perspective on the magnitude, source and implication of DIC flux from major Arctic rivers to the Arctic Ocean, Global Biogeochem. Cycles, doi:10.1029/2011GB004192, 2012a.
Tank, S. E., Raymond, P. A., Striegl, R. G., McClelland, J. W., Holmes, R. M., Fiske, G. J. and Peterson, B. J.: A land-to-ocean perspective on the magnitude, source and implication of DIC flux from major Arctic rivers to the Arctic Ocean, Global Biogeochem. Cycles, doi:10.1029/2011GB004192, 2012b.
Tank, S. E., Frey, K. E., Striegl, R. G., Raymond, P. A., Holmes, R. M., McClelland, J. W. and Peterson, B. J.: Landscape-level controls on dissolved carbon flux from diverse catchments of the circumboreal, Global Biogeochem. Cycles, doi:10.1029/2012GB004299, 2012c.
Tank, S. E., Striegl, R. G., McClelland, J. W. and Kokelj, S. V.: Multi-decadal increases in dissolved organic carbon and alkalinity flux from the Mackenzie drainage basin to the Arctic Ocean, Environ. Res. Lett., doi:10.1088/1748-9326/11/5/054015, 2016.
Tank, S. E., Fellman, J. B., Hood, E. and Kritzberg, E. S.: Beyond respiration: Controls on lateral carbon fluxes across the terrestrial-aquatic interface, Limnol. Oceanogr. Lett., doi:10.1002/lol2.10065, 2018.
Tanski, G., Lantuit, H., Ruttor, S., Knoblauch, C., Radosavljevic, B., Strauss, J., Wolter, J., Irrgang, A. M., Ramage, J. and Fritz, M.: Transformation of terrestrial organic matter along thermokarst-affected permafrost coasts in the Arctic, Sci. Total Environ., doi:10.1016/j.scitotenv.2016.12.152, 2017.
Tarnocai, C., Canadell, J. G., Schuur, E. A. G., Kuhry, P., Mazhitova, G. and Zimov, S.: Soil organic carbon pools in the northern circumpolar permafrost retion, Global Biogeochem. Cycles, doi:Gb2023\n10.1029/2008gb003327, 2009.
Teodoru, C. R., Del Giorgio, P. A., Prairie, Y. T. and Camire, M.: Patterns in pCO2 in boreal streams and rivers of northern Quebec, Canada, Global Biogeochem. Cycles, doi:10.1029/2008GB003404, 2009.
Tesi, T., Semiletov, I., Hugelius, G., Dudarev, O., Kuhry, P. and Gustafsson, Ö.: Composition

and fate of terrigenous organic matter along the Arctic land-ocean continuum in East Siberia: Insights from biomarkers and carbon isotopes, Geochim. Cosmochim. Acta, doi:10.1016/j.gca.2014.02.045, 2014.
Tootchi, A., Jost, A. and Ducharne, A.: Multi-source global wetland maps combining surface water imagery and groundwater constraints, Earth Syst. Sci. Data, doi:10.5194/essd-11-189-2019, 2019.
Tranvik, L. J., Downing, J. A., Cotner, J. B., Loiselle, S. A., Striegl, R. G., Ballatore, T. J., Dillon, P., Finlay, K., Fortino, K., Knoll, L. B., Kortelainen, P. L., Kutser, T., Larsen, S., Laurion, I., Leech, D. M., Leigh McCallister, S., McKnight, D. M., Melack, J. M., Overholt, E., Porter, J. A., Prairie, Y., Renwick, W. H., Roland, F., Sherman, B. S., Schindler, D. W., Sobek, S., Tremblay, A., Vanni, M. J., Verschoor, A. M., Von Wachenfeldt, E. and Weyhenmeyer, G. A.: Lakes and reservoirs as regulators of carbon cycling and climate, Limnol. Oceanogr., doi:10.4319/lo.2009.54.6_part_2.2298, 2009.
Venkiteswaran, J. J., Schiff, S. L. and Wallin, M. B.: Large carbon dioxide fluxes from headwater boreal and sub-boreal streams, PLoS One, doi:10.1371/journal.pone.0101756, 2014.
Vitousek, P. M. and Hobbie, S.: Heterotrophic nitrogen fixation in decomposing litter: Patterns and regulation, Ecology, doi:10.1890/0012-9658(2000)081[2366:HNFIDL]2.0.CO;2, 2000.
Vitousek, P. M. and Sanford, R. L.: Nutrient Cycling in Moist Tropical Forest, Ecology, doi:0.1146/annurev.es.17.110186.001033, 1986.
Van Vliet, M. T. H., Yearsley, J. R., Franssen, W. H. P., Ludwig, F., Haddeland, I., Lettenmaier, D. P. and Kabat, P.: Coupled daily streamflow and water temperature modelling in large river basins, Hydrol. Earth Syst. Sci., doi:10.5194/hess-16-4303-2012, 2012.
Van Vliet, M. T. H., Franssen, W. H. P., Yearsley, J. R., Ludwig, F., Haddeland, I., Lettenmaier, D. P. and Kabat, P.: Global river discharge and water temperature under climate change, Glob. Environ. Chang., doi:10.1016/j.gloenvcha.2012.11.002, 2013.
Vonk, J. E. and Gustafsson, Ö.: Permafrost-carbon complexities, Nat. Geosci., doi:10.1038/ngeo1937, 2013.
Vonk, J. E., Sanchez-Garca, L., Van Dongen, B. E., Alling, V., Kosmach, D., Charkin, A., Semiletov, I. P., Dudarev, O. V., Shakhova, N., Roos, P., Eglinton, T. I., Andersson, A. and Gustafsson, A.: Activation of old carbon by erosion of coastal and subsea permafrost in Arctic Siberia, Nature, doi:10.1038/nature11392, 2012.
Vonk, J. E., Mann, P. J., Davydov, S., Davydova, A., Spencer, R. G. M., Schade, J., Sobczak, W. V., Zimov, N., Zimov, S., Bulygina, E., Eglinton, T. I. and Holmes, R. M.: High biolability of ancient permafrost carbon upon thaw, Geophys. Res. Lett., doi:10.1002/grl.50348, 2013.
Vonk, J. E., Tank, S. E., Mann, P. J., Spencer, R. G. M., Treat, C. C., Striegl, R. G., Abbott, B. W. and Wickland, K. P.: Biodegradability of dissolved organic carbon in permafrost soils and aquatic systems: A meta-analysis, Biogeosciences, doi:10.5194/bg-12-6915-2015, 2015a.
Vonk, J. E., Thienpont, J. R., Rühland, K. M., Pisaric, M. F. J., Kokelj, S. V., Kimpe, L. E., Blais, J. M., Smol, J. P., Spencer, R. G. M., Mann, P. J., Dittmar, T., Eglinton, T. I., Mcintyre, C., Holmes, R. M., Zimov, N., Stubbins, A., Rudy, A. C. a, Lamoureux, S. F., Treitz, P., Collingwood, A., Rouse, W. R., Douglas, M. S. V, Hecky, R. E., Hershey, a. E., Kling, G. W., Lesack, L., Marsh, P., McDonald, M., Nicholson, B. J., Roulet, N. T., Smol, J. P., Murton, J. B., Lewkowicz, A. G., Harris, C., Lantz, T. C., Kokelj, S. V., Gergel, S. E., Henry, G. H. R., Tunnicliffe, J., Lacelle, D., Lantz, T. C., Chin, K., Fraser, R., Jin, H., Yu, Q., Lu, L., Guo, D., He,

5659 R., Yu, S., Sun, G., Li, Y., Harris, C., Lewkowicz, A. G., Grom, J. D., Pollard, W. H., Balser, A.
5660 W., Gooseff, M. N., Jones, J. B., Bowden, W. B., Anisimov, O. a. and Nelson, F. E.: Detecting
5661 the signature of permafrost thaw in Arctic rivers, Glob. Planet. Change,
5662 doi:10.1002/2015GL063498.Received, 2015b.
5663 Vonk, J. E., Tank, S. E., Bowden, W. B., Laurion, I., Vincent, W. F., Alekseychik, P., Amyot,
5664 M., Billet, M. F., Canário, J., Cory, R. M., Deshpande, B. N., Helbig, M., Jammet, M., Karlsson,
5665 J., Larouche, J., MacMillan, G., Rautio, M., Walter Anthony, K. M. and Wickland, K. P.:
5666 Reviews and Syntheses: Effects of permafrost thaw on arctic aquatic ecosystems,
5667 Biogeosciences Discuss., doi:10.5194/bgd-12-10719-2015, 2015c.
5668 Vorosmarty, C. J., Fekete, B. M., Meybeck, M. and Lammers, R. B.: Global system of rivers:
5669 Its role in organizing continental land mass and defining land-To-Ocean linkages, Global
5670 Biogeochem. Cycles, doi:10.1029/1999GB900092, 2000.
5671 Walz, J., Knoblauch, C., Böhme, L. and Pfeiffer, E. M.: Regulation of soil organic matter
5672 decomposition in permafrost-affected Siberian tundra soils - Impact of oxygen
5673 availability, freezing and thawing, temperature, and labile organic matter, Soil Biol.
5674 Biochem., doi:10.1016/j.soilbio.2017.03.001, 2017.
5675 Wang, T., Ottlé, C., Boone, A., Ciais, P., Brun, E., Morin, S., Krinner, G., Piao, S. and Peng, S.:
5676 Evaluation of an improved intermediate complexity snow scheme in the ORCHIDEE land
5677 surface model, J. Geophys. Res. Atmos., doi:10.1002/jgrd.50395, 2013.
5678 Wanninkhof, R. H.: Relationship between wind speed and gas exchange, J. Geophys. Res.,
5679 doi:10.1029/92JC00188, 1992.
5680 White, A. F. and Blum, A. E.: Effects of climate on chemical_ weathering in watersheds,
5681 Geochim. Cosmochim. Acta, doi:10.1016/0016-7037(95)00078-E, 1995.
5682 Whitefield, J., Winsor, P., McClelland, J. and Menemenlis, D.: A new river discharge and
5683 river temperature climatology data set for the pan-Arctic region, Ocean Model.,
5684 doi:10.1016/j.ocemod.2014.12.012, 2015.
5685 Wickland, K. P., Waldrop, M. P., Aiken, G. R., Koch, J. C., Jorgenson, M. T. and Striegl, R. G.:
5686 Dissolved organic carbon and nitrogen release from boreal Holocene permafrost and
5687 seasonally frozen soils of Alaska, Environ. Res. Lett., doi:10.1088/1748-9326/aac4ad,
5688 2018.
5689 Wild, B., Schnecker, J., Alves, R. J. E., Barsukov, P., Bárta, J., Čapek, P., Gentsch, N., Gittel, A.,
5690 Guggenberger, G., Lashchinskiy, N., Mikutta, R., Rusalimova, O., Šantrůčková, H.,
5691 Shibistova, O., Urich, T., Watzka, M., Zrazhevskaya, G. and Richter, A.: Input of easily
5692 available organic C and N stimulates microbial decomposition of soil organic matter in
5693 arctic permafrost soil, Soil Biol. Biochem., doi:10.1016/j.soilbio.2014.04.014, 2014.
5694 Wild, B., Gentsch, N., Capek, P., Diáková, K., Alves, R. J. E., Bárta, J., Gittel, A., Hugelius, G.,
5695 Knoltsch, A., Kuhry, P., Lashchinskiy, N., Mikutta, R., Palmtag, J., Schleper, C., Schnecker, J.,
5696 Shibistova, O., Takriti, M., Torsvik, V. L., Urich, T., Watzka, M., Šantrūcková, H.,
5697 Guggenberger, G. and Richter, A.: Plant-derived compounds stimulate the decomposition
5698 of organic matter in arctic permafrost soils, Sci. Rep., doi:10.1038/srep25607, 2016.
5699 Woods, G. C., Simpson, M. J., Pautler, B. G., Lamoureux, S. F., Lafrenière, M. J. and Simpson,
5700 A. J.: Evidence for the enhanced lability of dissolved organic matter following permafrost
5701 slope disturbance in the Canadian High Arctic, Geochim. Cosmochim. Acta,
5702 doi:10.1016/j.gca.2011.08.013, 2011.
5703 Wu, Y., Clarke, N. and Mulder, J.: Dissolved organic carbon concentrations in throughfall
5704 and soil waters at level II monitoring plots in norway: Short- and long-term variations,
5705 Water. Air. Soil Pollut., doi:10.1007/s11270-009-0073-1, 2010.
5706 Xue, K.: Tundra soil carbon is vulnerable to rapid microbial decomposition under

5707 climatewarming, Nat. Clim. Chang., doi:10.1038/NCLIMATE2940, 2017.
5708 Xue, K., Yuan, M. M., Shi, Z. J., Qin, Y., Deng, Y., Cheng, L., Wu, L., He, Z., Van Nostrand, J. D.,
5709 Bracho, R., Natali, S., Schuur, E. A. G., Luo, C., Konstantinidis, K. T., Wang, Q., Cole, J. R.,
5710 Tiedje, J. M., Luo, Y. and Zhou, J.: Tundra soil carbon is vulnerable to rapid microbial
5711 decomposition under climate warming, Nat. Clim. Chang., doi:10.1038/nclimate2940,
5712 2016.
5713 Yang, H., Zhou, F., Piao, S., Huang, M., Chen, A., Ciais, P., Li, Y., Lian, X., Peng, S. and Zeng,
5714 Z.: Regional patterns of future runoff changes from Earth system models constrained by
5715 observation, Geophys. Res. Lett., doi:10.1002/2017GL073454, 2017.
5716 Ye, B., Yang, D. and Kane, D. L.: Changes in Lena River streamflow hydrology: Human
5717 impacts versus natural variations, Water Resour. Res., doi:10.1029/2003WR001991,
5718 2003.
5719 Ye, B., Yang, D., Zhang, Z. and Kane, D. L.: Variation of hydrological regime with
5720 permafrost coverage over Lena Basin in Siberia, J. Geophys. Res. Atmos.,
5721 doi:10.1029/2008JD010537, 2009.
5722 Yu, Z.: Holocene carbon flux histories of the world's peatlands: Global carbon-cycle
5723 implications, Holocene, doi:10.1177/0959683610386982, 2011.
5724 Yue, C., Ciais, P., Zhu, D., Wang, T., Peng, S. S. and Piao, S. L.: How have past fire
5725 disturbances contributed to the current carbon balance of boreal ecosystems?,
5726 Biogeosciences, doi:10.5194/bg-13-675-2016, 2016.
5727 Zakharova, E. A., Pokrovsky, O. S., Dupré, B., Gaillardet, J. and Efimova, L. E.: Chemical
5728 weathering of silicate rocks in Karelia region and Kola peninsula, NW Russia: Assessing
5729 the effect of rock composition, wetlands and vegetation, Chem. Geol.,
5730 doi:10.1016/j.chemgeo.2007.03.018, 2007.
5731 Zhang, K., Kimball, J. S., Mu, Q., Jones, L. A., Goetz, S. J. and Running, S. W.: Satellite based
5732 analysis of northern ET trends and associated changes in the regional water balance
5733 from 1983 to 2005, J. Hydrol., doi:10.1016/j.jhydrol.2009.09.047, 2009.
5734 Zhang, X., Hutchings, J. A., Bianchi, T. S., Liu, Y., Arellano, A. R. and Schuur, E. A. G.:
5735 Importance of lateral flux and its percolation depth on organic carbon export in Arctic
5736 tundra soil: Implications from a soil leaching experiment, J. Geophys. Res.
5737 Biogeosciences, doi:10.1002/2016JG003754, 2017.
5738 Zhu, D., Peng, S., Ciais, P., Zech, R., Krinner, G., Zimov, S. and Grosse, G.: Simulating soil
5739 organic carbon in yedoma deposits during the Last Glacial Maximum in a land surface
5740 model, Geophys. Res. Lett., doi:10.1002/2016GL068874, 2016.
5741 Zimov, S. A., Schuur, E. A. G. and Stuart Chapin, F.: Permafrost and the global carbon
5742 budget, Science (80-.)., doi:10.1126/science.1128908, 2006.
5743 Zolkos, S., Tank, S. E. and Kokelj, S. V.: Mineral Weathering and the Permafrost Carbon-
5744 Climate Feedback, Geophys. Res. Lett., doi:10.1029/2018GL078748, 2018.
5745 Zona, D., Gioli, B., Commane, R., Lindaas, J., Wofsy, S. C. and Miller, C. E.: Cold season
5746 emissions dominate the Arctic tundra methane budget, Proc. Natl. Acad. Sci.,
5747 doi:10.1073/pnas.1516017113, 2015.
5748 Zubrzycki, S., Kutzbach, L., Grosse, G. and Desyatkin, A.: Organic carbon and total
5749 nitrogen stocks in soils of the Lena River Delta, Biogeosciences, doi:10.5194/bg-10-
5750 3507-2013, 2013.
5751